



1st Caprock Integrity & Gas Storage Symposium 2024
St-Ursanne, Switzerland

24–25 January 2024

Extended abstracts

www.cigss.ch

Published by Swiss Federal Office of Topography (swisstopo),
Mont Terri Underground Rock Laboratory, St-Ursanne, Switzerland

1st Caprock Integrity & Gas Storage Symposium 2024 – Extended abstracts

© 2024 swisstopo

The authors bear full responsibility for the contents of their contributions.

Edited by Martin Ziegler, Romain Nicol, David Jaeggi, Jonas Windisch and Christophe Nussbaum.

All rights reserved; no parts of this publication may be reproduced, stored or retrieved in any form or by any means without the prior written permission of the authors.

swisstopo received the right for online publishing.



Schweizerische Eidgenossenschaft
Confédération suisse
Confederazione Svizzera
Confederaziun svizra

Swiss Confederation

Federal Department of Defence,
Civil Protection and Sport DDPS
Federal Office of Topography swisstopo

PREFACE

In the context of the urgency of climate change and the need to drastically reduce greenhouse gases in the atmosphere, it is essential to capture and store unavoidable CO₂ emissions, alongside other vital emission reduction measures. Indeed, some CCS is essential to achieve the 2050 carbon neutrality targets that industrialised countries have set themselves. The Caprock Integrity & Gas Storage Symposium (CIGSS) aims at providing and establishing a platform for the exchange and discussion of scientific, technological, industrial, and regulatory advances related to the integrity of caprocks in the context of geological storage of CO₂ and gas storage in general. Purposely organised in Saint-Ursanne, with the support of the Mont Terri underground rock laboratory and its partners, the CIGSS benefits from the invaluable contribution and knowledge of the radioactive waste disposal community. Their experience is indispensable, particularly when it comes to gas migration in low-permeability rocks such as claystone, which is a promising host rock for nuclear waste disposal and caprock for CO₂ storage.

The first day of this 1st CIGSS is devoted to a symposium with academic community, government agencies, industry representatives and invited speakers. The following themes are on the agenda: public acceptance, regulation, site screening and exploration, characterization and behavior of geological reservoirs and caprocks, key research developments of geological storage of CO₂ and other gases like H₂, and expectation of CO₂ producers. The second day is devoted to scientific exchange and discussion during poster sessions, in the field of fault, caprock and borehole integrity, and gas storage in general.

In summary, the 2-day symposium is arranged around five core themes:

- Small-scale laboratory experiments
- Medium-scale rock laboratory experiments toward pilot-scale projects
- Local and regional geological and structural investigations of potential sites
- Numerical studies
- Innovative monitoring systems

The core themes will allow practitioners and researchers from diverse backgrounds to progress beyond current knowledge barriers, and lay out a framework for the evaluation of caprock integrity in claystone and possibly increasing the public acceptance of geological gas storage.

Guided tours of the Mont Terri underground rock laboratory and a symposium dinner complete the CIGSS program. Participants will be able to see for themselves the experiments being carried out in the low permeable Opalinus Clay in the fields of CO₂ storage and radioactive waste with focus on hydrogen migration.

COMMITTEES

Organizing Committee

Christophe Nussbaum.....	Swiss Federal Office of Topography (swisstopo)
David Jaeggi.....	Swiss Federal Office of Topography (swisstopo)
Martin Ziegler.....	Swiss Federal Office of Topography (swisstopo)

International Advisory and Review Board

Jamie Andrews.....	Equinor, Norway
Jens Birkholzer.....	Lawrence Berkeley National Laboratory (LBNL), USA
Frédéric Cappa.....	Géoazur Earth Sciences Laboratory, Université Côte d'Azur, France
Antonino Cilona.....	Shell, The Netherlands
Valentin Gischig.....	ETH Zurich (ETHZ), Switzerland
Yves Guglielmi.....	Lawrence Berkeley National Laboratory (LBNL), USA
David Jaeggi.....	Swiss Federal Office of Topography (swisstopo)
Martin Jiskra.....	Swiss Federal Office for the Environment (FOEN)
Rolf Kipfer.....	Swiss Federal Institute of Aquatic Science and Technology (EAWAG)
Michael Kühn.....	German Research Centre for Geosciences (GFZ)
Axel Liebscher.....	German Federal Company for Radioactive Waste Disposal (BGE)
Herfried Madritsch.....	Swiss Federal Office of Topography (swisstopo)
Roman Makhnenko.....	University Illinois, USA
Frédéric Mathurin.....	French Geological Survey (BRGM)
Andreas Möri.....	Swiss Federal Office of Topography (swisstopo)
Christian Minnig.....	Swiss Federal Office of Energy (SFOE)
Herwig Müller.....	Swiss National Cooperative for the Disposal of Radioactive Waste (nagra)
Christophe Nussbaum.....	Swiss Federal Office of Topography (swisstopo)
Philip Ringrose.....	Norwegian University of Science and Technology (NTNU)
Jean-Charles Robinet.....	French National Radioactive Waste Management Agency (ANDRA)
Jonny Rutqvist.....	Lawrence Berkeley National Laboratory (LBNL), USA
Elin Skurtveit.....	Norwegian Geotechnical Institute (NGI)
Victor Villarasa.....	Spanish National Research Council (CSIC)
Gabriela von Goerne.....	German Federal Institute for Geosciences and Natural Resources (BGR)
Christopher Wibberley.....	TotalEnergies, France
Stefan Wiemer.....	ETH Zurich (ETHZ), Switzerland
Alba Zappone.....	ETH Zurich (ETHZ), Switzerland
Martin Ziegler.....	Swiss Federal Office of Topography (swisstopo)

PROGRAMME OF DAY 1

Symposium with government agencies, industry representatives, academic world and invited speakers

- 08:30 **Registration opens / Mont Terri Visitor Centre**
- 09:00 **Welcome address**
Christophe Nussbaum (swisstopo)
- 09:10 **Session 1**
Geological carbon storage in Switzerland: current status and next steps
Chair: Christophe Nussbaum (swisstopo)
- 10:30 **Coffee break**
- 11:00 **Session 2**
Geological carbon storage worldwide: insights from research organisations
Chair: Jens Birkholzer (LBNL)
- 12:40 **Lunch**
- 13:45 **Session 3**
Geological carbon storage worldwide: insights from energy companies
Chair: Elin Skurtveit (NGI)
- 15:00 **Coffee break**
- 15:30 **Session 4**
Gas migration in shale and role of hydrogen
Chair: Axel Liebscher (BGE)
- 16:45 **Panel discussion**
Jens Birkholzer (LBNL)
Marcella Dean (Shell)
Martin Jiskra (FOEN)
Michael Kühn (GFZ, Helmholtz)
Philip Ringrose (NTNU)
Martin Saar (ETHZ)
Stefan Vannoni (cemsuissse)

Moderators: Gabriela von Goerne (BGR), Christophe Nussbaum (swisstopo)
- 17:30 **Appetiser**
- 18:30 **Transfer to dinner**

PROGRAMME OF DAY 2

Scientific conference

- 09:00 **Registration opens / Mont Terri Visitor Centre**
- 09:30 **Session 5 | Poster**
Small-scale laboratory experiments and transport models
- 10:45 **Session 6 | Poster**
Medium-scale rock laboratory experiments toward pilot-scale projects
and associated advances in numerical simulations and sensing technologies
- 12:00 **Lunch**
- 13:00 **Session 7 | Poster**
Local and regional geological and structural investigations
and monitoring of potential sites
- 14:30 **Rock laboratory visit**
Guides:
Myriam Agnel (ANDRA)
Yves Guglielmi (LBNL)
David Jaeggi (swisstopo)
Rolf Kipfer (EAWAG)
Mélanie Lundy (ANDRA)
Christophe Nussbaum (swisstopo)
Antonio P. Rinaldi (ETHZ/SED)
Senecio Schefer (swisstopo)
Alba Zappone (ETHZ/SED)
Martin Ziegler (swisstopo)
- 16:30 **Back at visitor centre and end of CIGSS**

TABLE OF CONTENTS

Preface	iii
Committees	iv
Programme of Day 1	v
Programme of Day 2	vi
Table of contents	vii

Session 1 — Geological carbon storage in Switzerland: current status and next steps

101 Establishing CO ₂ storage in Switzerland	1
MARTIN JISKRA AND CHRISTIAN MINNIG	
102 Current and planned activities of the Swiss Geological Survey in the context of geological carbon storage	3
DAVID JAEGGI, HERFRIED MADRITSCH, ANDREAS MÖRI, CHRISTOPHE NUSSBAUM AND MARTIN ZIEGLER	
103 Hard to abate sectors. How do we manage the challenge for the net zero target in climate policy on the way to 2050?	7
STEFAN VANNONI AND ROBIN QUARTIER	
104 From caprock integrity to system integration: lessons for siting of CO ₂ storage locations	8
THOMAS FLÜELER	

Session 2 — Geological carbon storage worldwide: insights from research organisations

201 How CCS can benefit from CO ₂ -Plume Geothermal (CPG)	13
MARTIN O. SAAR, TSUBASA ONISHI, KEVIN P. HAU, JASPER DE REUS AND MAHMOUD HEFNY	
202 Experiments of fault zone activation in caprock analogs: implications for CO ₂ sequestration	18
YVES GUGLIELMI AND JENS BIRKHOLZER	
203 Storing Swiss CO ₂ in Iceland and Switzerland: insights from DemoUpCarma and beyond	22
STEFAN WIEMER, ALBA ZAPPONE, ANTONIO PIO RINALDI, THANUSHIKA GUNATILAKE, JONAS JUNKER, ANNE OBERMANN, VIOLA BECATTINI, MARCO MAZZOTTO AND THE DEMOUPCARMA TEAM	
204 Multi-disciplinary monitoring of the Ketzin CO ₂ pilot site as successful concept for storage integrity assessment	26
MICHAEL KÜHN AND CORNELIA SCHMIDT-HATTENBERGER	

Session 3 — Geological carbon storage worldwide: insights from energy companies

301 Global status of saline aquifer CO ₂ storage and key challenges for scale-up	30
PHILIP RINGROSE	
302 CO ₂ storage site feasibility assessment and risk-based monitoring: an industry approach	34
MARCELLA DEAN, OWAIN TUCKER, KEES HINDRIKS AND NINO CILONA	
303 Structural geology and fault seal studies in CO ₂ storage evaluation	37
CHRISTOPHER WIBBERLEY, JADE DUTILLEUL AND RICHARD TOZER	

Session 4 — Gas migration in shale and role of hydrogen

401 Current issues on gas in radwaste deep geological repositories: example of Cigeo (France)	41
RÉMI DE LA VAISSIÈRE, JEAN TALANDIER, CHRISTOPHE DE LESQUEN AND GILLES ARMAND	
402 Microbial hydrogen transformation in the deep subsurface	45
RIZLAN BERNIER-LATMANI, CAMILLE ROLLAND AND OLIVIER LEUPIN	
403 Exploration for natural hydrogen	47
ERIC C. GAUCHER	

Session 5 — Small-scale laboratory experiments and transport models

501	Molecular scale understanding of gas transport in clays	48
	SERGEY CHURAKOV, JERRY OWUSU, KONSTANTINOS KARALIS, ATHANASIOS MOKOS AND NIKOLAOS PRASIANAKIS	
502	CO₂ sealing capacity of sandy and shaly Opalinus Clay	52
	HYUNBIN KIM, VICTOR VILARRASA AND ROMAN MAKHNENKO	
503	Experimental study of coupled hydro-chemo-mechanical processes of CO₂ injection into a low-permeability sandstone	56
	IMAN R. KIVI, DRAGAN GRGIC, MOHAMED MOUMNI, ATEFEH VAFAIE, JESUS CARRERA, SAMUEL KREVER AND VICTOR VILARRASA	
504	Characterizing elastic stiffness, creep, and in-situ stress and their anisotropies of clay shales using pressuremeter testing	60
	LANG LIU AND RICK CHALATURNYK	
505	Geochemical hydrogen-pore water-Opalinus Clay interactions	64
	CHRISTIAN OSTERTAG-HENNING	
506	Petrophysical and petrothermal characterization of caprock carbonate stringers: the Upper Muschelkalk in the Estopanyà syncline, South-Central Pyrenees	68
	PEDRO RAMIREZ-PEREZ, GABRIEL COFRAGE, ERNEST ONETTI, JUAN DIEGO MARTÍN-MARTÍN, JEAN-PIERRE SIZUN, IRENE CANTARERO AND ANNA TRAVÉ	
507	Microbial processes responsible for H₂ consumption in clay reservoirs	72
	CAMILLE ROLLAND, OLIVIER X. LEUPIN AND RIZLAN BERNIER-LATMANI	
508	Sealing capacity of a pre-fissured caprock to CO₂ injection (CS-C)	74
	ELENI STAVROPOULOU AND LYESSE LALOU	
509	Factors controlling acid interactions with carbonate rocks	78
	ATEFEH VAFAIE, JORDI CAMA, JOSEP M SOLER, DRAGAN GRGIC, IMAN R KIVI, SAMUEL KREVER AND VICTOR VILARRASA	
510	Project BiMiAb_H2: New experimental research to investigate hydrogen migration in reservoir and caprock layers	82
	PHILIPP WENIGER	
511	Seismic and ultrasonic monitoring of a shale seal exposed to CO₂: a laboratory study	83
	SERHII LOZOVYI, ZEENAT MANIAR, AND PIERRE CERASI	

Session 6 — Medium-scale rock laboratory experiments toward pilot-scale projects and associated advances in numerical simulations and sensing technologies

601	CO₂ leakage through a stimulated fault in a claystone caprock	87
	PRESELLI ANNAN, ANTONIO PIO RINALDI, ALBA ZAPPONE AND MARTIN BLUNT	
602	Fluid flow driven by rupture growth in low-permeability faults during high-pressure injection in shale caprocks	92
	YVES GUGLIELMI, FRÉDÉRIC CAPPÀ, CHRISTOPHE NUSSBAUM AND JENS BIRKHOEHLER	
603	Assessing caprock integrity in an acid gas storage project: a Middle East case	96
	MARTINA CERVELLI, NICOLÁS RANGEL JURADO AND FEDERICO GAMES	
604	CO₂ storage in salt basins: Influence of salt tectonics on seal integrity and containment risk	99
	SIÂN EVANS, SIMON BLONDEL, TORSTEN HANSEN, RIKKE BRUHN AND ALVAR BRAATHEN	
605	Increasing process understanding in gas migration: investigations using the TH2M modelling approach.	102
	VINAY KUMAR, GESA ZIEFLE AND JOBST MARBANN	
606	Fate of hydrogen gas injected in a clay-rich rock: an <i>in-situ</i> experiment	104
	MÉLANIE LUNDY, CHRISTIAN OSTERTAG-HENNING, MYRIAM AGNEL, STEFAN WECHNER, YANICK LETTRY AND AGNÈS VINSOT	
607	Hydro-geochemical scoping calculations for the CO₂ Long-term Periodic Injection Experiment (CO₂LPIE)	108
	JIN MA, PETER ALT-EPPING AND PAUL WERSIN	
608	Storage capacity assessment for CO₂/H₂S in a depleted gas condensate reservoir	111
	NICOLÁS RANGEL JURADO, MARTINA CERVELLI, YURIANNY ROJAS AND FEDERICO GAMES	
609	GCS caprock potential of the Triassic Haisborough Group, Southern North Sea: insights from an onshore UK analogue	115
	SIMON SCHNEIDER, MICHAEL FLOWERDEW, NIAL PATERSON, COLM PIERCE, MICHAEL POINTON, MICHELLE SHIERS, ADAM SZULC, STEPHEN VINCENT AND DAVID WARBURTON	

610	Field-scale hydro-mechanical simulation of a novel monitoring system for the CO₂ Long-Term Periodic Injection Experiment (CO₂LPIE) at the Mont Terri rock laboratory	117
	SRI KALYAN TANGIRALA, MARTIN ZIEGLER, ROMAN Y. MAKHNENKO AND VICTOR VILARRASA	
611	Using the miniRUEDI within the context of the Mont Terri Rock Laboratory: potential and challenges	121
	YAMA TOMONAGA, MARTIN ZIEGLER AND DAVID JAEGLI	
612	Fault slip in clay-rich rocks: influence of the interaction between water and clay minerals	125
	MARKUS RAST, CLAUDIO MADONNA, PAUL A. SELVADURAI, ANTONIO SALAZAR VÁSQUEZ,, QUINN WENNING AND JONAS B. RUH	
613	Combined numerical and experimental investigation of injection related effects in the CL experiment	129
	GESA ZIEFLE, THIES BEILECKE, SHUANG CHEN, MARKUS FURCHE, JÜRGEN HESSER, VINAY KUMAR, JOBST MAßMANN, CHRISTIAN OSTERTAG-HENNING	
614	A borehole modular multi-sensor monitoring system (MMMS)	133
	MARTIN ZIEGLER, TOBIAS FRITSCH AND STEFAN CZERNER	
615	CO₂LPIE: CO₂ Long-term Periodic Injection Experiment (CL)	137
	MARTIN ZIEGLER, DAVID JAEGLI, ALESSIA GRIGNASCHI, ROLF KIPFER, ANTONIO PIO RINALDI	

Session 7 — Local and regional geological and structural investigations and monitoring of potential sites

701	Distributed fibre-optic temperature monitoring in boreholes of a seasonal geothermal energy storage	141
	MATTHIAS BÜHLER, FRANK FISCHLI, MICHAEL ITEN, FALKO BETHMANN AND ANDRE EL-ALFY	
702	Modelling of factors affecting fault stability	145
	PIERRE CERASI, XIYANG XIE AND ANNA STROISZ	
703	Well integrity monitoring for large-scale CO₂ storage: the LEGACY project	149
	BASTIEN DUPUY, MICHAEL JORDAN, TJ ULICH,, HARVEY GOODMAN, ANDREW DELOREY, ROBERT GUYER AND BENJAMIN EMMEL	
704	Overview of structure, geometry, fluid flow and seismo-mechanics of clay-rich thrust faults drilled by the International Ocean Discovery Program (IODP) in active subduction margins: insights for fault seal analysis for CCS	153
	JADE DUTILLEUL AND CHRISTOPHER WIBBERLEY	
705	Evaluation of faulted topseal integrity for CCS: analogues from sub-surface post-mortem well analyses and shale-rich fault outcrops	157
	MARIA EL HAGE MOUSSA, CHRISTOPHER A. J. WIBBERLEY, JADE DUTILLEUL, JEAN-PAUL CALLOT AND NICOLAS E. BEAUDOIN	
706	Regional characterization of clay formations for multi-barrier CO₂ storage opportunities in North Germany	160
	FRANZ MAY, STEFAN KNOFF, ALEXANDRA RUALES AND GABRIELA VON GOERNE	
707	Workflow to determine the potential of leakage from CO₂ storage reservoirs along fractures and faults triggered by uplift	165
	RAFAEL F. MESQUITA, SAHYUO ACHUO DZE, NICK HARPERS, NATHANIEL FORBES INSKIP, FLORIAN DOSTER AND ANDREAS BUSCH	
708	Targeted CO₂ storage monitoring in a multi-layer stratigraphic system	169
	GEETARTHA DUTTA, RICARDO MARTINEZ, PHILIP RINGROSE AND JO EIDSVIK	

801	The Mont Terri URL: guided tour overview	173
	DAVID JAEGLI, JONAS WINDSICH AND MARTIN ZIEGLER	173

Establishing CO₂ storage in Switzerland

Martin Jiskra^{1*} and Christian Minnig^{2**}

1 Swiss Federal Office for the Environment (FOEN)

2 Swiss Federal Office for Energy (SFOE)

* martin.jiskra@bafu.admin.ch

** christian.minnig@bfe.admin.ch

Abstract

Switzerland must achieve its net-zero target by 2050. First and foremost, this requires a significant reduction in greenhouse gas emissions such as CO₂. Not all greenhouse gas emissions are entirely avoidable. That is why additional technologies are needed to capture or remove CO₂ and store it permanently. There are two types of technology: carbon capture and storage (CCS), which as the name suggests captures and stores fossil and process-based CO₂ at installations, thereby further reducing emissions, and negative emission technologies (NETs), which permanently remove CO₂ from the atmosphere. Both technologies are not yet widely available.

The Federal Council's long-term climate strategy of January 2021 shows that despite all measures to reduce the emissions from fossil energy in 2050 difficult to avoid greenhouse gas emissions will still be around, particularly from industry, waste treatment and agriculture. To deal with these emissions, technologies are needed to capture and store fossil and process-related CO₂ directly at installations (carbon capture and storage, CCS) or permanently remove CO₂ from the atmosphere (negative emission technologies, NETs). The Long-Term Climate Strategy estimates that annual hard-to-abate emissions from industry, waste recycling and agriculture will total around 12 million tonnes of CO₂eq in 2050, around 5 million tonnes of which could be avoided by means of CCS plants. The greenhouse gas emissions remaining after the use of CCS technologies – totaling just under 7 million tonnes of CO₂eq – would have to be offset by negative emissions. According to the Federal Council strategy, the focus here should be on domestic measures. However, since the achievable potential for permanent CO₂ storage in Switzerland may be limited by technical, environmental, economic and social factors, the Federal Council also remains open to measures abroad. To be able to deploy CCS and NET on a larger scale in Switzerland and abroad, appropriate infrastructure for CO₂ transport and permanent storage are needed.

Under the long-term climate strategy, the CO₂ captured in Switzerland should, if possible, be stored in Switzerland, either underground or in long-lasting products such as construction materials. This reflects the fact that exporting CO₂ is likely to remain a challenge, despite some promising international developments – not least because of high European demand facing limited proven storage capacity for CO₂. The guide value for domestic geological CO₂ storage according to the Energy Perspectives 2050+ is 3 million tonnes of CO₂ in 2050. According to initial SFOE estimates, this would require up to 10 geological storage sites, each with a yearly CO₂ capacity of 200'000 to 400'000 tonnes. Those sites would yet have to be successfully explored and developed. Theoretically, by 2050 a further 2.5 million tonnes of CO₂ per year could be stored in all of Switzerland's demolition concrete, via targeted carbonation. However, more recent estimates suggest that the achievable potential is likely to be significantly smaller. Due to uncertain storage capacity in Switzerland, the Energy Perspectives 2050+ expect significant quantities of domestic CO₂ to be exported to foreign storage sites, even in the long term (guide value of 4 million tonnes of CO₂ per year by 2050).

Today, the geological storage potential of Switzerland's subsurface is largely unknown. A number of potential storage complexes have been identified, but no nominal storage site has yet been identified. To mature from the current situation of undiscovered storage resources all the way to commercial storage resources, a number of barriers need to be tackled. These are: a) permanently storing CO₂ in the subsurface suffers from large economic and commercial risks. The lack of a viable business model prevents market participants to accept these risks and engage into the endeavor. b) As

the 26 cantons are the owners of their respective subsurface and in charge of regulating most activities therein, the regulatory regime for CO₂ storage is very heterogenous, generally poorly developed and has never been tested. The ensuing legal uncertainty for any market participant is considerable. c) not having an industrial history in mining or oil and gas production, Switzerland lacks domestic technical upstream competences. Isolated know-how can be found in small consulting companies or at universities, but integrated operational competence and experience in the E&P domain is largely missing. Developing CO₂ storage potential will thus rely heavily on technical competencies from abroad. d) public perception for domestic CO₂ remains uncertain.

Overcoming these systemic barriers will need time. In order for domestic CO₂ storage to move ahead in the meantime, alignment of the activities with the pioneering phase, defined in a report published in Mai 2022 by the Federal Council, is needed. Said report lies out how CCS and NET can gradually contribute to the long-term climate strategy and divides the evolution of the technology in two phases, a pioneering phase until 2030 and a targeted scaling phase from 2030 to 2050.

In said pioneering phase, the Confederation seeks to support the development of CCS and NET through targeted research funding and pilot projects, notably the P&D program of the SFOE and the subsidies program for novel technologies under the climate and innovation act. Furthermore, the SFOE in collaboration with the FOEN and swisstopo, answering a parliamentary motion, is seeking to enable a national prospection campaign to reduce the subsurface uncertainties and facilitate future exploration activity for CO₂ storage sites. For the scaling phase of CCS and NET beyond 2030 a development of the regulatory framework and financing conditions following the polluter-pays principle will be necessary to overcome the barriers laid out above. The Federal council will discuss by the End of 2024 specific proposals for new regulations and clarify the role of the state, cantons and the industry.

Current and planned activities of the Swiss Geological Survey in the context of geological carbon storage

David Jaeggi¹, Herfried Madritsch², Andreas Möri², Christophe Nussbaum¹ and Martin Ziegler¹

¹ Federal Office of Topography, Swiss Geological Survey, Saint-Ursanne, Switzerland

² Federal Office of Topography, Swiss Geological Survey, Wabern, Switzerland

* david.jaeggi@swisstopo.ch

1 Introduction

Given today's climate and energy challenges, the management of Switzerland's georesources is becoming increasingly important, leading to changes in the activities of the National Geological Survey. Currently, we are working on a holistic strategy of subsurface usage including the option of CO₂ storage. This strategy encompasses stakeholder coordination for a sustainable exploitation of the potential of georesources in a national action plan and the planning of a prospection program to acquire new geological data. Moreover, CO₂ storage related research in the Mont Terri underground rock laboratory (MT URL) has already been carried out since 2010. More recently we, together with ETH Zurich, have engaged in the assessment of repurposing an existing exploration well in the northernmost Swiss Midland for a pilot CO₂ injection test.

2 Overall strategy of swisstopo

Various options for CO₂ storage are being examined in the federal government's strategy, such as transport abroad with injection into basalts or existing oil and gas reservoirs and clarification of the domestic injection of CO₂ underground. The storage potential in Switzerland is still little known and initial estimates vary considerably and are subject to major uncertainties (Chevalier et al. 2010 and later). However, it is important that the possibilities of domestic deep geological disposal are properly investigated in situ in order to know more precisely how large the storage capacities are and to be able to better estimate future dependence on foreign storage capacities.

A large-scale, systematic exploration campaign, as called for in a political mandate, would provide a remedy here and clearly improve the level of knowledge about potential storage facilities in Switzerland. This would pave the way for testing storage in Switzerland and then scaling it up. If these exploration efforts are successful, the first commercial storage sites would be ready for operation from around 2040 in the best-case scenario. Until then, however, clarification of the safety of the proposed concept (caprock integrity) in the Swiss underground on the laboratory scale, such as CO₂LPIE (CO₂ Long-term Periodic Injection Experiment) in the Mont Terri rock laboratory, and eventually pilot injection tests in Switzerland's main target area for CO₂ storage (the Swiss Midland) can verify the suitability for safe and permanent storage. These two projects are led by swisstopo and are briefly described in the following two chapters below.

3 Experiments at the rock laboratory scale

The MT URL has been conducting research in the field of CCS since 2010. In an initial research phase, the main focus was on well integrity (e.g., Goodman et al. 2022) (Fig. 1). Are existing oil wells in the caprock also tight in the long term and what processes take place in the well casing, cementation and rock system? In a later phase, the experiments focused on the integrity of geological faults (fault integrity, e.g., Guglielmi et al. 2022). Under which conditions can tectonic faults in clay rocks be reactivated, what about the migration of fluids and CO₂ along such discontinuities, and do these reactivated faults seal again over time? These experiments are still ongoing, but one crucial component is still missing: the integrity of the rock matrix.

The behavior of the actual geological barrier far from faults and existing boreholes with regard to long-term CO₂ injection has not yet been investigated on the rock laboratory scale in the meter range (e.g., Makhnenko et al., 2017; Sciandra et al. 2023 in prep.). In addition, systems optimized for clay rocks and CCS are still lacking for efficient and cost-effective reservoir monitoring. Two years ago, on the initiative of BGR, swisstopo and Eawag/ETH-SED, the CO₂LPIE project began planning a major in-situ experiment to investigate the integrity of the matrix (see abstract #615). In addition to experimental monitoring, safety monitoring is also an important national issue and as a result, swisstopo began developing a modular multi-sensor monitoring system (MMMS) (see abstract #614) and thus also took the lead in the experiment. This system has now been successfully tested in two short boreholes and will be installed in observation boreholes in January/February 2024.

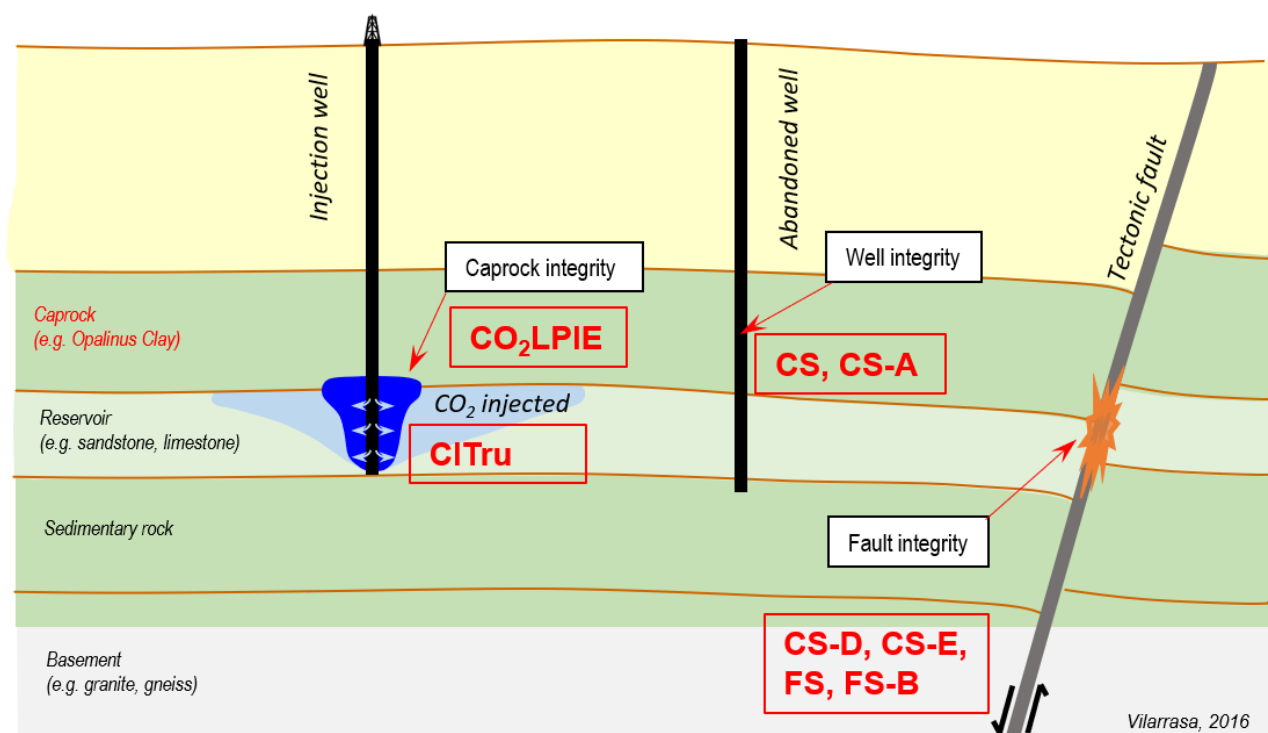


Fig. 1. Sketch of CCS experiment categories at the Mont Terri underground rock laboratory and CO₂ Injection test at Trüllikon (CITru) in the Swiss Midland.

The CO₂LPIE experiment will use an in-situ experimental setup in the MT URL to investigate the behavior of the Opalinus Clay with regard to periodic CO₂ injections. The aim is to explore which processes take place in the rock under the influence of the injected CO₂, how the rock-pore water-CO₂ system behaves in the long term and how safe the Opalinus Clay will be as a caprock and proxy for clay rocks worldwide. In order to achieve these goals, extensive modeling work, laboratory analyses and the development of a completely new multi-sensor system for permanent temporal and spatial monitoring of the processes in the subsurface are being carried out as part of CO₂LPIE.

Safety and safe operation supported by monitoring will be key issues in a future pilot project or effective producing reservoir. In addition to the technical feasibility of CCS in Switzerland, the safety of the environment and the population will play an equally important role and will have a direct influence on future public acceptance. Strategically, CO₂LPIE is particularly relevant for the federal government and Swiss industry. Switzerland must consider the possibility or even necessity of domestic CO₂ storage in order to reduce its dependence on foreign customers in the future. CO₂LPIE, with its clarifications on the safety and monitorability of a caprock and the associated public relations work (acceptance), forms a crucial link to other parallel projects, i.e., a play fairway analysis (PFA) regarding possible CO₂ reservoirs in Switzerland and pilot injection tests in the Swiss Midland. In addition, the industry is to be provided with the necessary technical information and tools to be able to compete with foreign competitors. CO₂LPIE is scientifically relevant because of its importance for the

reservoir complex, where, in addition to wells and faults (already being investigated at Mont Terri), the processes in the confining structure of the clay rock must also be understood and investigated. So far, there are numerous studies available about the rock behavior upon CO₂ injection from laboratory experiments (mm–cm scale) (e.g., Makhnenko et al. 2017) or from large-scale experiments (100–1000 m) (e.g., Ketzin, see Liebscher et al. 2013 or Sleipner and Snøhvit, see Eiken et al. 2011) but comprehensive data from the easily controllable and yet realistic rock laboratory scale on the meter to decameter scale are missing for caprock integrity.

Long-term CO₂ exposure experiments are necessary to (a) improve the understanding of dynamic processes on different time scales, (b) obtain reliable reaction rates for natural clay minerals, (c) determine in situ rock permeabilities for reactive CO₂ flux and changes due to geochemical rock alteration, and (d) calibrate or improve THMC models. Long-term periodic tests allow the discrimination of experimentally induced signals from the external influence, e.g., earth tides, with a better signal-to-noise ratio. These experiments improve the fundamental understanding of the joint inversion of, e.g., pressure and deformation data. The latter is ensured by the quasi-continuous monitoring of a comprehensive set of parameters for which the innovative MMMS was developed. Joint inversion is one of the most promising approaches for monitoring the gas reservoirs and the integrity of the overburden. CO₂LPIE furthermore combines the laboratory scale via model calculations with the rock laboratory scale and thus covers the entire scale spectrum below larger-scale pilot tests.

4 Scoping a CO₂ pilot injection test in an existing exploration borehole within the Swiss Molasse Basin

While the Opalinus Clay seems to represent an excellent caprock for future CO₂ storage in Switzerland, the potential of various hypothetical storage units in the Swiss Alpine foreland is less clear. According to previous assessments, the Schinznach Formation of the Triassic Upper Muschelkalk Group, a significant regional saline aquifer, is considered the most promising option. Its characterization with respect to CO₂ storage is based on rock matrix porosity/permeability analyses of drill cores from a number of deep boreholes and isolated hydrotest data. To this date, no in-situ tests to investigate actual CO₂ injectivity and verify storage capacity estimates have been carried out. In northern Switzerland, a region previously considered to be potentially suitable for CO₂ storage (Chevalier et al. 2010), the Swiss national cooperation for radioactive waste disposal (Nagra) has drilled a series of exploration wells. Swisstopo, together with ETH Zurich, has engaged into an assessment to what extent one of these wells near the village of Trüllikon (ZH) could be repurposed for pilot CO₂ injection test. The technical assessment could be based on an exceptional dataset provided by Nagra, including extensive borehole test data (geological, hydrogeological, and geomechanical) and a structural model based on the interpretation of 3D reflection seismics. The results indicate that the Bänkerjoch Formation immediately overlying the Muschelkalk Group represents a very effective sealing unit. The expected permeabilities of the storage unit are rather low, and so would be the CO₂ injectivities. From numerical modeling, the resulting CO₂ plume around the borehole is expected to be very small as well and its detection would present a major monitoring challenge. Nevertheless, from a technical perspective a CO₂ injection at this location is considered to be feasible. Although for no immediate commercial purpose, a pilot CO₂ Injection test at Trüllikon (CITru) is regarded to be a great CCS catalyst and capacity building point for the scientific and technical community in Switzerland. Ideally, CITru would be embedded into a broader community effort that includes modelling, validation, upscaling, resource exploration, and additional pilot sites.

References

- Chevalier, G, Diamond, LW & Leu, W. 2010. Potential for deep geological sequestration of CO₂ in Switzerland: a first appraisal. *Swiss J Geosci* 103, 427–455.
- Eiken, O, Ringrose, P, Hermanrud, C, Nazarian, B, Torp, TA, Høier, L. 2011. Lessons learned from 14 years of CCS operations: Sleipner, In Salah and Snøhvit, *Energy Procedia*, Volume 4, p. 5541–5548.

- Goodman, H, Rösli, U, Gisiger, J, Jaeggi, D, Minnig, C. 2022. Sealant tests at the Mont Terri CS-A experiment that address seepage of CO₂ behind casing in Carbon Dioxide Capture for Storage in Deep Geological Formations, Volume 5, K. F. Gerdes (Editor), p. 629–668.
- Guglielmi, Y, Ajo-Franklin, J, Birkholzer, J, Cappa, F, Cook, P, Hopp, C, Nussbaum, C, Rinaldi, AP, Robertson, M, Rodriguez-Tribaldos, V, Rutqvist, J, Shadoan, T, Soom, D, Wood, T, Zappone, A. 2022. Imaging leakage associated with caprock fault activation: Results from the fault slip experiment in MT. Terri Opalinus Clay analogue caprock in Carbon Dioxide Capture for Storage in Deep Geological Formations, Volume 5, K. F. Gerdes (Editor), p. 715–732.
- Liebscher, A, Möller, F, Bannach, A, Köhler, S, Wiebach, J, Schmidt-Hattenberger, C, Weiner, M, Pretschner, C, Ebert, K, Zemke, J. 2013. Injection operation and operational pressure–temperature monitoring at the CO₂ storage pilot site Ketzin, Germany—Design, results, recommendations, *International Journal of Greenhouse Gas Control* 15 (2013) 163–173.
- Makhnenko, RY, Vilarrasa, V, Mylnikov, D, Laloui, L. 2017. Hydromechanical aspects of CO₂ breakthrough into clay-rich caprock. *Energy Procedia*, 114, 3282–3290.
- Sciandra D, Rahimzadeh Kivi, I, Vilarrasa, V, Makhnenko, RY, Rebscher, D. 2023 (in preparation). Blind prediction of the hydro-mechanical response of Opalinus Clay to the CO₂ long-term periodic injection experiment (CO₂LPIE) at the Mont Terri rock laboratory, *Geomechanics and Geophysics for Geo-Energy*.

Hard to abate sectors. How do we manage the challenge for the net zero target in climate policy on the way to 2050?

Stefan Vannoni^{1*} and Robin Quartier^{2**}

¹ cemsuisse, Association of the Swiss Cement Industry, Marktgasse 53, 3011 Bern, Switzerland

² VBSA, Association of the Swiss waste treatment industry, Wankdorffeldstrasse 102, 3014 Bern, Switzerland

* stefan.vannoni@cemsuisse.ch

** quartier@vbsa.ch

Abstract

Emission from cement clinker kiln and from waste-to-energy plants are hard to abate. In order to reach net zero by 2050, carbon capture and storage will need to be deployed at a large scale on both these kinds of point sources. According to the ramp-up plan of the Swiss government, carbon capture on hard-to-abate point sources will have to reach 7 million tons of CO₂ per year by 2050. Most of the CO₂ captured will have to be permanently stored.

CO₂ capture units could be ordered today, and their energy consumption modelled. Accordingly, the costs associated with the capture of CO₂ can be calculated with reasonable accuracy. However, for now, the costs associated with transport and permanent storage of CO₂ are only very rough estimates at best. This is because the transcontinental infrastructure needed to transport and permanently store gigatons of CO₂ does not exist yet, not even as a blueprint. Moreover, it is not clear yet how and by whom this much needed new infrastructure will be financed.

At present, the operator of a large point source does not know if and at what cost he will be able to hand over the thousands of tons of CO₂ captured at his facility. Needless to say, with this degree of uncertainty, it is impossible to take the decision to invest tens and hundreds of millions CHF in a CO₂-capture facility.

The Swiss Confederation shall draw up a clear and reliable roadmap for the development of a CO₂-transport infrastructure as soon as possible. This roadmap should specifically define important milestones with possible actors, the contribution of the public authorities and necessary political processes, which have to be followed or newly established (e.g., for Public Private Partnerships). This, in turn, is a necessary basis for defining specific investments and processes on the journey to the net-zero goal of sectors and companies (within the meaning of Art. 5 "Klimagesetz").

In the very short run, we need information on Transport capacities on the Swiss railway network for the transport of CO₂ "freight wagons" towards Germany and Italy in 2030 and 2040. It is important to understand, if it is possible to prioritize freight transport over passenger transport. Also, we need sufficient amount of renewable and affordable energy in Switzerland in 2030, 2040 and 2050 – to reasonable prices.

Capacity for the permanent storage of CO₂ is poised to become a strategic resource. Access to storage capacity will be critical for the future of the Swiss industry. With this in mind, it is clear that the potential for storage in Switzerland needs to be carefully assessed. Finally, the whole idea of the geological storage of CO₂ only makes sense if the storage really is permanent. Society therefore expects science to provide very strong evidence of the permanence and long-term safety of geological storage.

From caprock integrity to system integration: lessons for siting of CO₂ storage locations

Thomas Flüeler^{1,2*}

¹ ETH Zurich, Institute for Environmental Decisions, Zurich, Switzerland

² Commission de suivi, République et Canton du Jura, Mont Terri Underground Rock Laboratory, Delémont, Switzerland

* thomas.flueeler@env.ethz.ch

1 Assessing a complex technology

Although science and society recognise the climate crisis as a serious problem, humankind has pursued a high greenhouse gas, esp. carbon dioxide, CO₂ emissions path to the atmosphere. Barriers to effective reductions exist at political, institutional and individual levels. Incentives, trading and enforcement mechanisms are weak or not in place, and large-scale lifestyle changes towards sustainable development are rare. In such a tangled situation, the characteristics of Carbon capture and storage, CCS seem attractive, negative emission paths even seem indispensable to reach the 1.5 °C goal (IEA 2023¹). It promises a – relatively – quick and technical, narrowly located but high-potential solution with no need for extensive efficiency improvement in dispersed facilities, equipment, appliances or “software” such as institutions and behaviour. The involved dimensions are manifold – there is no “one” method for analysis. Instead, cross-disciplinary investigations allow drawing lessons from contentious long-term environmental issues – necessary before embarking on this route on a large scale. The approach, laid out in Flüeler 2023, is a combination of disciplines and perspectives from systems theory, risk assessment, technology assessment and management. The six criteria below address issues proven to be crucial in technology policy debates.

2 Criterion 1: Need for deployment and comparative benefits

With the climate debate, CO₂ is recognised as a pollutant and waste at the back end of fossil fuel systems. As such it is as inseparable from, i.a., coal utilisation as radioactive waste is from nuclear fission utilisation. There has been a mention of closing the carbon cycle (Powicki 2007), comparable to the nuclear cycle (NEA 2000). Unlike nuclear waste, however, CO₂ is not tied to specific technologies but is also produced in conversion chains other than fossil systems (like deforestation) and can be reduced in such chains (afforestation with CO₂ sequestration) or in processes (building insulation with avoided CO₂ – negative – emissions). Consequently, CCS is in competition with other technologies regarding potential, efficiency and cost, and it must demonstrate its necessity and perform uncontroversially well. If hard-to-abate technologies such as the cement industry or municipal waste incinerators were in the focus, CCS could not be called a Trojan horse². At this stage (research and development, R&D; few pilots, low technology readiness level; unestablished concept) the performance of CCS has yet to be determined.

3 Criterion 2: Total-system analysis and safety concept

Even though the approach sounds thrilling as a technical solution, the CCS concept is not yet mature, and its technical potential cannot be reliably defined at this stage. We currently lack solid calculations of reserves (with relatively high profitability, i.e., economic perspectives, distinguishing between “proven”, “probable” and “possible” reserves. Somewhat contrary to Section 6 below, according to the latest (official) CCUS database by IEA, there was no STORAGE facility operational in 2022. Projected for 2024 is a storage capacity of 55 Mt.³. Furthermore, the CCS system performance cannot be assessed because overall conditions, including its embeddedness in economic, technological and environmental policies, must be set beforehand: with a total-system analysis.

System approach. CCS is not only a potentially powerful but also an ambiguous lever in the transition towards carbon-free economies. For all energetic technological lines of CCS (pre-combustion, post-

combustion and oxyfuel), a comprehensive life cycle analysis along the process chain of extraction of the energy carrier, transport, conversion, CO₂ capture, compression, transportation and storage phases shows a 10-40 % increase in resource use (e.g., coal and mining) if a “low-carbon” use of fossil energy is targeted (IPCC 2005; Wuppertal Institute et al. 2008). This implies a decrease in system efficiency to 65 %, currently 45 %, and an increase in classically toxic impact (NO_x, heavy metals, fine particles; Koornneef et al. 2008). Constraints on transportation distance and means are required (power plants close to storage sites, pipelines or tanker ports). In a long-term management plan, all components must be set in place in a timely manner so that coal provisioning, plant lifetime, storage volume and facility are synchronised. “Technical lessons learned” are not enough (EU CO₂ Network 2004) – it is the maturity and deployment of the overall system, not just its components, that counts. The definition of system boundaries and the choice of energy penalty values are crucial, esp. given the slim publicly available database on safety-relevant issues (Page et al. 2009, valid in 2023⁴).

It is recognised that CCS only has a bridging function (de Coninck 2008). This means that geoengineering tools must not substitute or hamper the development of renewables and efficiency measures because fossil fuels are finite. Critical is the length of the transition period that CCS (or the world energy system for that) should be given until the combination of efficiency measures and renewables takes effect. Arguably, it takes fewer efforts to “add” CCS to the existing energy infrastructure than it does to sustainably change the overall energy system (provision, distribution and consumption).

Overall, the system analysis must consider material and energy fluxes (and related stocks), the link of CCS with other energy (sub)systems, market integration and interplay of actors. CCS is “more than a strategy for ‘clean coal’” (IEA 2009c, 4); it must be adopted by biomass and gas power plants, “mixed” portfolios (coal/biomass/hydrogen) are possible. Thus “negative emission scenarios” providing net CO₂ reductions must be on the table. Carbon abatement cost curves (McKinsey 2015, Goldman Sachs 2019) put it in a nutshell: Conservation (efficiency) measures offer more for low-cost decarbonisation with less uncertainties but their curves steepen sharply; sequestration (esp. direct air carbon capture), however, has great uncertainty but provides an enormous long-term potential.

The system approach reveals how its compartments, functions and dynamics are related, whether this is optimised, to what goal and with what unintended consequences. An example in the nuclear field is the dysfunction (leakage) of Asse, a German low-level waste repository (Ilg et al. 2017). This leakage can be traced back to the fact that the site was not designed for waste disposal but misused as such after it had been exploited for rock salt. This process had major repercussions on the German disposal programme, incidentally built on the Gorleben site with the same host rock as in Asse. Hence abandoned oil and gas fields have to be carefully evaluated as potential CCS deposit sites, particularly as their deployment is attractive to exploiters in the form of profits, higher extraction yields due to CO₂ injection, CO₂ credits and disclaimers in the case of short-term liabilities.

Systemic features. Some argue that CCS is not a novel technological concept as CO₂ has long been injected into oil formations to yield additional oil (Enhanced Oil Recovery, EOR, Benson 2005). Radically different, though, are the goals and scales of CCS and EOR. The new intention with CCS is to seclude CO₂ for the common good (a sustainable climate), at an ample scale and for a very long time. This requires the implementation of a globally effective system, testing long-term safety performance of facilities and the overall system (with adequate control mechanisms) and, above all, the recognition of longevity as a decisive factor. Much of emitted CO₂ remains in the atmosphere for 100 years. The biosphere’s carbon cycle takes a long time to neutralise manmade CO₂. Its lifetime is up to 35,000 years (Archer 2005) if averaged out over its entire distribution, whereby “lifetime” refers to the time required to restore equilibrium after an increase in its concentration in the atmosphere.

Safety assessment. Safety analyses, called “performance assessments” in the context of nuclear waste, include scenario development, conceptual and mathematical models development, consequence analysis, uncertainty and sensitivity analysis and confidence building (IAEA Standards). Key questions like the isolation period needed or the robustness of the barrier concept must be answered.

Site selection and characterisation procedure. By definition, disposal facilities also concentrate hazards, which means that the selection of suitable sites is decisive. In the case of radioactive waste, efforts have been made in a range of national programmes to establish a safety first, systematic, transparent and participatory site selection (Switzerland, Germany, Canada or CoRWM for the UK).

4 Criterion 3: Dedicated internationally harmonised regulation and control

Because CCS is seen as part of the mitigation portfolio addressing climate crisis, straightforward international regulation is pivotal. In fact, it is a prerequisite for its effective deployment (Mace et al. 2007). Basic research (e.g., on modelling, system definitions, side effects and cost-benefit analyses of the wide basket of ideas in geoeengineering) requires massive but standardised resources. Applicants of non-commercial activities (such as demonstration projects) need funds, while affected stakeholders and NGOs need confidence in effective regulators. Monitoring and verification rely on international standards, transboundary transfer and trading require the existence of international inventories and transnational treaties and liability issues need regulation. The 2009 IEA Roadmap proposed comprehensive frameworks by 2020 (IEA 2009c, 36f.), while recommendations exist in rather generic forms (IRGC 2007, 2008, WRI 2008; EU 2009/18). At any rate, under the umbrella of ISO/TC 265, since 2011 the International Organization for Standardization, ISO has published 13 standards on different CCS aspects with 7 more under development⁵. Such steps revert to the criteria above; in order to, e.g., integrate CCS into the Clean Development Mechanism, CDM technical and organisational aspects must be fully covered, in the form of good site characterisations, thorough site-specific risk assessments and monitoring during and after operation (Dixon 2009), including accounting (Haefeli et al. 2005). Decisions are critical where host country regulatory capacities are insufficient. Pollak & Wilson (2008, 84) suggested giving “preference to sites that present lower seepage risk, such as offshore sites or sites that have well-characterized geology”. They concluded that “if a geological storage site approved by the CDM were to cause environmental, health or safety problems for the host country, it would damage not just the reputation of the CDM but also the reputation of CCS as a greenhouse gas mitigation technology” (ib., 85).

Regarding claims to national sovereignty over the sea, the recently inaugurated “Greensand” project under the North Sea is hailed to be on “the Danish subsoil” by Denmark’s climate minister⁶. Multinational radwaste repositories exhibit the complexity of the issue (IAEA 2004).

5 Criterion 4: Economic aspects (costs and incentives)

Costs depend on technology and a range of externally set assumptions including size, inception, promotion strategies in early phases and coverage of carbon penalty. Differences in abatement technology lines range from -100 EUR/t CO₂ avoided (for high-tech lighting) to +60 EUR/t CO₂ avoided by retrofitted gas power plants with CCS (McKinsey 2009, Goldman Sachs 2019). The abatement potential for CCS is substantial, albeit at a high cost. One asset of CCS is that it applies to hard-to-abate cement, iron/steel and chemical industries, or in biomass production with negative emissions (CO₂ yielded twice: when taken out of the atmosphere by plants and buried later on).

The bulk of costs (75 %) goes to capture technology, the rest to transportation, injection and monitoring (Plasynski et al. 2009). Currently (2021), the IEA states 40-120 USD/t for processes with “dilute” gas streams from iron/steel to cement production and power generation⁷. As to storage costs alone, the range is 2-20 EUR/t, in a “mature CCS industry”⁸. McKinsey (2009) assumed 4–12 EUR/t for early commercial plants. Against the nuclear experience and recent projections (100-190 USD/t for cement CCS; Goldman Sachs 2019), this low share may be questioned as research expenditure rose with greater knowledge and insight into the complex proof of long-term safety. Monitoring costs depend on the timeframe and specific regulatory quality requirements. CCS technology not being mature, R&D expenses accrue as economies of scale are not realised, and the lack of experience may explain lower-quality cost estimates. Furthermore, social costs accumulate, i.a., licensing pro-

cedures, decision uncertainties, delays or damages after abandonment⁹. We have discussed specific costs per kWh or t CO₂. It is, however, necessary to look at costs for a national or regional economy, e.g., a full-fledged operational CCS system as a fraction of the gross domestic product.

6 Criterion 5: Implementation

Since the 1990s CO₂ has been captured in the Sleipner field of now Equinor, a natural gas reserve in the North Sea. CO₂ would have been blown off had the Norwegian government not introduced a CO₂ tax of 25 EUR/t in 1991. There has been a great upturn of projects, experiments and industrial activities. Despite this, large-scale CCS deployment requires a satisfactory regulatory regime (Mace et al. 2007)¹⁰ and projects by major players such as Equinor, Shell or BP were shelved due to insecure financing, lacking public subsidies and inadequate tax incentives and carbon trading. Recent assessments confirm this view (IEA 2021). To date, there are 16 dedicated storage projects worldwide with a capacity of 10-30 Mt/yr¹¹, 39 are operational¹². From a broader perspective, carbon “lock-in” is common in energy systems: “fossil fuel-intensive systems perpetuate, delay or prevent the transition to low-carbon alternatives” (Sato et al. 2021). Power infrastructure is often tied to a high-emission path, systemically determined (centralised, cost-intensive) and aligned with vested interests. Coal may be a major domestic energy source and considered key to a country’s energy security.

7 Criterion 6: Societal issues

CCS system decisions involve many societal issues. After all, CCS long-term management reflects a fundamental distributional risk-benefit asymmetry, just as with nuclear waste, esp. local risks vs. general benefit and current generations’ benefits and power of decision vs. that of future generations. The decisive point is probably the long-term dimension. A common denominator of “acceptance” studies is the poor state of knowledge and the plea for “outreach” (Plasynski et al. 2009), following the “deficit model” where specialists just inform laypeople to close the “information gap” between them. Experience in the nuclear field shows: It is not enough. The decision-making process from a generic CCS approval to site selection, risk assessment, monitoring and closure must be transparent, open, fair and accountable, with well-defined decision criteria. Yet, recent “best practice” guides subsume demographic trends and land use under “social context analysis” (NETL 2017). Research finds that public participation is still instrumentally motivated by project proponents (Reins 2017). Given that the sequestration risks are minimised (esp. earthquakes or contamination of drinking water aquifers), public acceptance of CCS may be higher than of nuclear waste as the safety periods greatly differ: under 10,000 years for CO₂, around 1 million years high-level nuclear waste.

8 Some conclusions

CCS highlights the tension between the advantage of a “quick fix” and the disadvantages posed by the long-term leakage risk and, from a technology policy perspective, the danger of perpetuating carbon lock-in. Since innovation not only consists of technological progress but is also an integration of technical, conceptual, organisational and societal processes, a narrow perspective is prone to fail. Respect the following: • Expand the notion of time (period of isolation, safety assessment, geological processes, implementation of the CCS system); • Integrate scales (spatial, temporal, institutional) into overall energy system(s), markets and regulation; • Consider CO₂ disposal as a goal in itself, not a “by-product” of other economic activities; • Optimise CCS to environmental performance (effectiveness, efficiency and timing, e.g., new “capture-ready” coal plants commissioned provided that old ones are shut down); • Settle major issues (above) before large actors (states and companies) deploy CCS as *fait accompli* (technically and generating accountable CO₂ certificates); • Take action before political pressures and/or environmental failures (such as spillouts) make it compulsory.

References

Flüeler, T. 2023. Governance of radioactive waste, special waste and carbon storage. Literacy in dealing with long-term controversial sociotechnical issues. Springer Nature Switzerland, Cham. 145 pp. All references may be found with open access in Chapter 2: https://link.springer.com/chapter/10.1007/978-3-031-03902-7_2

Footnotes (weblinks of 2023-12-26):

¹www.iea.org/reports/net-zero-roadmap-a-global-pathway-to-keep-the-15-0c-goal-in-reach, 9.2023

²de Coninck 2008, <https://doi.org/10.1016/j.enpol.2007.11.013>

³www.iea.org/data-and-statistics/data-tools/ccus-projects-explorer

⁴<https://co2re.co/>, www.iea.org/data-and-statistics/data-tools/ccus-projects-explorer

⁵www.iso.org/committee/648607.html

⁶www.carboncapturejournal.com/news/first-carbon-storage-at-project-greensand/5441.aspx?Category=all, 3.2023

⁷www.iea.org/commentaries/is-carbon-capture-too-expensive

⁸<https://zeroemissionsplatform.eu/co2-storage-cost/>, 2.2020

⁹www.rff.org/publications/journal-articles/comprehensive-evidence-implies-a-higher-social-cost-of-co2/, 9.2022

¹⁰EU Directive, rather vague: <https://eur-lex.europa.eu/legal-content/EN/TXT/?uri=CELEX:32009L0031>

¹¹www.iea.org/data-and-statistics/data-product/ccus-projects-database, 3.2023

¹²www.statista.com/statistics/726624/large-scale-carbon-capture-and-storage-projects-worldwide-by-status

How CCS can benefit from CO₂-Plume Geothermal (CPG)

Martin O. Saar^{1*}, Tsubasa Onishi¹, Kevin P. Hau¹, Jasper de Reus¹ and Mahmoud Hefny¹

¹ Geothermal Energy and Geofluids (GEG) group, Department of Earth Sciences, ETH Zurich, Zurich, Switzerland

* saarm@ethz.ch

1 Introduction

CO₂-Plume Geothermal (CPG) systems (Fig. 1) use naturally permeable reservoirs at 2-5 km depth, targeted for CO₂ Capture and (geologic) Sequestration (CCS) to reduce climate change and to expand the resource base of renewable geothermal energy (Randolph and Saar, 2011a). These reservoirs typically include depleted oil/gas reservoirs and deep saline formations. CPG recognizes CO₂ as a resource rather than a waste product to be discarded. Consequently, CCS is expanded to include utilization of CO₂, resulting in CO₂ Capture, Utilization and Sequestration (CCUS). The usage of subsurface CO₂ to extract geothermal energy doubles to triples the geothermal energy extraction rate, compared to using groundwater or brine under our base-case conditions, while ultimately geologically sequestering 100 % of the CO₂ (Adams et al., 2015, 2021).

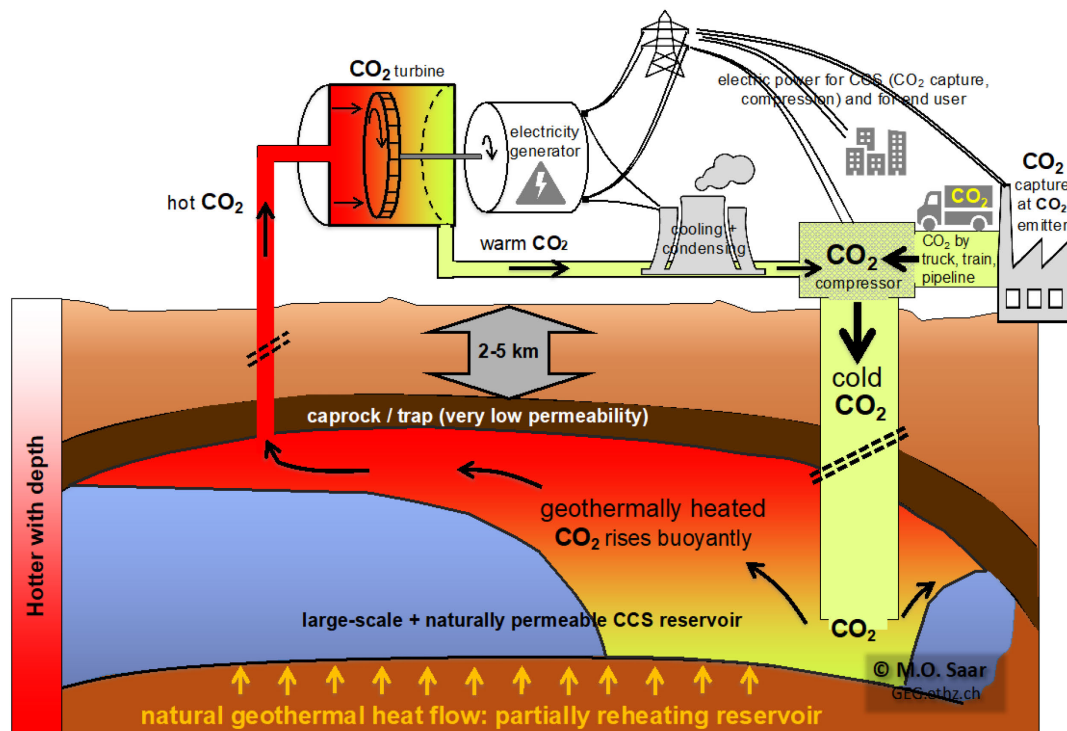


Fig. 1. Conceptual image of a CO₂-Plume Geothermal (CPG) system. CO₂ from a CO₂ point source is transported and injected into a suitable reservoir formation underneath a caprock. As the CO₂ spreads and buoyantly rises in the reservoir, collecting underneath the caprock, due to its lower density than that of water or hydrocarbons, it is heated by the geothermal energy. Once the CO₂ reaches a production well, it is produced back to the land surface, expanded directly in a CO₂ turbine, and finally cooled and condensed for reinjection (Randolph and Saar, 2011; Adams et al., 2015, 2021; Garapati et al., 2015; Ezekiel et al., 2021, 2022). (Figure by M.O. Saar, modified from Brehme et al., *Nature Communications Engineering* – under revision, 2023).

While CPG requires CCS to be added to, CPG provides multiple benefits to CCS, resulting in a symbiosis. In fact, it was the capability of CPG to support CCS that the inventors of CPG (Saar, Randolph, and Kuehn) originally had in mind with CPG, even though at the time (2009), not all benefits listed here had been envisioned yet. The benefits of adding CPG to CCS, resulting in CCUS, envisioned from the very beginning are:

- 1) CPG providing heat and electricity to the CCS operations, from the CO₂ capture to the injection processes, and
- 2) CPG revenue from (thermal/electric) power sales essentially subsidizing CCS operations (Randolph and Saar, 2011b).

Both heat/electric power supply and revenue would help reduce the extra costs of adding CCS to other operations, from power generation at fossil-fuelled or bioenergy power plants to non-power-plant applications that also result in point-source and hard-to-abate CO₂ emissions, such as cement manufacturing or biofuel refining. More recently, we have identified additional potential benefits of adding CPG to CCS, namely:

- 3) Reducing reservoir pressure to enable safer and/or more storage of CO₂.
- 4) Providing continuous CO₂ injection even if only intermittent injection of new CO₂ takes place.
- 5) Potentially helping with public acceptance of CCS as not just a waste is stored but also geothermal energy is produced.
- 6) Synergies with CCS monitoring: Instead of installing pure observation wells, information is gathered using (future) CPG production wells (i.e., observation wells that pay for themselves).
- 7) Increased storage efficiency due to sweep improvement. As with waterflooding, production and injection can be balanced to improve the overall sweep.
- 8) Directional control of the plume, particularly relevant in the US, where the CO₂ plume needs to remain within the permit area.
- 9) Redundancy: (heat depleted) producers can be converted to injectors.

In this contribution, we consider several of the above benefits to CCS of adding CPG to CCS.

2 CPG providing heat/electricity and/or revenue to CCS

Inherently, CCS operations require a significant amount of energy, resulting in a huge cost penalty to any CO₂ emitter. Thus, while the costs of CCS are higher than the financial penalties put on CO₂ emitters through regulatory frameworks, such as cap and trade systems, it is cheaper to pay the financial penalty. By reducing CCS costs via CPG-add-on, the threshold, where it is cheaper to add CCS to operations than paying the (cap and trade) penalty is reached earlier. The first two points in the introduction aim exactly at this cost reduction:

- 1) CPG providing heat and electricity to the CCS operations, from the CO₂ capture to the injection processes, and
- 2) CPG revenue from (thermal/electric) power sales essentially subsidizing CCS operations.

Important to note is here that CPG provides about two to three times the thermal, and thus electric, power than groundwater-based geothermal systems under our base-case conditions (2.5 km deep reservoir at 100°C, 50 mD permeability, 300m thickness) as shown in Randolph and Saar (GRL, 2011), Adams et al. (2015, 2021), and Fig. 2. This thermal and/or electric power can be directly used to power CCS operations and/or for sales.

Fig. 2 shows in the left and middle panels the electricity output per 1 km² reservoir footprint with an inverted 5-spot well pattern for two different geothermal energy extraction fluids, CO₂ (used in CPG) and water, respectively. The right panel shows the ratio of electrical power output from CPG to that of water-based geothermal systems. The results show that, for constant parameters, such as geothermal gradient and wellbore radius, utilizing CO₂ as the subsurface energy extraction fluid provides electricity at higher rates (W_e), compared to using groundwater. CO₂ yields comparatively more power than groundwater, particularly in shallower reservoirs (between 2 and 5 km) and at lower reservoir transmissivities, i.e., the product of reservoir permeability and thickness (see also Randolph and Saar, 2011a; Adams et al., 2015). This advantage is attributed to the lower kinematic viscosity of CO₂, enabling higher geothermal circulation rates, thereby enhancing advective heat transfer through the reservoir and from the reservoir to the land surface, where the thermal power is either

directly used or, as shown here, converted to electricity. For conversion to electricity the CO₂ in the CPG system is directly expanded in the turbine, whereas the heat energy in the groundwater-based geothermal system is first transferred to a secondary loop via a heat exchanger, where the secondary loop typically runs an Organic Rankine Cycle, as is also done here. Due to space limitations, the details cannot be shown here, but can be reviewed in many geothermal energy and CPG publications, such as Randolph and Saar (2011a), Adams et al. (2015, 2021), Garapati et al. (2015), and Ezekiel et al. (2021).

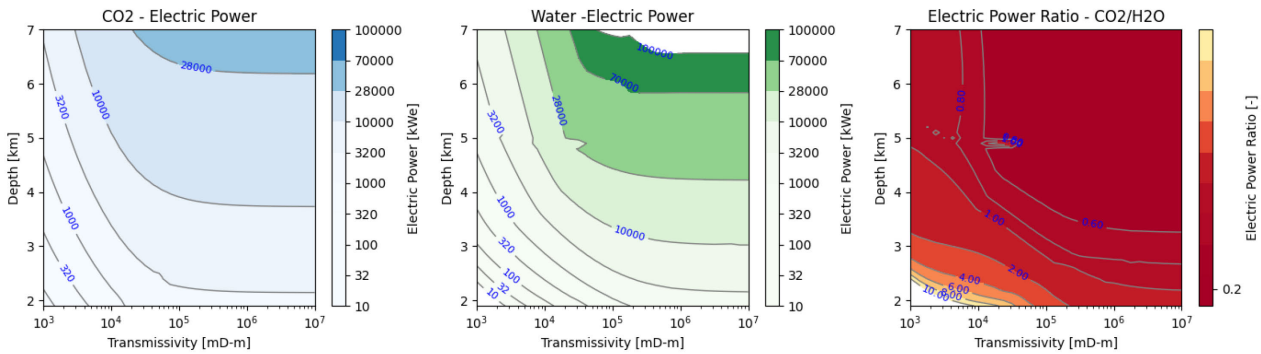


Fig. 2. Potential for CO₂ Plume Geothermal systems to outperform traditional water-based geothermal systems in terms of electric power generation under certain geological conditions. The assumed temperature gradient is 35°C/km, the well diameter 41 cm, the mean annual surface heat rejection temperature 15°C, and the approach temperature 7°C. For CPG systems, the CO₂ is directly expanded in a turbine. For groundwater-based systems, the heat energy is transferred to an organic rankine cycle, where an organic fluid is expanded in a turbine.

3 CPG energy extraction reduces the CO₂ pressure in the reservoir

CCS can benefit from CPG being added to it in other ways. One additional benefit of adding CPG to CCS is that the extraction of heat energy results in a significant reduction in the CO₂ pressure in the reservoir (Fig. 3) due to the significant thermal expansion coefficient of supercritical CO₂, improving the likelihood that the caprock integrity is maintained during CO₂ injection into the reservoir.

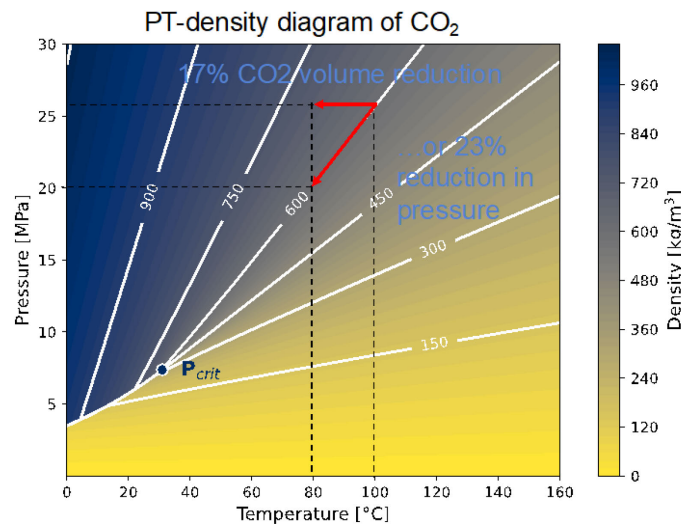


Fig. 3. Diagram showing the impact of reservoir energy (heat) extraction on the density of supercritical CO₂. Thus, the removal of heat enhances the CO₂ storage potential by decreasing the volume of CO₂ and/or reducing the reservoir pressure. The example indicated by the red arrows show that a 20 °C temperature reduction at isobaric conditions results in a 17 % reduction in CO₂ volume or a 23 % reduction in CO₂ pressure, assuming a constant CO₂ volume. The thermophysical CO₂ properties are computed using the Coolprop library (Bell et al., 2014).

4 CPG facilitates intermittent CO₂ injection

As CPG produces and reinjects CO₂, it provides continuous CO₂ injection for sites, where new CO₂, coming from the CO₂ capture facility, is injected only intermittently. One example is the Aquistore CCS site in Canada, which acts as a buffer storage site, where CO₂ from the Boundary Dam coal-fired power plant is injected at Aquistore only when it is not being sold to the Weyburn Enhanced Oil Recovery (EOR) site. When no (or too little) CO₂ is injected at a location, brine backflow into the (near) wellbore region can occur, which in turn can yield mineral precipitation/scaling, with potentially detrimental consequences to the well injectivity index. Thus, by regulating CO₂ production and reinjection during CPG operations, to increase during times of reduced or paused injection of new CO₂ coming from the capture facility, a rather constant bottom-hole injection pressure can be maintained. This in turn reduces the likelihood of brine backflow, mineral precipitation, and reductions in the well injectivity index.

5 Further ways in which CPG may support CCS

CPG is expected to support CCS in several other ways, briefly listed in the introduction. This includes the potential to improve public acceptance of CCS operations when CO₂ is not just a waste that needs to be permanently sequestered but also a working fluid that can be used to extract geothermal energy at significantly higher rates than when groundwater is used, all else being equal, while still ultimately sequestering all CO₂. One can also envision that instead of drilling observations wells, which can be expensive, particularly when well casings have to be installed at shallower depths to protect freshwater resources, full-diameter CPG production wells are rather installed. These wells could be used first for (pressure, CO₂ arrival, etc.) monitoring and later for CO₂ production and much later for CO₂ injection. Such full-scale wells could also be used early on for brine production, supporting CO₂ plume management, for example to provide directional control on the CO₂ plume emplacement and to ensure the CO₂ remains within the boundaries of the permit region. Furthermore, such first brine and later CO₂ production wells would enable balancing the injection and production rates, which should improve the sweep, thereby increasing the CO₂ storage efficiency.

Finally, the redundancy that the additional CPG (production) wells provide is potentially highly beneficial to CCS operations as (heat depleted) CO₂ producers can be converted to CO₂ injectors (planned or unplanned). For example, if, at the start of CCS operations (for example due to different than expected geology), the CCS system is CO₂-injection-limited, so that it could be more expensive to idle the CO₂ capture plant than to go below capacity of the CPG plant. In this scenario it could make more sense to convert CO₂ producers to injectors, while drilling additional wells (reducing planned injection overcapacity needed, i.e., redundant injectors in case of CCS). For heat depleted wells, this occurs at the end of operation, when reservoir pressures are high, resulting in lower pressure differentials being available to operate the CO₂ injectors below fracture pressure. Therefore, by converting CO₂ producers to injectors would spread the injection over more wells.

6 Disadvantages of adding CPG to CCS

There are also some disadvantages to adding CPG to CCS, such as puncturing the caprock with additional wells, needing to make sure that no water is injected along with the reinjected CO₂, and issues concerning permitting, as in many cases CCS permits and, in some cases, (full) CO₂ storage credits (e.g., 45Q in the US) are only given when it is assured that the CO₂ is not back-produced. However, these issues appear to not be insurmountable and, in our opinion, seem to be considerably outweighed by the benefits that CPG operations can provide to CCS operations. And concerning the most significant concern, namely puncturing the caprock with additional wells, these extra wells are not necessarily truly in addition, as briefly discussed in Section 5, as monitoring wells and additional injection wells would likely have to be installed in any case and as extra wells may be needed for active plume management. Also, by reducing the CO₂ pressure in the reservoir (Section 3), CPG contributes significantly to caprock integrity, in our opinion far outweighing the concerns associated with adding further wells that may be needed anyway eventually.

7 Conclusion

While it may at first seem counterintuitive to produce back to the land surface the CO₂ that has been painstakingly, and at high costs, captured and injected deep underground for CCS, this approach can provide several benefits to CCS, compared to only CO₂ injection. In this contribution, we have outlined several such ways in which CCS can benefit from CO₂-Plume Geothermal (CPG) based CO₂ and energy production. Briefly, these benefits include: 1) heat/electricity supply to CCS operations, 2) revenue to subsidize CCS, 3) reducing CO₂ pressure in the reservoir enabling more and/or safer CO₂ injection, 4) providing continuous CO₂ injection to facilitate only intermittent injection of newly captured CO₂, 5) improving public acceptance when also using the subsurface CO₂ as a high-efficiency geothermal energy extraction working fluid and not just treating it as a waste fluid, 6) providing additional full-scale wells that can be used as monitoring wells, as brine production wells (for CO₂ plume management), as CO₂ production wells (once sufficient pore-space CO₂ saturation is reached around the production well inlet (Buckley and Leverett, 1942; Hau, 2020; Ezekiel et al., 2022), and as CO₂ injection wells, providing better pressure control, directional control on CO₂ migration and redundancy, while improving sweep efficiency and related CO₂ storage efficiency. The disadvantages of adding CPG to CCS mentioned in Section 6, such as puncturing the caprock with additional wells, needing to make sure that no water is injected along with the reinjected CO₂, and issues concerning permitting, appear to be surmountable. Finally, in our opinion, the potential benefits of adding CPG to CCS, briefly discussed above, seem to considerably outweigh the above-mentioned disadvantages of doing so.

References

- Adams, B. M., T. H. Kuehn, J. M. Bielicki, J. B. Randolph, and M. O. Saar (2015). "A comparison of electric power output of CO₂ Plume Geothermal (CPG) and brine geothermal systems for varying reservoir conditions". In: *Applied Energy* 140, pp. 365–377. <https://doi.org/10.1016/j.apenergy.2014.11.043>
- Adams, B. M., D. Vogler, T. H. Kuehn, J. M. Bielicki, N. Garapati, and M. O. Saar (2021). "Heat depletion in sedimentary basins and its effect on the design and electric power output of CO₂ Plume Geothermal (CPG) systems". In: *Renewable Energy* 172, pp. 1393–1403. <https://doi.org/10.1016/j.renene.2020.11.145>
- Bell, I. H., Wronski, J., Quoilin, S., and Lemort, V. (2014). "Pure and Pseudo-pure Fluid Thermophysical Property Evaluation and the Open-Source Thermophysical Property Library CoolProp". In: *Industrial & Engineering Chemistry Research* 53(6), pp. 2498–2508. <https://doi.org/10.1021/ie4033999>
- Buckley, S.E. and M.C. Leverett (1942). "Mechanism of fluid displacements in sands". In: *Transactions of the AIME*. 146 (146): 107–116. <https://doi.org/10.2118/942107-G>
- Ezekiel, J., D. Kumbhat, A. Ebigbo, B.M. Adams, and M.O. Saar (2021). "Sensitivity of Reservoir and Operational Parameters on the Energy Extraction Performance of Combined CO₂-EGR-CPG Systems". In: *Energies*, 14:6122. <https://doi.org/10.3390/en14196122>
- Ezekiel, J., B.M. Adams, M.O. Saar, and A. Ebigbo (2022). "Numerical analysis and optimization of the performance of CO₂-Plume Geothermal (CPG) production wells and implications for electric power generation". In: *Geothermics*, 98/102270, 2022. <https://doi.org/10.1016/j.geothermics.2021.102270>
- Garapati, N., J.B. Randolph, and M.O. Saar (2015). "Brine displacement by CO₂, energy extraction rates, and lifespan of a CO₂-limited CO₂ Plume Geothermal (CPG) system with a horizontal production well". In: *Geothermics*, 55:182–194. <https://doi.org/10.1016/j.geothermics.2015.02.005>
- Hau, K.P., A. Rangriz Shokri, E. Nickel, R.J. Chalaturnyk, and M.O. Saar (2020). "On the Suitability of the Aquistore CCS-site for a CO₂-Circulation Test". In: *Proceedings of the World Geothermal Congress 2020+1*.
- Randolph, J. B. and M. O. Saar (2011a). "Combining geothermal energy capture with geologic carbon dioxide sequestration". In: *Geophysical Research Letters* 38.10, n/a–n/a. <https://doi.org/10.1029/2011gl047265>
- Randolph, J. B. and M. O. Saar (2011b). "Coupling carbon dioxide sequestration with geothermal energy capture in naturally permeable, porous geologic formations: Implications for CO₂ sequestration". In: *Energy Procedia* 4, pp. 2206–2213. <https://doi.org/10.1016/j.egypro.2011.02.108>

Experiments of fault zone activation in caprock analogs: implications for CO₂ sequestration

Yves Guglielmi^{1*} and Jens Birkholzer¹

¹ Energy Geosciences Division, Lawrence Berkeley National Laboratory, Berkeley, California

* yguglielmi@lbl.gov

Abstract

Since 2015, the observations on tens-of-meter scale experiments of fault activation by fluid injection conducted in the Mont Terri shales allow exploring how aseismic and seismic events may jeopardize the integrity of a sealing caprock overlying a CO₂ sequestration reservoir. These experiments demonstrated that a significant $\sim 10^5$ maximum fault permeability increase can occur along an initially $\sim 10^{-15}$ m² permeability shale fault zone with a >50 % clay content. When fluid injection ends, a $\sim 10^2$ m² permeability decrease related to fluid pressure drops and fault creep occurs within a few months following the experiment while return to initial permeability could take several decades. Fault hydromechanical behavior strongly depends on confining and deviatoric stresses, and on the evolution from the dilatant strain softening of the bulk fault zone towards localized slip on the principal shear surface. This is caused by multiple fracture opening favored by the softness of the shale, and by the structure of the fault zone that prevents fluids from diffusing into the adjacent damage zone. Experiments show a large amount of slow aseismic failure while infrequent small-magnitude seismicity ($M_w < -2.5$) is observed outside the pressurized leakage patch. In terms of fault activation in caprocks, these experiments highlight the continuity between aseismic fault slip leading to increased permeability and induced seismicity. Moreover, they show that the volumetric deformation of a fault zone should be better monitored and considered in models describing the loss of seal integrity.

1 Introduction

For carbon capture and geological storage (CCS) to become a viable emissions reduction and climate mitigation strategy, the world will need to sequester carbon dioxide (CO₂) in the deep subsurface at an unprecedented scale. Such an amount of industrial CO₂ storage may cause basin-scale fluid pressurization of up to several tens of bars, which raises questions about storage integrity and induced seismicity (Birkholzer and Zhou, 2009; Birkholzer et al., 2015). Many questions remain about fault reactivation and CO₂ leakage through faulted caprocks — such as how such pathways can be created in initially low permeable fault zones, whether they may fully extend across the caprock, how long will they remain permeable, and what are the expected leakage rates—in particular when considering major industrial-scale projects with long-term large-scale pressure buildup. Theoretical papers based on fully coupled hydromechanical numerical modeling tend to show that even if a fault in a shale formation undergoes seismic slip, leakage through a caprock is unlikely to occur at a significant level because of (1) the high ductility of such typically clay-rich faults (Vilarrasa and Makhnenko, 2017) and (2) the heterogeneous nature of faults intersecting multilayered shale/sandstone sequences (Rutqvist et al., 2016). However, as demonstrated at the laboratory scale, gas injection into shale samples can create discrete dilatant pathways associated with a localized pressurization of a fault-type discontinuity (Cuss and Harrington, 2016). It was furthermore shown that such discrete leakage and slip is possible without any observable fault reactivation, whatever the orientation of the fault towards stress (Cuss et al., 2015). And at the field scale, the observation of natural seeps proves that faults can allow for complex upward migration of CO₂ (Nicol et al., 2017). Laboratory scale tests performed at the centimeter scale hardly represent the complexity of an often several meter thick and compartmentalized fault zone, and obviously cannot reproduce large magnitude induced earthquakes. Industrial sites provide “empirical” insights but under operational constraints that intrinsically limit the control of the experimental conditions despite the pioneering work by Ra-

leigh et al. (1976). In contrast, in situ experiments at the tens-of-meter scale allow controlled activation of pre-existing faults by fluid injection, provide access to the complex architecture of the entire fault, and with high-resolution monitoring in place offer an opportunity for tracking fault slip and induced seismicity close to the nucleation zone.

2 Field scale experiments

Amann et al. (2018) conducted fault reactivation experiments in deep crystalline rocks at the Grimsel site (Switzerland) in order to study the seismic-hydromechanical behavior of faults during deep geothermal reservoir stimulations. Few such experiments have recently been conducted in reservoir and in caprock analogs to study the relationship between fault leakage and induced seismicity (Guglielmi et al., 2015a; Michael et al., 2019; Zappone et al., 2021). The key idea is to pressurize a sealed section of a borehole intersecting a fault zone by injecting a fluid (i.e., pure water or a CO₂-in-brine solution) in order to trigger millimeter-scale slip by lowering the effective normal stress acting on the fault. As an example, the experimental design of the meso-scale experiments at Mont Terri as described in Guglielmi et al. (2015) is a setup with an injection borehole crossing the entire fault zone and a number of monitoring boreholes nearby (Fig. 1). The section of the injection borehole that intersects the fault is isolated by two inflatable packers and contains a high-resolution probe (the SIMFIP probe) that allows the continuous monitoring of three-dimensional displacements of the fault synchronously with injection pressure and flowrate (Guglielmi et al., 2014). The monitoring boreholes may be instrumented with a similar SIMFIP probe and with different types of seismic sensors. A typical activation experiment consists of increasing the pressure step-by-step in the injection zone until fault slip is triggered. When fault is at slip, pressure is maintained for several minutes to study the relationships between slip, opening, permeability variations and induced micro-seismicity. All instruments are synchronized and permanently monitor during the entire experiment.

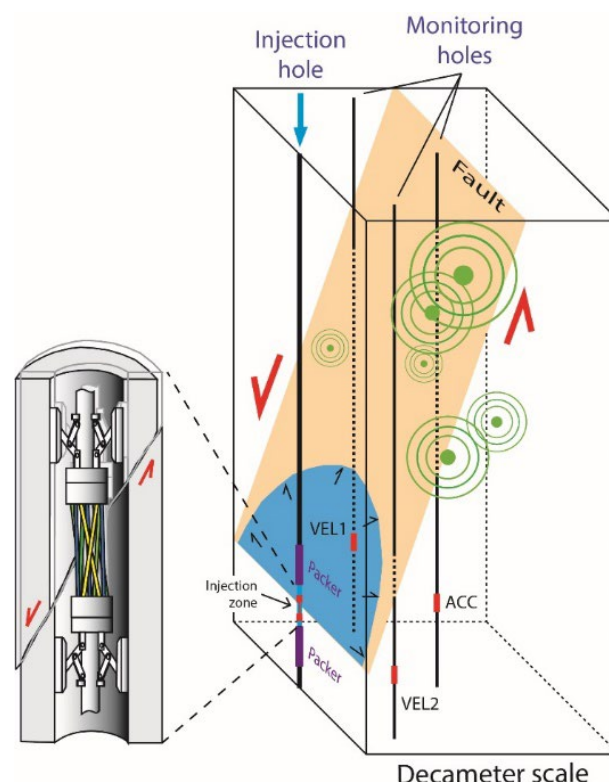


Fig. 1. Fault activation experiment concept caused by fluid injection. Block diagram on the right shows the typical fault activation setting (modified from Guglielmi et al., 2015). Green circles schematically represent seismic events. Blue half circle figures the pressurized fault patch. The three-dimensional SIMFIP fault displacement sensor is shown on the left (not to scale). This sensor is a deforming cage that records fault movements while being clamped on each of the fault compartments. VEL1, VEL2 and ACC are seismic sensors.

3 Lessons learned

Three important takeaways from controlled fault activation experiments are (1) that significant leakage rates were produced by the local activation of initially stable and seismically inactive faults, (2) that leakage in shale faults was associated to a large fault volume dilation preceded by slip on a principal shear surface, and (3) that the experiments generated a large amount of aseismic slow slip and a few seismic events. Models that only allow fluid flow when fault is rupturing and that consider the evolution of the volumetric fault zone plasticity may better estimate the loss of integrity of a cap rock.

The test geometry of the meso-scale experiments is of course quite different from CO₂ storage projects where injection occurs into a deep yet sufficiently permeable reservoir rock, pressure increases gradually at the injection point, and a pressurized zone grows within the reservoir as a function of time. Ultimately, this pressurized zone may encounter a fault that intersects both the reservoir and the overlying caprock. In the reservoir, faults may act as mixed conduit-barrier system, which can block further migration in the reservoir and rather drive the pressure increase up and down along the fault damage zone, accompanied with dilatant slip and aseismic rupture along the fault. One first key parameter is thus the difference between the along and across fault zone permeability, and how much lower the across fault permeability is from the intact injection reservoir permeability. The second key parameter the nature of the volumetric dilatant strain softening of the fault, potentially leading to contrasted leakage and induced seismicity scenarios.

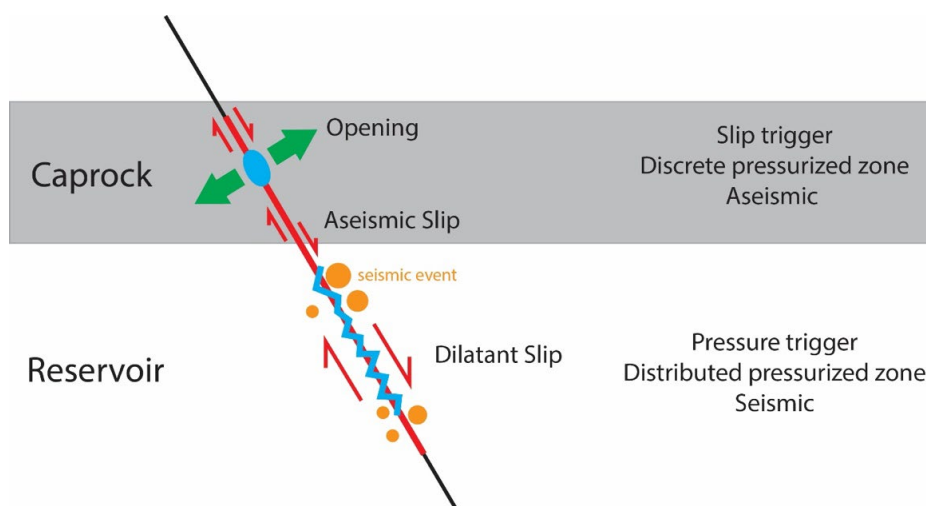


Fig. 2. Comparison of fault activation mechanisms in a conceptual reservoir-caprock system.

As shown in Fig. 2, the worst case scenario is that both the pressure propagation and aseismic slow rupture along the reservoir fault favor fluid penetration into the overlying shale fault segment in the caprock. And as we learned from the shale fault experiments, this in turn can trigger rupture nucleation in the caprock associated with an accelerated fluid migration, which is mostly aseismic and thus hard to detect. As the aseismic rupture continues to propagate, it may encounter a seismogenic zone where it could then rapidly create a larger magnitude earthquake and a larger permeable fault patch. Fig. 2 also highlights that the pressurized patch in the reservoir segment of the fault is likely more distributed along the fault compared to the shale segment where a more compact patch is expected. This has a significant impact on the mode of rupture and on the faults' seismic behavior. In permeable reservoirs like limestone/granite, high-pressure fluids invade a given rock volume, which then increases the chance to encounter a critically stressed frictional fault and cause a seismic event. In a caprock setting, on the other hand, due to the low permeability of the shale fault, fluids can only migrate into the fault if some opening occurs which then may be followed by aseismic slip; there may be little impact on the neighboring shale volume and little interaction with other faults in the vicinity. Moreover, the large amount of observed slow slip highlights that fault leakage and induced seismicity may occur decades after the start of a CO₂ storage project.

References

- Amann, F., Gischig, V., Evans, K., Doetsch, J., Jalali, R., Valley, B., Krietsch, H., Dutler, N., Villiger, L., Brixel, B., Klepikova, M., Kittila, A., Madonna, C., Wiemer, S., O. Saar, M., Loew, S., Driesner, T., Maurer, H. & Giardini, D. 2018. The seismo-hydromechanical behavior during deep geothermal reservoir stimulations: open questions tackled in a decameter-scale in situ stimulation experiment. *Solid Earth*, 9(1), 115-137.
- Birkholzer, J.T., Zhou, Q. 2009. Basin-scale hydrogeologic impacts of CO₂ storage: Capacity and regulatory implications, *International Journal of Greenhouse Gas Control*, 3(6), 745-756.
- Birkholzer, J.T., Oldenburg, C.O., Zhou, Q. 2015. CO₂ migration and pressure evolution in deep saline aquifers. Special issue on state of the art – 10 Years on from IPCC/SRCCS, *International Journal of Greenhouse Gas Control*, 40, 203-220.
- Cuss, R. J., Harrington, J. F., Noy, D. J., Sathar, S. and S. Norris 2015. An experimental study of the flow of gas along synthetic faults of varying orientation to the stress field: Implications for performance assessment of radioactive waste disposal, *J. Geophys. Res. Solid Earth*, 120, 3932–3945. <https://doi.org/10.1002/2014JB011333>
- Cuss, R.J. and Harrington, J.F. 2016. An experimental study of the potential for fault reactivation during changes in gas and pore-water pressure. *International Journal of Greenhouse Gas Control*, 53, 41-55.
- Guglielmi, Y., Cappa, F., Lanc, H., Janowczyk, J.B., Rutqvist, J., Tsang, C.-F., Wang, J.S.Y. 2014. ISRM suggested method for step-rate injection method for fracture in-situ properties (SIMFIP): Using a 3-component Borehole Deformation Sensor. *Rock Mechanics and Rock Engineering* 47, 303–311.
- Guglielmi, Y., Cappa, F., Avouac, J.P., Henry, P., Elsworth, D. 2015. Seismicity triggered by fluid-injection-induced aseismic slip. *Science* 348, 1224. <https://doi.org/10.1126/science.aab0476>
- Michael, K., Avijegon, A., Ricard, L., Strand, J., Freifeld, B., Woitt, M., Pervukhina, M., Tertysnikov, K., Pevzner, R., Rachakonda, P., Larcher, A., Dance, T., Myers, M., Delle-Piane, C., Feitz, A., Stalker, L., Myers, J., Langhi, L., and Hortle A. 2019. The CSIRO In-Situ Laboratory – A facility For CO₂ injection testing and monitoring in a fault zone; ECCSEL Workshop Underground Laboratories for CO₂ geological storage research, 5-6 June 2019, Nancy, France, 2019.
- Nicol, A., Seebeck, H., Field, B., McNamara, D., Childs, C, Craig, J., Rolland, A. 2017. Fault permeability and CO₂ storage. 13th International Conference on Greenhouse Gas Control Technologies, GHGT-13, 14-18 November 2016, Lausanne, Switzerland, *Energy Procedia* 114 (2017) 3229–3236.
- Raleigh, C.B., Healy J.H. and Bredehoeft J.D. 1976. An experiment in earthquake control at Rangely. *Colorado. Science*, 191, 1230–1237.
- Rutqvist, J., Rinaldi, A.P., Cappa, F., Jeanne, P., Mazzoldi, A., Urpi, L., Guglielmi, Y., Vilarrasa, V. 2016. Fault activation and induced seismicity in geological carbon storage: Lessons learned from recent modeling studies. *Journal of Rock Mechanics and Geotechnical Engineering*, Volume 8, Issue 6, 2016, Pages 789-804, ISSN 1674-7755. <https://doi.org/10.1016/j.jrmge.2016.09.001>
- Vilarrasa and Makhnenko, 2017. Caprock integrity and induced seismicity from laboratory and numerical experiments, *Energy Procedia*, Volume 125, Pages 494-503, ISSN 1876-6102. <https://doi.org/10.1016/j.egypro.2017.08.172>
- Zappone, A., Rinaldi, A.P., Grab, M., Wenning, Q.C., Roques, C., Madonna, C., Obermann, A.C., Bernasconi, S.M., Brennwald, M.S., Kipfer, R., Soom, F., Cook, P., Guglielmi, Y., Nussbaum, C., Giardini, D., Mazzotti, M. and Stefan Wiemer 2021. Fault sealing and caprock integrity for CO₂ storage: an in-situ injection experiment. *Solid Earth*, 12, 319–343, 2021. <https://doi.org/10.5194/se-12-319-2021>

Storing Swiss CO₂ in Iceland and Switzerland: insights from DemoUpCarma and beyond

Stefan Wiemer¹, Alba Zappone¹, Antonio Pio Rinaldi¹, Thanushika Gunatilake¹, Jonas Junker¹, Anne Obermann¹, Viola Becattini, Marco Mazzotto and the DemoUpCarma team

¹ Swiss Seismological Service, ETH Zurich, Switzerland

² Department of Mechanical and Process Engineering, ETH Zurich, Switzerland

* stefan.wiemer@sed.ethz.ch

1 The need and options for sequestering Swiss CO₂

For Switzerland to meet its climate goal, carbon dioxide (CO₂) emissions must be curbed dramatically in the next three decades. Technology and infrastructural changes to eliminate distributed CO₂ emissions in sectors such as mobility and buildings are mandatory, and they are on the way; this will not be enough. There is an emerging consensus in the scientific community, in politics, responsible offices, and in society that even after transitioning to renewables for heating and mobility needs, Switzerland will need to capture, transport and store millions of tons of CO₂ per year from sizeable Swiss point sources (CO₂ capture, transport, and storage; CCTS). While Carbon Capture and Use (CCUS) is essential and, in some cases, such as CO₂ used in concrete already being widely used, there is likely not enough capacity and cost are a limiting factor. Recent scenarios published by SFOE and the Joint Activity Scenarios and Modelling (JASM, www.sccer-iasm.ch) agree that without CO₂ CCTS as an additional means, the net-zero emission target cannot be achieved (Panos et al., 2021; Guidati et al., 2021) This is also a clear conclusion of the federal councils 2022 report on Carbon capture and storage (CCS) and negative emission technologies (NETs). For storing CO₂ captured from hard-to-abate emission sources, Switzerland has, in principle, several options:

1. Storage in saline aquifers or depleted oil and gas fields in the North Sea
2. Enhanced mineralization
3. Sequestration of CO₂ in Basalts, for example, in Iceland
4. Storage in saline aquifers in the Molasse Basin in Switzerland

Below, we will summarise recent activities related to options 3 and 4.

2 Capturing and Storing CO₂ in Concrete and in Iceland: DemoUpCarma

DemoUpCARMA (Demonstration and Upscaling of CARbon dioxide MANagement solutions for a net-zero Switzerland) and its sister project DemoUpStorage are pilot projects led by ETH Zurich (www.demoupcarma.ethz.ch). They aim to demonstrate the implementation and scale-up of two pathways leading to negative emissions:

- **Pathway 1:** CO₂ utilization and permanent storage in primary and recycled concrete in Switzerland using a novel technology.
- **Pathway 2:** CO₂ transport and permanent storage in Basalts in Iceland, in partnership with Carbfix.

An overview of the DemoUpCarma workflow is shown in Fig. 1.

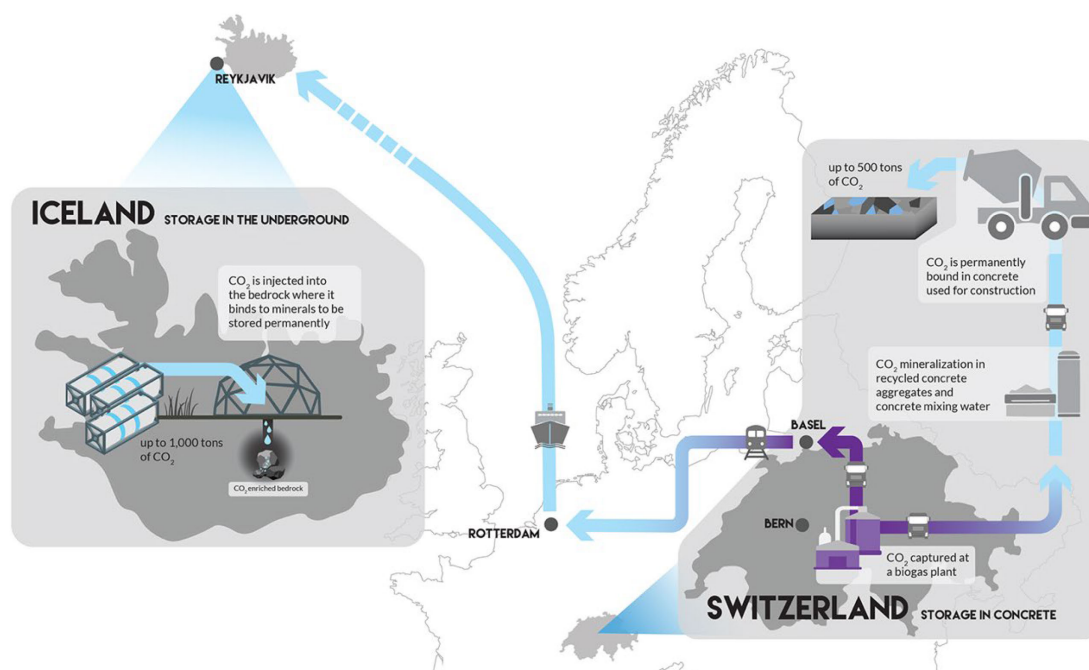


Fig. 1. Schematic representation of the DemoUpCarma pathways for CCUS and CCTS.

DemoUpCarma is a broad consortium of partners from science and industry, funded in parts by the Swiss Federal Office of Energy. The project used about 1000 tons of carbon dioxide emissions from a wastewater treatment plant in Bern. We performed a life cycle analysis that covered the entire chain – from the capture and liquefaction of CO₂ at the point of origin to its transport and permanent storage. The project has demonstrated that both pathways are technically feasible and positively impact climate. In all the examples examined, the amount of CO₂ stored exceeded the emissions produced along the transport chain. When storing in recycled demolition concrete, the efficiency and thus the ratio between stored emissions and resulting new emissions is 90 %; when transporting Swiss CO₂ and storing it in a geological reservoir in Iceland, it's around 80 %. This efficiency should improve in the future as most of the new emissions arise from transporting the containers by rail and ship, and some of these modes of transport still use energy from coal-fired power stations and fossil fuels. If CO₂ is to be exported on a large scale, constructing a pipeline would be a potential solution.

The DemoUpCARMA project was the first to demonstrate a CO₂ supply chain from capture and transport to geological storage in Icelandic basalt. Biogenic CO₂ is captured and liquefied at ARA Bern. From there, it is transported by truck in special containers to Weil am Rhein, Germany, where it is then transported by rail to the port of Rotterdam in the Netherlands, and onwards by sea freight to Iceland. In Iceland, the container is transported from the port to the geological reservoir by truck. So far, 80 tons of CO₂ have been transported to Iceland, and about 500 tons more will be transported until the project is over in late 2024. A life-cycle assessment has shown that the entire supply chain causes significantly fewer greenhouse gas emissions than are avoided through geological storage.

In Iceland, the Swiss CO₂ is mixed with seawater and injected into the basaltic subsoil through a specially constructed borehole at 300 to 400 meters at a site near Helgukvík (Fig. 2). Previously, the partner company Carbfix had been dissolving the CO₂ in freshwater to mineralize it underground (Snæbjörnsdóttir et al., 2020). We installed an extensive monitoring network (Fig. 3) with additional boreholes to investigate whether the procedure and the mineralization processes also work with seawater and to monitor the mineralization process with geophysical and geochemical methods. We mainly use repeated cross-hole active seismic imaging as well as continuous electrical resistance measurements to track the migration and mineralization of CO₂.

3 CO₂ storage options in Switzerland

CO₂ storage in Switzerland can be the most economical and ecological option; it has also been shown to be attractive to the population because it creates a self-sufficient value chain in Switzerland. The first study on the potential CO₂ storage capacity in Switzerland was carried out by Chevalier et al. (2010). It was a first-order appraisal based solely on geological data and criteria available at that time. The primary targets for CO₂ storage in Switzerland are saline aquifers in the Swiss Molasse Basin and the adjacent Folded Jura. The authors adopted the approach and criteria established in the literature adapted for the Swiss case. By carrying out both a basin-wide and an aquifer-wide analysis and by accounting for the many uncertainties, they estimated a large potential for CO₂ geological storage in the Swiss Molasse Basin, namely of the order of 2500 Mt CO₂. The same authors revisited this first appraisal based on new data acquired in the last decade (Diamond et al., 2019). The main factors determining whether an aquifer formation can serve as an industrial-scale reservoir for gas storage are rock-matrix porosity, rock-matrix permeability and the porosity and permeability of any fracture networks. Current industrial techniques require rock-matrix porosities >10 vol.-% and permeability > 10 mD to inject gas efficiently. Considering these factors, the most promising part of the Upper Muschelkalk is the 20–30 m thick layer known as the Trigonodus Dolomit, which is hydraulically sealed above the Gipskeuper layer. The theoretical CO₂ storage capacity was in 2019 re-estimated to be ~52 Mt CO₂. However, this assessment is based on several assumptions and minimal data; several scientists have questioned the evaluation and argued that the actual storage potential may be much more significant, especially if fracture permeability can be enhanced.

To advance the knowledge on CO₂ storage options in Switzerland and to engage in a dialog with society on CCS, swisstopo and ETH, with support from the Swiss Federal Office of Energy (SFOE) and the Federal Office for the Environment (FOEN), are promoting the CITru project (CO₂-pilot Injection at Trüllikon). The goal of the project is «*To test in a pilot project the injectivity of CO₂ into a nationally important potential CO₂-storage complex in a highly explored region of Switzerland*». CITru will demonstrate for the first time in Switzerland the injection of liquid CO₂ at a modest scale (up to 25 000 tons of CO₂) into a saline aquifer to test optimal injection geometries and strategies, maximizing the amount of CO₂ that can be safely injected into tight and tilted formations common in the Swiss underground. The behaviour and spreading of the injected CO₂ are closely monitored during and after the injection phase. CITru, as a showcase (lighthouse) project, will improve the public perception and awareness of the general challenges and solutions for CCS and demonstrate the feasibility of safe and permanent storage of CO₂ in Switzerland's geological subsurface.

References

- Chevalier, G., Diamond, L. W. & Leu, W. Potential for deep geological sequestration of CO₂ in Switzerland: a first appraisal. *Swiss J. Geosci.* 103, 427–455 (2010).
- Diamond, L.W., L. Aschwanden, A. Admand, D, Egli (2019), Revised potential of the Upper Muschelkalk Formation (Central Swiss Plateau) for CO₂ storage and geothermal electricity, SCCER-SoR. http://static.seismo.ethz.ch/sccer-soe/Annual_Conference_2019/AC19_S3a_08_Diamond.pdf
- Guidati, Gianfranco, Adriana Marcucci, and Domenico Giardini (2021). Probabilistic Assessment of the Swiss Energy Strategy - Scenario analysis with the SES-ETH model. Tech. Rep. ETH Zurich - JASM. https://sccer-jasm.ch/JASMPapers/JASM_results_ses_eth.pdf
- Panos, E., Kober, T., Ramachandran, K., Hirschberg, S. (2021). Long-term energy transformation pathways - Integrated scenario analysis with the Swiss TIMES energy systems model. Tech. rep. PSI - JASM. https://sccer-jasm.ch/JASMPapers/JASM_results_stem.pdf
- Snæbjörnsdóttir, S.Ó., Sigfússon, B., Marieni, C., Goldberg, D., Gislason, S.R. and Oelkers, E.H. (2020). Carbon dioxide storage through mineral carbonation, *Nature Reviews Earth & Environment*, 1, 90-102. <https://doi.org/10.1038/s43017-019-0011-8>

Multi-disciplinary monitoring of the Ketzin CO₂ pilot site as successful concept for storage integrity assessment

Michael Kühn^{1*} and Cornelia Schmidt-Hattenberger¹

¹ GFZ German Research Centre for Geosciences, Telegrafenberg, Potsdam, Germany

* michael.kuehn@gfz-potsdam.de

1 Introduction

In the context of the international climate policy, carbon dioxide (CO₂) capture and geological storage is seen as a potential measure for reducing anthropogenic greenhouse gas emissions. The CO₂ pilot site in Ketzin, Brandenburg, was the first European onshore CO₂ storage project and the only project of its kind in Germany to date (Kühn et al., 2015; Schmidt-Hattenberger et al., 2019). At this research site, the complete life cycle of a CO₂ storage facility was investigated in accordance with the European CCS Directive 2009/31/EC. During the regular injection phase from 2008 to 2013, an amount of 67,000 t of CO₂ was stored in a saline aquifer at a depth of about 650 m.

2 Ketzin pilot site

Since 2004, scientific investigations on underground storage of CO₂ had been conducted within a context of several large-scale national research-projects, with rich international participation. Of primary interest were the specific processes during the injection of CO₂ and the subsequent propagation of the CO₂ plume within the storage horizon. Datasets were gathered and documented by a comprehensive monitoring programme (Möller et al., 2012; Bergmann et al., 2016, Szizybalski et al., 2017). In the long run, these data also helped to safely operate the storage complex and assess the impact on its environment (webpage of the project - <https://www.co2ketzin.de/en/home>).

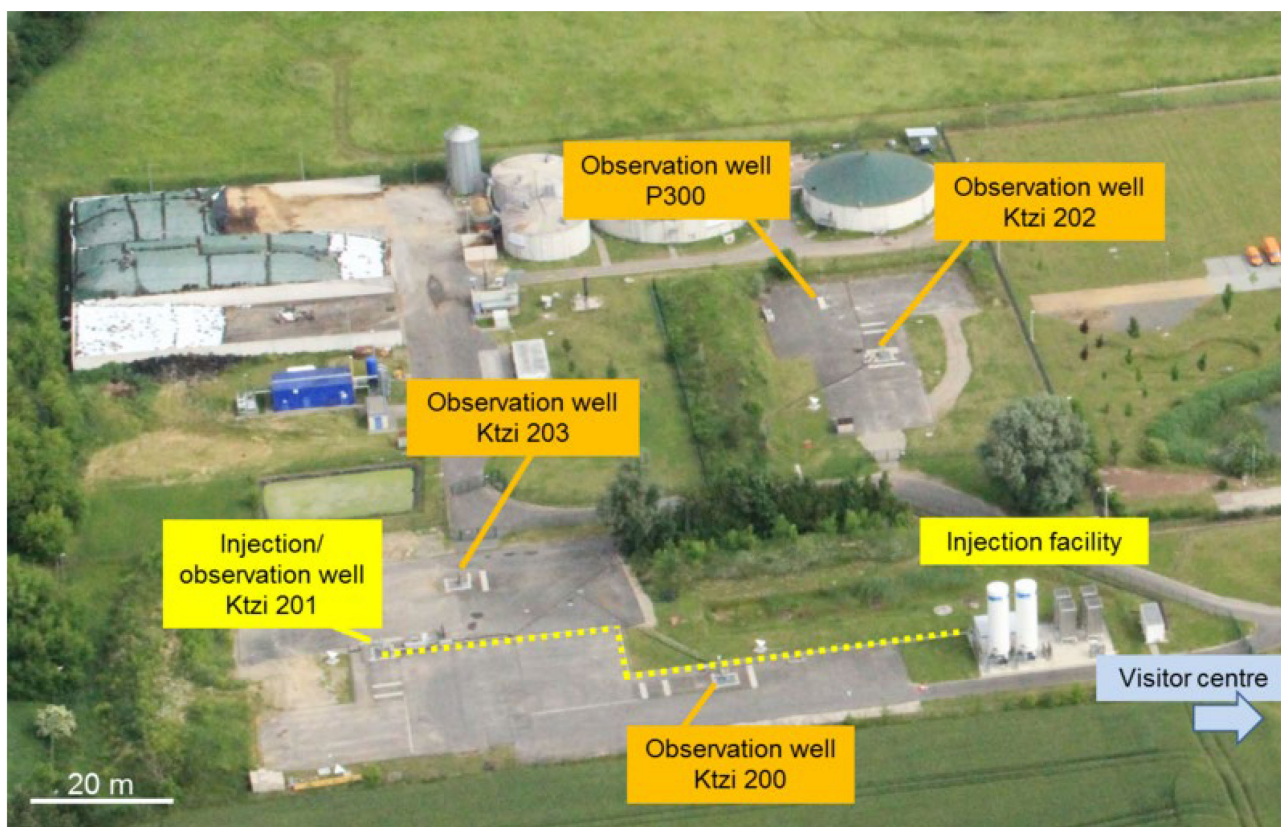


Fig. 1. Aerial view of the pilot site in Ketzin with all five wells.

The co-ordination of these works was done by the GFZ German Research Centre for Geosciences in Potsdam. All projects were supervised by the mining authority of the state of Brandenburg (LBGR) in Cottbus. From the beginning, the city of Ketzin/Havel has supported the overall project.

In total, five wells were drilled in 2007, 2011 and 2012 (Figs. 1 and 2). Suitable rock formations for CO₂ storage were located at 630 to 650 m depth at the Ketzin site consisting of porous sandstone layers, that can store CO₂ in their pores. The CO₂ injection itself, was operated by GFZ since 30th June 2008 and ended, as scheduled on 29th August 2013. During that period 67,271 t of CO₂ were stored in the reservoir.

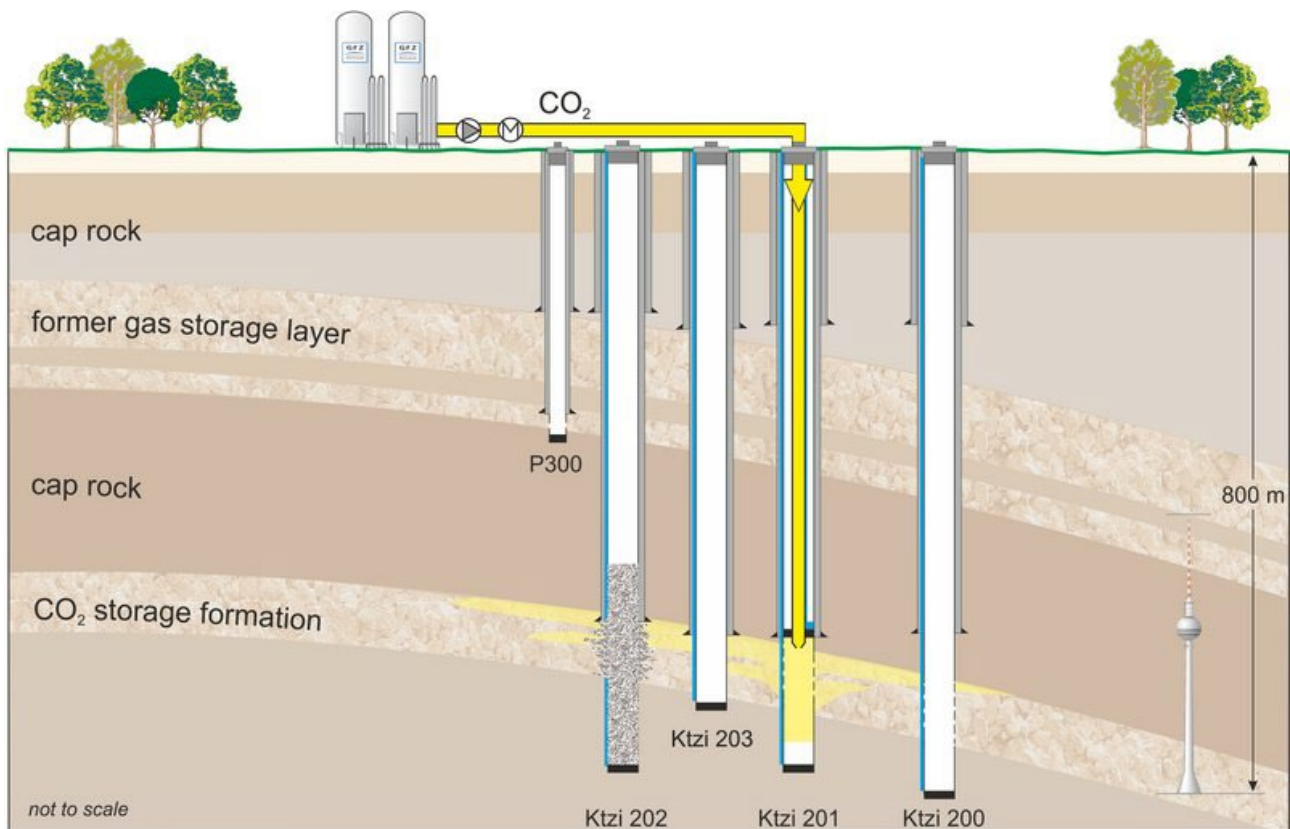


Fig. 2. Schematic vertical profile of the Ketzin pilot site. The dome-like structure of the layers is indicated. For comparison: Berlin TV Tower (368 m height). In 2013, the observation well Ktzi 202 was partially abandoned. The complete abandonment of this well was finally done in 2015 (Schmidt-Hattenberger et al., 2018).

At Ketzin, the layers are not lying horizontally but are arched (Fig. 2). The CO₂ was injected into the reservoir at the southern flank of this dome-like structure. For this, the injection well Ktzi 201 was used, which besides the other deep wells (Ktzi 200, 202 and 203) also served as an observation well to monitor the distribution of the CO₂ in the underground.

The reservoir is sealed by overlying 165 m thick shaly cap rocks. These cap rocks, together with the dome-like structure, ensure a controlled and limited distribution of the CO₂. The shallower well P300 ends above these cap rocks and was used for the monitoring of their tightness.

3 Multi-disciplinary monitoring

The propagation of the injected CO₂ and its fluid-rock-interactions were investigated with an observation program of various geoscientific methods on the surface and also in the subsurface. Both the storage horizon of the sandstone layers (reservoir) and the overlying thick clay rocks (caprock), which seal the reservoir horizon upwards, had to be monitored. A multi-disciplinary monitoring concept was developed for the Ketzin site (Lüth et al., 2020; Martens et al., 2012), which included a

combination of different geophysical and geochemical methods and covered different temporal (periodic and permanent measurements) and spatial scales (dm, m, km). The official requirements for the monitoring of the geological storage included the following tasks:

- (1) Determination of the CO₂ arrival at the observation wells
- (2) Investigation of the propagation behaviour of the CO₂ distribution
- (3) Safety monitoring to ensure the tightness and integrity of the storage complex

During the CO₂ injection, the geophysical monitoring provided data on the lateral and vertical propagation of the CO₂ plume. From the extent of this CO₂ distribution around the injection well, the CO₂ gas saturation in the porous sandstone can be inferred. The storage physics parameters obtained from the seismic repeat measurements (Bergmann et al., 2016) served for decision-making for control of the CO₂ injection and fluid propagation in the subsurface. Besides the 3D geophysical measurements, petro-physical and geomechanical laboratory experiments were carried out on rock samples under in-situ pressure and temperature conditions (Zemke et al., 2010; Kummerow and Spangenberg, 2011). The results of the geophysical measurements significantly supported the calibration of the numerical simulation models (Kempka and Kühn 2013) and thus improved the reliability of the long-term forecast and risk assessment for the storage facility.

4 Storage integrity assessment

Static and dynamic geological models are important tools for storage operations, as they complement monitoring methods and provide forecasts for the operational management. To study the dynamic behaviour of the CO₂ plume in the subsurface, a static geological model is required. This is used as the basis for the numerical simulations of the CO₂ propagation, together with existing data from hydraulic, thermal, geochemical and mechanical processes. For example, information from existing old boreholes (data from borehole logs, core samples) and from hydraulic testing (injection and production of fluid) could be used to evaluate estimates about channel/non-channel facies at different depths at Ketzin (Norden and Frykman 2013).

The assessment of the storage integrity of the CO₂ injection at Ketzin was based on the multi-disciplinary monitoring program comprising a combination of geophysical and geochemical methods to observe the migration and spatial distribution of CO₂ in the underground. This comprehensive information was used to build the static geological model and run dynamic simulations and numerical scenarios.

5 Conclusions and recommendations

For the Ketzin pilot site a storage integrity assessment was performed based on multi-disciplinary monitoring. From the integrated results it can be concluded that: (i) storage of CO₂ at the Ketzin was safe and reliable at all times; (ii) it has been proven that no CO₂ escaped during the pilot test; (iii) the interactions between fluid and rock induced by the injected CO₂ did not affect the integrity of the reservoir and cap rocks; and (iv) computer simulations have reproduced the temporal and spatial behaviour of the injected CO₂ and are suitable tools for assessing the long-term behaviour of the reservoir (Liebscher et al., 2012, Lüth et al., 2015).

The successful implementation of a CO₂ storage project also includes gaining acceptance by the local population. A transparent information strategy comprising all steps of the project is key to that and highly recommended. At the Ketzin site, regular information of the local politicians and authorities about the CO₂ storage technology and all associated construction measures on site began even before the start of the project. There was also cooperation with local educational institutions, such as schools and universities, and a weekly visitor day was set up for interested guests with a guided tour of the test site (Szyzibalski et al. 2014). Through this very successful public outreach concept, the project was able to gain local and regional acceptance.

The Ketzin project was successfully completed in 2017 with the backfilling of the boreholes and dismantling of the surface facilities. The results form a template for follow-up projects on an industrial scale, and they are also fed into national and international standardisation work in the form of knowledge transfer.

References

- Bergmann, P., Diersch, M., Götz, J., Ivandic, M., Ivanova, A., Juhlin, C., Kummerow, J., Liebscher, A., Lüth, S., Meekes, S., Norden, B., Schmidt-Hattenberger, C., Wagner, F. M., & Zhang, F. (2016). Review on geophysical monitoring of CO₂ injection at Ketzin, Germany. *Journal of Petroleum Science and Engineering*, 139, 112–136. <https://doi.org/10.1016/j.petrol.2015.12.007>
- Kempka, T., & Kühn, M. (2013). Numerical simulations of CO₂ arrival times and reservoir pressure coincide with observations from the Ketzin pilot site, Germany. *Environmental Earth Sciences*, 70(8), 3675–3685. <https://doi.org/10.1007/s12665-013-2614-6>
- Kummerow, J., & Spangenberg, E. (2011). Experimental evaluation of the impact of the interactions of CO₂-SO₂ brine, and reservoir rock on petrophysical properties: A case study from the Ketzin test site, Germany. *Geochemistry, Geophysics, Geosystems*, 12(5). <https://doi.org/10.1029/2010GC003469>
- Kühn, M., Liebscher, A., Martens, S., Möller, F., Kempka, T., & Streibel, M. (2015). Safe Operation of Geological CO₂ Storage Using the Example of the Pilot Site in Ketzin. In W. Kuckshinrichs & J.-F. Hake (Eds.), *Carbon capture, storage and use: Technical economic environmental and societal perspectives* (pp. 127–143). Springer. https://doi.org/10.1007/978-3-319-11943-4_6
- Liebscher, A., Martens, S., Möller, F., Lüth, S., Schmidt-Hattenberger, C., Kempka, T., Szzybalski, A., & Kühn, M. (2012). Überwachung und Modellierung der geologischen CO₂-Speicherung - Erfahrungen vom Pilotstandort Ketzin, Brandenburg (Deutschland). *Geotechnik*, 35(3), 177–186. <https://doi.org/10.1002/gete.201200005>
- Lüth, S., Henniges, J., Ivandic, M., Juhlin, C., Kempka, T., Norden, B., Rippe, D., & Schmidt-Hattenberger, C. (2020). Geophysical monitoring of the injection and postclosure phases at the Ketzin pilot site. In J. Kasahara, M. S. Zhdanov, & H. Mikada (Eds.), *Active geophysical monitoring* (pp. 523–561). Elsevier. <https://doi.org/10.1016/B978-0-08-102684-7.00025-X>
- Lüth, S., Ivanova, A., & Kempka, T. (2015). Conformity assessment of monitoring and simulation of CO₂ storage: A case study from the Ketzin pilot site. *International Journal of Greenhouse Gas Control*, 42, 329–339.
- Norden, B., & Frykman, P. (2013). Geological modelling of the Triassic Stuttgart Formation at the Ketzin CO₂ storage site, Germany. *International Journal of Greenhouse Gas Control*, 19, 756–774. <https://doi.org/10.1016/j.ijggc.2013.04.019>
- Martens, S., Kempka, T., Liebscher, A., Lüth, S., Möller, F., Myrntinen, A., Norden, B., Schmidt-Hattenberger, C., Zimmer, M., & Kühn, M. (2012). Europe's longest-operating on-shore CO₂ storage site at Ketzin, Germany: a progress report after three years of injection. *Environmental Earth Sciences*, 67(2), 323–334.
- Möller, F., Liebscher, A., Martens, S., Schmidt-Hattenberger, C., & Kühn, M. (2012). Yearly operational datasets of the CO₂ storage pilot site Ketzin, Germany. <https://doi.org/10.2312/GFZ.B103-12066>
- Schmidt-Hattenberger, C., Lüth, S., Rippe, D., Wiese, B.U., Pilz, P., Hierold, J., Zimmer, M., & Kühn, M. (2019). Nutzung des geologischen Untergrunds zur stofflichen Speicherung. *System Erde*, 9(1). <https://doi.org/10.2312/GFZ.SYS-ERDE.09.01.2>
- Schmidt-Hattenberger, C., Bergmann, P., Labitzke, T., Wagner, F.M., & Rippe, D. (2016). Permanent crosshole electrical resistivity tomography (ERT) as an established method for the long-term CO₂ monitoring at the Ketzin pilot site. *International Journal of Greenhouse Gas Control*, 52, 432–448. <https://doi.org/10.1016/j.ijggc.2016.07.024>
- Szzybalski, A., Zimmer, M., Pilz, P., & Liebscher, A. (2017). Results from twelve years of continuous monitoring of the soil CO₂ flux at the Ketzin CO₂ storage pilot site, Germany. *Energy Procedia*, 125, 543–548. <https://doi.org/10.1016/j.egypro.2017.08.186>
- Szzybalski, A., Kollersberger, T., Möller, F., Martens, S., Liebscher, A., & Kühn, M. (2014). Communication Supporting the Research on CO₂ Storage at the Ketzin Pilot Site, Germany – A Status Report after Ten Years of Public Outreach. *Energy Procedia*, 51, 274–280. <https://doi.org/10.1016/j.egypro.2014.07.032>
- Zemke, K., Liebscher, A., & Wandrey, M. (2010). Petrophysical analysis to investigate the effects of carbon dioxide storage in a subsurface saline aquifer at Ketzin, Germany (CO₂SINK). *International Journal of Greenhouse Gas Control*, 4(6), 990–999.

Global status of saline aquifer CO₂ storage and key challenges for scale-up

Philip Ringrose^{1*}

¹ Norwegian University of Science and Technology, Trondheim, Norway

* philip.ringrose@ntnu.no

1 Global CCS status and scale-up needs

Reducing global CO₂ emissions to atmosphere is a major challenge. Over the last 5 years global emissions have flattened but not yet started falling, and economically viable pathways to significant reductions in emissions remain elusive. Good progress has been made in Europe, where the EU's net emissions in 2022 were 31 % lower than in 1990 and even 49 % lower in the UK. However, more aggressive decarbonisation rates are needed in the coming years, with the main actions being (i) the addition of new renewable energy sources, (ii) electrification of power systems, (iii) efficiency measures, (iv) increased use of bioenergy and (v) further deployment of CO₂ capture, utilization, and storage (CCUS). Using the IEA Sustainable Development Scenario as a framework (IEA 2020), the 'CCUS tool' only needs to handle about 14 % of these emissions reductions by 2050; however, that contribution is vital as CCUS plays a key role in cutting emissions in difficult to decarbonize sectors of our economies. The global contribution to emissions reductions via CCS needs to reach around seven Gigatonnes per annum (Gtpa) by 2050.

There are currently 30 large-scale CCS projects in operation globally, with another 11 in construction and over 150 projects in various stages of development (GCCSI, 2022). Of the 30 operating projects, most use CO₂ enhanced oil recovery as the storage mechanism, but already nine use saline aquifers as the storage mechanism. Looking ahead saline aquifer storage is expected to become the dominant destination for captured sources of CO₂. Some of the longer-running saline aquifer storage projects where much experience has been shared and published include Sleipner and Snøhvit (in Norway), Quest and Aquistore (in Canada) and IBDP (in the USA). Selected digital datasets from these projects are also shared via the co2datashare.org platform.

The current global capture capacity of operating CCS projects is 42 Mtpa, and if all the CCS projects currently in construction and development were deployed this would rise to nearly 250 Mtpa (GCCSI, 2022). However, this capacity needs to increase to 1 Gtpa by 2030 and then to 7 Gtpa by 2050 (using the IEA Sustainable Development Scenario as a framework, IEA 2020). Initially, this capture capacity is mainly needed for decarbonising coal, natural gas and industry, but beyond around 2040 negative emissions technology (Direct Air Capture and Biomass capture) needs to increase significantly and eventually dominate in order to meet the 2DS climate scenario goals.

2 Summary of trapping mechanisms

The CO₂ trapping mechanisms operating in saline aquifer storage systems have been extensively discussed in the published literature (e.g., Metz et al., 2005; Ch. 5; Bradshaw et al. 2007) and can be broadly summarised in terms of (a) structural and stratigraphic trapping, (b) residual CO₂ trapping, (c) solubility trapping and (d) mineral trapping. Although the rates of these processes and their relative importance are site specific and somewhat uncertain, there is general agreement that the concepts are qualitatively correct and that the processes work to make CO₂ storage more secure as a function of time. The initially mobile dense-phase CO₂ gradually becomes trapped by capillary forces, both at the pore scale and the formation scale, and also dissolved in the brine phase or precipitated as mineral phases.

Fig. 1 illustrates how these processes are likely to develop in a dipping saline aquifer unit. Each site will have different expressions and magnitudes of these processes depending on the detailed geology, but general learnings from projects so far suggests that significant fractions do become trapped

by residual CO₂ and solubility trapping processes (Ringrose et al. 2021), strengthening the case for secure long-term storage in saline aquifers.

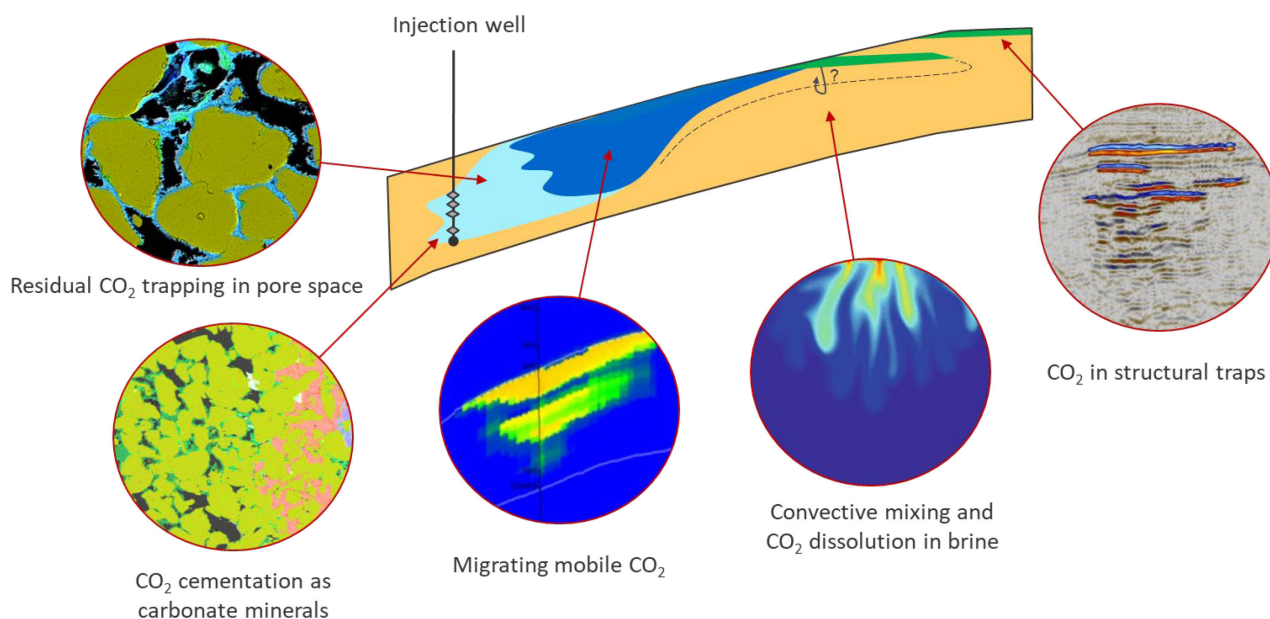


Fig. 1. Conceptual sketch of CO₂ trapping mechanisms in a dipping saline aquifer unit (modified from Ringrose 2023, inset images courtesy of Equinor and Ranganathan et al. 2012).

3 Key challenges for global scale-up

As we confront the question of global scale-up of CCS to meet the climate goals, the key technical question for geoscientists and subsurface-resource engineers is then: What would it take to achieve Gigatonne-scale CO₂ storage? We review this question by looking at five main concerns:

1. Are there enough suitable rock formations?
2. What about the pressure and injectivity limitations?
3. Will large-scale CO₂ injection cause fracturing and earthquakes?
4. Will our society allow storage activities to proceed?
5. Are there sufficient financial incentives?

The first concern is relatively easy to address – potential storage resources are overwhelmingly available, both in the world's sedimentary basins and in the prolific near-surface volcanic (mafic) rock systems. The more pertinent question is can we exploit these resources in an economically viable manner. Using historical hydrocarbon industry drilling data, Ringrose & Meckel (2019) argued that around 12,000 CO₂ injection wells would be needed globally to reach the 7 Gtpa rate by 2050 using the world's sedimentary basins. This is a relatively modest well count compared to the 41,000 wells drilled worldwide in 2021 for hydrocarbon exploration and production. This CO₂-well rate model can be presented in various ways; for example, cumulative storage of 1 Gt by 2050 would need around 20 CO₂ injection wells by 2030 rising to around 60 by 2040 (Fig. 2).

The pressure management and injectivity concerns represent important constraints on the economically achievable levels of storage. To help understand these limits, Ringrose & Meckel (2019) proposed an analytical pressure model to explore ways to optimize the reservoir pressure rise for multiple injection projects in sedimentary basins, where the estimated volume stored per project, $V_{project}$, is given by Eq. 1:

$$V_{project} = I_C \left[p_{well} - p_{init} + \int_i^f A p_D(t_D) \right] + F_b \quad \text{Eq. (1)}$$

where I_c is the well injectivity, P_{well} is the injection well operating pressure, P_{init} is the initial reservoir pressure, $A_{\text{D}}(t_{\text{D}})$ is a characteristic pressure function, and F_b is a volume flux boundary condition. The integration of the characteristic pressure function is between the limits P_{init} and P_{final} , where P_{final} would be determined with reference to a pressure limiting condition controlled by the geomechanical response of the formation.

To test this approach, we applied this function to a simplified model of the fault blocks of the Smeaheia storage prospects region offshore Norway (Ringrose et al., 2022). The study showed how Gt-scale storage in the prospect was plausible and illustrated how larger fault blocks need to be prioritised to optimize the use of the available storage resources.

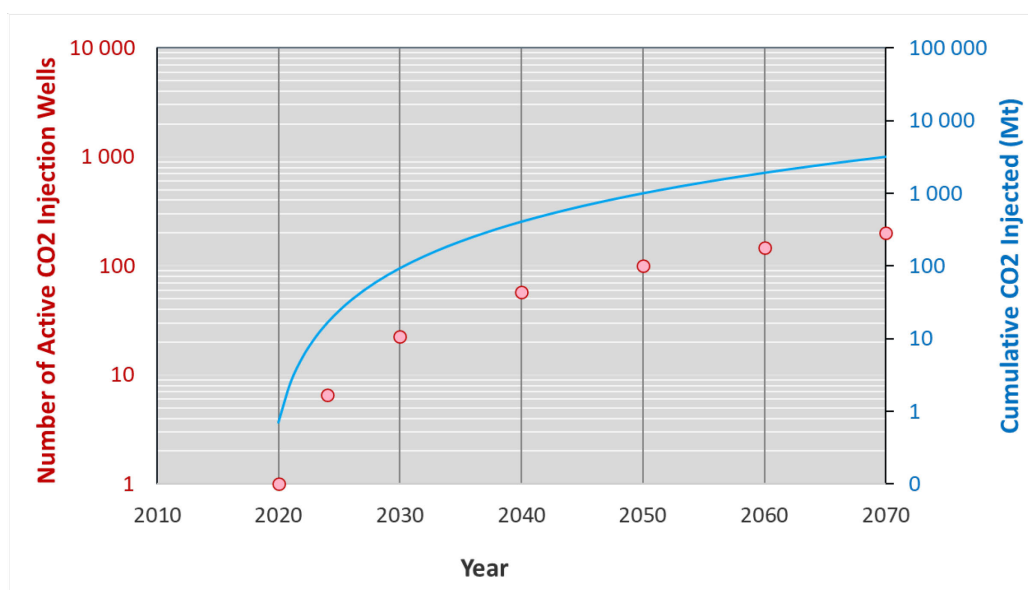


Fig. 2. Example model of the number of injection wells needed to reach a cumulative CO₂ storage of 1 Gigatonne by 2050, assuming well #1 is drilled in 2020. The function is $N_{\text{wells}} = T^{1.355}$ (time in years).

The third question of the potential for induced fractures and seismicity associated with large-scale CO₂ storage is harder to conclude on. However, proactive mitigation and monitoring efforts can address these concerns. Firstly, maximum injection pressures need to be carefully managed within a framework of accurate geomechanical datasets and models, and secondly good baseline seismicity assessments are needed to ensure successful discrimination between natural and induced seismicity. Zarifi et al. (2023) report recent work on improving background seismicity monitoring in preparation for large-scale CO₂ storage offshore Norway. They characterise the normal levels of background tectonic seismicity observed in this region and demonstrate ways to significantly improve event localisation and detection. Seismicity monitoring using sparse seismic sensor arrays and fibre-optic detection systems are emerging as a key tool for enabling the cost-effective monitoring systems needed to ensure safe storage.

4 Social and economic risks and benefits

The socio-economic factors are arguably the more significant hurdles to achieving Gigatonne-scale CCS when compared with the technical challenges (Trupp et al. 2022). Several socio-political factors have historically impeded CCS project developments, including public scepticism/opposition, lengthy permitting processes, and a lack of financial support for CCS. Encouragingly, these framing conditions are beginning to improve, and many new CCS developments have been recently announced around the world. However, progress with CCS project development is still too slow compared to the rates of decarbonisation needed. If we can get to the point where it becomes both economically viable and socially accepted for industry to develop multiple CCS facilities, then we can be confident that Gigatonne-scale CO₂ storage is technically achievable. It is furthermore important to realise that, while CCS is initially mainly needed for decarbonising fossil fuels, these CO₂ storage resources will

be increasingly used to support negative emissions technology. Scaling up CO₂ storage thus has multiple benefits, both for decarbonising existing emissions systems (CCS) and for enabling Carbon Dioxide Removal (CDR).

References

- Bradshaw, J., Bachu, S., Bonijoly, D., Burruss, R., Holloway, S., Christensen, N.P. and Mathiassen, O.M., 2007. CO₂ storage capacity estimation: issues and development of standards. *International journal of greenhouse gas control*, 1(1), pp.62–68. [https://doi.org/10.1016/S1750-5836\(07\)00027-8](https://doi.org/10.1016/S1750-5836(07)00027-8)
- IEA (2020) CCUS in Clean Energy Transitions, IEA, Paris. <https://www.iea.org/reports/ccus-in-clean-energy-transitions>
- GCCSI (2022) Global status of CCS report. <https://status22.globalccsinstitute.com/2022-status-report/global-status-of-ccs/>
- Metz, B. (Ed.) 2005. Carbon dioxide capture and storage: special report of the intergovernmental panel on climate change. Cambridge University Press.
- Ranganathan, P., Farajzadeh, R., Bruining, H. 2012. Numerical Simulation of Natural Convection in Heterogeneous Porous media for CO₂ Geological Storage. *Transport in Porous Media* 95, 25–54. <https://doi.org/10.1007/s11242-012-0031-z>
- Ringrose, P.S. & Meckel, T.A., 2019. Maturing global CO₂ storage resources on offshore continental margins to achieve 2DS emissions reductions. *Scientific reports*, 9(1), 17944. <https://doi.org/10.1038/s41598-019-54363-z>
- Ringrose, P.S., Furre, A.K., Gilfillan, S.M., Krevor, S., Landrø, M., Leslie, R., Meckel, T., Nazarian, B. and Zahid, A., 2021. Storage of carbon dioxide in saline aquifers: Physicochemical processes, key constraints, and scale-up potential. *Annual Review of Chemical and Biomolecular Engineering*, 12, pp.471–494. <https://doi.org/10.1146/annurev-chembio-eng-093020-091447>
- Ringrose, P., Guo, T., Nybråten, E., Thompson, N., Wu, L., Worthington, R., Nazarian, B. & Santi, A., 2022, September. Gigatonne-Scale CO₂ Storage: Analytical Frameworks for Optimizing Multiple Projects in Sedimentary Basins. In Sixth International Conference on Fault and Top Seals (Extended abstract). European Association of Geoscientists & Engineers. <https://doi.org/10.3997/2214-4609.202243017>
- Ringrose, P., 2023. Storage of Carbon Dioxide in Saline Aquifers: Building confidence by forecasting and monitoring. Society of Exploration Geophysicists. 152 pp. <https://doi.org/10.1190/1.9781560803959>
- Trupp, M., Ringrose, P., Hovorka, S. and Whittaker, S., 2022. Risk-sharing is vital for up-scaling CCS, to combat climate change. 16th International Conference on Greenhouse Gas Control Technologies, GHGT-16. Available at SSRN: <https://ssrn.com/abstract=4284770> or <http://dx.doi.org/10.2139/ssrn.4284770>
- Zarifi, Z., Köhler, A., Ringrose, P., Ottemöller, L., Furre, A.K., Hansteen, F., Jerkins, A., Oye, V., Dehghan Niri, R. and Bakke, R., 2023. Background Seismicity Monitoring to Prepare for Large-Scale CO₂ Storage Offshore Norway. *Seismological Research Letters*, 94(2A), pp.775–791. <https://doi.org/10.1785/0220220178>

CO₂ storage site feasibility assessment and risk-based monitoring: an industry approach

Marcella Dean¹, Owain Tucker², Kees Hindriks¹ and Nino Cilona¹

¹ Shell Global Solutions International B.V., The Netherlands

² Shell Research Limited, UK

* marcella.dean@shell.com

1 Introduction

Carbon Capture and Storage (CCS) is a critical technology solution to achieve Net Zero ambitions targeted by countries and industry alike. This requires deploying CCS at giga-tonne scale and ensuring that CO₂ injected into the subsurface remains securely in the ground as intended.

To establish technical CO₂ storage site feasibility, a comprehensive characterisation of the subsurface is required. This includes the geosphere, hydrosphere, biosphere, and all wells in the area which could potentially be affected.

To guide this assessment, we use the concept of five pillars of storage site feasibility (Fig. 1).

- 1) **Capacity:** Does the site have the storage capacity required?
- 2) **Containment:** Can the site contain CO₂ indefinitely?
- 3) **Transport & Injectivity:** Can CO₂ be transported to the site safely and economically? Can sustained injection be maintained at the required rates?
- 4) **Monitoring & Remediation:** Can the injected CO₂ be monitored, and remedial activities be deployed within economic limits?
- 5) **Stakeholders:** Can we provide the evidence to align stakeholders?

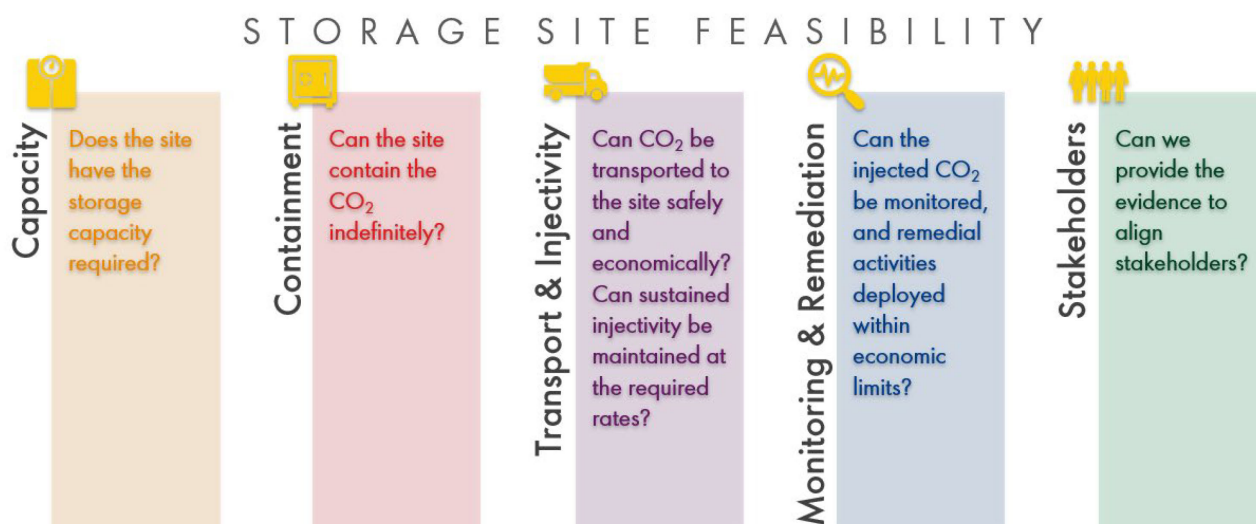


Fig. 1. The five pillars describing the key requirements to establish CO₂ storage site feasibility.

2 Industry approach and experience

We combine all geological and engineered aspects of CO₂ storage together using the bowtie risk management framework (Fig. 2). This approach is widely used in the energy industry and beyond (de Ruijter & Guldenmund, 2014). Specifically, we use the bowtie to assess and manage all credible subsurface risks related to containment (CO₂ and existing pore fluids) or fault reactivation and subsequent induced microseismicity. Within this framework, threats (i.e., mechanisms that can lead to loss of containment/induced seismicity) are investigated and barriers (i.e., selection of natural or

engineered features and actions that prevent unintended migration or seismicity) are identified. Monitoring technologies are key elements of active barriers in a bowtie, which are made up of a sensor, a control response, and a corrective action.

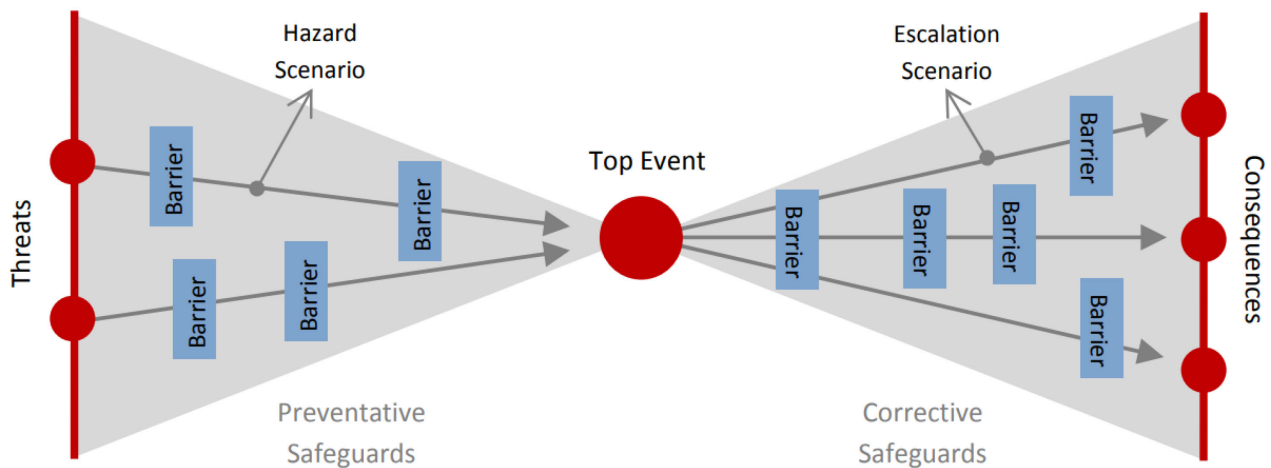


Fig. 2. A simplified bowtie showing the basic elements used to aid risk assessment.

The monitoring actions and technologies are documented in a risk-based Measurement, Monitoring and Verification (MMV) plan (Bourne et al., 2017; Dean & Tucker, 2017). MMV is a fundamental requirement for a storage permit in Europe and other countries with CCS regulations. In addition to fulfilling a regulatory requirement, the purpose of MMV is to verify containment and demonstrate conformance, i.e., provide evidence for understanding the long-term behaviour of the CO₂ plume.

It consists of a base case monitoring plan which includes a comprehensive baseline to establish the *status quo* before injection and a contingency monitoring plan to address alerts that cannot be resolved with the available information. MMV links risk assessment to timely corrective actions and provides data to investigate the credibility of stakeholder challenges. In countries where CCS regulations exist, MMV data and insights will be regularly presented to the responsible authorities, demonstrating evidence in support of containment and conformance (Fig. 3). MMV can be adapted over time aligned with the most current risk assessment of the CO₂ storage complex and ultimately enables industry to hand-over the site back to the responsible authorities.

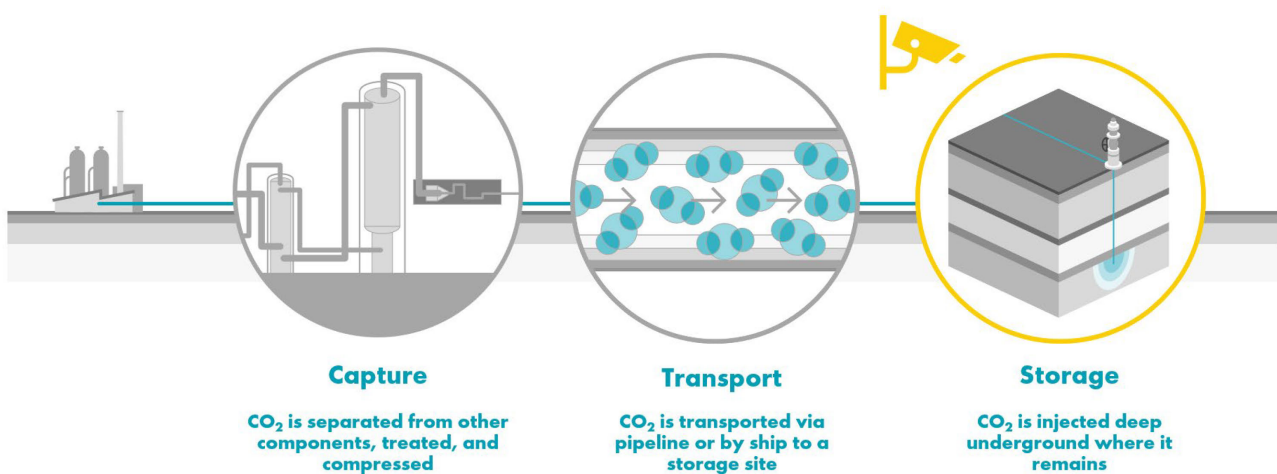


Fig. 3. MMV provides evidence for long-term storage of the injected CO₂ and is critical for safeguarding the entire CCS value chain. MMV data are used to demonstrate evidence in support of containment and conformance.

Well containment, fault, and top seal integrity assessments are all required to determine the feasibility of a site for permanent storage of CO₂. At Shell, we have developed workflows and tools to evaluate all credible, site-specific risks. These workflows focus on key elements such as the injection reservoir, wells, caprock, underburden, and interconnected fields. Detailed modeling studies are employed not only to qualify containment risks but also to define the operational strategy, which includes CO₂ injection locations, injection pressures, and variation of reservoir pressure/temperature.

This thorough subsurface characterization not only instills confidence in the safety and durability of CO₂ storage at the identified site but also serves as a prerequisite for obtaining storage permits. The methodology can be applied globally allowing a more efficient advancement for similar storage projects.

References

- Bourne, S, Crouch, S, Smith, M. 2014. A risk-based framework for measurement, monitoring and verification of the Quest CCS Project, Alberta, Canada. *International Journal of Greenhouse Gas Control* 26, 109-126. <http://dx.doi.org/10.1016/j.ijggc.2014.04.026>
- Dean, M, Tucker, O. 2017. A risk-based framework for Measurement, Monitoring and Verification (MMV) of the Goldeneye storage complex for the Peterhead CCS project, UK. *International Journal of Greenhouse Gas Control* 61, 1-15. <http://dx.doi.org/10.1016/j.ijggc.2017.03.014>
- De Ruijter, A, Guldenmund, F. 2014. The bowtie method: A review. *Safety Science* 88, 211-218. <https://doi.org/10.1016/j.ssci.2016.03.001>

Structural geology and fault seal studies in CO₂ storage evaluation

Christopher Wibberley^{1*}, Jade Dutilleul¹ and Richard Tozer¹

¹ TotalEnergies, CSTJF, Av. Larribau, 64018 Pau, France

* christopher.wibberley@totalenergies.com

1 Overview

Structural geology is critical to many aspects of CS (CO₂ storage) projects, from geometrical definition of traps through guided seismic interpretation, to fault sealing, compartmentalisation and faulted overburden integrity. From an oil and gas E&P company perspective, the learning curve as we move beyond hydrocarbon projects to CS includes an understanding of the differences in timescales of migration, trapping and leakage. Applications of structural geology to CS projects vary across the spectrum between exploration activities, development project studies and R&D, underpinned by a fundamental understanding of tectonic events and their timing including active tectonics.

2 Introduction

For regional exploration of storage aquifers, particularly in basin screening, structural geology starts at the basin-to-regional scale geodynamics and tectonic history before zooming in to particular potential storage complexes. Structural interpretation and fault mapping / ranking are required to constrain connected aquifer and containment limits. In CS development projects, interpretation of geological structure and fault analysis at the scale of the reservoir is essential for containment and maximum injection pressure evaluation, both in terms of fluid leakage and also if the faults could potentially be weak points to the mechanical integrity of the system. Propagation of the aquifer pressure front downwards within the fault zone into the basement or deeper units could increase the risk of induced seismicity which needs to be qualitatively risked before a more detailed geomechanical assessment.

3 Exploration activities

Structural geology in CS exploration, particularly for screening, starts with an understanding of the basin from regional-scale geodynamics and tectonic history before zooming in to specific potential storage complexes. Structural interpretation for connected aquifer limits - on which resource evaluations depend - is necessarily guided by the larger-scale regional picture, and this is especially the case in regions of poor data quality such as sparse 2D seismic. Fault mapping and ranking - in some cases aided by new machine learning techniques - is part of the regional screening work aiding the identification of structural containment limits (Fig. 1) and, along with regional pressure evaluations, is important for understanding aquifer continuity. In cases where boundary or overburden fault integrity is identified as an issue early in the process, structural geologists can also advise the geomechanics team on the tectonic stress regime along with fault geometrical and strength parameters to use in their models for maximum injection pressure evaluation.

Uncertainties in the extent of a connected aquifer can depend on a structural model. Accurately defined and structurally consistent fault boundaries are necessary for the geometrical definition of fault disconnections and connected aquifer limits. In terms of risks and geological probability of success, structural geology is an integral part of containment risking and identification of potential leakage pathways where boundary faults are critical. Risking injectivity may require an evaluation of fault compartmentalization, including estimation of sub-seismic fault density and impact on bulk permeability reduction.

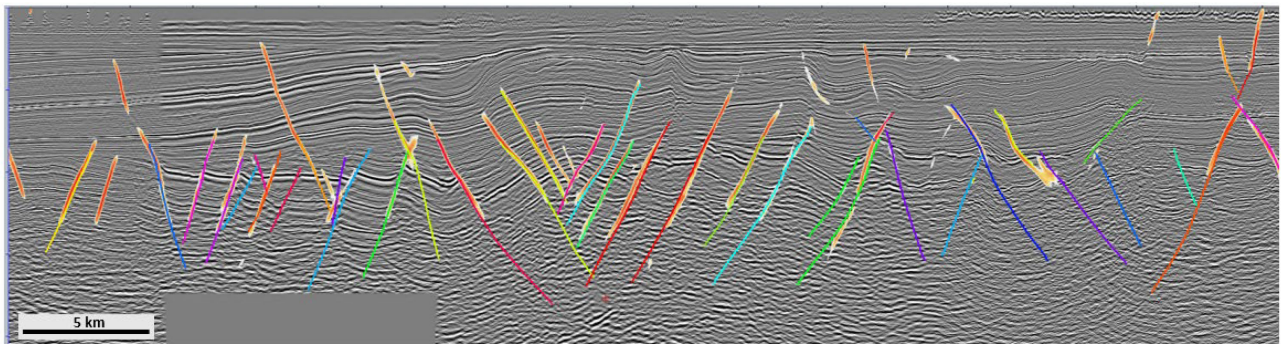


Fig. 1. Example of a fault probability cube from machine learning on seismic in regional fault mapping for a CS exploration project (from Edouard Le Garzic). Fault probability attribute colour scale is white to red, other colours are individually picked faults.

4 CS development projects

For containment, interpretation of geological structure and fault analysis is essential for CS development projects at the scale of the reservoir, both in terms of fluid leakage / sealing and also if the faults could potentially be weak points to the mechanical integrity of the system. For fault sealing, both the geometrical configuration of reservoir juxtapositions and/or disconnections needs to be considered, along with the fault composition (e.g., shale gouge permeability, or that CO₂ may dissolve carbonate-cemented faults), and calibration and prediction of the fault petrophysical properties for leakage (Fig. 2).

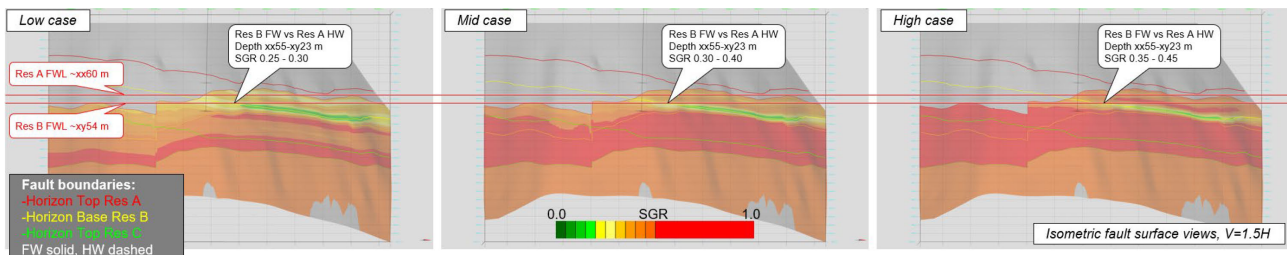


Fig. 2. Example of a fault reservoir juxtaposition analysis with fault property predictions (low – mid – high cases) for a CS development project in aquifers of a depleted gas field (by Richard Tozer).

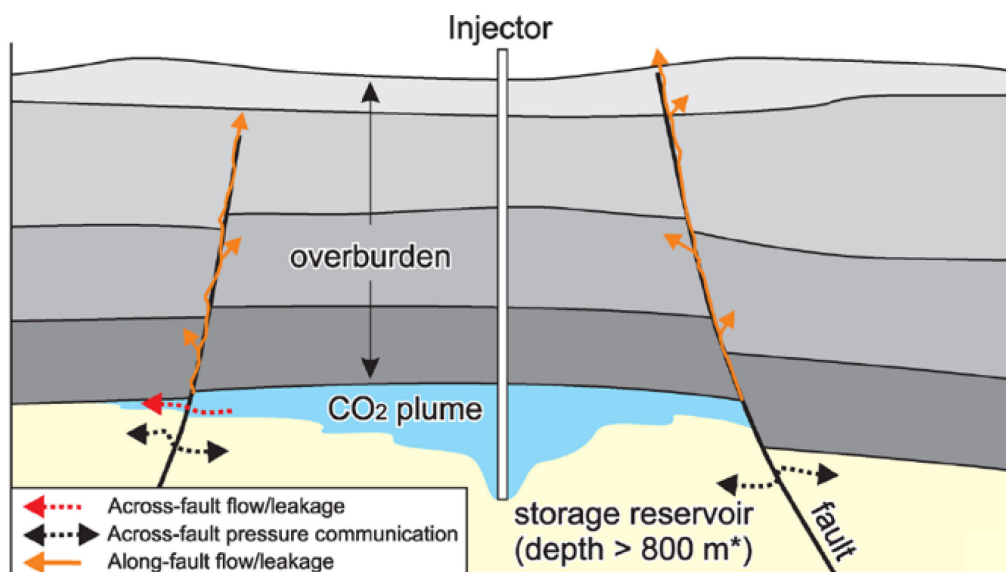


Fig. 3. Potential leakage pathways of a CO₂ plume from a fault-bounded trap. It is also important to consider the effect of the aquifer pressure front migrating ahead of the CO₂ plume (from Wu et al. 2022).

Whilst leakage across the fault may lead to propagation of the plume beyond the envisaged containment limits (Fig. 3), potential up-fault leakage into the overburden via a connected network could provide a different challenge in terms of surface or near-surface hazards. Furthermore, propagation of the aquifer pressure front downwards within the fault zone into the basement or deeper units could increase the risk of induced seismicity which needs to be qualitatively risked before a more detailed geomechanical assessment. Fault reactivation also represents a risk for CO₂ retention as it may lead to the migration of CO₂ into a shallower reservoir formation.

5 Some current and future research directions

Structural geology encompassed a wide range of scales for classic hydrocarbon exploration and development, and equally so for CS projects. Hence research also needs to cover scales across the scale spectrum from basin-wide to individual faults. From a naturalistic point of view, the questions we seek to answer include: what are the geological parameters most likely to make a fault susceptible to CO₂ leakage without mechanical reactivation, what can we learn from naturally-occurring CO₂ seeps via fault zones and how can we transform these findings into a predictive approach for CS exploration and ranking basins or different sectors in a basin in terms of leakage risk? (Fig. 4). How can the heritage of knowledge and data from the subsurface on hydrocarbon trapping against faults be leveraged to our advantage when we consider the different mechanisms and timescales coming into play for CO₂ trapping in a sequestration project?

Prediction of the maximum injection pressure that a fault can withstand, along with the behaviour of the fault as fluid pressure increases (leakage prior to fault slip? seismic slip versus aseismic creep?) are also subjects of research. These are more focused at contributing to geomechanical modelling of the coupled hydro-mechanical response of the faults to fluid pressure increases, from well-constrained laboratory tests on realistic materials as fault rock analogues, complemented by in-situ tests, to study the hydro-mechanical response of the fault and provide more realistic quantitative parameters such as frictional behaviour and permeability changes.

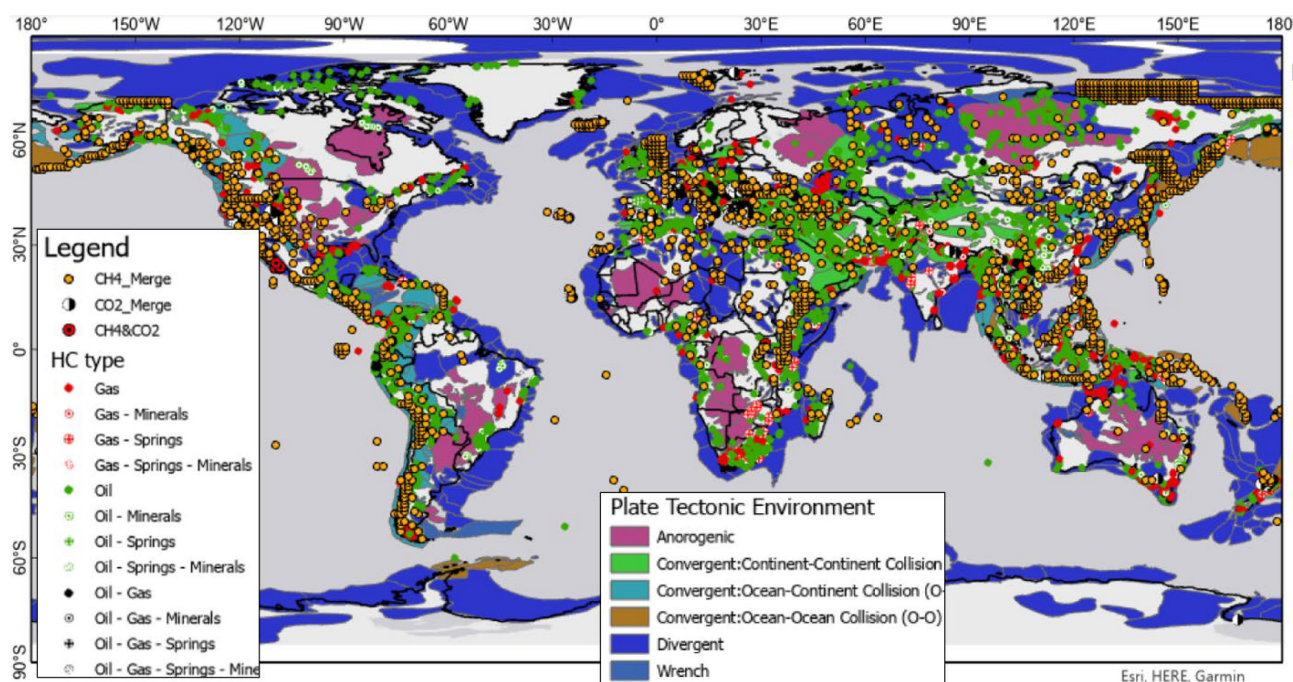


Fig. 4. Global distribution of CO₂ and CH₄ leakage overlying the sedimentary basins illustrating their different plate tectonic environments modified from GETECH (from Levendal et al. 2022).

6 Final statement and epilogue

As a final word, whilst the experience gained from subsurface structural geology, seals and traps coming from hydrocarbon exploration and production activities over the last few decades proves

valuable for new and on-going CS projects – from exploration of regional aquifers to injection into depleted fields - the differences must not be underestimated. Aspects in which structural geology, including faults and fracture analyses, become involved these differences are mainly in the trapping mechanisms and timescales of interest (intermediate between geological hydrocarbon trapping and field compartmentalization through the life of a producing field), but also in the overall nature of the project including leakage risking as a project goes to sanction phases.

References

- Levendal, T, Henry, P, Wibberley, C, Gassier, G, Boisson, M. 2022. A global review of natural leakage of gases: case studies representing geological factors conducive to vertical fluid flow. 16th International Conference on Greenhouse Gas Control Technologies, GHGT-16, October 2022, Lyon, France.
- Wu, L, Thorsen, R, Ottesen, S, Meneguolo, R, Hartvedt, K, Ringrose, P, Nazarian, B. 2022. Significance of fault seal in assessing CO₂ storage capacity and containment risks – an example from the Horda Platform, northern North Sea. *Pet. Geosci*, 28. <https://doi.org/10.1144/petgeo2020-102>

Current issues on gas in radwaste deep geological repositories: example of Cigeo (France)

Rémi de La Vaissière^{1*}, Jean Talandier², Christophe de Lesquen² and Gilles Armand¹

¹ ANDRA, Meuse/Haute-Marne Underground Research Laboratory, Bure, France

² ANDRA, Chatenay-Malabry, France

* remi.delavaissiere@andra.fr

1 Introduction

The French national radioactive waste management agency (Andra) has developed, through the last twenty years, an underground research laboratory (Meuse/Haute-Marne URL) to study a possible radioactive waste repository in a claystone formation. It is located in the Callovo-Oxfordian claystone (COx) encountered at a depth between 420 to 550 m near the village of Bure, in the eastern Paris Basin, France. The first objective of this URL was to characterize the confining properties of the clay through in situ hydrogeological tests, chemical measurements, diffusion experiments and the effect of excavation work on surrounding rock mass. One of the goals was to demonstrate that the construction and operation of a geological repository would not introduce pathways for radionuclides migration. The program evolved to address issues related to demonstration and optimization of various repository components (such as tunnels support, waste cells, seals, etc.). In this framework, understanding the migration of gas produced by corrosion of metals, microbial degradation and radiolysis of water within a Deep Geological Repository for radioactive waste (DGR) is of importance for assessing the performance and long-term evolution of the repository.

Once the gas solubility limit is reached and if the rate of gas production exceeds the rate of diffusion of dissolved gas in the pore-water of the host rock and the engineered barriers, a gas phase will form and accumulate until the associated pressure buildup is large enough to overcome the hydraulic pressure and the capillary resistance of the surrounding confining rock (two-phase flow). If the gas pressure increases and exceeds a threshold depending mainly on the stress state in the host rock, its tensile strength and the presence of heterogeneities, tensile (mode I) fractures are formed, in which the gas moves much more quickly. The evacuation capacity of the gas by the processes described above and the kinetic of the gas pressure rise control both the creation of tensile fractures and their extension. A particular transfer mode may appear for a pressure level lower than the fracturing pressure (Marschall et al., 2005). This mode results in the opening of localized paths (channels) through which the gas will flow. Referred to as dilatancy or microcracking, this phenomenon is contingent upon the material's local stress state and microstructure. Importantly, this mechanism is exclusive to porous clay-based and salt materials. Consequently, gas fracturing may damage the rock mass around and could affect the safety function of the host rock. It is important to note that due to the strength of the CO_x claystone and the depth of the main level of the Cigéo project, an excavation induced fractures network appears during the excavation around the openings depending of the orientation of the opening versus the major horizontal stress as observed at the Meuse/Haute-Marne URL (Armand et al., 2014), meaning that the principal process is more fracture propagation rather than fracture initiation.

To investigate these mechanisms, Andra has conducted two field-scale experiments to examine the mechanisms controlling gas entry and gas migration in the CO_x claystone at the URL. Those experiments, called PGZ1 and PGZ3, were designed to study the migration of nitrogen in the host rock using gas injection tests in packed off sections of boreholes.

In this extended abstract, we summarize the most recent observations obtained in the PGZ3 experiment but before we recall the main results obtained with PGZ1.

2 PGZ1 results

The data analysis of PGZ1 experiment and a two-phase flow modelling revealed that gas percolates first in the borehole damaged zone (BDZ) but that a small quantity of gas migrates through the intact host rock (de La Vaissière et al., 2014). Two distinct mechanisms for gas transfer were observed in this saturated porous medium. First, two-phase flow is controlled by the generalized Darcy equation for both liquid and gas phases. Second, at higher pressure levels rock fracturing is induced by gas with very low viscosity and high compressibility. In relation to the dilatant pathway phenomenon, on-site observations don't definitively confirm the occurrence of this specific gas transfer mode in clay media as observed on sample tests. The observations indicate that the threshold pressure for fracturing depends on the kinetics of pressure increase (de La Vaissière et al., 2019). The pressure range where both modes of gas transfer occur is relatively narrow for CO_x claystone.

An important point regarding safety issues for a radioactive waste repository project is that even if a gas fracture is generated, it will naturally close when the pressure drops, as evidenced by the permeability measurements made before and after gas fracturing.

3 PGZ3 experiment

To gain a better understanding of how gas injection kinetics affect the fracturing process, ongoing work involves investigating the influence of the BDZ, especially its elliptical shape, and the stress applied by packers at the borehole wall. A new experiment called PGZ3 with new boreholes and gas injection tests is being conducted to more comprehensively characterize the gas fracturing process, mainly at which gas pressure level fracture propagates.

3.1 PGZ3 layout

In the continuity of PGZ1 experiment, 9 boreholes have been drilled since 2020 and defined a new phase of the experiment called "PGZ3" (Tab. 1). Among these boreholes, six are horizontal, all sharing an identical length of approximately 35 meters. They are equipped with a multiple packer system designed to monitor water and gas pressures in five isolated intervals, using the same device as employed in the PGZ1 experiment. Each borehole's packers are 1.5 m in length, and the intervals are 1 meter long, except for interval #01, which is only 20 cm long at the dead end of the borehole.

Tab. 1. PGZ3 boreholes detailed

N° borehole	Completion installation	Length (m)	diameter (mm)	orientation vs sigma H
	MM/YYYY	m	mm	// or ⊥
PGZ1002	01/2020	35	76	⊥
PGZ1003	01/2020	35	76	//
PGZ3001	04/2021	35	76	//
PGZ3002	04/2021	35	76	⊥
PGZ3004	03/2022	35	146	⊥
PGZ3005	06/2023	32	76	vertical
PGZ3006	07/2023	37	76	vertical
PGZ3007	07/2023	49	76	vertical
PGZ5301	04/2021	35	146	//

The horizontal boreholes are oriented along principal horizontal stresses where the shape of the induced fractures network is different. The remaining three boreholes are vertical, with varying lengths. For each completion, two intervals are selected to perform a "fast" gas injection test (with an injection phase duration of a few hours) and a "slow" gas injection test (with an injection phase duration of several months). The objective is to reach the fracturing pressure of the rock. Prior to gas injection, water permeability tests are carried out in these intervals. The slow gas injection protocol will consist of several stages of gas injection at constant flow rate (RI) separated by pressure recovery phases.

3.2 Observations

Since 2020, several series of "fast" gas injections with high flow rates (~ 500 mLn/min) were carried out in the PGZ1002, PGZ1003 in the interval #04 and in interval #03 for PGZ5301 and are summarized in Tab. 2.

Tab. 2. Fast gas injection tests in PGZ3 boreholes

N° borehole	phases/date (DD/MM/YYYY)	gas flow rate (mLn/min)	max gas pressure (MPa)	new fracture formed	remarks
PGZ1002	RI1: 02/12/2020	500	12.96	Yes	Opening?
	RI2: 09/02/2021	500	14.54	Yes	Re-opening?
	RI3-RI4: 23- 24/04/2021	500	13.60	Yes	Re-opening
PGZ1003	RI1: 02/12/2020	500	14.28	Yes	Opening
	RI2: 09/02/2021	500	14.53	Yes	Re-opening
	RI3-RI4: 23- 24/04/2021	500	13.96	Yes	Re-opening
PGZ5301	Rix: 02/05/2022	5000	11.99	No	maximum flowmeter output

The measurements clearly indicate a leakage i.e., gas flow "along borehole" for all the boreholes (not presented). In the case of PGZ5301, gas leakage along the borehole was so great that it was not possible to go beyond 12 MPa with an injection rate at maximum capacity. For PGZ1002 and PGZ1003, preliminary analyses (pressure signature during pressure build-up and during the shut-in phase) seem to show that, despite this gas flow along the borehole at the interface, pressure responses are dominated not by the behavior of this interface, but by the mechanical behavior of the rock, with the existence of pre-existing fissure(s) corresponding to the excavation induced fractures in the damaged zone of the borehole. The evolution of pressure in the two tests is in fact similar to that observed in hydraulic fracturing. Further analysis is needed to better understand the orientation of the fracture(s) which was/ere created.

Several series of "slow" gas injections were carried out in different boreholes which are summarized in Tab. 3.

Tab. 3. Slow gas injection tests in PGZ3 boreholes

N° borehole	start/end (MM/YYYY)	interval	gas flow rate (mLn/min)	max gas pressure (MPa)	New fracture formed	remarks
PGZ1002	01/2023 -> 04/2023	02	50	13.77	Yes	equipressure in all intervals
PGZ1003	02/2023 -> 05/2023	02	12	12.33	No	impossible to increase pressure beyond this, even by increasing flow rate
PGZ3001	10/2021 -> 03/2023	02	6	13.10	Yes	Equipressure; except interval #05
PGZ3002	10/2021 -> 05/2023	02	120	10.61	No	maximum flowmeter output
PGZ5301	10/2021 -> 03/2022	04	60	8.36	No	packer failure: # PPK02 -> 06/10/2021 # PPK04 -> 30/03/2022

It systematically appears that gas percolates along the borehole either at the interface with the rock, or via the BDZ. This phenomenon was not observed in the tests carried out in the PGZ1 boreholes. All the boreholes drilled were air-drilled, and the horizontal boreholes had numerous breakouts. These breakouts mean that the borehole wall is not circular, making contact between the packer gum and the rock imperfect. This poor contact is not visible when the CO_x claystone is resaturated due to the self-sealing capacity of the claystone. However, as soon as gas is injected, this hydraulic

clogging disappears, allowing the gas to percolate along the borehole. This observation is nevertheless very interesting, because if we consider a borehole as a scale model of a DGR gallery, and the packers represent a perfectly sealed zone, gas can still percolate at the interfaces/BDZ regardless of the gas permeability of the seal itself.

For three boreholes, due to the leakage achieving the fracturing pressure was not possible despite efforts to increase the pressure. In the case of borehole PZG5301, the initial program was altered to facilitate a rapid gas injection rate in interval #03 due to the loss of one packer in interval #04. In PGZ3001, equipressure is evident in intervals #01 to #04 since October 2022 (Fig. 1). After reaching a pressure of 13.1 MPa, it proved impossible to elevate the pressure beyond 12.6 MPa. Inflections in the pressure measurements emerged around 12.3–12.4 MPa, indicating fracture reopening and closing. The presence of leaks along the borehole complicates data analysis.

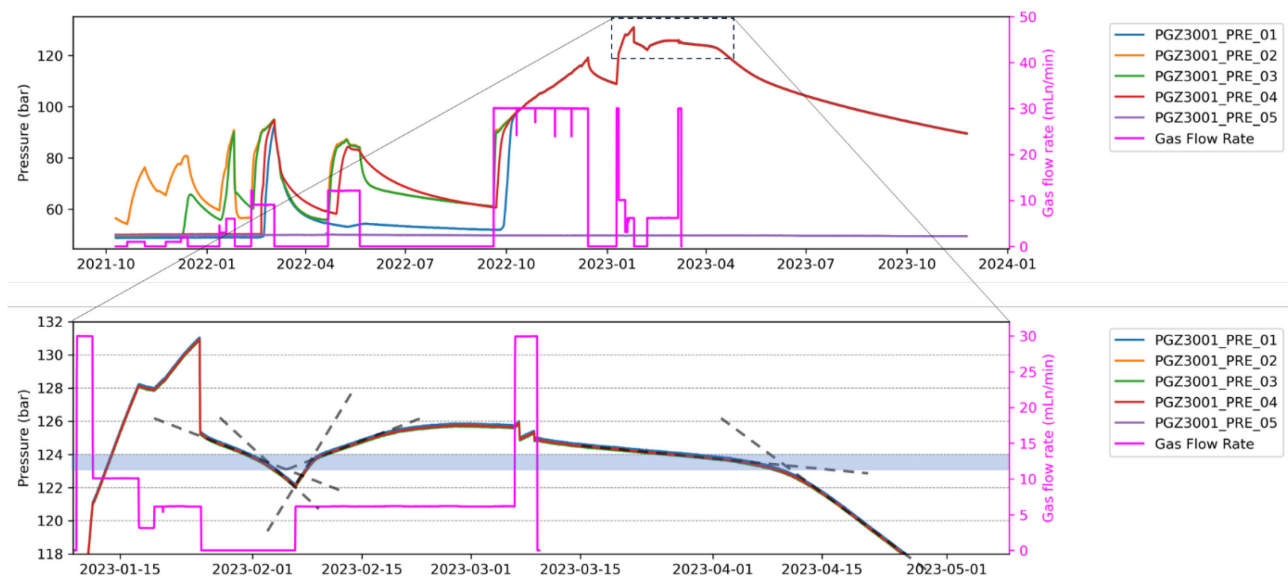


Fig. 1. Pressure and gas flow measurements in PGZ3001 borehole during slow gas injection test. Bottom: zoom at high pressure level.

4 Conclusion

The results from PGZ1 and the ongoing PGZ3 experiment highlight the nuanced factors influencing gas migration, including borehole conditions and injection kinetics. An important finding reveals the significance of interfaces where gas can circulate, providing essential knowledge for optimizing repository design and ensuring the long-term integrity of DGR in clay formations. However, it is crucial to emphasize that further detailed data analysis is warranted to enhance our understanding of the repository's long-term performance.

References

- Armand, G., Leveau, F., Nussbaum, C., de La Vaissière, R., Noiret, A., Jaeggi, D., ... & Righini, C. (2014). Geometry and properties of the excavation-induced fractures at the Meuse/Haute-Marne URL drifts. *Rock mechanics and rock engineering*, 47(1), 21–41.
- de La Vaissière, R., Gerard, P., Radu, J. P., Charlier, R., Collin, F., Granet, S., ... & Helmlinger, B. (2014). Gas injection test in the Callovo-Oxfordian claystone: data analysis and numerical modelling. Geological Society, London, Special Publications, 400(1), 427-441.
- Ajayi, T., Gomes, JS, Bera, A. 2019. A review of CO₂ storage in geological formations emphasizing modeling, monitoring and capacity estimation approaches. *Pet. Sci.* 16, 1028–1063.
- de La Vaissière, R., Talandier, J., Armand, G., Vu, M. N., & Cornet, F. H. (2019, June). From two-phase flow to gas fracturing into Callovo-oxfordian claystone. In *ARMA US Rock Mechanics/Geomechanics Symposium* (pp. ARMA-2019). ARMA.
- Marschall, P., Horseman, S., & Gimmi, T. (2005). Characterisation of gas transport properties of the Opalinus Clay, a potential host rock formation for radioactive waste disposal. *Oil & gas science and technology*, 60(1), 121–139.

Microbial hydrogen transformation in the deep subsurface

Rizlan Bernier-Latmani^{1*}, Camille Rolland¹ and Olivier Leupin²

¹ Ecole Polytechnique Fédérale de Lausanne, EPFL, Lausanne, Switzerland

² National Cooperative for the Disposal of Radioactive Waste, Wetingen, Switzerland

* rizlan.bernier-latmani@epfl.ch

Abstract

Hydrogen (H₂) is present in the subsurface either due to natural processes (e.g., serpentinization), to its storage as an energy source, or to its formation *in situ* through, for instance, nuclear waste storage. However, in the anoxic subsurface, H₂ serves as a major electron donor for microorganisms, resulting in microbial processes such as sulfate reduction (if sulfate is present) and methane production (if CO₂ or other substrates are available). There are several engineering applications for which a thorough understanding and ability to control the factors influencing the extent and the rate of H₂-dependent metabolism in the subsurface is critical.

One is nuclear waste disposal because of the production of large amount of H₂ from anoxic corrosion of steel. In the past 10 years, several studies have considered the microbial transformation of H₂ in Opalinus Clay (the rock formation chosen for the storage of nuclear waste) at the Mont Terri Underground Rock Laboratory (URL). The first was to evidence the potential for H₂ consumption by microorganisms in a borehole (Bagnoud et al., 2016a, 2016b) (Fig. 1). H₂ was consumed primarily through the reduction of aqueous sulfate. The next experiment investigated H₂ consumption in the backfill considered for the repository (sand/bentonite) and showed both sulfate reduction and methanogenesis (Rolland et al., 2024). Finally, an ongoing experiment shows the evolution of the gas phase in the same backfill solid phase and demonstrates the consumption of H₂ and production of hydrogen sulfide and methane (see abstract #507 of this volume), demonstrating the occurrence of several concurrent hydrogenotrophic microbial metabolisms.

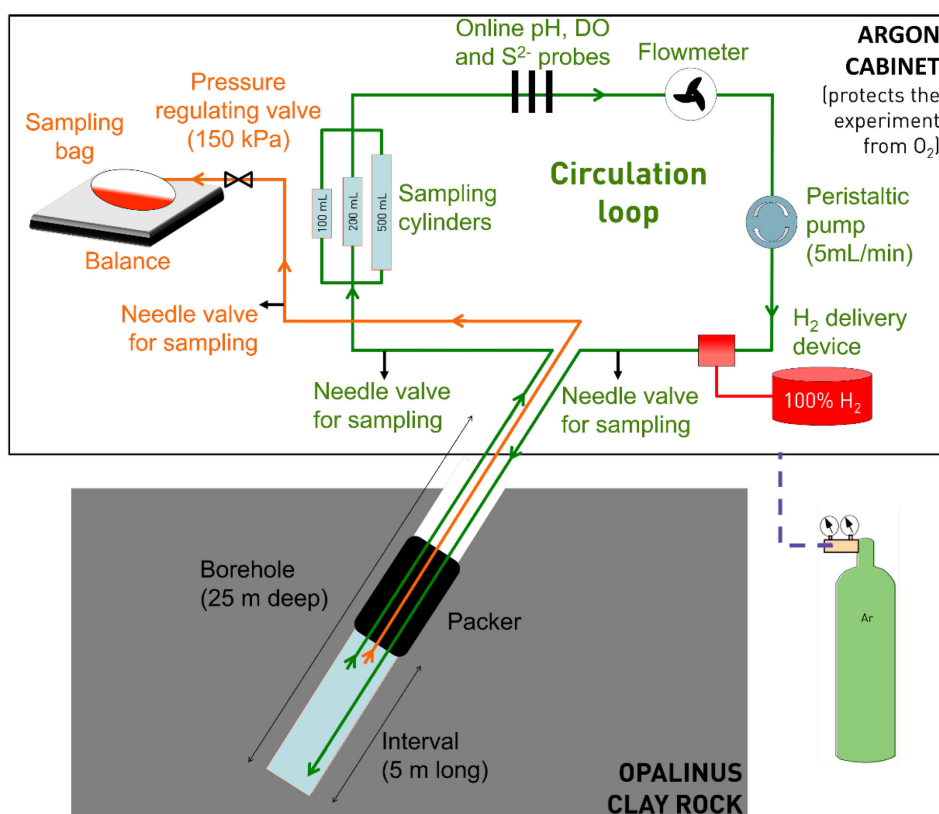


Fig. 1. Set-up of experiment evaluating microbial activity upon the injection of H₂ into the borehole.

A second emerging application is the biological conversion of H_2 and CO_2 into methane for storage and later injection into the natural gas grid (Rüdisüli et al., 2023). Here, we present experimental approaches to characterize H_2 -dependent microbial activity in a reservoir rock and controls on its rate and extent. The approach entails a proof-of-concept experiment at Mont Terri URL to manipulate the microbial community and optimize the rate of formation of methane from H_2 and CO_2 for engineered subsurface biological methanation (Fig. 2).

Thus, we propose to leverage the microbial transformation of H_2 in the subsurface for engineering applications by building on the fundamental scientific investigations that have taken place in the past decade.

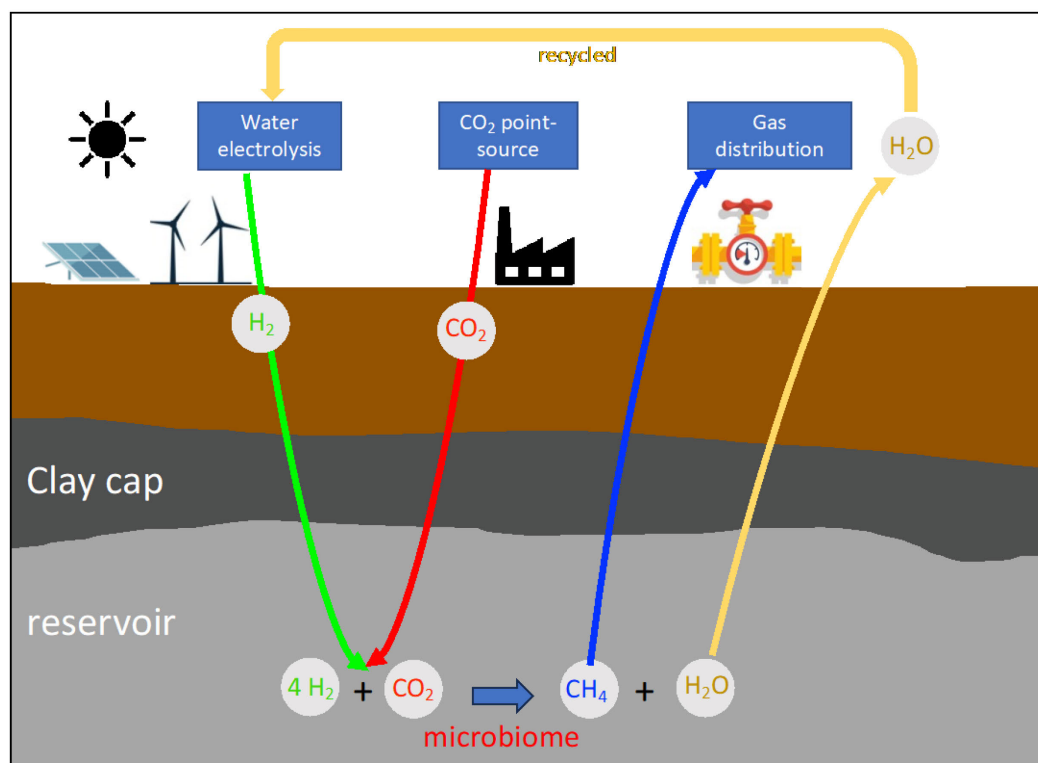


Fig. 2. Concept for underground methanation.

References

- Bagnoud, A., Chourey, K., Hettich, R.L., de Bruijn, I., Andersson, A.F., Leupin, O.X., et al. 2016a. Reconstructing a hydrogen-driven microbial metabolic network in Opalinus Clay rock. *Nat Commun* 7, 12770. <https://doi.org/10.1038/ncomms12770>
- Bagnoud, A., Leupin, O., Schwyn, B., and Bernier-Latmani, R. 2016b. Rates of microbial hydrogen oxidation and sulfate reduction in Opalinus Clay rock. *Applied Geochemistry* 72, 42–50. <https://doi.org/10.1016/j.apgeochem.2016.06.011>
- Rolland, C., Burzan, N., Leupin, O.X., Boylan, A.A., Fruttschi, M., Wang, S., Jacquemin, N. and Bernier-Latmani, R. 2024. Microbial hydrogen sinks in the sand-bentonite backfill material for a radioactive waste deep geological disposal. Submitted.
- Rüdisüli, M., Mutschler, R., Sinan L. Teske, S.L., Sidler, D., van den Heuvel, D., Diamond, L.W., Orehoung, K., Eggimann, S. 2023. Potential of renewable surplus electricity for power-to-gas and geo-methanation in Switzerland. *International Journal of hydrogen energy*. 48, 14527–14542.

Exploration for natural hydrogen

Eric C. Gaucher^{1*}

¹ Lavoisier H₂ Geoconsult

* eric.gaucher@lavoisierh2.com

Abstract

Hydrogen will play a key role in managing the transition from fossil fuels to renewable energy sources. Today, hydrogen is almost exclusively manufactured, which consumes a lot of energy. Natural hydrogen, which has been explored in various geological sites around the world, could be an additional source to cover the huge recent and future human demand. We will describe several cases showing the research and industrial efforts done for this exploration. Production potential also exists in the Alps. We'll be taking a closer look at effective exploration strategies in the Alps.

Molecular scale understanding of gas transport in clays

Sergey Churakov^{1,2}, Jerry Owusu^{1,2}, Konstantinos Karalis², Athanasios Mocos¹ & Nikolaos Prasianakis¹

¹ Laboratory for Waste Management, Paul Scherrer Institute, Villigen-PS, Switzerland

² Institute of Geology, University of Berne, Switzerland

* sergey.churakov@psi.ch

Abstract

Molecular scale mechanism of gas transport in clay rich materials was investigated by Molecular Dynamics (MD), Random Walk and Lattice Boltzmann simulations methods at partially and fully saturated conditions as function of pore size distribution and temperature. Analysing the molecular scale diffusion trajectories of Ar, CH₄, CO₂, H₂ and He, it was possible to derive a general relationship between the molecular diffusivity, pore size and effective radius of gas molecules at saturated conditions. Furthermore, taking into account the geometric factor available from diffusion studies with tritiated water in various rocks, a semi-empirical relationship for diffusivity of gases in clay rocks has been formulated based on their effective radius or, if available, self-diffusion of gas tracer in bulk water. For the first time, gas transport in partially saturated clay pores and the partition coefficient of gas molecules between low density, gas rich, and high density, water rich phase were derived by equilibrium and non-equilibrium molecular dynamics simulation. Interestingly, the presence of dissolved gas leads to an increase of the swelling pressure, caused by higher gas solubility under elevated pressure. The nonequilibrium molecular dynamics simulations conducted for partially saturated clay pores provide the viscosity and slip length for advective transport in gas, including surface absorbed water films, which are important parameters in macroscopic and pore scale gas transport modelling. Mechanistic insight into gas transport obtained by molecular simulations provides information about the condition under which the transition between molecular (bulk-like) and Knudsen (surface collision controlled) diffusion of gas in confined space sets on.

1 Introduction

In low-permeability, saturated clays, the primary mode of gas transport is through the diffusion of dissolved gas in the porewater, when the gas generation rate is low. If the rate of gas generation exceeds the diffusive flux, free gas phase can form in the large pores. Under such conditions, gas transport mechanism may transition from diffusion of dissolved gases in liquid phase to the gas diffusion in partially de-saturated gas filled pores. It is crucial to understand and account for these phenomena as they can have significant implications on the safety of geological repositories and caprock integrity.

Within EURAD-GAS project, molecular and pore scale simulations were applied to gain a better understanding of diffusion in porous clay media. For that, two kinds of simulations were performed: molecular dynamics and pore-scale simulations. The molecular dynamics simulations investigate diffusion within small pores (e.g., few nanometers), while the pore scale simulation examines the effect of porosity, connectivity, and arrangement of particles on microscopic diffusion (e.g., hundreds of nanometers). The microscopic transport parameters obtained from the pore scale simulation can be used in other models at the continuum scale. To obtain a more comprehensive understanding of diffusion in porous clay media, an upscaling method is applied in pore-scale simulations, which incorporates mechanisms occurring below the Representative Elementary Volume. Such an approach considers both the pore-scale properties and complexities, as well as the local clay interaction properties (i.e., the local diffusive coefficients obtained from molecular dynamics simulations).

The successful validation of this approach for water diffusivity was achieved through a comparison of the 3D simulations of water transport in complex porous geometry obtained by molecular dynamics simulations (including full interatomic interactions) with the upscaling approach, using random

walk simulation of non-interacting particles and lattice-based representation of pores and clay particles (Churakov & Gimmi, 2011). Equilibrium molecular dynamics simulation was applied to understand the diffusion mechanism of dissolved gases in a smectite clay nanopore. The influence of pore size, gas species, and temperature on the molecular scale diffusive transport was further explored. Equilibrium molecular dynamics was used to understand the diffusion of gases in a partially saturated smectite nanopores and how gas partitions between the gas-rich phase and the water phase in the nanopore. Furthermore, non-equilibrium molecular dynamics was applied to investigate the dynamics of viscous gas flow in the nanopore. It has been also shown that the dissolution of solutes in saturated porous clay materials can change the swelling behaviour of the clay materials, which, in turn, can change the porosity and thereby change the transport properties. An upscaling approach was developed in which sample scale effective diffusivity of gas molecules were obtained by Random Walk and lattice Boltzmann simulation methods based on an explicit model for clay particle arrangement and pore size dependent diffusion coefficients obtained by molecular dynamics simulations.

2 Diffusion of gases in fully saturated conditions

Equilibrium MD simulations were conducted for saturated montmorillonite pores at different pore sizes, temperature and concentrations of gases (Owusu et al., 2022). To investigate the dependence of the mobility of gases in Na-Montmorillonite (Na-MMT) interlayer nanopores on pore size and temperature, a series of simulations were performed for 5 gases (He, H₂, CO₂, Ar, CH₄) at 7 different nanopore sizes ranging from 1 to 3 nm. Simulations were performed at temperatures of 300, 350, and 375 K (see Fig. 1a,b). Na-MMT was used as a proxy model for clays in which gas transport is controlled by 2-20 nm sized intergranular pores.

An increase in the diffusion coefficient (D) of gases with increasing temperature is observed in the clay nanopore. This behaviour is expected and consistent with experimental and theoretical studies. However, for different pore sizes, the D value of the gases increases at different rates. For example, when the temperature increases from 300 to 350 K, the D value for He gas increases from 2.59×10^{-9} to 5.18×10^{-9} m²/s for a pore size of 1.0 nm, an increase of about 2 times, while it is only about 1.5 times higher for a pore size of 2.6 nm (increase from 7.58×10^{-9} to 11.60×10^{-9} m²/s). It can be concluded that the diffusion coefficient of gases confined in Na-MMT increases with increasing pore size (see Fig. 1a) and shows different temperature-pore size dependence. This relationship is also supported by several previous studies, where for example, Wang et al. (2018) reported in their MD simulation that the self-diffusion of CH₄ in Ca-MMT increases with increasing interlayer pore size in the range of 1.8 - 50 nm.

To better understand the influence of clay surface on the gas migration, the diffusion coefficients of the gas in the clay layer nanopore were normalized by the diffusion coefficient of the gas in the bulk water (D₀) predicted by the MD simulation. The curves in Fig. 1a represent an average value for all temperatures and follows the conclusion of Wang et al. (2016), that the ratio at different temperatures almost converges to a single curve as a function of pore spacing, indicating an empirical correlation. Due to the limited transport space, diffusion of entrapped species through the clay layers is hindered. Therefore, the diffusion coefficients of gases are slower under confinement than in bulk due to the specific interaction between the solvent, gas molecules and the clay surface. As the size of the nanopores increases, the D of the gases shows a monotonically increasing trend and asymptotically approaches the value of the bulk. However, this behaviour is different for each gas. H₂ approaches the bulk value faster than, for example, CH₄. This highlights that the effect of confinement is different for different gases. The regression fit of apparent diffusion coefficient in Boom clay (Fig. 1c,d) could be obtained given the formula:

$$D_a = \frac{D_0}{G} \left(1 - \frac{k_c}{h_{av}} \right) \quad \text{Eq. (1)}$$

where D_a is the apparent diffusion coefficient of the gas, D₀ is the diffusion coefficient of the gas in bulk water, G is the geometric factor, k_c is the interaction parameter between the fluid and the solid

and h_{av} average pore width. In most diffusion experiments, a single effective or pore diffusion coefficient is given, which is an average sum over all pore sizes. These simple formulations, such as Eq. (1) are useful for testing theories and explaining experimental results by providing a microscopic view. In addition, they provide a basis for easy incorporation into an up-scaling framework, such as Lattice Boltzmann or Random Walk methods, which can be advantageous in linking nanoscale simulations with macroscale measurements.

3 Diffusion of gases in partially saturated conditions

Equilibrium and non-equilibrium molecular dynamics simulations reported below were conducted for partially saturated montmorillonite pores at different pore size distribution, temperature and concentrations of gases and published in Owusu et al. (2023). The self-diffusion coefficient of gas molecules in the gas phase at temperatures of 300 K as a function of the gas-filled pore width, normalized to the diffusion coefficient in the bulk (D_0) was calculated and, is shown in Fig. 1e,f.

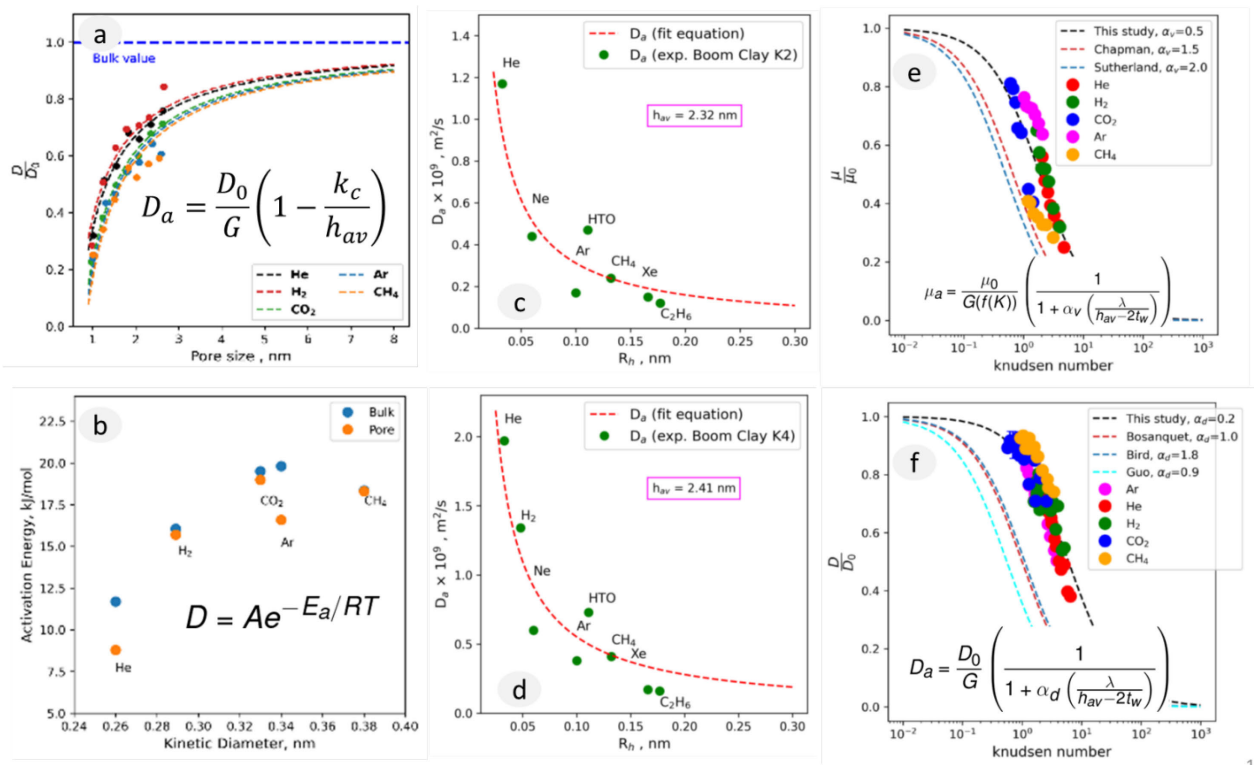


Fig. 1. Molecular scale and effective transport parameters of Ar, He, H₂, CO₂ and CH₄ obtained by molecular dynamics simulations (Owusu et al., 2022; Owusu et al., 2023), where D_0 - bulk diffusion coefficient, G - geometric factor, D_a - apparent diffusion coefficient, h_{av} - average pore width, K_c - surface interaction parameter, D_p - pore diffusion coefficient, R_h – hydrodynamic radius, α_d - Bosanquet parameter, t_w - water film thickness, μ_0 bulk dynamic viscosity, μ_a - apparent dynamic viscosity, E_a and A – activation energy and preexponential factor, T – temperature, R – thermodynamic gas constant. Experimental data for gas diffusivity are taken from (Jacops et al., 2017).

The results show that the diffusion coefficient increase with the interlayer pore size and asymptotically converges towards the value obtained in the bulk state. The results showed that He gas specifically, was strongly affected by confinement compared to other gases, possibly due to the so-called Knudsen effects. To investigate this, the mean free path of the gas molecules was calculated based on the collisions in the trajectories of the molecular dynamics simulations and compared with the calculations of the mean free path performed with kinetic theory, which agreed well.

The Knudsen number was calculated from the mean free path and the gas-filled pore sizes. A diagram showing the relationship between the diffusion coefficient and the Knudsen number is shown

in Fig. 1(right). A mathematical equation developed from the graph after the Bosanquet approximation (Pollard & Present, 1948; Krishna & van Baten, 2012) is given as:

$$\frac{D}{D_0} = \frac{1}{1 + \alpha_d \left(\frac{\lambda}{h - 2t_w} \right)} \quad \text{Eq. (2)}$$

where D_0 represents the bulk diffusion coefficient in the gas phase at 12 MPa, λ denotes the mean free path of the gas at 12 MPa, h is the width of the pore, t_w is the thickness of the adsorbed water film, which varies with the degree of saturation. The parameter α_d is the Bosanquet correction parameter obtained through fitting and has a value of 0.2. Based on the work of Yin et al. (2019), the identification of three gas diffusion regimes can be made in a porous media, determined by the local Knudsen number. The regimes are characterized by K_n values of ≤ 0.1 , $0.1 < K_n < 10$, and $K_n \geq 10$. In the case of molecular diffusion ($K_n \leq 0.1$), intermolecular collisions are dominant. When Knudsen diffusion occurs ($K_n \geq 10$), the dominant collisions are between molecules and a solid wall. In the case of transition diffusion ($0.1 < K_n < 10$), significant intermolecular collisions and collisions between molecules and the solid wall occur. The Knudsen number ranges from 0.6 to 6 in the aforementioned simulations, indicating that diffusion is in the transition regime, and not purely in the molecular diffusion regime. These effects thus have to be taken into account in the gas transport simulations.

References

- Churakov, S. V. and Gimmi, T. (2011). Up-scaling of molecular diffusion coefficients in clays: A two-step approach. *The Journal of Physical Chemistry C*, 115(14):6703–6714.
- Jacops, E., Maes, N., Bruggeman, C., and Grade, A. (2017). Measuring diffusion coefficients of dissolved He and Ar in three potential clay host formations: Boom clay, Callovo-Oxfordian clay and Opalinus Clay. Geological Society, London, Special Publications, 443(1):349–360.
- Krishna, R. and van Baten, J. M. (2012). Investigating the validity of the bosanquet formula for estimation of diffusivities in mesopores. *Chemical engineering science*, 69(1):684–688.
- Owusu, JP; Karalis, K; Prasianakis NP; Churakov, SV (2022) Mobility of Dissolved Gases in Smec-tites under Saturated Conditions: Effects of Pore Size, Gas Types, Temperature, and Surface Inter-action. *JPC* 126, 17441-17455.
- Owusu, JP; Karalis, K; Prasianakis NP; Churakov, SV (2023) Diffusion and Gas Flow Dynamics in Partially Saturated Smectites *JPC* 127, pp.14425–14438.
- Pollard, W. and Present, R. D. (1948). On gaseous self-diffusion in long capillary tubes. *Physical Review*, 73(7):762.
- Yin, Y., Qu, Z., and Zhang, J. (2019). Multiple diffusion mechanisms of shale gas in nanoporous organic matter predicted by the local diffusivity lattice boltzmann model. *International Journal of Heat and Mass Transfer*, 143:118571.
- Wang, S., Feng, Q., Zha, M., Javadpour, F., and Hu, Q. (2018). Supercritical methane diffusion in shale nanopores: effects of pressure, mineral types, and moisture content. *Energy & fuels*, 32(1):169–180.
- Wang, S., Javadpour, F., and Feng, Q. (2016). Molecular dynamics simulations of oil transport through inorganic nanopores in shale. *Fuel*, 171:74–86.

CO₂ sealing capacity of sandy and shaly Opalinus Clay

Hyunbin Kim^{1*}, Victor Vilarrasa² and Roman Makhnenko¹

¹ Department of Civil and Environmental Engineering, University of Illinois at Urbana-Champaign, Urbana, IL, USA.

² Global Change Research Group, IMEDEA, CSIC-UIB, Esporles, Spain

* hyunbin3@illinois.edu

Abstract

Successful geologic CO₂ storage in saline aquifers necessitates the presence of caprock formation with low permeability and high CO₂ breakthrough pressure. The sealing capacity of a caprock can be compromised if heterogeneities are present in the formation, as well as by other factors such as structure disturbance and deformation due to changes in stress and temperature. The CO₂ Long-term Periodic Injection Experiment (CO₂LPIE) at the Mont Terri Underground Rock Laboratory, Switzerland, aims to quantify the advance of CO₂ in Opalinus Clay, an anisotropic and heterogeneous clay-rich rock. In this study, the laboratory-scale tests of sandy and shaly facies of Opalinus Clay (OPA) are conducted to evaluate their sealing capacity. After reaching full saturation with brine, the permeability and CO₂ breakthrough pressure are measured. The sandy specimen exhibits a permeability several times higher than that of the shaly specimen, mainly due to its larger porosity and dominant pore size. Since the pore space of sandy OPA contains more macropores, its breakthrough pressure is lower than that of shaly OPA (4 and 9 MPa, respectively). Methods involving the indirect evaluation of capillary pressure (e.g., porosimetry) are explored and indicate a limited implication for proper characterization of the effect of mineralogy and confinement. This suggests that the direct measurements under representative in-situ conditions should be utilized for Opalinus Clay formation.

1 Introduction

Geologic carbon dioxide (CO₂) storage in deep saline aquifers requires presence of a porous reservoir (e.g., sandstone or limestone) conformably overlain by a low-permeability caprock formation with a high capillary entry pressure. The sealing capacity of a caprock is commonly denoted as the breakthrough pressure, which represents the maximum CO₂ column height that can be retained in the underlying reservoir before CO₂ entry occurs. It could be compromised by various processes, including the reactivation of faults, geochemical reactions between fluids and solid, thermo-hydro-mechanical effects on deformation, and the presence of preferential pathways (Rutqvist and Tsang, 2002). Identifying the role of mineralogical composition in sealing capacity thus allows for a comprehensive understanding of the serviceability of the CO₂ storage for a geologic timescale.

To achieve this understanding, field experiments in rock laboratories can be invaluable. In particular, the CO₂ Long-term Periodic Injection Experiment (CO₂LPIE) project aims to investigate the sealing capacity of a caprock in response to direct CO₂ injection at the decameter scale. CO₂LPIE will be conducted in a highly monitored environment at the Mont Terri Underground Rock Laboratory, Switzerland, where Opalinus Clay (OPA) serves as a representative caprock for CO₂ storage (Vilarrasa and Makhnenko, 2017; Sciandra et al., 2022). This stiff overconsolidated shale is divided into several facies that are inconsistent across the region. Sandy and shaly facies of OPA specimens from different galleries are tested in this study. The grain size distributions indicate that shaly OPA contains more clay-size particles (60 %) and less silt-size particles (35 %) compared to sandy OPA (40 % and 50 %, respectively). Mercury intrusion porosimetry (MIP) is utilized to evaluate the pore structure of sandy and shaly OPA (Fig. 1a). The measured dominant pore size is 28 nm for sandy and 20 nm for shaly OPA, comparable to other claystones (~ 10 nm, Dewhurst et al., 1999; Espinoza and Santamaria, 2017). The effective porosity ϕ is calculated to be 0.13 for sandy and 0.12 for shaly OPA.

The intrinsic (single-phase) permeability of sandy and shaly facies of OPA is directly measured using a core flooding system under different effective mean stresses. The breakthrough pressure of sandy and shaly OPA is then assessed in the same system under a given effective mean stress. The CO₂

breakthrough pressure is also determined through an indirect method based on MIP data and capillary properties in the water-CO₂-rock system. The comparison between the two methods sheds light on any disparities in the breakthrough pressure values.

2 Methodology

The tests conducted in the core flooding system involve a cylindrical specimen with a diameter of 50 mm and length of 95–100 mm. A membrane envelops the specimen to prevent confining fluid (hydraulic oil) from infiltrating it, and the lateral confining pressure is applied using a pressure controller. The passive resistant axial stress arises from the constraint of axial deformation parallel to the flow direction. Before the test, two syringe pumps filled with water are connected to the upstream and downstream sides to achieve full saturation using the back-pressure technique (Black and Lee, 1973). Once the specimen is fully saturated, a constant pore pressure gradient is initially implemented for the permeability tests under different effective mean stresses. During the permeability test, the fluid flow is constrained in the direction perpendicular to the bedding planes. For the breakthrough test, the upstream pump is filled with liquid CO₂ and its pressure increases in a stepwise manner until the differential pressure Δp_f between CO₂ and water overcomes the breakthrough pressure and the continuous CO₂ flow is achieved (called the “stepwise method”). The upstream CO₂ volume is monitored during measurements to elucidate the onset of the breakthrough process.

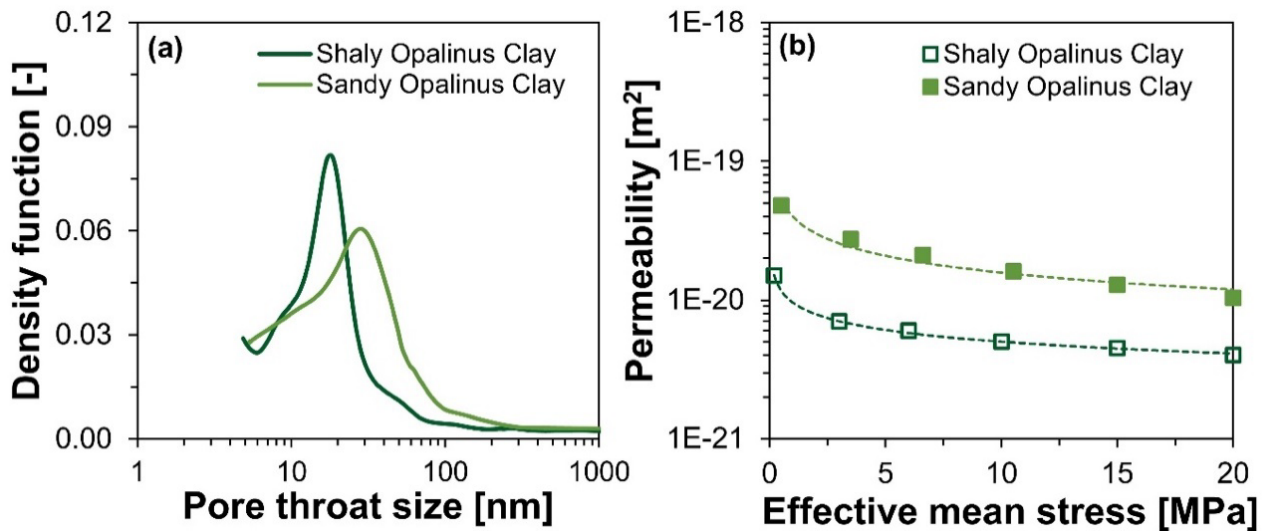


Fig. 1. Sandy vs. shaly Opalinus Clay: (a) pore size distribution and (b) stress-dependent permeability.

The direct experimental assessment of breakthrough pressure has the advantage of replicating representative in-situ conditions in the laboratory, but it requires intricate and time-consuming procedures. As an alternative, the indirect method is widely accepted for estimating the capillary pressure ψ curve based on the mercury injection pressure p_{Hg} -fluid saturation relationship obtained from the MIP, along with the capillary properties of a given wetting-nonwetting fluid-rock system (Equation 1). The indirect method should be used with caution since the MIP does not account for in-situ conditions that may influence the breakthrough pressure. In this approach, water saturation is assumed to be equivalent to mercury vapor (wetting fluid) saturation at a given mercury (nonwetting fluid) pressure.

$$\psi = -\frac{\gamma \cos \theta}{\gamma_{Hg} \cos \theta_{Hg}} p_{Hg} \quad \text{Eq. (1)}$$

Here θ_{Hg} is the contact angle of mercury with solid surface (140 °) and γ_{Hg} is the surface tension of mercury in contact with its vapor (0.48 Nm⁻¹). The capillary properties are taken as $\gamma = 0.03$ Nm⁻¹ and $\theta = 30$ ° under $p_f = 8$ MPa and $T = 22$ °C – the same conditions as for the direct measurements (Espinoza and Santamaria, 2010).

3 Results and discussion

Fig. 1b depicts the intrinsic permeability k of sandy and shaly facies of OPA as a function of the effective mean stress P' . In both cases, k exhibits an exponential decrease with P' . Sandy OPA demonstrates permeability 3–4 times higher than that of the shaly counterpart mainly due to its larger porosity and dominant size, and lower specific surface area. The permeability of both OPA specimens falls within the same order of magnitude ($\sim 10^{-20}$ m²) – similar to that for shales with $\phi \approx 0.1$ (Neuzil, 2019), satisfying the criterion for a potential caprock for geologic CO₂ storage (Dewhurst et al., 1999).

Fig. 2 displays the results of the CO₂ breakthrough pressure test with sandy OPA specimen. The accuracy of the direct method is associated with the increment in upstream CO₂ pressure (Ito et al., 2011), such that a 1 MPa/step is applied in this study. The time interval between two pressure steps is approximately 2 days to ensure pore pressure equilibrium inside the specimen. The tests in the core flooding system are conducted under P' higher than the in-situ value of 2.2 MPa (Martin and Lanyon, 2003) to effectively prevent extremely low normal stress acting in the flow direction and generation of new fractures.

Under the differential pressure Δp_f of 1 and 2 MPa, CO₂ comes in contact with the specimen but does not pass through it (Fig. 2). The upstream CO₂ volume changes due to the increase in the injection pressure at the beginning of each stage, but the CO₂ flow rates eventually become zero. Interestingly, the test with sandy OPA allows for distinguishing between the capillary entry pressure and breakthrough pressure. CO₂ starts penetrating the specimen under $\Delta p_f = 3$ MPa; however, the interconnected CO₂-rich phase may not be developed throughout the specimen, hindering the breakthrough process due to the presence of local heterogeneities or the observation scale. After overcoming the pore entry pressure, CO₂ displaces pore water with a relatively constant flow rate whereby the CO₂ breakthrough pressure is measured to be 4 MPa. The discrepancy between the entry and breakthrough pressures may become insignificant for homogeneous specimens on a laboratory scale.

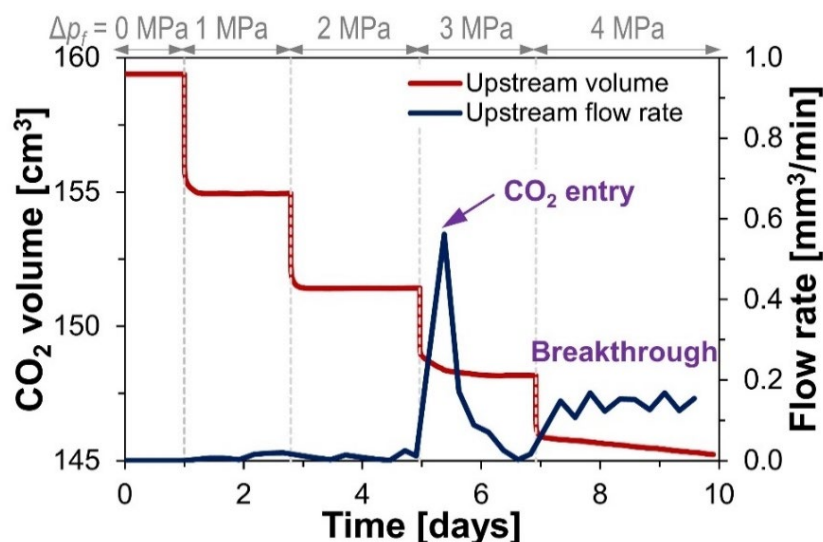


Fig. 2. Upstream CO₂ volume and corresponding flow rate profiles in measurements of breakthrough pressure for sandy Opalinus Clay under 9 MPa effective mean stress.

The indirect method is applied to sandy and shaly OPA, and its result is compared with the direct measurement. In general, the indirect method yields lower breakthrough pressure (1.8 MPa for sandy and 3.6 MPa for shaly OPA) compared to the direct measurements (4 MPa for sandy and 9 MPa for shaly OPA; Vilarrasa and Makhnenko, 2017). This discrepancy primarily stems from the differences in the utilized effective mean stresses. The samples in the MIP test experience zero effective confinement. However, the specimens and their pore throats could be compressed under

the representative in-situ stress condition during the direct measurements, hindering the CO₂ breakthrough. The influence of the effective mean stress on the breakthrough pressure is more pronounced for the shaly specimen mainly due to its higher compressibility. Other sources for the discrepancy are (1) geochemical reactions (e.g., swelling of clay minerals in OPA), (2) uncertainty in values of capillary properties, and (3) phenomenological difference between the capillary entry and breakthrough pressures.

4 Conclusions

Sandy and shaly facies of Opalinus Clay (OPA) are examined to investigate the effect of mineralogical composition on their sealing capacity, especially the intrinsic permeability and CO₂ breakthrough pressure. The permeability of sandy OPA is several times higher than that of shaly OPA, yet both facies still satisfy the criterion for a potential caprock ($k \leq 10^{-18} \text{ m}^2$). Using a stepwise injection method, the direct measurement of breakthrough pressure reveals that the value for the sandy specimen is 5 MPa smaller than that of the shaly counterpart (4 MPa vs. 9 MPa), primarily due to the wider pore distribution and larger dominant size. The CO₂-water capillary pressure curve can be predicted from the porosimetry data, enabling the indirect estimation of the capillary entry pressure. The direct measurement yields higher breakthrough pressure values compared to the indirect method since it can account for the effect of confinement and geochemical reactions. The discrepancy between the direct and indirect methods is more pronounced for the shaly specimen due to its lower stiffness. Consequently, the direct method under representative in-situ conditions should be adopted for Opalinus Clay. The measured parameters are used as inputs for a 3D model of Long-Term Periodic CO₂ injection – CO₂LPIE experiment currently being performed at Mont Terri URL (Sciandra et al., 2022).

Acknowledgements

H.K. and R.M. acknowledge the support from US National Science Foundation grant CMMI-2239630. The Opalinus Clay cores were graciously provided by swisstopo. V.V. acknowledges funding from the European Research Council (ERC) under the European Union's Horizon 2020 Research and Innovation Program through the Starting Grant GEoREST (www.georest.eu) under Grant agreement No. 801809. IMEDEA-CSIC-UIB is an accredited "Maria de Maeztu Excellence Unit" (Grant CEX2021-001198, funded by MCIN/AEI/10.13039/501100011033).

References

- Black, D.K., Lee, K.L. 1973. Saturating laboratory samples by back pressure. *J. Soil Mech. and Found. Divi.*, 99, 75–93. <https://doi.org/10.1061/JSFEAQ.0001847>
- Dewhurst, D.N., Yang, Y., Aplin, A.C. 1999. Permeability and fluid flow in natural mudstones. *Geolog. Soci., London, Special Publications*, 158, 23–43. <https://doi.org/10.1144/GSL.SP.1999.158.01.03>
- Espinoza, D.N., Santamarina, J.C. 2010. Water-CO₂-mineral systems: interfacial tension, contact angle, and diffusion – implications to CO₂ geological storage. *Water Res. Resear.*, 46, W07537. <https://doi.org/10.1029/2009WR008634>
- Espinoza, D. N., Santamarina, J. C. (2017). CO₂ breakthrough-Caprock sealing efficiency and integrity for carbon geological storage. *International Journal of Greenhouse Gas Control*, 66, 218–229. <https://doi.org/10.1016/j.ijggc.2017.09.019>
- Ito, D., Akaku, K., Okabe, T., Takahashi, T., Tsuji, T. 2011. Measurement of threshold capillary pressure for seal rocks using the step-by-step approach and the residual pressure approach. *Energy Procedia*, 4, 5211-5218. <https://doi.org/10.1016/j.egypro.2011.02.499>
- Martin, C. D., Lanyon, G. W. 2003. Measurement of in-situ stress in weak rocks at Mont Terri Rock Laboratory, Switzerland. *Int. J. of Rock Mech. and Mining Sci.*, 40(7-8), 1077-1088. [https://doi.org/10.1016/S1365-1609\(03\)00113-8](https://doi.org/10.1016/S1365-1609(03)00113-8)
- Neuzil, C.E. 2019. Permeability of clays and shales. *Annual Review of Earth and Planetary Sciences*, 47, 247–273. <https://doi.org/10.1146/annurev-earth-053018-060437>
- Rutqvist, J., Tsang, C. F. 2002. A study of caprock hydromechanical changes associated with CO₂-injection into a brine formation. *Environ. Geol.*, 42, 296–305. <https://doi.org/10.1007/s00254-001-0499-2>
- Sciandra, D., Rahimzadeh Kivi, I., Vilarrasa, V., Makhnenko, R.Y., Rebscher, D. 2022. Blind prediction of the hydro-mechanical response of Opalinus Clay to the CO₂ long-term periodic injection experiment (CO₂LPIE) at the Mont Terri rock laboratory. *Geomech. Geophys. Geoenerg. Georesour.*, 8(5), 166. <https://doi.org/10.1007/s40948-022-00442-x>
- Vilarrasa, V., Makhnenko, R. Y. 2017. Caprock integrity and induced seismicity from laboratory and numerical experiments. *Energy Procedia*, 125, 494–503. <https://doi.org/10.1016/j.egypro.2017.08.172>

Experimental study of coupled hydro-chemo-mechanical processes of CO₂ injection into a low-permeability sandstone

Iman R. Kivi^{1*}, Dragan Grgic², Mohamed Moumni², Atefeh Vafaie¹, Jesus Carrera³, Samuel Krevor¹ and Victor Vilarrasa⁴

¹ Department of Earth Science and Engineering, Imperial College London, London, UK

² Laboratoire GeoRessources, Université de Lorraine, CNRS, 54000, Nancy, France

³ Institute of Environmental Assessment and Water Research, Spanish National Research Council (IDAEA-CSIC), Barcelona, Spain

⁴ Global Change Research Group (GCRG), IMEDEA, CSIC-UIB, Esporles, Spain

* i.rahimzadeh-kivi@imperial.ac.uk

1 Introduction

Mitigation of the climate crisis and averting its worst consequences require rapid, deep and vast decarbonization (IEA 2023). The majority of pathways proposed to achieve this goal include large-scale deployment of carbon capture and storage (CCS) (Krevor et al. 2023). Accordingly, several gigatons (Gt) of CO₂ need to be annually captured from large, hard-to-abate industrial sources and injected into deep geological formations in the coming decades. However, the subsurface response to massive CO₂ injection is complex. Carbon dioxide injection results in a series of coupled thermo-hydro-mechanical-chemical processes that impose primary controls on CO₂ flow and storage performance underground (Rutqvist 2012; Vilarrasa et al. 2019; Kivi et al. 2022). Dissolution of CO₂ in the pore fluid creates acidic environments, which induce a series of chemical reactions with rock (Gaus 2010). These reactions, often discussed in terms of mineral dissolution and precipitation, could take place in different sedimentary rocks and alter their hydraulic and mechanical properties (see Vafaie et al. 2023 for a review).

Experimental and numerical studies consider CO₂-fluid-rock interactions with simplifying assumptions about the impacts of the subsurface stress state. Laboratory experiments are commonly performed under hydrostatic stress conditions. Geochemical databases used for numerical simulations only consider the potential effects of pressure and temperature on reaction kinetics (Palandri, Kharaka 2004). However, the dominant stress conditions in the subsurface is anisotropic. Macroscopic differential stresses of a few megapascals could result in localized stress at grain contacts by factors as large as 100, imposing non-negligible impacts on the chemical potential of minerals (Wheeler 2018). This concept has been broadly leveraged to study a variety of reactions at varying depths in Earth (Wheeler 2020).

One reaction of relevance to CO₂ storage is pressure solution. Pressure solution involves preferential mineral dissolution at stressed grain-to-grain contacts and subsequent precipitation on free mineral surfaces (Gratier et al. 2013) with potential implications for long-term rock deformation at CCS sites (Grgic 2011). Yet, the possible effects of stress on fluid reactions with stressed mineral surfaces in the short term are less well understood.

We have recently initiated a study to understand the effect of stress on the kinetics of aqueous CO₂ reactions with porous rocks. We here briefly present the adopted methodology and some preliminary observations from the laboratory experiments. Complementary experiments combined with coupled reactive transport and deformation simulations are required to better resolve the involved processes.

2 Methodology

We perform laboratory experiments of CO₂-saturated water injection into two specimens from Rotliegend Sandstone, which serves as a candidate reservoir for CO₂ storage in the UK Southern North Sea. The samples have an average initial porosity of 0.14 and a low permeability of 2×10^{-17} m². Such low-permeability rocks occur as thin or thick interbedding layers in the storage

reservoir and are crossed by the buoyant CO₂, affecting CO₂ flow and storage behavior in the sub-surface. The rock is composed of 44 wt.-% Quartz, 27 wt.-% Clays, 20 wt.-% carbonates, dominantly dolomite, and 9 wt.-% anhydrites. Hydrostatic loading tests under drained, undrained and unjacketed conditions are performed before the main experiments to extract the poroelastic properties of the rock.

Experiments are performed under two different stress conditions: (1) hydrostatic stress of 15 MPa and (2) confining stress of 8 MPa and axial stress of 29 MPa, providing the same mean effective stress as in the first scenario but an elevated deviatoric stress of 21 MPa (see Fig. 1 for the setup). The specimens are initially saturated with water. A total of 70 nominal pore volumes of CO₂-saturated water with a pH of 3.13, calculated from the PhreeqC code (Parkhurst and Appelo, 2013) at the reactor temperature of 25 °C and pressure of 5 MPa, are injected at constant rates in a way that results in identical initial differential pressures across the specimens subject to 5 MPa backpressure. The choice of identical injection pressures allows us to isolate possible effects of stress on reaction kinetics from those of pore pressure. One should note that the stress-dependent permeability of the rock results in different injection rates in the two specimens. Outflow solution samples are regularly collected during the experiments for chemistry analysis to quantify the amount of dissolved minerals. Micro CT imaging is also carried out on samples before and after flow-through experiments to diagnose the evolution of pore structure as a result of chemical reactions. However, these complementary analyses have not yet been interpreted and are not presented here.

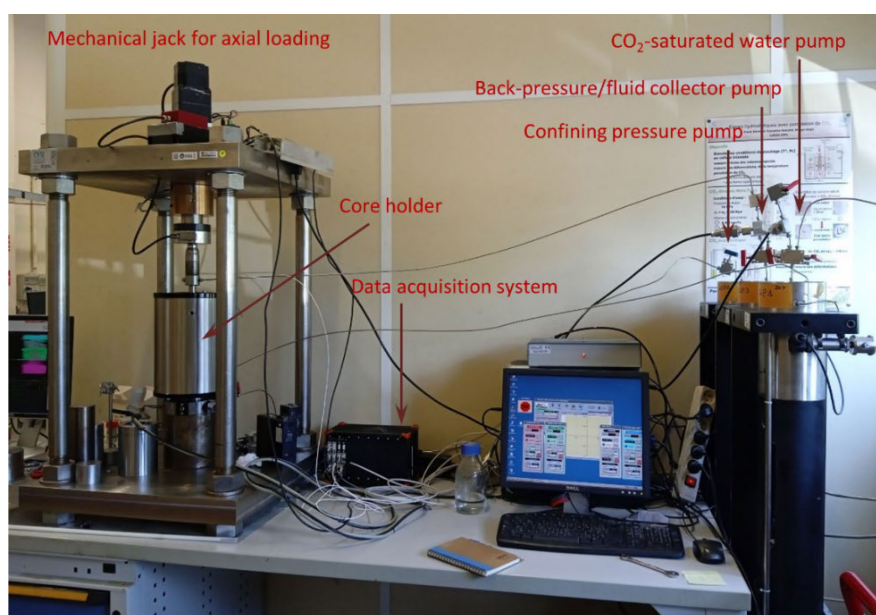


Fig. 1. Photograph of the flow-through setup used in this study (photograph by I.R. Kivi).

3 Results and discussions

The evolutions of pore pressure and rock deformation –following the sign convention of geomechanical, i.e., positive under compression– are shown in Fig. 2. The upstream pressure initially increases, reaches a peak and then decreases continuously with time (Fig. 2a). Little differences are observed between the two pressure evolution curves. Primary analysis of the data shows that the porosity and permeability increase by 0.5 % and a factor of around 1.5, respectively, for both specimens. In contrast to the upstream pressure, the measured strains continuously decrease with time, implying rock expansion (Fig. 2b). The steep expansion trend at the beginning corresponds to the initial increase in pore pressure, which drives down the applied effective stress on the rock. Subsequent expansion instead has its origin in geochemical interactions. This behavior can be explained by the theory of poroelasticity, from which one can write (Zimmerman 1986)

$$\varepsilon_v = C_b P - C_p p \quad \text{Eq. (1)}$$

where ε_v is the volumetric strain (compression positive), P is the mean stress and p is the pore pressure. C_b and C_p are the bulk skeleton compressibility and pore compressibility, respectively. We write the volumetric response of the porous media in incremental form as

$$d\varepsilon_v = dC_b P + C_b dP - dC_p p - C_p dp \quad \text{Eq. (2)}$$

where an infinitesimal change of pore pressure and mean stress in a chemically degrading rock causes an infinitesimal volumetric deformation. While the mean stress is constant, i.e., $dP = 0$, and the first and fourth terms on the right-hand side of Eq. (2) are positive, the rock expansion implies $dC_p > 0$, which means an increase in pore compressibility or equivalently pore stiffness weakening.

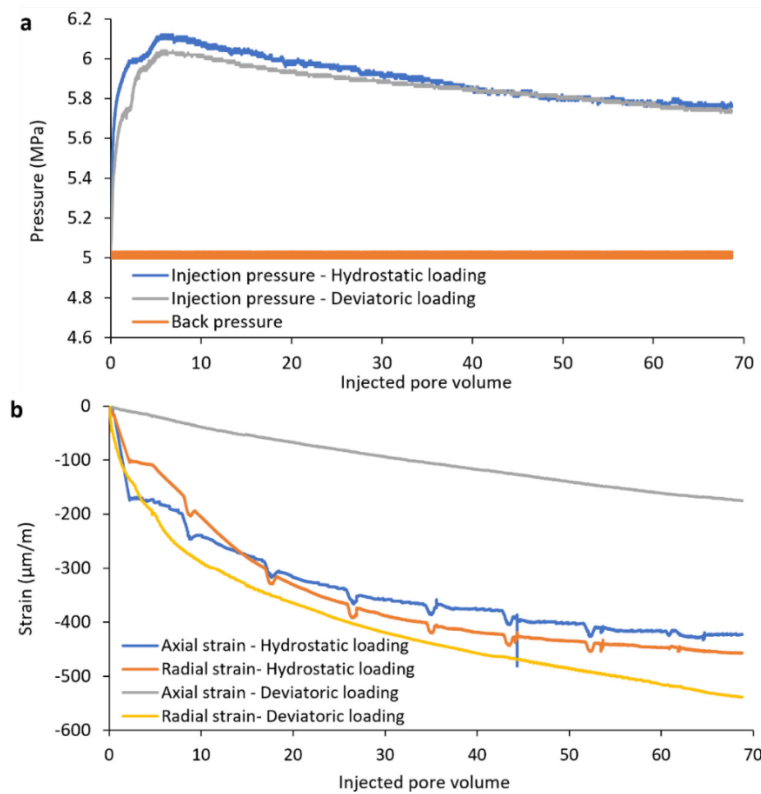


Fig. 2. Temporal evolution of (a) pore pressure and (b) deformation for the conducted experiments.

Although the observed trends are generally similar in both tests, some meaningful differences are evident. First, the evolutions of both pore pressure and deformation under hydrostatic loading gradually attenuate with time approaching nearly constant values at the end of injection. This trend shows that the accessible surface area of the fast-reacting minerals becomes progressively limited or the extent of reactions evolves non-linearly with the increase in pore compressibility in the course of the experiment. In contrast, a steadier profile of pore pressure and deformation changes is established under deviatoric loading. Nevertheless, the experiment was stopped after injecting 70 pore volumes of CO_2 -saturated water for the sake of comparison with the other one and could not be resumed because strain gauges were removed from the specimen surface for micro-CT imaging of the post-injection pore structures. Second, reaction-induced rock deformation under deviatoric loading features more pronounced anisotropy (Fig. 2b). While the radial strain under deviatoric loading is generally comparable to those established axially and radially under hydrostatic conditions, the corresponding axial deformation is smaller by a factor of approximately 3. This behavior could originate from micro-channeling of flow and transport along the specimen, favoring preferential stiffness degradation in the lateral direction. Although the rock specimen is more prone to micro-fracturing under elevated deviatoric stress (Kivi et al. 2018), the applied axial stress in the experiment was far below the failure stress threshold measured to be around 100 MPa. Explaining the observed anisotropic behavior warrants further micro-structural evidence from micro-CT images.

4 Conclusions

We have performed flow-through experiments of CO₂-saturated water injection into two sandstone specimens under hydrostatic and deviatoric stress conditions to resolve the effect of stress on chemical reaction kinetics. Preliminary analyses of the data point to slight increases in porosity and permeability and pore stiffness weakening. The observed trends are generally similar in the two experiments while some meaningful differences including more pronounced, anisotropic expansion under deviatoric loading also exist. A detailed assessment of the evolution of pore structure using micro-CT images and coupled hydro-chemo-mechanical simulations of the experiments should allow for a more detailed assessment of the underlying mechanisms.

Acknowledgments

I.R.K. and V.V. acknowledge support by the PCI2021-122077-2B project (www.easygeocarbon.com) funded by MCIN/AEI/10.13039/501100011033 and the European Union NextGenerationEU/PRTR. I.R.K. and S.K. acknowledge funding from the Engineering and Physical Sciences Research Council through the UKRI Postdoc Guarantee Award THMC4CCS [Grant number EP/X026019/1]. V.V. also acknowledges support from the Spanish Ministry of Science and Innovation through the project HydroPore (PID2019-106887GB-C32). IMEDEA-CSIC-UIB is an accredited "Maria de Maeztu Excellence Unit" (Grant CEX2021-001198, funded by MCIN/AEI/10.13039/501100011033).

References

- IEA, 2023. Net Zero Roadmap: A Global Pathway to Keep the 1.5 °C Goal in Reach, IEA, Paris.
- Gaus, I. 2010. Role and impact of CO₂-rock interactions during CO₂ storage in sedimentary rocks. *Int. J. Greenhouse Gas Control* 4(1), 73–89. <https://doi.org/10.1016/j.ijggc.2009.09.015>
- Gratier JP, Dysthe DK, Renard F. 2013. The role of pressure solution creep in the ductility of the earth's upper crust. In: Dmowska R. (ed) *Advances in Geophysics*, Vol 54. Elsevier, Amsterdam, pp 47–179. <https://doi.org/10.1016/b978-0-12-38094-0-7.00002-0>
- Grgic, D. 2011. Influence of CO₂ on the long-term chemomechanical behavior of an oolitic limestone. *J. Geophys. Res.: Solid Earth* 116(B7). <https://doi.org/10.1029/2010JB008176>
- Kivi, IR, Makhnenko, RY, Vilarrasa, V. 2022. Two-phase flow mechanisms controlling CO₂ intrusion into shaly caprock. *Transp. Porous Media* 141(3), 771–798. <https://doi.org/10.1007/s11242-022-01748-w>
- Kivi, IR, Ameri, M, Molladavoodi, H. 2018. An experimental investigation on deformation and failure behavior of carbonaceous Garau shale in Lurestan Basin, west Iran: Application in shale gas development. *J. Nat. Gas Sci. Eng.* 55, 135–153. <https://doi.org/10.1016/j.jngse.2018.04.028>
- Krevor, S, De Coninck, H, Gasda, SE, Ghaleigh, NS, de Gooyert, V, Hajibeygi, H, Juanes, R, Neufeld, J, Roberts, JJ, Swennenhuis, F. 2023. Subsurface carbon dioxide and hydrogen storage for a sustainable energy future. *Nat. Rev. Earth Environ.* 4(2), 102–118. <https://doi.org/10.1038/s43017-022-00376-8>
- Palandri, JL, Kharaka, YK. 2004. A compilation of rate parameters of water-mineral interaction kinetics for application to geochemical modeling. Geological Survey, Report. 71 pp.
- Parkhurst, D.L., Appelo, C.A.J., 2013. Description of input and examples for PHREEQC version 3—a computer program for speciation, batch-reaction, one-dimensional transport, and inverse geochemical calculations. *US Geol. Surv. Techn. Methods* 6 (A43), 497.
- Paterson, MS. 1973. Non-hydrostatic thermodynamics and its geologic applications. *Rev. Geophys. Space Phys.* 11, 355–389. <https://doi.org/10.1029/RG011i002p00355>
- Rutqvist, J. 2012. The geomechanics of CO₂ storage in deep sedimentary formations. *Geotech. Geol. Eng.* 30, 525–551. <https://doi.org/10.1007/s10706-011-9491-0>
- Vafaie, A, Cama, J, Soler, JM, Kivi, IR, Vilarrasa, V. 2023. Chemo-hydro-mechanical effects of CO₂ injection on reservoir and seal rocks: A review on laboratory experiments. *Renewable Sustainable Energy Rev.* 178, 113270. <https://doi.org/10.1016/j.rser.2023.113270>
- Vilarrasa, V, Carrera, J, Olivella, S, Rutqvist, J, Laloui, L. 2019. Induced seismicity in geologic carbon storage. *Solid Earth*, 10(3), 871–892. <https://doi.org/10.5194/se-10-871-2019>
- Wheeler, J. 2018. The effects of stress on reactions in the Earth: Sometimes rather mean, usually normal, always important. *J. Metamorph. Geol.* 36(4), 439–461. <https://doi.org/10.1111/jmg.12299>
- Wheeler, J., 2020. A unifying basis for the interplay of stress and chemical processes in the Earth: support from diverse experiments. *Contrib. Mineral. Petrol.* 175(12), 116. <https://doi.org/10.1007/s00410-020-01750-9>
- Zimmerman RW, Somerton WH, King MS. 1986. Compressibility of porous rocks. *J Geophys Res.* 91, 12765–12777. <https://doi.org/10.1029/JB091iB12p12765>

Characterizing elastic stiffness, creep, and in-situ stress and their anisotropies of clay shales using pressuremeter testing

Lang Liu^{1*} and Rick Chalaturnyk²

¹ SINTEF, Trondheim, Norway

² University of Alberta, Edmonton, Canada

* lang.liu@sintef.no

1 Pressuremeter Testing and Example Tests in Shales

Pressuremeter testing (PMT) has been considered an effective in-situ method to determine the geotechnical parameters of the ground at shallow depths (Clarke, 1995). With the advances in the pressure capacity and displacement measurement resolution of the testing equipment, PMT has also been carried out in deep rock formations (Hughes & Whittle, 2023; Liu et al., 2021). The internal caliper equipped in the pressuremeter probe allows for the precise measurement of borehole deformation at a resolution as high as about 0.1 μm , and the multiple sets of calipers sitting at different diametric axes can capture the anisotropy of the borehole deformation during PMT (Fig. 1). Measurement of in-situ geomechanical properties have been considered important in assessing and controlling the integrity of host rock/caprock and other relevant geological structures in subsurface stimulation and storage projects. In this work, we will discuss the use of PMT in characterizing rock anisotropy and in-situ stress anisotropy in clay shales from our recent field observations and experimental study.

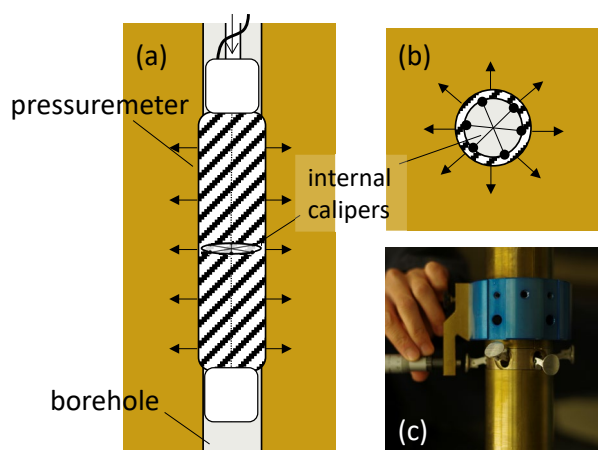


Fig. 1. Schematics of pressuremeter testing in (a) borehole side and (b) cross-section views; (c) high-resolution internal calipers under laboratory calibration.

2 Influence and Interpretation of Rock Anisotropy

In a recent field campaign at the Mont Terri Rock Laboratory, a series of PMTs were carried out in three boreholes to characterize the in-situ elastic stiffness of Opalinus Clay (Liu et al., 2022b). The dipping angle of the Opalinus Clay at the test site is approximately 40° . Two boreholes were oriented perpendicular to bedding, and the third one, borehole BGC-A6, was drilled horizontally and oriented parallel to bedding (Fig. 2). For the PMT in BGC-A6, because of the variation of borehole compliance with respect to the bedding plane, the borehole deformation also varies with the azimuth angle θ , which can be distinguished using the data obtained from the calipers at three diametric axes (Fig. 3). In these tests, at different pressure levels, a pressure hold with about 5 minutes duration was attempted, followed by an unload-reload cycle with a strain amplitude $\Delta\varepsilon_{c,unload}$ of about 0.05 %. The data from the pressure hold was used to estimate the creep deformation of the borehole, while the data from the unloading step was used to determine the elastic moduli of the borehole.

Fig. 4 shows the borehole moduli G^* and creep strain $\Delta\epsilon_{c,creep}^*$ determined using the data obtained at different caliper axes. Based on the closed-form solution derived by Amadei and Savage (1991), the borehole moduli can be calculated for rocks characterized using transversely isotropic elasticity with five independent parameters. A good fit on the test data is obtained with reasonable choices of values for these parameters (Fig. 4). Both fits of G^* and $\Delta\epsilon_{c,creep}^*$ show the preferential anisotropies with the maximum moduli and the minimum creep oriented parallel to bedding indicating the influence of the rock anisotropy.

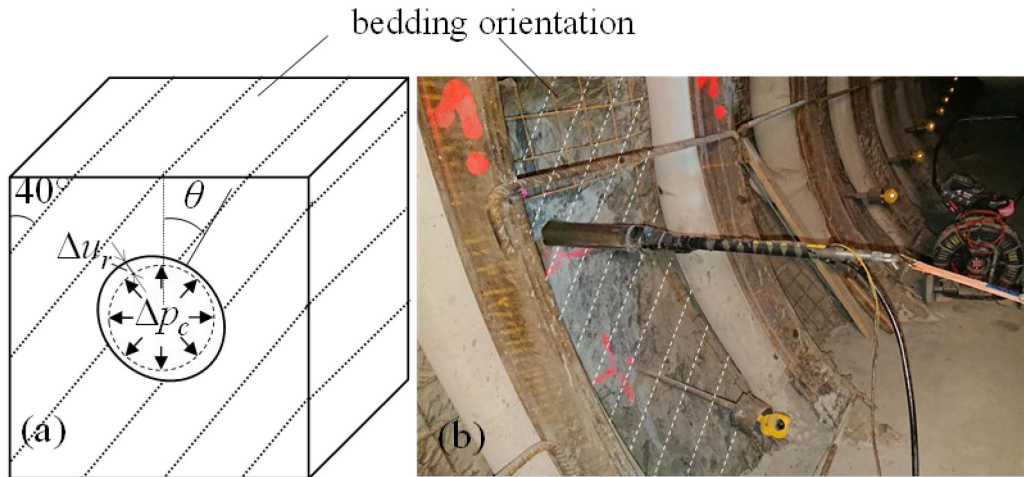


Fig. 2. PMT in a horizontal borehole (BGC-A6) oriented parallel to bedding: (a) schematic diagram and (b) field test at the Mont Terri rock laboratory.

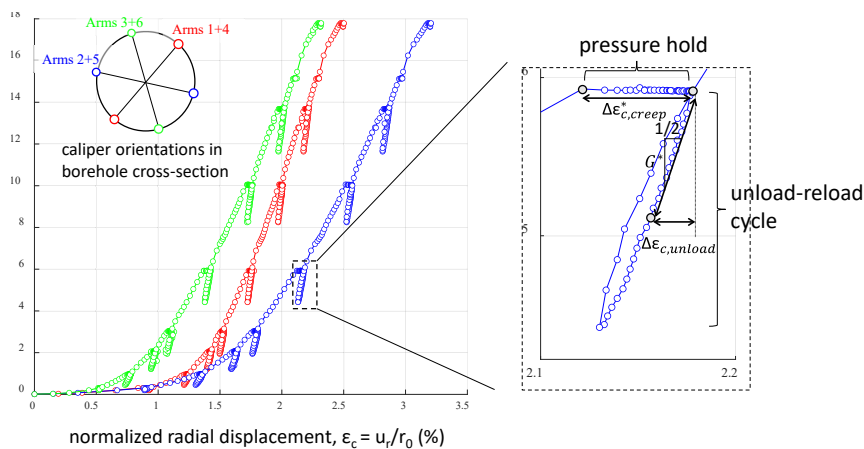


Fig. 3. Pressuremeter test data at the borehole depth of 4.5m in borehole BGC-A6.

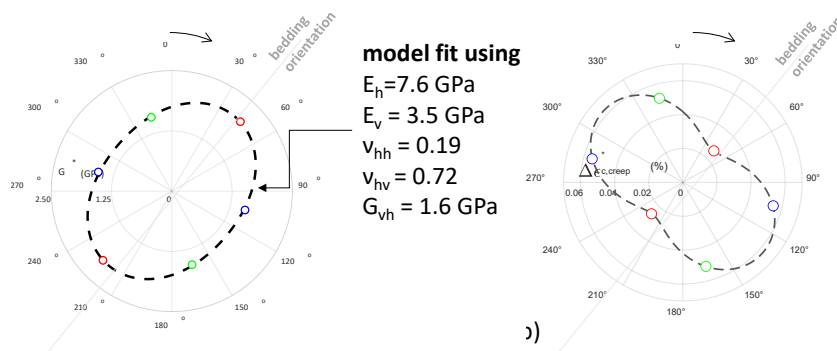


Fig. 4. Variation of (a) borehole moduli and (b) creep deformation with borehole azimuth from PMT measurements (dots) and model fits (lines).

3 Influence and Interpretation of In-situ Stress Anisotropy

An experimental program was implemented by Liu et al. (2018) to study the influence of the anisotropic in-situ stresses on the PMT in clay shales. In this program, Portland cement was mixed with kaolinite and water to produce a large cubic analog specimen with Young's modulus of about 2 GPa and uniaxial compressive strength of about 10 MPa. The specimen was initially confined under polyaxial boundary stresses (σ_v , σ_H , and σ_h) before a PMT was conducted in its pre-drilled center hole (Fig. 5a). Three different sets of boundary stresses were used on the three specimens, respectively. Fig. 5b shows the borehole deformation measured by three pairs of calipers from one test with $\sigma_H = 3.25$ MPa, $\sigma_h = 2.15$ MPa, and $\sigma_v = 2.6$ MPa. A divergence of test data was observed from the measurements at the three caliper axes after the borehole expansion became nonlinear due to plastic deformation. This was attributed to the anisotropic stress field in the near-borehole region even when the uniform borehole pressure was imposed (Liu et al., 2021). The observation can be explained as a *reversed borehole breakout* that occurs in a ductile manner and is considered an indicator of in-situ horizontal stress anisotropy.

An interpretation of this in-situ horizontal stress anisotropy is possible when a geomechanical model can predict the anisotropic borehole deformation captured from PMT. Fig. 5b also shows the fit of the test data predicted using a finite element model where all the boundary conditions except σ_H and σ_h are defined according to the experiment. An inversion procedure was implemented to iteratively update the values of σ_H and σ_h in the model until the predicted borehole deformation at all three caliper axes satisfyingly matched the test data when the misfit could no longer be reduced (Fig. 5c). The inverted σ_H and σ_h values from the model prediction reasonably agree with that used in the experiment (with errors of 12 % to σ_H and 1 % to σ_h), suggesting its promising potential in the in-situ stress determination in ductile caprock formations where the conventional approach can be ineffective (Yuan et al., 2013).

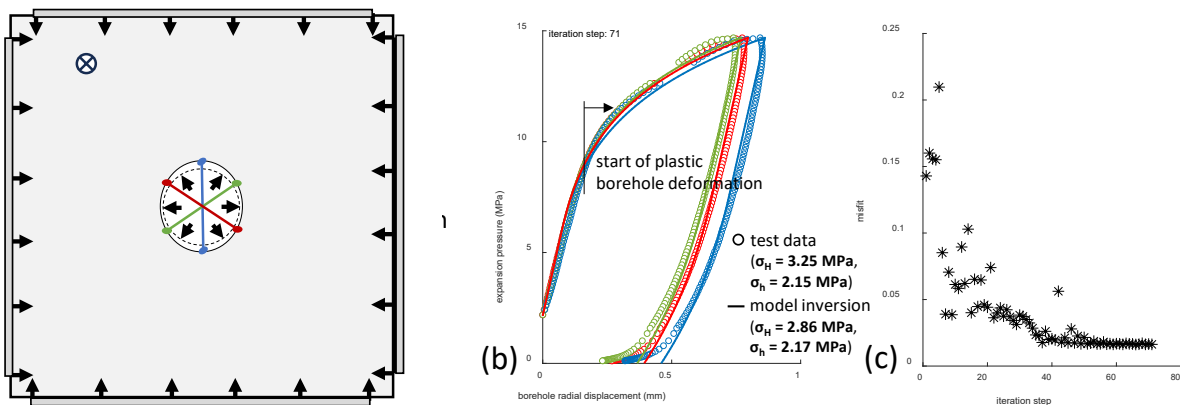


Fig. 5. (a) Schematic diagram of pressuremeter test in a soft cement specimen under polyaxial boundary stresses reported by Liu et al. (2018); (b) test data obtained by three calipers and model prediction from an analysis to invert boundary stresses σ_H and σ_h ; (c) minimization of misfit through the inversion.

4 Challenges and Recommendations

Like many in-situ testing methods, the interpretation of PMT data can be strongly influenced by the initial quality of the borehole. Limiting the borehole disturbance is challenging when drilling in weak clay shales, such as the Opalinus Clay, because of their sensitivities to changes in moisture, temperature, and stress. Because damage can be induced by swelling when the clay shale is in contact with water, air or oil-based drilling mud has been mostly used in drilling. Unloading from the in-situ stresses can also lead to localized overstressing damage, and/or the structural failure that was often observed when drilling in parallel to the bedding plane, for example, from cases at the Mont Terri

(Fig. 6). The model used in the interpretation should properly account for these borehole disturbances, otherwise, the elastic moduli would be underestimated (Liu et al., 2022a). The localized borehole damage can also affect the local stress field near the borehole, complicating the analysis of the *reversed borehole breakout* from PMT and therefore making it difficult to determine the in-situ stress anisotropy. It may be desired to load the borehole to a pressure level as high as practicable so that the intact formation beyond the near-borehole disturbance zone can be sufficiently impacted. On the other hand, if the initial borehole damage is caused by overstressing and is detectable by downhole tools, it by itself can be used as a good indicator for the interpretation of directions and perhaps the magnitude of the in-situ stresses (Zoback et al., 2003).

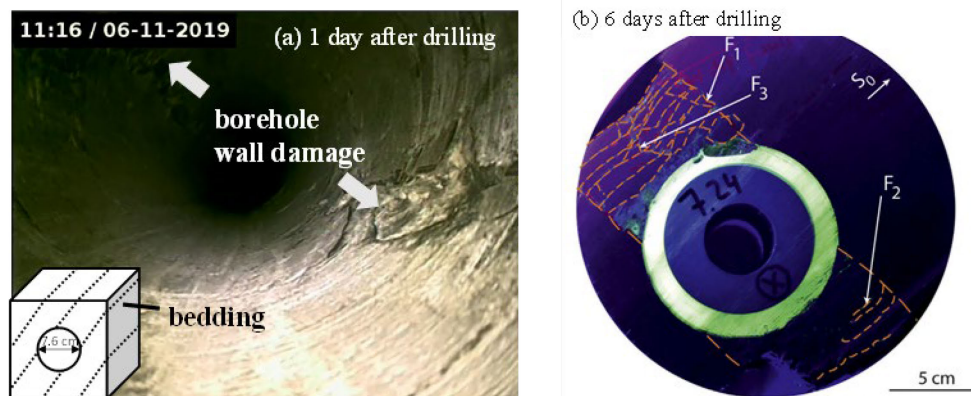


Fig. 6. (a) local borehole wall damage perpendicular to bedding observed in borehole BGC-A6 before PMT; (b) buckling-like failure (marked by F_1 , F_2 , and F_3) along bedding beyond the borehole wall observed from an overcored borehole section (Kupferschmied et al., 2015).

References

- Amadei, B, Savage, WZ. 1991. Analysis of borehole expansion and gallery tests in anisotropic rock masses. *Int. J. Rock Mech. Min. Sci.* 28, 383–396. [https://doi.org/10.1016/0148-9062\(91\)90077-Y](https://doi.org/10.1016/0148-9062(91)90077-Y)
- Clarke, BG. 1995. *Pressuremeters in geotechnical design*, 1st ed. ed. CRC Press, London.
- Hughes, J, Whittle, R. 2023. *High Resolution Pressuremeters and Geotechnical Engineering*, 1st Ed. ed, High Resolution Pressuremeters and Geotechnical Engineering. CRC Press. <https://doi.org/10.1201/9781003200680>
- Kupferschmied, N, Wild, KM, Amann, F, Nussbaum, C, Jaeggi, D, Badertscher, N. 2015. Time-dependent fracture formation around a borehole in a clay shale. *Int. J. Rock Mech. Min. Sci.* 77, 105–114. <https://doi.org/10.1016/j.ijrmms.2015.03.027>
- Liu, L, Chalaturnyk, R, Deisman, N, Zambrano-Narvaez, G. 2021. Anisotropic borehole response from pressuremeter testing in deep clay shale formations. *Can. Geotech. J.* 58, 1159–1179. <https://doi.org/10.1139/cgj-2019-0801>
- Liu, L, Deisman, N, Chalaturnyk, R. 2022a. Elastic stiffness modelling of Opalinus Clay based on laboratory measurements with implications for in-situ testing. *Rock Mech. Rock Eng.*
- Liu, L, Fu, H, Chalaturnyk, R, Weng, D. 2018. An experimental study of pressuremeter testing under polyaxial boundary stress condition, *Proceedings of GeoShanghai 2018 International Conference: Multi-physics Processes in Soil Mechanics and Advances in Geotechnical Testing*. Springer Singapore. <https://doi.org/10.1007/978-981-13-0095-0>
- Liu, L, Giger, SB, Martin, D, Chalaturnyk, R, Schuster, K, Deisman, N, Keller, L. 2022b. In-situ shear modulus determination by pressuremeter tests in Opalinus Clay and reconciliation with laboratory tests. *Rock Mech. Rock Eng.*
- Yuan, Y, Xu, B, Palmgren, C. 2013. Design of caprock integrity in thermal stimulation of shallow oil-sands reservoirs. *J. Can. Pet. Technol.* 52, 266–278. <https://doi.org/10.2118/149371-PA>
- Zoback, MD, Barton, CA, Brudy, M, Castillo, DA, Finkbeiner, T, Grollmund, BR, Moos, DB, Peska, P, Ward, CD, Wiprut, DJ. 2003. Determination of stress orientation and magnitude in deep wells. *Int. J. Rock Mech. Min. Sci.* 40, 1049–1076. <https://doi.org/10.1016/j.ijrmms.2003.07.001>

Geochemical hydrogen-pore water-Opalinus Clay interactions

Christian Ostertag-Henning^{1*}

¹ Federal Institute for Geosciences and Natural Resources, Hannover, Germany

* christian.ostertag-henning@bgr.de

1 Introduction

During the long-term subsurface storage of high-level nuclear waste there are two main processes that will produce molecular hydrogen (H₂): One is the radiolytic decomposition of water and organic matter by the ionizing radiation yielding hydrogen atoms (Bonin et al. 2000), which may recombine to form molecular hydrogen. The second are the redox reactions of water with the metal canisters yielding the reduction of water to molecular hydrogen with the concomitant oxidation of, e.g., iron on the canister surfaces (Xu et al. 2008). Both processes will result in significant formation of molecular hydrogen, which is considered as a factor for the possible pressure buildup in the subsurface repository. The molecular hydrogen might be present as dissolved hydrogen in the pore water in the technical barrier or the host rock, but it might form a new or transfer into an existing gas phase as well. In addition to the pressure buildup, the dissolved molecular hydrogen is changing the redox conditions and resulting in redox reactions with dissolved ions or with the exposed mineral surfaces, too. The microbial community present in the repository will use the molecular hydrogen resulting in increased microbial activity and the formation of secondary products, e.g., if sulfate-reducing bacteria are oxidizing the molecular hydrogen, sulfide might be produced with impact on the further corrosion of canisters (Bagnoud et al. 2016).

In the context of subsurface storage of molecular hydrogen as an energy carrier, the geochemical and microbial reactions oxidizing hydrogen in the reservoir rocks and at the contact with the cap rock are equally important. They determine the loss of hydrogen by these reactions, and might invoke changes in the composition of back-produced gas, e.g., by presence of hydrogen sulfide due to reactions with iron sulfide (pyrite) or microbial sulfate reduction. They might alter also the cap rock by geochemical reactions inducing dissolution, and hence porosity and permeability changes.

Therefore, several studies have investigated the reactions producing hydrogen – and its microbial or geochemical oxidation and migration in barrier or host rock materials as well as reservoir and cap rocks. In the context of ongoing work at the Federal Institute for Geosciences and Natural Resources in Hannover, Germany, different aspects of the formation (by radiolysis and redox reactions / corrosion) and oxidation of molecular hydrogen are being investigated. In this contribution, results from geochemical reactions of Opalinus Clay rock material – both a host rock for high-level nuclear waste and possible cap rock in subsurface reservoirs - with molecular hydrogen are presented focusing on the oxidation rates of H₂ and reactions responsible or influenced by this redox reaction.

2 Material and Methods

A series of gas-fluid-rock experiments in closed gold capsules with pulverized Opalinus Clay rock material from the subsurface lab in Mont Terri, Switzerland, have been conducted. The rock material has been cored in the Mont Terri HE-F project from the shaly facies in the Opalinus Clay in the vicinity of the MI niche in borehole BHE-F1. An interval in the core between 2.0 and 2.2 m was selected, crushed, freeze-dried and ground gently with an agate mortar and pestle taking care to minimize heating and exposure to atmospheric oxygen. The pulverized rock material was stored under an argon atmosphere. The mineralogical and chemical composition of this sample is described in Helten et al. (2022) and is similar to published data for the shaly facies of the Opalinus Clay in the subsurface lab (Gaucher et al. 2003).

For the experiments, 200 mg of this rock material was weighed into gold capsules with an outer diameter of 5 mm, a wall thickness of 0.2 mm and a length of 60 mm welded close at one end. Then

a volume of 50 μl of HPLC-grade water was added, and the gold capsule connected to a gas-filling apparatus. There the gas phase was replaced by either a gas mixture of $\text{H}_2\text{:Ne:Ar}$ (ratio 5:1:4) or pure Ar (control samples for identifying the background geochemical fluid-rock reactions) at 5 bars absolute pressure. The noble gases argon and neon were added as tracers for a very accurate determination of the amount of H_2 added into the gold capsules and calculation of the molar amounts oxidized, and to ensure that gas loss due to leaks during the experiments and the analyses could be excluded. Then the gold capsule was cold-welded on the other side still connected to the gas-filling device, disconnected and finally arc-welded. The experiments were performed in high pressure reactors at temperatures of 80, 120, 160 and 200 °C at 200 bars pressure for a duration of one week. After the experiment, the gold capsules were retrieved from the high-pressure reactors, cleaned, and stored in N_2 -purged headspace glass vials with a gas-tight septum. Before analyses, the gold capsules were pierced through the septum to release the gases into the bulk gas phase of the headspace vial. Then the concentration of the gases was analyzed with a modified refinery gas chromatographic analyzer. The molar amounts of gases were calculated using the pressure and gas phase volume of the headspace vial. The amount of hydrogen oxidized was determined by subtracting the determined final amount of H_2 from the initial amount of H_2 present in the gold capsule derived from the amounts of both Ar and Ne and the known initial gas mixture composition. The experiments and analyses were carried out in duplicate for each set of conditions.

3 Results and Interpretation

The control experiments with only argon in the gas phase documented that no formation of H_2 was occurring under the investigated conditions up to 200 °C. The major gaseous product was carbon dioxide (CO_2). The amounts of released CO_2 were increasing with increasing temperature from 1300 nmol at 80 °C to 18000 nmol at 200 °C. The range of amounts of CO_2 released are in line with findings of Helten et al. (2022) using the same rock sample but different fluid:rock masses and experimental system. As described there, most of the CO_2 is formed due to dissolution reactions of the carbonate minerals present, but at elevated temperatures, part of the CO_2 is from oxidation of organic matter as well. In addition to CO_2 , small amounts of hydrocarbons, most abundant methane (CH_4), are present after the experiments, again increasing in molar amounts from 0.6 nmol at 80°C to 4 nmol at 200 °C. The hydrocarbons are formed by thermal decomposition of the organic matter, and possibly to a small extent by desorption from the rock material. The ratio of the saturated alkane ethane (C_2H_6) to the unsaturated alkene ethene (C_2H_4) at 200 °C is 1.6. No carbon monoxide or hydrogen sulfide was detected after the control experiments with the initially pure argon gas phase.

The experiments with ca. 55000 nmol H_2 present initially in the gas phase exhibited a significant oxidation of H_2 over the experiment: From a loss of 7500 nmol at 80 °C the loss increased to 29600 nmol at 200 °C. The amount of CO_2 present after the experiments was similar to the control experiments in the increase with temperature yielding 18000 nmol at 200 °C. But at lower temperatures, the amount of CO_2 present was lower than in the control experiments at 80 and 120 °C. In addition, for the experiments at 160 and 200 °C, there were small amounts of carbon monoxide present after the experiments, 38 and 110 nmol. The amounts of hydrocarbons present were again small and increasing with temperature, but in comparison to the control experiments at the same temperatures significantly elevated, e.g., the experiment at 200 °C had twice the amount of CH_4 and C_2H_6 . The ratio of $\text{C}_2\text{H}_6\text{:C}_2\text{H}_4$ was 10 instead of 1.6 as in the control experiments. No hydrogen sulfide was detected in the gas phase after the experiments.

The changes in the gas phase allow the determination of extent of oxidation rates of H_2 at each condition, ranging from 14 % at 80 and 120 °C to 33 % at 160 °C to 55 % at 200 °C within a week. The changes in the overall gas composition add further insights into reactions contributing to the H_2 oxidation. The absence of hydrogen sulfide in the gas phase after the experiment does not rule out the redox reaction between pyrite and H_2 , but indicates that if this reaction occurred, all the produced sulfide was precipitating with available metals to, e.g., iron monosulfide. Most likely the oxidation of Fe^{2+} in pyrite and clay minerals is responsible for the observed oxidation of the H_2 , but the increased

amounts of hydrocarbons in presence of H_2 , and the increase in more-H-rich alkanes over alkenes ($C_2H_6:C_2H_4$) point to H_2 losses due to reaction with organic matter as well. The presence of CO indicates the reduction of CO_2 by H_2 at temperatures above 120 °C in the presence of surplus H_2 .

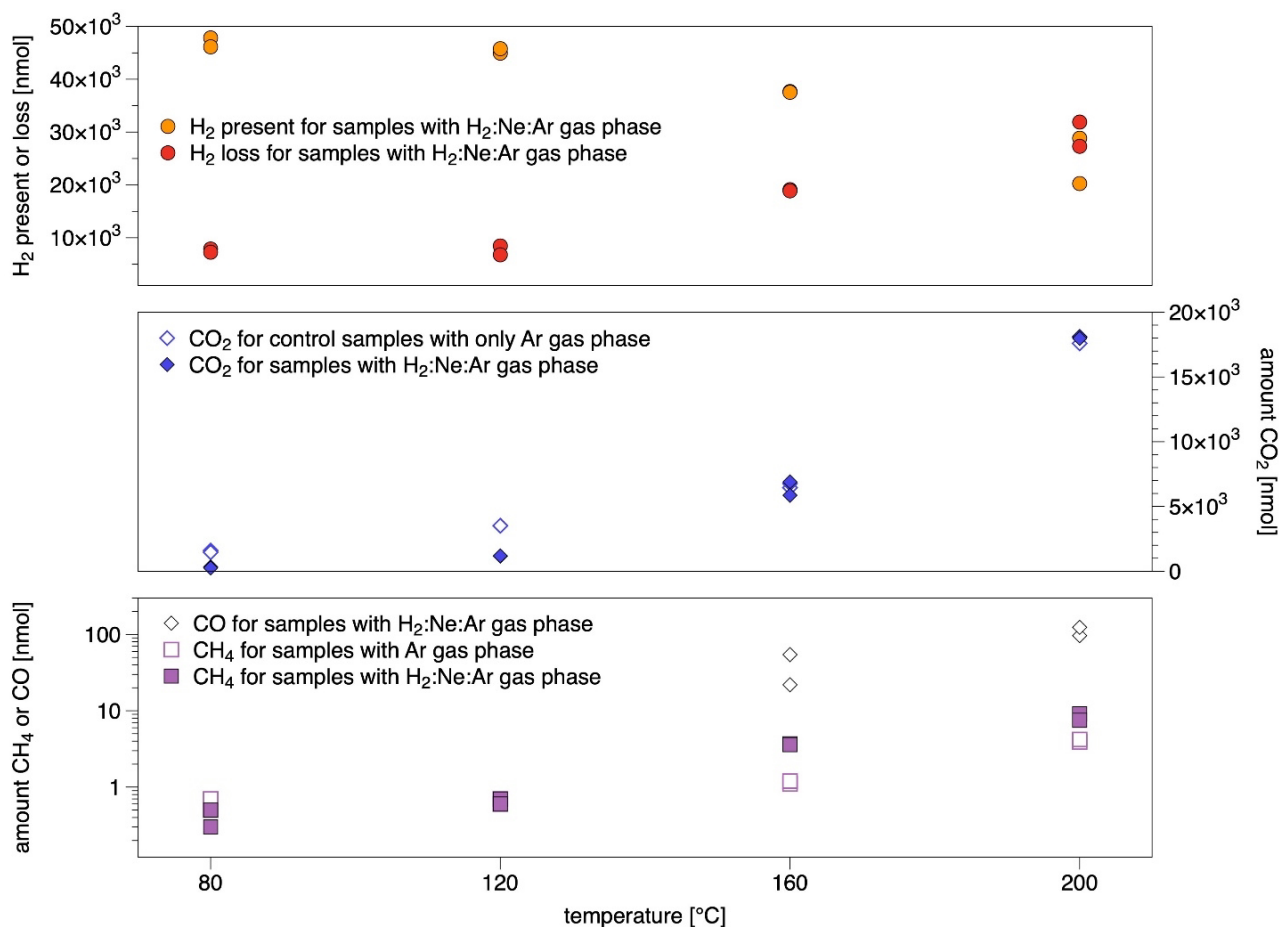


Fig. 1. Molar amounts of gases present after the experiments of Opalinus Clay rock material with and without initial H_2 present at temperatures of 80 to 200 °C and 200 bars for one week duration.

The observed oxidation of H_2 documents rapid redox reactions with mineral surfaces at the conditions investigated. In addition, the redox reactions during the H_2 oxidation might change the pH of the pore water inducing further mineral dissolution in the cap rock. The reaction of H_2 with organic matter in rocks at these conditions has not been described before, the production of CO is most likely related to the reduction of CO_2 by H_2 catalyzed at reactive mineral surfaces. The results are equally important for the subsurface storage of H_2 if the Opalinus Clay is considered as cap rock as for storage of nuclear waste in the Opalinus Clay as host rock. Ongoing studies on the fate of H_2 in the Opalinus Clay, e.g., the HT (Vinsot et al. 2014) and MA experiments in the Mont Terri consortium, will benefit from these data on abiotic geochemical oxidation rates of H_2 and the related processes for the interpretation of diffusion and microbial oxidation rate determinations.

These preliminary data will be complemented by experiments with larger rock masses in flexible gold cells that will allow a detailed investigation of not only the H_2 oxidation rates by analyzing gas phase composition, but in addition the changes in fluid composition during the experiment and the changes in the solid rock material/minerals as well (cf. Helten et al., 2022).

References

- Bagnoud, A, Leupin, O, Schwyn, B, Bernier-Latmani, R 2016. Rates of microbial hydrogen oxidation and sulfate reduction in Opalinus Clay rock. *Appl. Geochem.* 72, 42–50. <https://doi.org/10.1016/j.apgeochem.2016.06.011>
- Bonin, B, Colin, M, Dutfoy, A 2000. Pressure building during the early stages of gas production in a radioactive waste repository. *J. Nuc. Mat.* 281, 1–14. [https://doi.org/10.1016/S0022-3115\(00\)00184-7](https://doi.org/10.1016/S0022-3115(00)00184-7)

- Gaucher, E, Fernandez, AM, Waber, HN 2003. Annex 9: Rock and Mineral Characterisation of the Opalinus Clay Formation. p. 281-303. In: Pearson et al.: Mont Terri Project – Geochemistry of Water in the Opalinus Clay Formation at the Mont Terri Rock Laboratory.
- Helten, O, Ostertag-Henning, C, Bach, W, Hinrichs, K-H 2022. Generation and decomposition of low-molecular weight organic acids in hydrous pyrolysis experiments with Opalinus Clay rock. *Org. Geochem.* 172, 104481. <https://doi.org/10.1016/j.orggeochem.2022.104481>
- [Vinsot, A](#), Appelo, CAJ, Lundy, M, Wechner, S, Lettry, Y, Lerouge, C, Fernandez, A, Labat, M, Tournassat, C, de Canniere, P, Schwyn, B, McKelvie, J, Dewonck, S, Bossart, P, Delay, J 2014. In situ diffusion test of hydrogen gas in the Opalinus Clay. *Geol. Soc. Spec. Publ.* 400, 563–578. <https://doi.org/10.1144/SP400.12>
- Xu, T, Senger, R, Finsterle, S 2008. Corrosion-induced gas generation in a nuclear waste repository: Reactive geochemistry and multiphase flow effects. *Appl. Geochem.* 23, 3423–3433. <https://doi.org/10.1016/j.apgeochem.2008.07.012>

Petrophysical and petrothermal characterization of caprock carbonate stringers: the Upper Muschelkalk in the Estopanyà syncline, South-Central Pyrenees

Pedro Ramirez-Perez^{1*}, Gabriel Cofrade¹, Ernest Onetti¹, Juan Diego Martín-Martín¹, Jean-Pierre Sizun², Irene Cantarero¹ and Anna Travé¹

¹ SGR Geologia Sedimentària, Departament de Mineralogia, Petrologia i Geologia Aplicada, Facultat de Ciències de la Terra, Universitat de Barcelona (UB), c/Martí i Franquès s/n. 08028 Barcelona, Spain

² Chrono-Environnement, UMR CNRS 6249, Université de Franche-Comté, 16, Route de Gray, Besançon Cedex 25030, France

* pramirezperez@ub.edu

1 Introduction

The current climate and energy context calls for a better understanding of geological reservoirs to develop carbon-neutral alternative energy exploitation. In recent decades, energy research has focused on studying hydrocarbon plays for alternative energy purposes. Among them, salt structures have become one of the most popular settings for geothermal energy, Carbon Capture and Storage (CCS), and underground hydrogen storage (Duffy et al., 2023) However, salt walls and diapirs frequently exhibit a heterogeneous internal composition that represents an important exploitation risk. Consequently, it is necessary to implement detailed characterization of salt structures based on well-defined outcrop analogs and high-resolution seismics (Marín et al., 2023).

In this regard, the evaluation of the potential of salt structures as reservoirs for CCS or geothermal energy requires their structural characterization and mapping and a good assessment of the reservoir conditions (i.e., pressure and temperature) and the petrophysical properties of the reservoir rocks (porosity, permeability, and thermal conductivity). Following this line, the petrophysical characterisation of salt plays has been more focused on the rock salt (i.e., halite and other viscous evaporites) than on the heterolithic bodies embedded in it (i.e., evaporite, carbonate, siliciclastic or volcanic rocks), that were transported and deformed by salt flow.

In this contribution, we present an approach to the petrophysical and petrothermal attributes of the Upper Muschelkalk unit (M3) stringers within the caprock deposits of the Estopanyà syncline (South-Central Pyrenees, NE Spain). The study presents preliminary results of the mapping, and stratigraphy of the stringers and of the petrophysical characterisation of the connected porosity, permeability, P-wave velocity, and thermal conductivity and effusivity of the M3 limestones, which have been the target of similar studies in other sites of Europe (i.e., the Upper Rhine Graben). Thus, our study aims to contribute to outcrop analog research for CCS and geothermal energy by presenting the characterization of the M3 stringers of the Estopanyà syncline.

2 Geological setting

The Estopanyà syncline is a seismic scale (10 km long by 7 km wide) tectonic structure located in the western part of the South-Central Pyrenean zone within the Serres Marginals thrust sheet. The syncline shows a Late Triassic to Oligocene sedimentary sequence sub-divided into a pre-orogenic (Late Triassic-Santonian) and a syn-orogenic (Santonian-Oligocene) succession. The Maastrichtian to Oligocene stratigraphy was strongly controlled by the growth of two salt walls in the limbs of the Estopanyà syncline that evolved, due to the advance of the Alpine compressional front, from salt-inflated NNW-SSE oriented structural ridges in the Upper Cretaceous-Paleocene and were exposed as salt-walls during the compressional onset in the Serres Marginals (Early Ypresian) (Ramirez-Perez et al., in prep.).

Thin-skinned deformation in the Southern Pyrenees was greatly controlled by the disposition of the preorogenic Middle-Upper Triassic evaporites of the Muschelkalk and Keuper facies. The distribution and migration of these units encompassed different tectonic transport ratios of the supra-salt sedimentary cover during the piggyback advance of the compressional front, forming an orogenic curvature known as the South-Central Pyrenean Zone. This structural realm is full of diapiric exposures evolved during the main compressional pulse in the Serres Marginals thrust sheet (Late Eocene – Oligocene). The Layered Evaporite Sequence (LES) that formed the current diapir exposures in the South-Central Pyrenean Zone includes three evaporitic intervals: The Middle Muschelkalk (M2) facies, and the Lower and Middle Keuper (K1 and K2) facies. Despite the former interval was never identified directly on the surface, the existence of misoriented and disrupted heterometric carbonate blocks of the Upper Muschelkalk (M3) facies indicates the existence of a detachment layer beneath them (Cofrade et al., 2023b). The Triassic LES was intruded by sill-like dolerites at the end of the Triassic, which currently appear as misoriented heterometric bodies within the caprock exposures.

The Upper Muschelkalk (M3) is the principal non-evaporitic level of the Triassic LES and consists of a carbonate unit formed by inter-to-supratidal limestones. The lower M3 interval is formed by tabular centimetre-thick layers of mudstones and fine-grained dolostones interbedded with marls and grey mudrocks, whereas the upper M3 is formed by up to meter-thick oolitic packstones and grainstones. During salt mobilization, the M3 was disrupted, fragmented, and transported within the salt flow and the subsequent salt structures. Near the surface, the most soluble evaporites (i.e., halite and other chlorides) were dissolved leading to the accumulation of the less soluble materials of the LES (i.e., gypsum and mudrocks), forming a dissolution matrix that embeds decameter thick and laterally extensive dolerites and M3 stringers (Cofrade et al., 2023a).

3 Methods

The characterization of the Upper Muschelkalk stringers in the Estopanyà syncline is based on fieldwork and laboratory analyses. Mapping of the stringers was made by Remote Sensing Mapping (RSM) using QGis (v3.28) free software and a high-resolution Digital Terrain Model (DTM) constructed with 2 m x 2 m LiDAR data. Mapping was quality-controlled in the field by comparing the cartographic trace of the identified stringers with already published geological maps and aerial 5 m/pixel resolution images. Fieldwork also included the sampling of the M3 limestones for petrological studies and petrophysical and petrothermal measurements. Field observations and laboratory data were completed with thin section descriptions using an Axiophot Zeiss optical microscope. Special attention was placed on defining rock composition and texture and pore-space geometry and potential connectivity, which can affect the petrophysical attributes of the rocks.

The measurement of the petrophysical properties was performed in two rock cubes of 175 cm³ (5 x 5 x 7 cm in size, one oriented parallel to bedding and another oriented perpendicular to it) following the procedures of Ramirez-Perez et al., (2023a). The P-wave velocity was measured using a portable Pundit 6 system (CNS Electronics LTD) operating at a regular frequency of 1 MHz. For the petrothermal analysis, samples were sawn using a high-precision manual saw to obtain 3 x 3 x 3-4 cm-sized rock cubes with two smooth surfaces (one parallel and another perpendicular to the bedding). Sample preparation and laboratory conditions followed Ramirez-Perez et al., (2023b). In the next section, we present petrophysical and petrothermal data from two samples of the Upper Muschelkalk stringers in the Estopanyà syncline (EST-1 and 6).

The thermal properties of the samples were measured using a C-Therm TCi thermal analyser using the Modified Transient Plane Source Method (MTPS). For each cube, a loop of 3 to 5 consecutive measures was done. After each measurement, a value was given by the TCi analyser and when completing the loop, a mean thermal conductivity value with its Relative Standard Deviation (RSD) was acquired. A minimum of 2 cubes are measured for each sample, depending on their petrological heterogeneity. The data of each cube were then averaged to calculate a representative value for the analysed sample, however, values placing an RSD over 2 % were deleted from their respective loops to accomplish the technical requirements of the TCi analyser.

4 Results

4.1 Field description of the Upper Muschelkalk stringers in Estopanyà

The Upper Muschelkalk (M3) crops out as tabular meter to kilometre laterally extensive limestone blocks embedded in a non-cohesive and strongly altered matrix (i.e., caprock matrix, Fig. 1A). The polarity of the M3 stringers is difficult to determine owing to the intense deformation of the limestone bodies due to salt flow and diapirism, which also folds and fractures the tabular succession of the lower M3 intervals (Fig. 1 B,C,D). Consequently, in the absence of clear stratigraphic or sedimentological attitudes (i.e., bioturbation, mud-cracks, Fig. 1E) the polarity of the M3 stringers cannot be always determined.

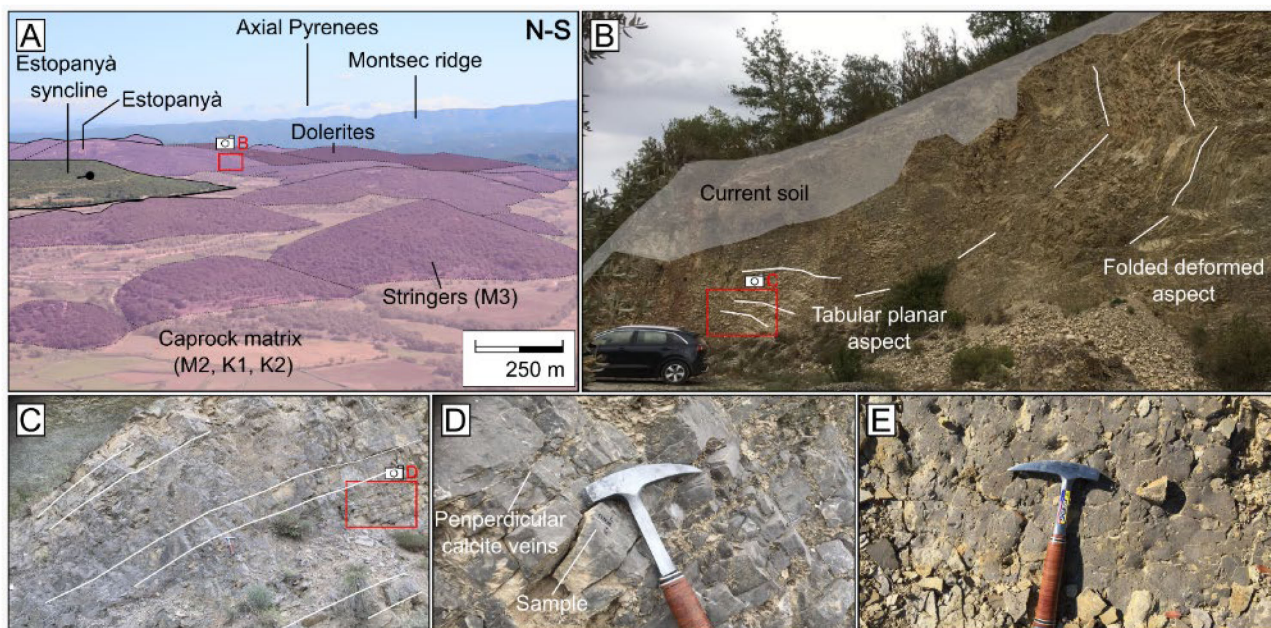


Fig. 1. Field images of the Upper Muschelkalk (M3) stringers in Estopanyà. A) Interpreted image from the southern limb of the syncline, the M3 stringers and dolerites form hills whereas the caprock matrix (mudrocks and gypsums of M2, K1, and K2 facies) crops in the fields. B) Tabular and folded aspects of the lower M3 denoting the deformation of the stringers. C) Tabular planar facies of the lower M3, centimeter- and decimeter-thick mudstone layers are packed in metric successions. D) Detail of the lower M3. Note the slight planar lamination and perpendicular to bedding centimeter-sized calcite-cemented fractures. E) Mud cracks are common base marks in the lower M3 allowing to determine the polarity of the stringers.

4.2 Petrology, petrophysics, and petrothermics of the Upper Muschelkalk in Estopanyà

The studied samples pertain to the lower M3 interval and present massive textures with very isolated millimetre-sized vug porosity. Open to slightly cemented fractures were observed perpendicular to bedding, with a millimetre amplitude and up to 1 cm longitude. Planar lamination is inferred in thin sections owing to slight changes in the grain size of the micrite matrix.

The petrophysical results agree with the moderate porosity and permeability inferred from the petrological description. The connected porosity of samples ranges between 2.07-2.49 %, whilst permeability reaches 10^{-2} mD, one order of magnitude over the instrumental threshold value. P-wave velocities vary from 6000 to 6055 ms^{-1} for dry conditions and become more dispersed for water-saturated measurements (5854 to 6122 ms^{-1}), probably because of the occurrence of open fractures that lowered the P-wave velocities. For all the analyzed properties, except for P-wave velocity in saturated conditions, the obtained values are not dependent on the measure orientation.

Thermal conductivity varies from 2.464 to 2.972 $\text{Wm}^{-1}\text{K}^{-1}$ in the case of EST-1 and from 3.176 to 3.234 $\text{Wm}^{-1}\text{K}^{-1}$ in EST-6, independently on the measurement orientation. Similarly, the thermal effusivity of EST-1 varies from 2158.8 to 2415.9 $\text{Ws}^{0.5}\text{m}^{-2}\text{K}^{-1}$, whilst it is between 2523.2 and

2557.2 $\text{Ws}^{0.5}\text{m}^{-2}\text{K}^{-1}$ for EST-6. These results indicate a very small variation in the thermal properties of the studied samples denoting that neither the petrology nor the petrophysics affects the studied thermal properties.

5 Final remarks and further work

Our very first results reveal clustered values of connected porosity, permeability, and P-wave velocity, whilst thermal properties vary slightly between samples. Such results point out to low permeability of the Upper Muschelkalk stringers that, combined with the measured moderate thermal conductivities, will result in moderately good reservoir properties for gas storage. However, low porosities will reduce the storage capacity of the M3 stringers. The presented petrophysical and petrothermal analysis cannot be considered fully representative of the Upper Muschelkalk stringers, and thus, more sampling and laboratory measurements are necessary to properly discuss the properties of these stringers and their potential for CCS or geothermal energy production. However, our contribution presents a new perspective on the caprock deposits of the South Pyrenean Zone and their potential for carbon-neutral energy production.

References

- Cofrade, G., Závada, P., Krýza, O., Cantarero, I., Gratacós, Ò., Ferrer, O., Adineh, S., Ramirez-Perez, P., Roca, E., & Travé, A. (2023a). The kinematics of a salt sheet recorded in an array of distorted intrasalt stringers (Les Avellanes Diapir – South-Central Pyrenees). *Journal of Structural Geology*, 176, 104963. <https://doi.org/10.1016/J.JSG.2023.104963>
- Cofrade, G., Cantarero, I., Gratacós, Ò., Ferrer, O., Ramirez-Perez, P., Travé, A., & Roca, E. (2023b). Allochthonous salt advance recorded by the adjacent syn-kinematic sedimentation: Example from the Les Avellanes diapir (South Central Pyrenees). *Global and Planetary Change*, 220, 104020. <https://doi.org/10.1016/J.GLOPLACHA.2022.104020>
- Duffy, O., Hudec, M., Peel, F., Apps, G., Bump, A., Moscardelli, L., Dooley, T., Bhattacharya, S., Wisian, K., & Shuster, M. (2023). The Role of Salt Tectonics in the Energy Transition: An Overview and Future Challenges. *Tektonika*, 1(1). <https://doi.org/10.55575/TEKTONIKA2023.1.1.11>
- Marín, D., Cardozo, N., & Escalona, A. (2023). Compositional variation of the Zechstein Group in the Norwegian North Sea: Implications for underground storage in salt caverns. *Basin Research*, 35(4), 1460–1485. <https://doi.org/10.1111/BRE.12761>
- Ramirez-Perez, P., Cantarero, I., Cofrade, G., Muñoz-López, D., Cruset, D., Sizun, J. P., & Travé, A. (2023a). Petrological, petrophysical and petrothermal study of a folded sedimentary succession: the Oliana anticline (Southern Pyrenees), outcrop analogue of a geothermal reservoir. *Global and Planetary Change*, 222, 104057. <https://doi.org/10.1016/J.GLOPLACHA.2023.104057>
- Ramirez-Perez, P., Cantarero, I., Cofrade, G., Muñoz-López, D., Cruset, D., Sizun, J. P., & Travé, A. (2023b). Petrophysical and petrothermal dataset of the sedimentary succession in the Oliana anticline (Southern Pyrenees). *Data in Brief*, 48. <https://doi.org/10.1016/j.dib.2023.109086>
- Ramirez-Perez, P., Cofrade, G., Martín-Martín, J. D., & Travé, A. (in prep.). Stratigraphic Evolution of a Salt-Walled Basin: The Influence of Diapirism and Compressional Tectonics on the Sedimentary Record of the Estopanyà Syncline (South-Central Pyrenees). <https://doi.org/10.2139/SSRN.4604076>

Microbial processes responsible for H₂ consumption in clay reservoirs

Camille Rolland^{1*}, Olivier X. Leupin² and Rizlan Bernier-Latmani¹

¹ Ecole Polytechnique Fédérale de Lausanne, EPFL, Lausanne, Switzerland

² National Cooperative for the Disposal of Radioactive Waste, Wettingen, Switzerland

* camille.rolland@epfl.ch

Abstract

Hydrogen gas (H₂) is taking center stage in the development of projects related to sustainable energy sources, and the quest for geological hydrogen and/or a subsurface storage option is progressing. In both cases, a caprock, likely clay rock is necessary. However, H₂ is also a readily available source of energy for microbial communities (Greening et al., 2016; Hensdorf et al., 2017; Gregory et al., 2019). Its oxidation is coupled to microbial metabolism such as sulfate reduction, iron reduction, or methanogenesis. If H₂ storage in clay-capped, porous underground reservoirs is to be a viable option, its consumption by microorganisms should be characterized and, ideally, inhibited. Alternatively, H₂ could be converted to methane while sequestering CO₂, in which case H₂ consumption should be enhanced. A better understanding of the rate(s), control(s), and engineering potential of microbial H₂ oxidation in the deep subsurface is needed to provide the parameters required to design H₂ storage/transformation systems underground.

The most significant amount of work carried out on the topic of H₂ conversion in the subsurface has been performed in the context of the safe disposal of nuclear waste in a deep geological repository (e.g., Bagnoud et al., 2016a, 2016b). Thus, we can leverage that knowledge for H₂ storage applications. More specifically, having a thorough understanding of the factors controlling the rate of H₂ consumption, and of the impact of microbial activity on deep subsurface reservoirs, will be critical to choosing appropriate locations for the implementation of H₂ storage or CO₂ to methane conversion in the subsurface.

Here, we present an *in-situ* experiment in the Mont Terri Underground Rock Laboratory (URL) that was designed with the storage of radioactive waste in mind but whose approach and results are also relevant for the abovementioned applications. The Mont Terri URL intersects the Opalinus Clay geological layer which was selected for the storage of radioactive waste in Switzerland. In this context, H₂ production will result from anoxic corrosion of low and intermediate level waste steel containers, threatening the integrity of the host rock. The transport of gases (produced in the disposal caverns) to the operational tunnel will limit the overpressure. As an additional safety parameter, the capacity of microorganisms to act as a H₂ sink is being considered. The small pore space and low water activity in undisturbed Opalinus Clay rock limit microbial metabolism and growth. Thus, the proposed strategy is to backfill the operational tunnels with porous material to allow microbial growth and the concomitant consumption of H₂. Our experiment aims at quantifying the microbial H₂ consumption rate in this environment, and deconvoluting the underlying microbial processes and dynamics, as well as the associated geochemical processes.

The experiment consists of a borehole, drilled in Opalinus Clay rock, and feeding porewater to gas-tight reactors packed with porous medium (sand-bentonite 80/20 (wt.-%)). The latter corresponds to material being considered for gallery backfill in a nuclear waste repository. The experiment aims at quantifying the microbial H₂ consumption rate in this environment, and deconvoluting the underlying microbial processes and their dynamics, as well as associated geochemical processes. To reconstruct expected repository conditions, porous medium is only partially saturated with Opalinus Clay porewater and pulse injections of H₂ (100 %) are applied to the reactor, establishing a gas overpressure of 4 bars. The gas pressure and composition are monitored daily, allowing the determination of microbial H₂ consumption and methane production rates. Porewater chemistry reveals the extent of

sulfate and iron consumption. Finally, the microbial community composition and distribution and the speciation of redox-sensitive elements (Fe, S) are characterized in a spatially-resolved manner. This work lays the methodological groundwork for the type of investigation that will constrain the effectiveness of subsurface reservoirs for H₂ storage and conversion.

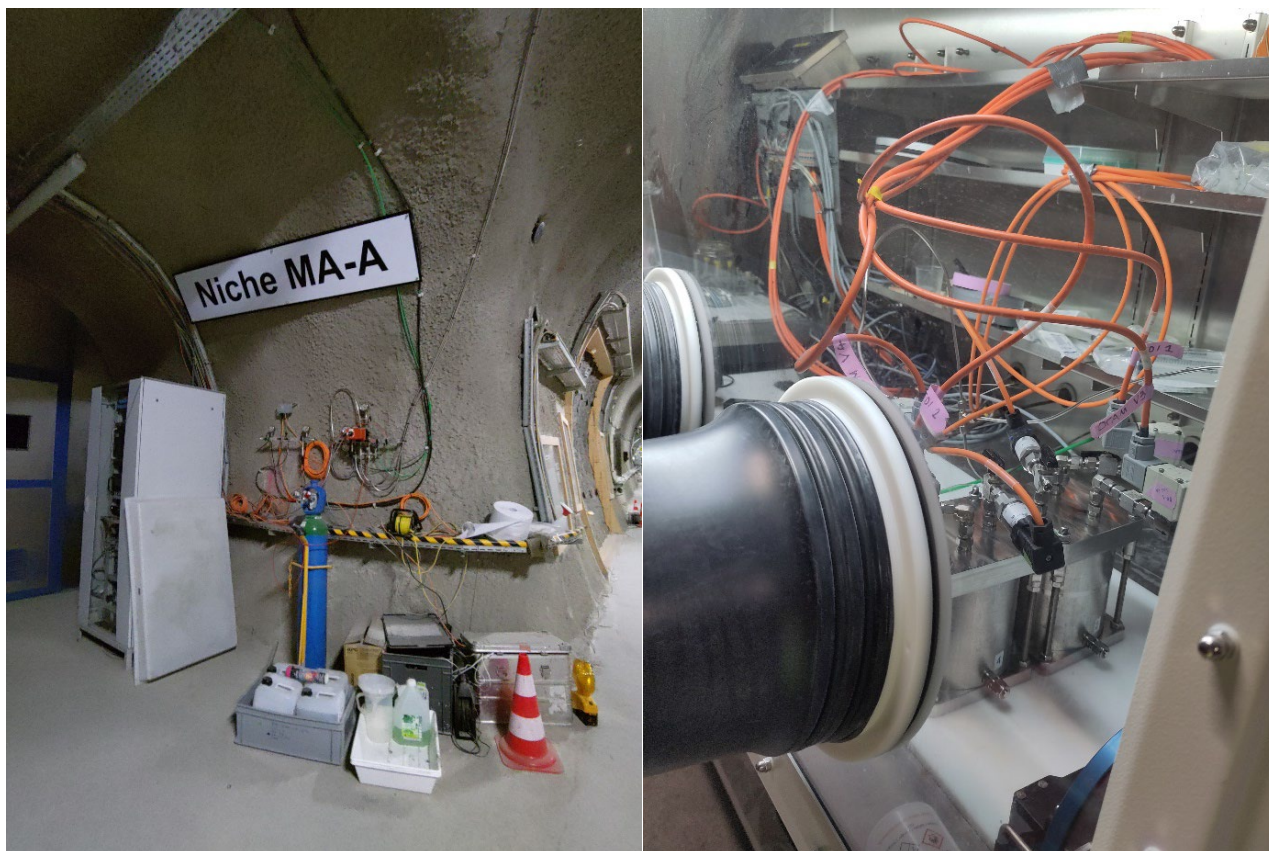


Fig. 1. (Left) Niche MA-A in the Mont Terri Underground Rock Laboratory. (Right) Reactors installed in the anoxic chamber, equipped with pressure sensors, and electro-valves for H₂ injections and gas sampling (photographs by C. Rolland).

References

- Bagnoud, A., Chourey, K., Hettich, R. L., de Bruijn, I., Andersson, A. F., Leupin, O. X., et al. (2016a). Reconstructing a H₂-driven microbial metabolic network in Opalinus Clay rock. *Nat Commun* 7, 12770. <https://doi.org/10.1038/ncomms12770>
- Bagnoud, A., Leupin, O., Schwyn, B., and Bernier-Latmani, R. (2016b). Rates of microbial H₂ oxidation and sulfate reduction in Opalinus Clay rock. *Applied Geochemistry* 72, 42–50. <https://doi.org/10.1016/j.apgeochem.2016.06.011>
- Greening, C., Biswas, A., Carere, C. R., Jackson, C. J., Taylor, M. C., Stott, M. B., et al. (2016). Genomic and metagenomic surveys of hydrogenase distribution indicate H₂ is a widely utilised energy source for microbial growth and survival. *ISME J* 10, 761–777. <https://doi.org/10.1038/ismej.2015.153>
- Gregory, S., Barnett, M., Field, L., and Milodowski, A. (2019). Subsurface Microbial H₂ Cycling: Natural Occurrence and Implications for Industry. *Microorganisms* 7, 53. <https://doi.org/10.3390/microorganisms7020053>
- Hernsdorf, A. W., Amano, Y., Miyakawa, K., Ise, K., Suzuki, Y., Anantharaman, K., et al. (2017). Potential for microbial H₂ and metal transformations associated with novel bacteria and archaea in deep terrestrial subsurface sediments. *ISME J* 11, 1915–1929. <https://doi.org/10.1038/ismej.2017.39>

Sealing capacity of a pre-fissured caprock to CO₂ injection (CS-C)

Eleni Stavropoulou^{1*} and Lyesse Laloui¹

¹ École Polytechnique Fédérale de Lausanne (EPFL), Laboratory for Soil Mechanics (LMS), EPFL-ENAC-LMS, Station 18, 1015 Lausanne, Switzerland

* eleni.stavropoulou@epfl.ch

1 Introduction

The integrity of low-permeability caprocks such as shales, is crucial for CO₂ containment, particularly at early times when the buoyancy of the injected CO₂ might drive upward migration, or in cases where the reservoir is overpressured during injection. In such situations, the transport behaviour of fractures, either naturally pre-existing or induced, in the sealing unit becomes crucial for evaluating the safety of injected CO₂. The sealing and transport properties of intact Opalinus Clay make it a good caprock candidate for geological CO₂ storage: CO₂ entry pressures between 2 and 6 MPa and water permeability in the order of 10⁻²⁰ m² (Minardi et al. 2021, Stavropoulou & Laloui, 2022a). Therefore, for lower CO₂ overpressures, leakage through low-permeability caprocks requires the presence of fractures. The long-term evolution of such potential conduits is highly uncertain and dependent on an intricate coupling between geomechanical and hydrogeological processes. For instance, the Opalinus Clay has been shown to induce self-sealing in conductivity due to clay swelling when in contact with water (Voltolini & Ajo-Franklin, 2020). However, the impact of CO₂ flowing through micro-fractures in shaly caprocks is not yet well understood as different competing mechanisms take place (e.g., caprock desiccation, local effective stress modification) (Stavropoulou & Laloui, 2022b). In this work, the processes associated with the role, initiation and propagation of fissures in caprocks are studied aiming at relating the results to field conditions: reactivation of faults or other potential leakage pathways. CO₂ injection is performed in a pre-fissured Opalinus Clay sample and the hydromechanical response of the material is analysed with quantitative image analysis of real-time x-ray tomographies. The impact of CO₂ injection on the sealing capacity of the material is studied and compared to previous results of CO₂ breakthrough.

2 Methodology and Tools

In this campaign, CO₂ breakthrough is studied in an Opalinus Clay sample that was naturally pre-fissured during the rehydration process where the material was free to swell under atmospheric pressure conditions. The pre-existing fissure has an orientation parallel to the bedding plane of the material, which in this case is parallel to the longest axis of the cylindrical sample. The impact of the pre-existing fissure on the sealing capacity of the sample is investigated with real time x-ray imaging during CO₂ injection. CO₂ injection is performed stepwise, parallel to the axis of the main-pre-existing fissure and under isotropic confinement. More precisely, isotropic confinement of 10 MPa is applied and CO₂ is introduced from the upstream side of the sample at different pressure levels: 1 MPa, 2 MPa, 3 MPa and 4 MPa. The test has taken place under controlled temperature conditions equal to 25 °C ± 0.5 °C.

To study the sealing capacity of the caprock material, a new high pressure mini-cell has been designed that allows CO₂ injection during live x-ray tomography (XRCT). This original cell can reproduce conditions representative to the field including high loading stress (max. 30 MPa) and pore pressure (max. 16 MPa). The mini-cell is designed to host cylindrical samples of 5 mm diameter and 10 mm height. Small samples allow faster testing intervals but also better image resolution in the x-ray tomograph. A resolution of 6 µm/px is obtained for a scan duration of 1 h.

The result of an x-ray tomography is a 3D x-ray attenuation map of the scanned sample that is associated with the 3D density map of the material. Advanced image analysis enables the measurement of the micro-structural changes of the material in 3D. The volumetric response of the caprock

material during the different stress/pressure steps is calculated with Digital Volume Correlation (DVC) using the open-source SPAM software (Stamati et al. 2020).

3 CO₂ injection in pre-fissured Opalinus Clay

CO₂ injection is performed in a pre-fissured Opalinus Clay sample under isotropic confinement. An initial confining stress $p = 3$ MPa is applied (scan 00) that is increased to 10 MPa (scan 01). Water is then introduced in the downstream line of the sample in contact with the top side of the sample under atmospheric pressure during 2 days (scan 02). CO₂ is introduced from the bottom of the sample (upstream line) and injected under drained conditions at four different pressure levels: 1 MPa (scan 03), 2 MPa (scan 04), 3 MPa (scan 05) and 4 MPa (scan 06). A final scan (07) is performed after unloading the sample to zero pore pressure and confining stress. The middle horizontal and vertical slice of the sample at each scan are presented in Fig. 1.

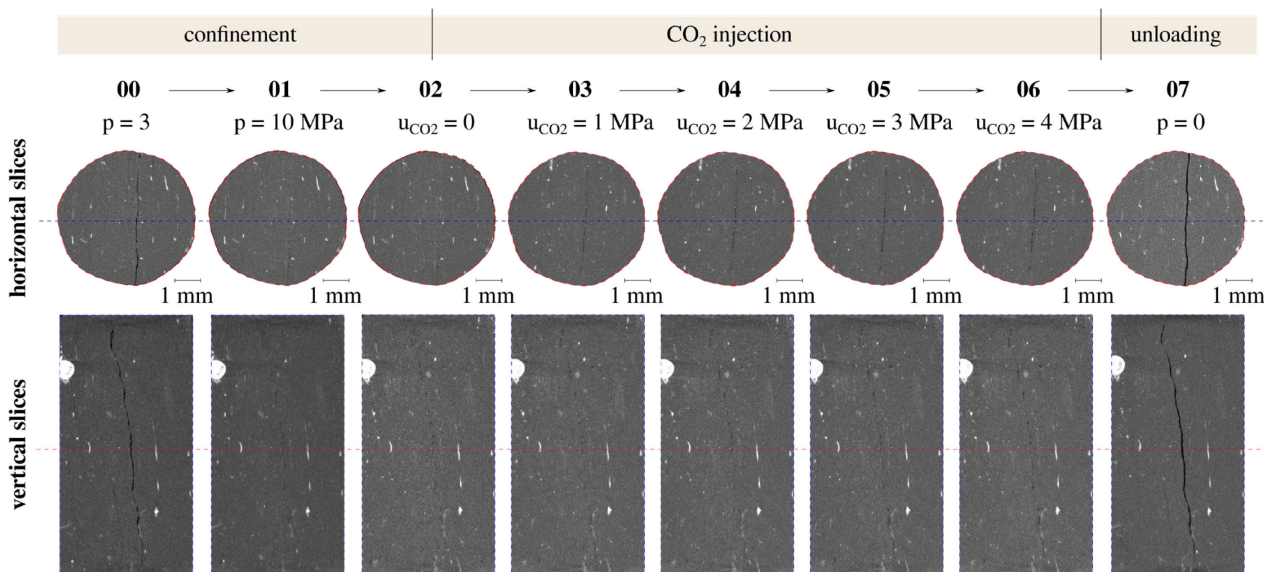


Fig. 1. Horizontal and vertical slices of the x-ray tomographies during the different testing phases – the straight dashed lines indicate the location of the corresponding perpendicular slices.

The evolution of the 3D micro-structure during the different stages (confinement, CO₂ injection, unloading) is analysed directly from the acquired images. A main pre-existing fissure that goes through the entire height of the sample is clearly visible (darker grey values in scan 00) – see vertical slice. Several additional micro-fissures are also detectable, with orientation parallel to the main one. Increase of the confining stress (from 3 MPa to 10 MPa in scan 01) results in reduction of the main fissure which nearly disappears after 2 days of confinement and introduction of water on the top side under atmospheric pressure (scan 02) that seemed to enhance the self-sealing response of the material.

CO₂ is introduced in pure gaseous form from the bottom of the sample at increasing steps of 1 MPa. The time duration of each injection step is 20 min followed by 1 hour of scanning. This relatively short injection and exposure time to gaseous CO₂ minimises phenomena related to rock mineral alteration (dissolution). As revealed from the horizontal slices, the main pre-existing fissure opens already after the first CO₂ injection level (scan 03). The aperture of the fissure slightly increases at each increase of the injection pressure level. Fissure opening is clearer in the middle horizontal slices, and it becomes more visible from scan 05 onwards in the vertical slices.

To better understand the mechanical response of the material, the total and local volumetric strain of the sample are calculated with DVC. For the calculation of the total volumetric strain, each scan is compared to scan 02 ($p = 10$ MPa and $u_{\text{CO}_2} = 0$) which is used as reference scan. During the application of confinement (00 to 02) the sample compacts by nearly 1 % (negative strain). Once CO₂ is introduced (03 to 06) the sample starts swelling slightly (positive strain) in an increased way

at each injection pressure increase: 0.05 %, 0.12 %, 0.19 % and 0.29 % for $u_{\text{CO}_2} = 1 \text{ MPa}$, 2 MPa, 3 MPa and 4 MPa respectively. As suggested by Stavropoulou & Laloui (2022a), swelling response of the material indicates breakthrough that in this test seems to occur already at 1 MPa. This is indeed possible given the presence of the main fissure that remains partially open and seemingly serves as a breakthrough conduit. Finally, after unloading, the sample swells by a total of around 2.5 % (scan 07).

To better understand the occurring kinematics, local DVC is performed using again scan 02 as a reference scan. The 3D map of volumetric strain of the sample after application of confinement (00-02) and post-CO₂ injection unloading (02-07) are presented in Fig. 2.

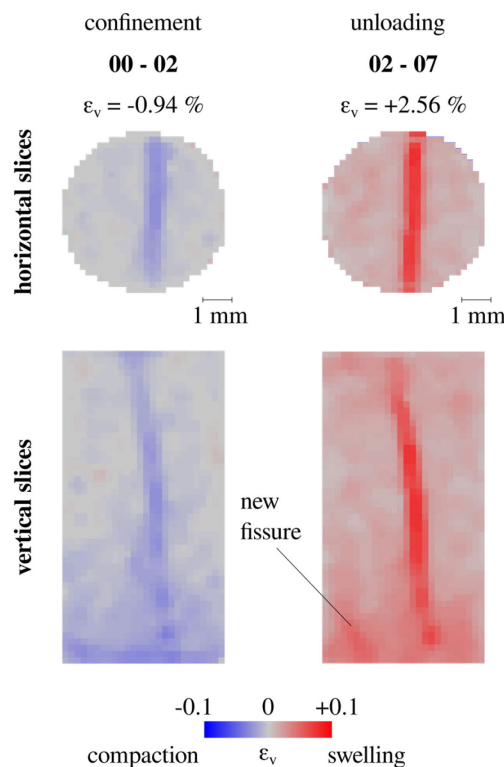


Fig. 2. Horizontal and vertical slices of the calculated volumetric strain during the application of isotropic confinement (00-02) and after unloading (02-07).

During application of confinement, compaction is calculated with maximum values (10 %) around the pre-fissured zone as seen from both horizontal and vertical slices (00-02). After stress and pore pressure release, the material relaxes and a swelling response is observed (02-07). There is a localised pronounced swelling response around the pre-existing fissure but also around the bottom part of the sample. This pronounced swelling at the bottom of the sample suggests a damaged zone that can be confirmed by the existence of minor micro-fissures visible at this resolution. The volumetric map 02-07 shows that release of CO₂ pressure and confinement, result in re-opening of the main pre-existing fissure at the bottom of the sample and a global relaxation of the material throughout its height. Interestingly, a more pronounced swelling zone is measured at the bottom of the sample with a discrete zone at the left side that indicates the creation of a new fissure.

4 Volumetric response of the fissured zone

To understand the evolution and contribution of the pre-existing fissures to CO₂ breakthrough, a quantitative analysis of the fissures' volume is performed. The acquired x-ray tomographies are segmented and the evolution of the volume of the fissures is calculated during the different applied boundary conditions. After application of confinement and before CO₂ injection, the pre-existing fissure closes by 98 % (scan 02). CO₂ injection results in fissure opening already during the first pressure level (1 MPa – scan 03) by 3 % (reference scan 02). During the following two injection steps,

2 and 3 MPa, the fissure opens further by 4 % at each pressure increase, while it remains stable during the last injection step (0.7 % at 4 MPa – scan 06). This response combined with the localised volumetric map of the sample suggests that until $u_{CO_2} = 3$ MPa (scan 04), the main pre-existing fissure serves as the principal CO_2 conduit. The pronounced swelling of the intact material at the bottom of the sample combined with the stabilisation of the fissure at $u_{CO_2} = 4$ MPa, indicates CO_2 entry in the material, i.e., breakthrough pressure from 3 to 4 MPa. This range is coherent with the breakthrough values stated in literature (Espinoza & Santamarina, 2017) at a similar level of effective stress (10 MPa) and even suggests a narrower range. However, this interpretation remains a speculation and needs to be confirmed with additional measurements.

5 Conclusions

Fissures can have a significant impact on caprock integrity in the context of carbon capture and storage (CCS) projects or any other subsurface containment scenarios. They can locally increase the permeability of the caprock and serve as direct pathways for the upward migration of CO_2 , reducing its ability to act as an effective seal. If these pre-existing or created fissures connect the storage reservoir to the overlying rock layers or the surface, they can compromise the containment of the injected fluids, leading to potential CO_2 leakage and environmental risks.

In this work, 3D imaging of a pre-fissured caprock sample revealed that the main fissure drives the hydromechanical response of the material until a certain injection level. The fissure starts re-opening already at low CO_2 overpressure (1 MPa) and keep opening until a certain overpressure level (3 MPa) where does not seem to further evolve (4 MPa). The fissure kinematics combined with the overall volumetric response of the sample suggest that at the final injection step the contribution of the fissure to CO_2 migration is stable and CO_2 breakthrough in the matrix of the material takes place. Given the short time period of the injection phase, diffusive flow is not considered for the analysis of the material's response (Busch et al. 2008).

The exact CO_2 breakthrough pathway in the caprock is not easy to predict because of the extremely small pore size (nano-metric scale) and the high micro-structural heterogeneity of the material. The connected pore space (including fissures) is supposed to drive flow and breakthrough phenomena; however, the different competing mechanisms (e.g., desiccation, local effective stress modification) may result in the collapse of initially conductive pathways and the creation of new ones. For instance, the volumetric response of the material after unloading revealed a pronounced swelling response at the bottom of the sample overall and locally: increased strain in a region that resembles to a created fissure conduit. In the future activities, injection experiments (in-situ and ex-situ the tomograph) will be performed under higher confining stress and will target for the first time combined hydraulic measurements (inflow/outflow) and localised kinematics in pre-fissured samples.

References

- Busch, A., Alles, S., Gensterblum, Y., Prinz, D., Dewhurst, D. N., Raven, M. D., Stanje, H., & Krooss, B. M. (2008). Carbon dioxide storage potential of shales. *International journal of greenhouse gas control*, 2(3), 297-308.
- Espinoza, D. N., & Santamarina, J. C. (2017). CO_2 breakthrough - Caprock sealing efficiency and integrity for carbon geological storage. *International Journal of Greenhouse Gas Control*, 66, 218–229.
- Minardi, A., Stavropoulou, E., Kim, T., Ferrari, A., & Laloui, L. (2021). Experimental assessment of the hydro-mechanical behaviour of a shale caprock during CO_2 injection. *International Journal of Greenhouse Gas Control*, 106, 103225.
- Stamati, O., Andò, E., Roubin, E., Cailletaud, R., Wiebicke, M., Pinzon, G., Couture, C., Hurley, R., Caulk, R., Caillerie, D. and Matsushima, T., ... & Birmipilis, G. (2020). Spam: software for practical analysis of materials. *Journal of Open Source Software*, 5(51), 2286.
- Stavropoulou, E., & Laloui, L. (2022a). Evaluating CO_2 breakthrough in a shaly caprock material: a multi-scale experimental approach. *Scientific Reports*, 12(1), 10706.
- Stavropoulou, E., & Laloui, L. (2022b). Insights into the interaction of a shale with CO_2 . *Solid Earth*, 13(12), 1823-1841.
- Voltolini, M., & Ajo-Franklin, J. B. (2020). The sealing mechanisms of a fracture in opalinus clay as revealed by in situ synchrotron x-ray micro-tomography. *Frontiers in Earth Science*, 8, 207.

Factors controlling acid interactions with carbonate rocks

Atefeh Vafaie^{1*}, Jordi Cama², Josep M Soler², Dragan Grgic³, Iman R Kivi⁴, Samuel Krevor¹ and Victor Vilarrasa⁴

¹ Department of Earth Science and Engineering, Imperial College London, London SW7 2AZ, United Kingdom

² Institute of Environmental Assessment and Water Research, Spanish National Research Council (IDAEA-CSIC), Barcelona, Spain

³ GeoResources Laboratory, National School of Geology, University of Lorraine, Vandoeuvre-lès-Nancy, France

⁴ Global Change Research Group (GCRG), IMEDEA, CSIC-UIB, Esporles, Spain

* a.vafaie@imperial.ac.uk

1 Introduction

Large-scale storage of CO₂ in deep saline aquifers is a promising technology for mitigating atmospheric CO₂ emissions and global climate change (Metz 2005, Ringrose et al. 2021). When stored in the aquifer CO₂ acidifies the resident brine. This induces mineral dissolution which may cause changes in the pore structure and hydromechanical properties of the rock, particularly in carbonate rocks with fast-dissolving minerals (Gaus, 2010). These changes may in turn exert an influence on reservoir injectivity, mechanical integrity, and storage capacity (Rohmer et al. 2016, Wang et al. 2023). An understanding of these changes is indispensable to optimize and secure large-scale CO₂ storage projects and is the goal of this study (Vafaie et al. 2023a).

To achieve this goal, we perform flow-through experiments on cylindrical cores of a permeable limestone with two different acidic solutions (1) dissolved-CO₂, a weak acid, and (2) HCl, a strong acid commonly used agent for acid stimulation operations in carbonate hydrocarbon reservoirs. We use a combination of evaluation techniques, e.g., effluent chemistry analysis, X-ray imaging, porosity and permeability measurements, and mechanical loading tests to quantify acid-induced changes in the hydromechanical properties of the studied samples. Further, we rely on the comparison between these two sets of experiments to discuss the effects of acid type and pore structure heterogeneities on flow and reactions in carbonate rocks.

2 Material and methods

Three cylindrical core samples (samples *N1* to *N3*) of Pont Du Gard Limestone (~100 % calcite) with a diameter of 25 mm and a length between 50-75 mm are used in this study. Samples *N1* and *N2* are injected respectively with CO₂-saturated water ($P_{CO_2} = 100$ bar & $T = 60$ °C) and HCl solutions (atmospheric pressure and $T = 60$ °C) of the same pH (= 3.13) using the same flow rate (0.15 mL/min) for 14 days. Sample *N3* is not injected with these acidic solutions. Instead, it is used to measure the stiffness and strength of intact limestone (for more details see Vafaie et al. 2023b). We combine x-ray imaging, porosity, and permeability measurements on the core samples before and after percolation experiments with effluent chemistry analysis (outflow [Ca] variations) to assess the evolution of pore structure and hydraulic properties of the rock. Ultrasonic velocity measurements and uniaxial loading tests are also conducted on both intact and acid-altered cores to evaluate the changes in elastic constants (Young's, bulk, and shear moduli) and uniaxial compressive strength (UCS) of the rock.

3 Results

Fig. 1 shows the variation of outflow [Ca] versus time in percolation experiments. In both experiments [Ca] is > 0 illustrating continuous calcite dissolution. Outflow Ca concentration is up to 25 times higher in the CO₂-saturated water experiment (*N1*) than in the HCl test (*N2*). Although the flow rate and pH of the injected solutions are the same, the buffering capacity of the CO₂-saturated water is much higher. As a result, there is much more hydrogen ion available per unit volume of fluid in the CO₂-water system compared with the HCl system.

The observed trends in [Ca] are different for the two experiments and correlated with the injected acidic solution. In the CO₂ injection experiment, we first observe an initial peak for outflow [Ca] associated with the propagation of dissolution front across the core. This initial peak (day 1) is followed by a substantial decrease in outflow Ca concentration (days 2 to 5) due to the formation of preferential flow paths inside the sample, which diminishes the accessible reactive surface area with time. Eventually, the Ca concentration becomes constant at the core outlet (from day 5 on) that results from the complete localization of flow and dissolution reaction and an approximately constant surface area. In the HCl experiment, however, outflow [Ca] is almost constant throughout the whole experiment. The steady release of Ca in this case, translated as a constant calcite dissolution rate, is characterized by an almost constant reactive surface area.

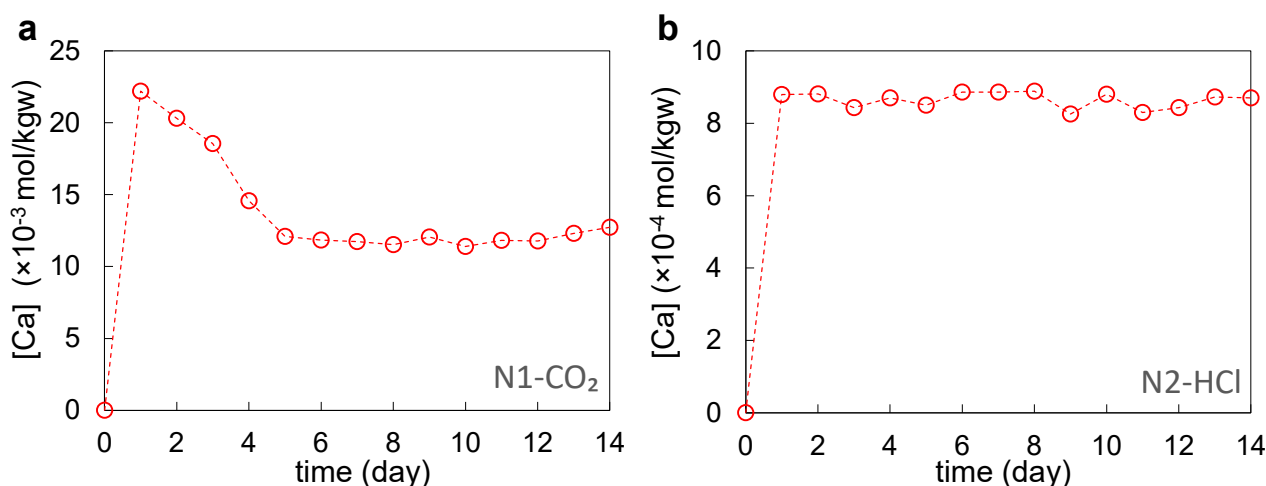


Fig. 1. Variation in outflow Ca concentration versus time for (a) CO₂-saturated water experiment and (b) HCl experiment.

Continuous calcite dissolution leads to porosity enhancements in both experiments. As expected, porosity enhancement is much larger in sample *N1* ($\Delta\phi=5.5\%$) than in sample *N2* ($\Delta\phi=0.3\%$) in agreement with outflow [Ca] content (Fig. 1). Fig. 2 depicts X-ray porosity profiles along the length of samples *N1* (Fig. 2a) and *N2* (Fig. 2b) before and after percolation experiments. These porosity profiles show that the porosity enhancement is non-uniform across the limestone cores. In the CO₂-injection case, porosity increases along the whole length of the sample although it is much more pronounced near the core inlet. In contrast, in the HCl-treated sample (*N2*) porosity increase only occurs at the core inlet forming a compact dissolution pattern.

In both experiments, the permeability of the cores increases because of porosity enhancement. In the HCl-treated sample (*N2*), permeability increases by a factor of 3 (from 1.0×10^{-13} to 3.2×10^{-13}). In the CO₂-treated core (*N1*), though, the permeability increase is of 3 orders of magnitude (from 8.1×10^{-14} to 8.3×10^{-11}). This substantial increase in permeability is caused by the formation of a large wormhole inside the sample *N1* as illustrated in Fig. 2c.

Compressional (V_p) and shear (V_s) wave velocities decrease with increases in the porosity of the samples correlated with reductions in elastic moduli of the rock. Nevertheless, attenuations in V_p and V_s are more definite in the CO₂ injection experiment tied up with larger porosity enhancement in this case (Fig. 3a). The tests for stress-strain behavior of the cores indicate a sharp decrease in both static Young's modulus (up to 38%) and UCS (up to 65%) of the acid-injected samples compared to intact one (sample *N3*) (Fig. 4b, c).

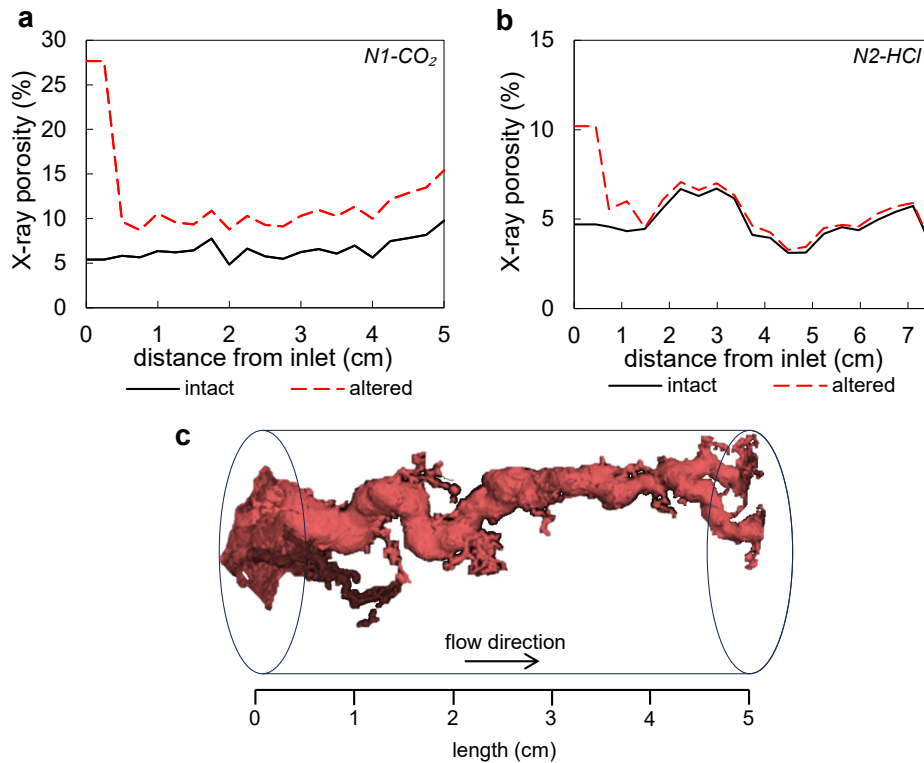


Fig. 2. Average x-ray porosity profile across the cores before (black solid line) and after (red dashed line) percolation experiments: (a) CO₂-saturated water experiment and (b) HCl experiment. (c) 3D reconstruction, from X-ray images, of porosity increase and wormhole formation due to calcite dissolution in sample N1.

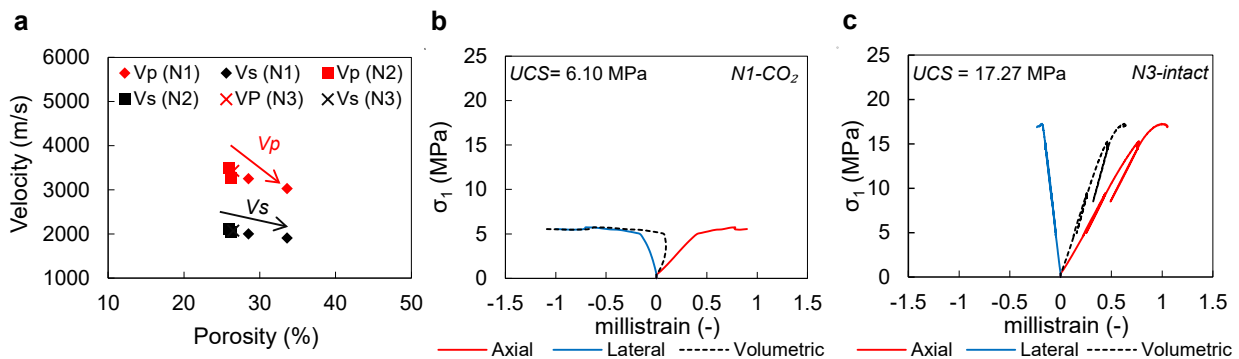


Fig. 3. (a) variation in the ultrasonic velocity as a function of porosity in the intact and acid-treated samples. Higher porosity-lower velocity data for samples N1 and N2 refers to the post-injection state. Stress-strain response of (a) CO₂-treated and (c) intact limestone cores.

4 Discussion

We have observed that continuous calcite dissolution causes different changes in the rock pore structure and forms different dissolution patterns inside the studied samples. Although we used similar flow regimes as estimated by the Peclet number, the ratio of advection to diffusion rate ($Pe \approx 3$) in both experiments, a change in calcite dissolution kinetics (H^+ activity and/or calcite reactive surface area) must be responsible for the development of two distinct dissolution patterns in the studied samples. Since the pH (H^+ activity) of both injected solutions is the same, a change in the reactive surface area must be behind the variations in calcite dissolution rate and outflow [Ca]. The pore structure heterogeneity evidenced by X-ray imaging of samples may lead to small differences in outflow [Ca] evolution but not different dissolution trends. The change in accessible reactive surface area is therefore caused by the acid type as the main different parameter between the two acid-rock systems, which needs to be considered when evaluating acid-rock interactions.

The partial dissociation of dissolved CO₂ (weak acid) and its buffering capacity provides a low pH solution (pH < 5) across sample *N1* leading to wormhole formation in this case. However, HCl is a strong acid that dissociates completely into its ions and strongly dissolves calcite at its first contact with the limestone core (i.e., core inlet). Strong calcite dissolution at the core inlet results in a fast increase in the pH (no buffering effect) preventing the advancement of dissolution front inside the core and rendering a compact dissolution pattern.

In both cases, observed dissolution patterns deviate from what is suggested by the traditional approach, i.e., calculated Peclet ($Pe \approx 3$) and Damkohler numbers, i.e., the ratio of reaction rate to advective flux ($Da \approx 10^{-4}$) for the studied samples. Although for $Pe > 1$ and $Da < 10^{-3}$, a uniform dissolution pattern is expected to occur, wormholing regime, and compact dissolution are observed in our experiments. This deviation is caused mainly by the pore space heterogeneity and acid type, particularly acidic solutions' buffering capacity that is not reflected in these numbers. Hence, the traditional Pe - Da diagrams should be updated by incorporating these features for a more general description of changes in the texture of rocks undergoing reactions applicable to CO₂ storage.

5 Summary

This work provides new insights into the evolutions of the pore structure and hydraulic and mechanical properties of a permeable limestone percolated with two different acidic solutions: CO₂-saturated water (weak acid) and HCl (strong acid). For the given flow regime and the pH range used, acid type, and particularly its buffering capacity, chiefly controls the difference in the pore structure alterations and dissolution patterns. The complete dissociation of the strong acid (HCl) leads to the formation of a compact dissolution, while partial dissociation of the weak acid (CO₂-saturated water) and its buffering effect brings about wormhole formation. Under both conditions, heterogeneities in the pore structure of the limestone cores influence the dissolution pattern, deviating from the dissolution pattern suggested by dimensionless Pe and Da numbers.

References

- Gaus, I. 2010. Role and impact of CO₂-rock interactions during CO₂ storage in sedimentary rocks. *Int. J. Greenhouse Gas Control* 4(1), 73–89. <https://doi.org/10.1016/j.ijggc.2009.09.015>
- Golfier, F, Zarcone, C, Bazin, B, Lenormand, R, Lasseux, D, Quintard, M. 2002. On the ability of a Darcy-scale model to capture wormhole formation during the dissolution of a porous medium. *J. Fluid. Mech.* 457, 213–54. <https://doi.org/10.1017/S0022112002007735>
- Metz, B, Davidson, O, De Coninck, H, Loos, M, Meyer, L. 2005. Carbon Dioxide Capture and Storage. Summary for Policymakers. IPCC.
- Ringrose, PS, Furre, AK, Gilfillan, SM, Krevor, S, Landrø, M, Leslie, R, et al. 2021. Storage of carbon dioxide in saline aquifers: Physicochemical processes, key constraints, and scale-up potential. *Annu. Rev. Chem. Biomol. Eng.* 12,471–94. <https://doi.org/10.1146/annurev-chembioeng-093020-091447>
- Rohmer, J, Pluymakers, A, Renard, F. 2016. Mechano-chemical interactions in sedimentary rocks in the context of CO₂ storage: Weak acid, weak effects? *Earth Sci. Rev.* 157, 86–110. <https://doi.org/10.1016/j.earscirev.2016.03.009>
- Vafaie, A, Cama, J, Soler, JM, Kivi, IR, Vilarrasa, V. 2023a. Chemo-hydro-mechanical effects of CO₂ injection on reservoir and seal rocks: A review on laboratory experiments. *Renewable Sustainable Energy Rev.* 178, p.113270. <https://doi.org/10.1016/j.rser.2023.113270>
- Vafaie, A, Cama, J, Soler, JM, Grgic, D, Vilarrasa, V. 2023b. Chemo-hydro-mechanical effects of CO₂ injection into a permeable limestone. *Int. J. Coal Geol.* 1;278:104359. <https://doi.org/10.1016/j.coal.2023.104359>
- Wang, K, Ma, L, Taylor, KG. 2023. Microstructure changes as a response to CO₂ storage in sedimentary rocks: Recent developments and future challenges. *Fuel* 1, 333:126403. <https://doi.org/10.1016/j.fuel.2022.126403>

Project BiMiAb_H2: New experimental research to investigate hydrogen migration in reservoir and caprock layers

Philipp Weniger^{1*}

¹ Federal Institute for Geosciences and Natural Resources (BGR), Hannover, Germany

* philipp.weniger@bgr.de

Abstract

The integrity of caprocks is a key safety requirement for long-term containment of nuclear waste as well as safe underground gas storage. Recently, underground gas storage sites in porous rock formations as well as in salt caverns are considered for underground hydrogen storage (UHS). Geochemical and microbiological processes in geological formations and their impact on storage integrity and reservoir performance are some of the main R&D demands for the implementation of UHS. The project "Generation, Migration and Degradation of Hydrogen – BiMiAb-H2" was developed within the framework of the BGR concept "Geoscientific contributions to the implementation of the national hydrogen strategy" to investigate reservoir and caprock formations and typical fluid-rock combinations for hydrogen storage. In this context, new experimental capabilities are being developed to investigate hydrogen storage and transport mechanisms at different scales, from diffusion to migration in different flow regimes, ranging from diffusion to single and multi-phase continuum flow. New laboratory methods are designed to mimic 'in-situ' conditions by approximating pressure, temperature, geochemical fluid composition as well as microbiome of underground gas storage sites in Germany to enable a quantitative investigation of the influence of geochemical and microbial processes on reservoir performance and caprock integrity.

This paper provides an overview of the new experimental setups developed at BGR, sample selection from relevant geological formations and the experimental and analytical workflow.

Seismic and ultrasonic monitoring of a shale seal exposed to CO₂: a laboratory study

Serhii Lozovyi^{1*}, Zeenat Maniar^{2,3} and Pierre Cerasi¹

¹ SINTEF Industry, Trondheim, Norway

² GEUS, Copenhagen, Denmark

³ University of Copenhagen, Copenhagen, Denmark

* serhii.lozovyi@sintef.no

Abstract

The process of capturing carbon dioxide and containing it underground involves strategically placing the gas within a porous rock bed, sealed off by an overlying non-permeable layer, typically consisting of shales. Monitoring the displacement of CO₂ within these underground layers through time-lapse seismic surveys enables tracking of the CO₂ plume over time and assessing the integrity of the sealing layer. To measure alterations in the acoustic properties of caprock induced by CO₂, such as changes in Young's modulus, Poisson's ratio, and the velocities of compressional and shear waves, we conducted a laboratory experiment on caprock from the Lille John-2 appraisal well in the southern part of the Danish North Sea. The experiment was performed at in situ stress state using a combination of low-frequency oscillation measurement and high-frequency wave transmission measurement, both with and without the presence of CO₂. We observed a reduction in all measured elastic properties at both ultrasonic and seismic frequencies, ranging from 3-6 %, when the sample was exposed to CO₂. These results suggest that carbon dioxide can have a limited impact on the integrity of the tested rock, indicating its potential as a caprock seal for CO₂ storage. However, the effect of CO₂ exposure on wave propagation should be carefully accounted for in time-lapse seismic surveys to ensure accurate monitoring of storage and injection operations.

1 Motivation

Carbon Capture and Storage (CCS) has been identified as a key technology in mitigating atmospheric CO₂ levels, crucial for meeting the goals of the Paris Agreement. The Intergovernmental Panel on Climate Change (IPCC) defines CCS as the process of capturing CO₂ from industrial and energy-related sources, transporting it to a storage site, and isolating it long-term from the atmosphere. The feasibility of CCS hinges on the long-term geological storage of CO₂. This concept faces challenges due to the porous nature of storage formations and potential leakage pathways, necessitating CO₂ containment over periods exceeding 10,000 years (Alcalde et al. 2018). The integrity of geological seals is vital in preventing CO₂ escape, with studies emphasizing the importance of understanding storage conformance, seal integrity, and the physical properties of storage sites. Additionally, the interaction of CO₂ with geological formations, involving mechanisms like hydraulic fracturing and CO₂ diffusion, can lead to either sealing or increased porosity and CO₂ migration. These interactions are mainly influenced by reactions with minerals such as calcite and feldspar (Gaus 2010; Choi et al. 2021; Xu et al. 2022). The exposure of caprock materials like shales to CO₂ also raises concerns about altered mechanical properties, potentially impacting the effectiveness and integrity of storage sites. Thus, while CCS presents a promising approach for CO₂ reduction, it faces significant challenges in ensuring long-term storage integrity, understanding CO₂-rock interactions, and effective monitoring, all of which are critical for its success in climate change mitigation.

2 Materials and methods

To study changes in the elastic properties of a potential sealing material exposed to CO₂, we utilized shale rock from the Lille John-2 well, located in the southern part of the Danish North Sea. The sample was taken from a depth of 1183 m, has a porosity of 31 %, and a total clay mineral content of 57 %. It is saturated with in-situ brine and was sealed to preserve saturation during all transporta-

tion stages. A cylindrical core plug sample was cored with symmetry axis perpendicular to the bedding planes. The estimated lithostatic pressure in-situ is 25 MPa, and the pore pressure is 12.4 MPa. For the laboratory experiment on a core plug under in-situ stress conditions, we used SINTEF's low-frequency apparatus (Szewczyk et al. 2016). This apparatus is designed for measurements on a cylindrical sample with a diameter of 1 inch and a length of 2 inches. The measurements include static strains in axial and radial directions, and dynamic measurements of Young's modulus and Poisson's ratio at seismic frequencies of 1-150 Hz, as well as ultrasonic velocity measurements in the axial direction (P- and S-waves).

The experimental procedure involved initial loading to the estimated in-situ stress and two fluid exposure stages: first, the sample was exposed to brine with a chemical composition equivalent to in-situ conditions; second, the sample was exposed to carbon dioxide (20 %) dissolved in the in-situ equivalent brine. During the test, we measured the vertical Young's modulus and Poisson's ratio in the frequency range of 1-150 Hz by applying sinusoidal uniaxial stress oscillations with an amplitude of 1 micro-strain, and pulse-transmission measurements of P-wave velocity at 500 kHz and S-wave velocity at 250 kHz.

3 Results and Discussion

The results of seismic and ultrasonic measurements before CO₂ exposure and their respective changes in absolute and relative values after CO₂ exposure are presented in Tab. 1. The test timeline, showing the evolution of vertical Young's modulus and Poisson's ratio at seismic frequencies, is depicted in Fig. 1. The evolution of P-wave and S-wave velocities over time is illustrated in Fig. 2. During the brine exposure stage, which lasted until 836 hours, the sample had sufficient time to consolidate and equilibrate at restored in-situ stress conditions; this was also confirmed by monitoring static strains. Upon introducing CO₂-saturated brine, a slow yet distinguishable process of CO₂-induced alterations in both seismic and ultrasonic properties was observed. This process appeared nearly complete at 1400 hours, but the test continued until 2000 hours to confirm these observations. The changes in rock properties at the end of the CO₂ exposure stage are summarized in Tab. 1. It should be noted that this study does not address anisotropy; however, due to the anisotropic nature of shale rocks, a direct comparison between measured seismic and ultrasonic parameters is not provided.

Tab. 1. Elastic and acoustic properties of Lille John-2 shale at in-situ stress conditions, and their respective changes after CO₂ exposure

Parameter	Absolute value before CO ₂ exposure	Absolute change after CO ₂ exposure	Relative change after CO ₂ exposure
Vertical Young's modulus (1-87 Hz)	4.56 GPa	-0.17 GPa	-3.7 %
Vertical Poisson's ratio (1-87 Hz)	0.401	-0.026	-6.4 %
Vertical P-wave velocity (500kHz)	2598 m/s	-115 m/s	-4.4 %
Vertical S-wave velocity (250kHz)	1593 m/s	-53 m/s	-3.3 %

Our study is conceptually similar to the work reported by Rørheim et al. (2021), in which the authors performed an experiment on Draupne Shale. However, they observed no clear changes in either seismic or ultrasonic properties. The authors attribute the absence of CO₂-induced changes in rock properties to Draupne Shale being calcite-poor and therefore resilient to the acidic action of CO₂. In comparison, Draupne Shale has a porosity of 15 %, which is half that of the Lille John-2 shale used in our study. Furthermore, Draupne Shale contains 0.8 % calcite, compared to 1.3 % in Lille John-2. These differences likely explain why we observed a small, but clear, reduction in all measured elastic and acoustic rock properties. The higher porosity in Lille John-2 shale facilitates easier CO₂ penetration and dissolution of calcite minerals, affecting the rock-frame properties.

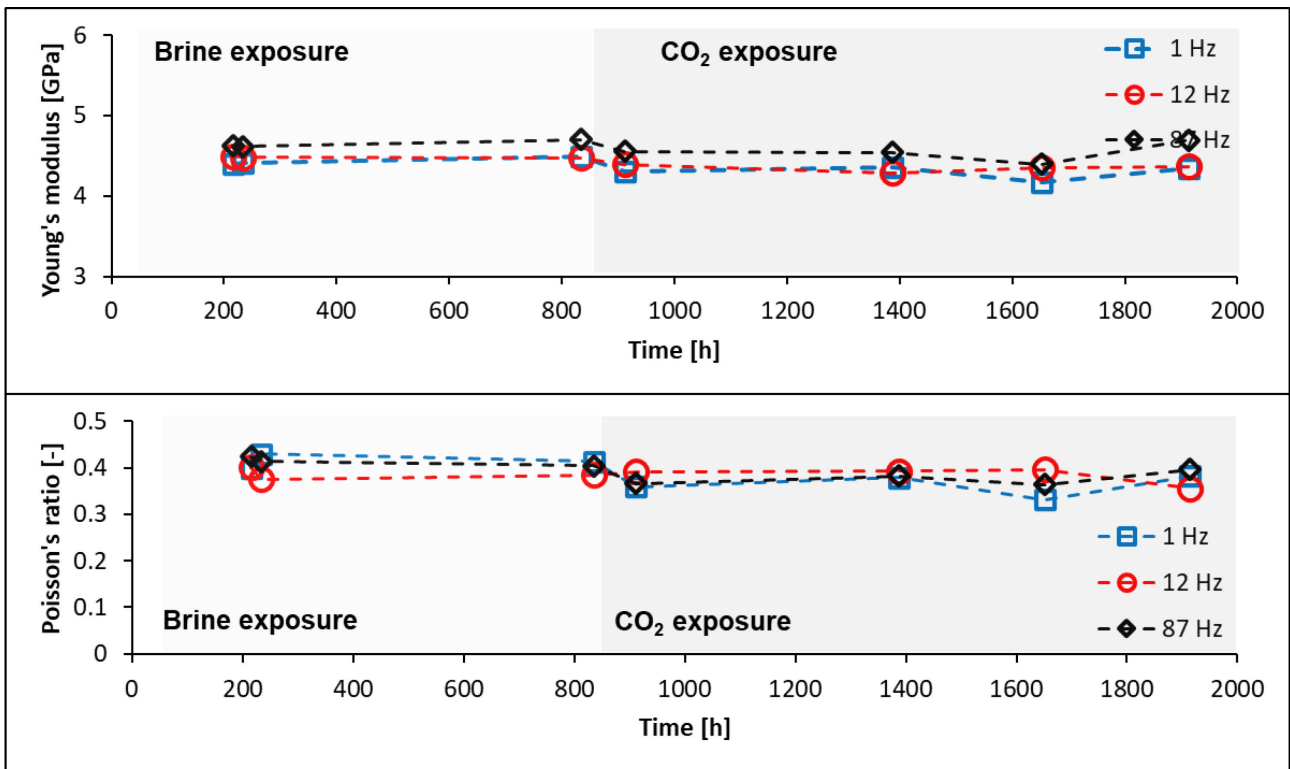


Fig. 1. Seismic results: Young's modulus (top) and Poisson's ration (bottom) as functions of test time. The results are shown for three frequencies: 1 Hz (squares), 12 Hz (circles), and 87 Hz (diamonds).

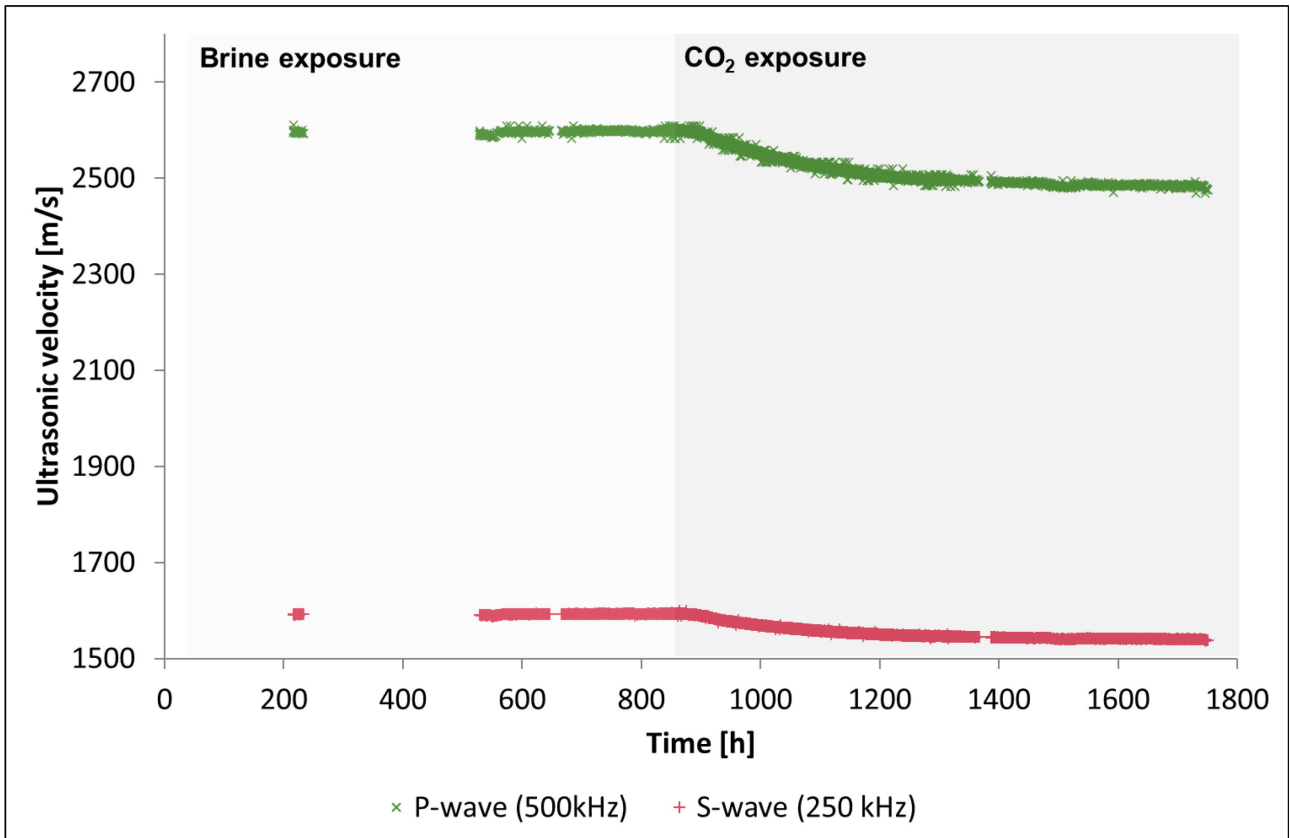


Fig. 2. Ultrasonic results obtained with pulse-transmission measurements.

4 Conclusions

This study demonstrated the impact of CO₂ exposure on the elastic and acoustic properties of Lille John-2 shale under in-situ stress conditions. The observed reduction of 3-6 % in properties such as Young's modulus, Poisson's ratio, and P- and S-wave velocities indicates that interactions between CO₂ and shale can lead to measurable changes in rock properties, an aspect that should not be ignored. While the integrity of the rock might not be significantly compromised, these observations are crucial for understanding the seismic response of shale formations acting as sealing caprock over CO₂ sequestration reservoirs, and therefore can help in accurate time-lapse seismic monitoring. Our findings enhance the understanding of CO₂-rock interactions, emphasizing the role of rock porosity and mineral content. This research bridges the gap between laboratory and field studies, offering insights into frequency-sensitive attributes that are essential for correlating lab-based findings with field observations in CO₂ sequestration studies.

References

- Alcalde J, Flude S, Wilkinson M, et al. (2018) Estimating geological CO₂ storage security to deliver on climate mitigation. *Nat Commun* 9:2201. <https://doi.org/10.1038/s41467-018-04423-1>
- Choi C-S, Kim J, Song J-J (2021) Analysis of shale property changes after geochemical interaction under CO₂ sequestration conditions. *Energy* 214:118933. <https://doi.org/10.1016/j.energy.2020.118933>
- Gaus I (2010) Role and impact of CO₂-rock interactions during CO₂ storage in sedimentary rocks. *International Journal of Greenhouse Gas Control* 4:73–89. <https://doi.org/10.1016/j.ijggc.2009.09.015>
- Rørheim S, Bhuiyan MH, Bauer A, Cerasi PR (2021) On the effect of CO₂ on seismic and ultrasonic properties: a novel shale experiment. *Energies* 14:5007. <https://doi.org/10.3390/en14165007>
- Szewczyk D, Bauer A, Holt RM (2016) A new laboratory apparatus for the measurement of seismic dispersion under deviatoric stress conditions. *Geophysical Prospecting* 64:789–798. <https://doi.org/10.1111/1365-2478.12425>
- Xu T, Wang J, Lyu W, Zhang Y, Yu Y (2022) Experimental study of diffusion and formation mineral change in supercritical CO₂ huff and puff process of shale reservoir. *Lithosphere* 2022:6171981. <https://doi.org/10.2113/2022/6171981>

CO₂ leakage through a stimulated fault in a claystone caprock

Prescelli Annan^{1*}, Antonio Pio Rinaldi¹, Alba Zappone¹ and Martin Blunt²

¹ Swiss Seismological Service (SED) at ETH Zurich

² Faculty of Engineering, Department of Earth Science & Engineering, Imperial College London

* pannan@sed.ethz.ch

Abstract

To ensure the safety and viability of CO₂ storage efforts, it is crucial to understand the impact of fluid injection on fault reactivation and CO₂ storage security. This study focuses on the results of a carbon sequestration experiment (CS-D) conducted at the Mont Terri underground rock laboratory in Switzerland. The experiment involved monitoring the injection of CO₂ brine into a fault zone within Opalinus Claystone, an analogue caprock, to better understand leakage processes at shallow depths.

This paper presents post-processing results from the analysis of pressure and deformation data obtained over a 12-month period, during which a micro-stimulation activity designed to emulate induced CO₂ leakage was conducted. The primary objective was to evaluate the effect of micro-stimulation on the fault's permeability and transmissivity. The results show an increase in flow rate from 0.035 ml/min to ~6 ml/min following the micro-stimulation, indicating a dynamic permeability enhancement of two orders of magnitude.

The semi-analytical solutions used in this study conclude a permeability increase during the micro-stimulation from 1.0×10^{-18} to 1.7×10^{-16} m² in linear flow model (A), and from 7.2×10^{-20} to 1.4×10^{-17} m² in radial flow model (B). When injecting at constant pressure, the flow rate decayed over several weeks, indicating fault resealing and a decrease in permeability. At all times, the permeability is sufficiently low that CO₂ in its own phase is unlikely to escape. Finally, the study validates the results using Theis' and Cooper-Jacob wellhead solutions. The outcomes of this study have significant implications for the safety and success of CO₂ storage efforts, providing a better understanding of the factors that impact fault reactivation and CO₂ storage security.

1 Introduction

Most potential GCS storage locations in saline aquifers are overlain by claystone caprocks. The Opalinus claystone (OPA) provides a good analogue for a common caprock (e.g., Zappone et al. 2021). It is necessary to evaluate and de-risk faults during storage site selection and characterisation, so this research holds significance for facilitating the deployment of commercial-scale CO₂ storage in a variety of geological settings.

The Mont Terri rock laboratory (MTRL), Switzerland hosted the CS-D experiment investigating CO₂ injection and fluid propagation observations. The experiment was in operation between November 2018 and June 2021. This paper presents data acquired as part of a micro-stimulation experiment; the concluding step of CS-D after 14 months of constant head injection and monitoring (September 2020 – January 2021). Fluid was injected directly into an anisotropic fault zone with the aim of simulating changes in leakage conditions through a faulted caprock.

High-resolution data was collected from sensors installed in a set of seven boreholes intersecting a heterogeneous fault zone with scaly clay lenses and fault gouge referred to as the Main Fault. The CS-D experiment utilises the setup of the MTRL Niche CO₂, with an overburden of ~340 m, so bears relevance for CO₂ storage at shallow depths.

2 Methods

The concept underlying the final phase CS-D experiments was to investigate the effects of a localised increase in flow-rate in a faulted caprock; exploring micro-stimulation induced potential reactivation of single or minor fractures within a heterogenous fault. The micro-stimulation injection directly into the upper fault zone exceeded fault opening pressure through injection of CO₂-saturated brine at a constant flow rate of modest magnitude. In Fig. 1a, the micro-stimulation protocol comprised multiple tests conducted with a constant flow-rate injection, with magnitudes increasing stepwise from 3 to 100 ml/min. This study analysed pressure signals, and deformation profiles through a fibre optic distributed strain sensing (DSS) network. The monitoring system enabled continuous, fully automated measurements as detailed in Zappone et al. 2021.

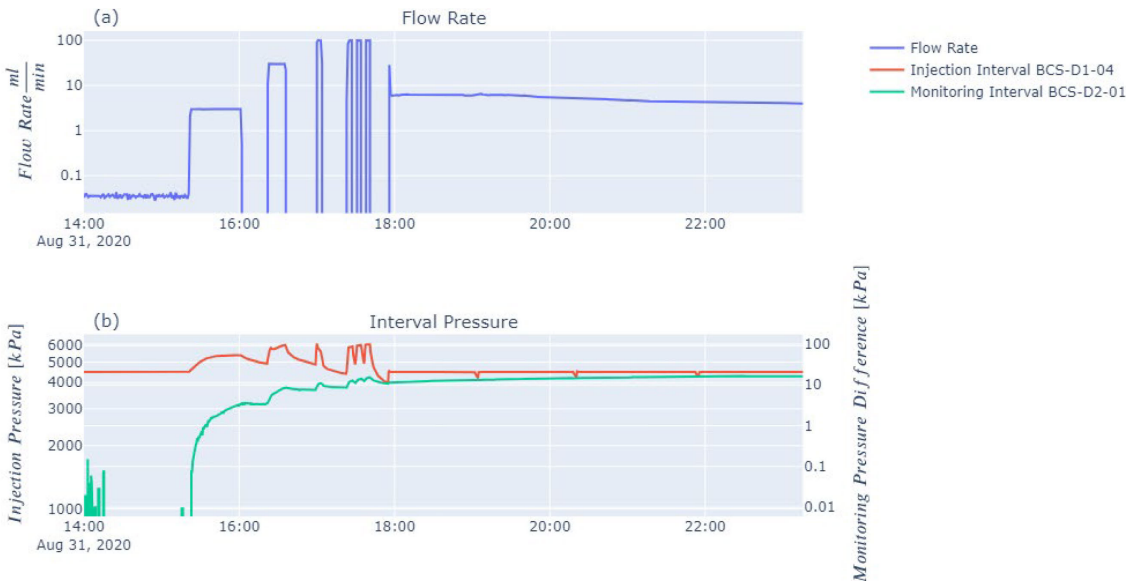


Fig. 1. a) Flow rate [ml/min] during the micro-stimulation. (b) High-resolution pressure measurements detailing the poroelastic response during the micro-stimulation. Interval pressure measured at the injection interval BCS-D1-Q4 (red) and primary monitoring interval BCS-D2-M1 (green, secondary y axis).

3 Results

After the micro-stimulation, the injection returned to constant-pressure injection at 4.5 MPa. When constant pressure injection was resumed, the flow rate was ~ 6 ml/min; significantly larger than the pre-stimulation rate of 0.035 ml/min. Long-term flow rate remained three times greater than the unstimulated value. A rapid increase in flow rate was observed during the micro-stimulation, followed by a rapid flow-rate decline despite constant pressure injection.

In this study a quantitative analysis of permeability and other hydraulic parameters was derived from the temporal evolution of flow rate and pressure using simplifying assumptions and well-established semi-analytical solutions, such as Darcy's Law. Two flow models were explored in this study: Linear flow model (A), and radial flow model (B) to assess uncertainty in flow geometry. After the micro-stimulation, hydraulic parameters exhibit a 50 % reduction in less than a week.

Distributed fibre optic strain-sensing (DSS) reveals significant but localised deformation in boreholes (BCS-D3 and BCS-D5) intersecting the fault zone roughly equidistant ~ 2.5 m from the injection interval. Strain is centred along the uppermost scaly-clay fault interface. Correlation between datasets indicates that the generation of additional permeability is caused by fracture aperture opening.

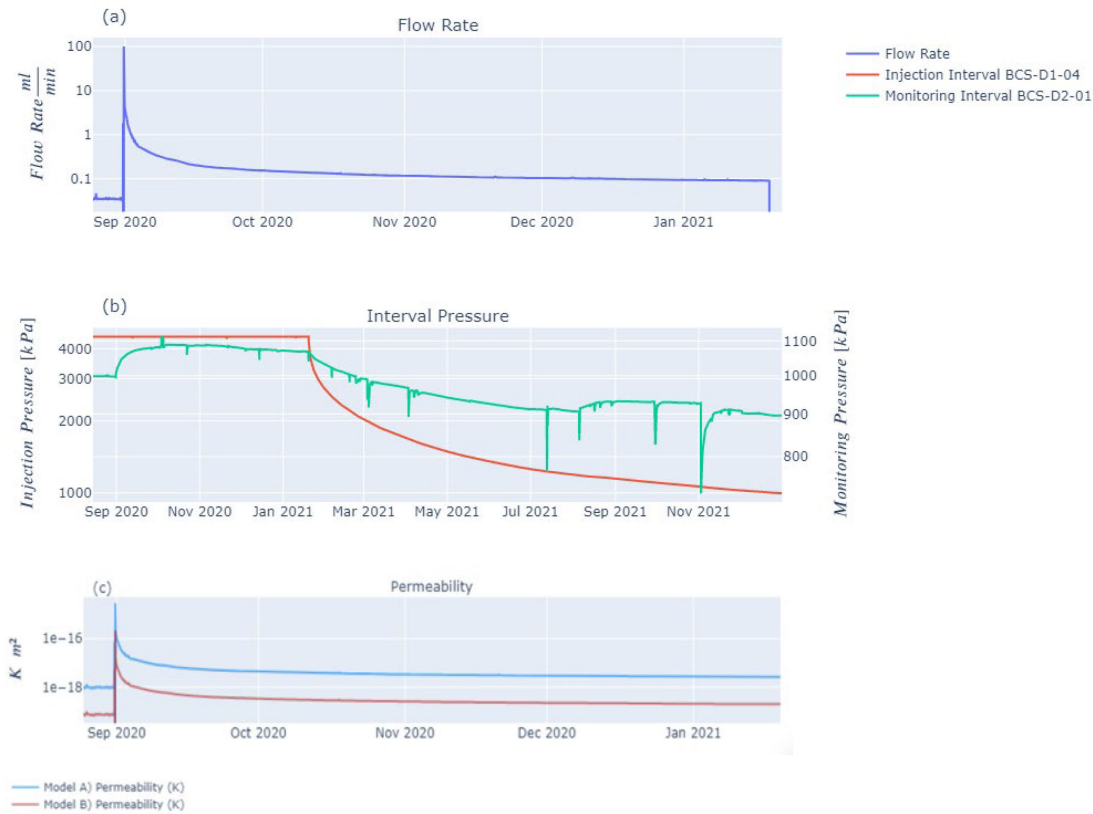


Fig. 2. (a) Flow rate during the 5 months following the micro-stimulation. (b) Injection and monitoring interval pressure measurements for 16 months following the micro-stimulation. (c) Temporal evolution of permeability from analytical flow models (A) and (B).

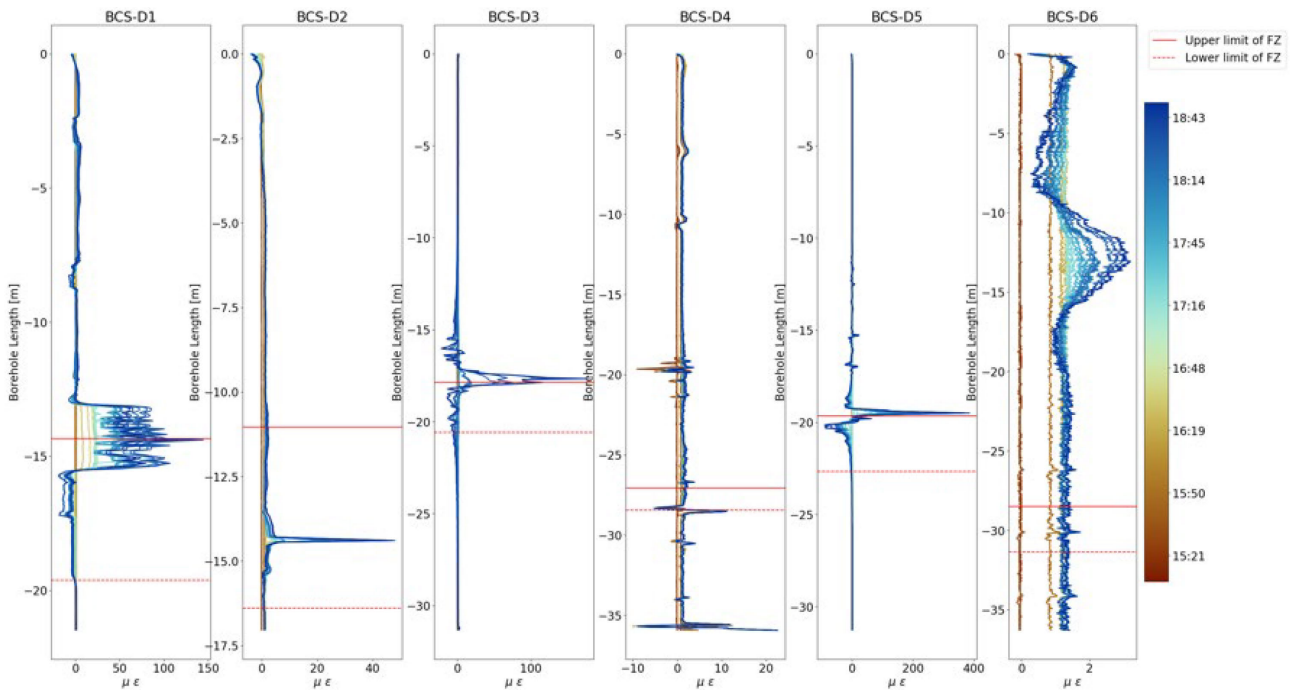


Fig. 3. DSS measurements from fibre optic arrays installed in boreholes BCS-D1 to BCS-D6. High-resolution Neubrex data covering the day of micro-stimulation 31/08/2020. Upper and lower limits of scaly-clay Main Fault zone delimited by red lines (after Grab et al. 2020; Zappone et al. 2021).

Tab. 1: Summative table containing representative values for key parameters. The following abbreviations were used: pre-ST = pre-stimulation; ST = stimulated value (onset of constant-pressure injection); post-ST = 7 days post-stimulation

Property	Unit	Model (A)			Model (B)		
		pre-ST	ST	post-ST	pre-ST	ST	post-ST
Volumetric flow rate Q	[m ³ /s]	5.5×10^{-10}	1.1×10^{-7}	6.0×10^{-9}	:	:	:
Darcy velocity q	[m/s]	1.2×10^{-9}	2.2×10^{-7}	1.3×10^{-8}	1.2×10^{-10}	2.2×10^{-8}	1.3×10^{-9}
Permeability K	[m ²]	1.0×10^{-18}	1.7×10^{-16}	1.0×10^{-17}	7.2×10^{-20}	1.4×10^{-17}	8.0×10^{-19}
Transmissivity T	[m ² /s]	1.3×10^{-11}	2.4×10^{-9}	1.4×10^{-10}	1.0×10^{-12}	1.9×10^{-10}	1.0×10^{-11}
Storativity S	[-]		9.0×10^{-6}				

4 Discussion

This study concludes that the micro-stimulation event induced partial fault reactivation, as supported by an elevated derived permeability during the event, and the rapid response time in deformation profiles - in contrast to the system’s typically sluggish behaviour. In such anisotropic and fractured media, the more probable mechanism for reactivation involves dilatancy of pre-existing fault planes and anisotropy induced by fluid pressure. Strain accommodation at the fault zone-host rock interface was predictable, attributed to the lower mechanical strength of fault gouge, resulting from abundant microstructures and mineralogical heterogeneity including a reduced percentage of hard particles, such as quartz grains (Laurich et al., 2018).

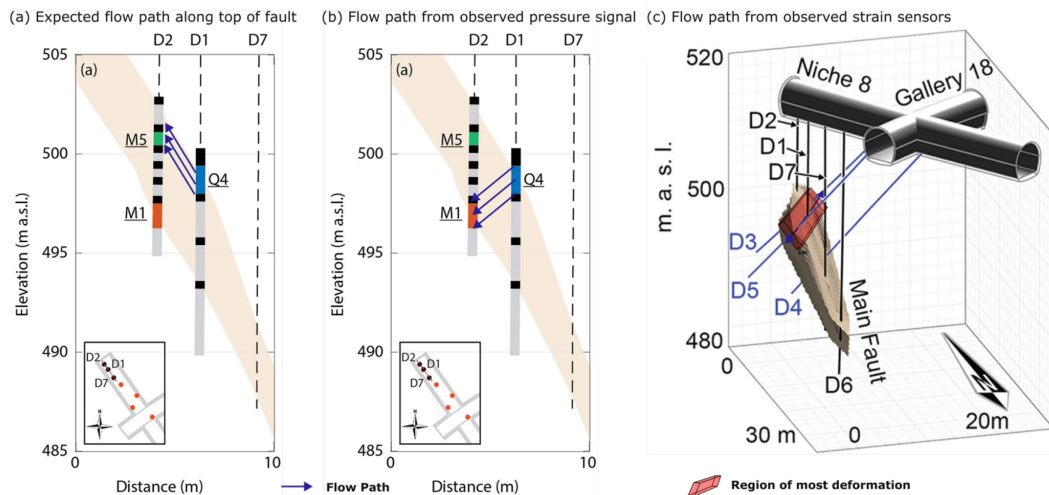


Fig. 4. (a) Expected flow path upwards along fault interface from injection interval. (b) Interpreted flow path from pressure signal observed in BCS-D2 interval 01. (c) Plane of most deformation upper fault zone interface, along fault strike from strain-sensing dataset, projected onto the Main Fault. Figures adapted from Zappone et al. (2020).

Ambiguity persists on the exact orientation and nature of the fractures-microfractures which govern flow. Absence of a strong pressure signal in BCS-D2 interval sensors 5-6 suggests fluid flow was directed from the injection interval down through the fault zone, as illustrated in Fig. 4 (b). This contrasts with predicted flow along the top of the fault zone, shown in Fig. 4 (a), but in line with the orientation of the most critically stressed fracture families, as determined in-situ by Guglielmi et al. (2020).

5 Conclusions

To evaluate how CO₂-saturated water injection impacts the sealing integrity in Opalinus Claystone, an analogue caprock, this study investigated temporal trends during constant pressure CO₂-saturated water injection into a fault zone after a micro-stimulation phase. This study found the following:

- The micro-stimulation enhances flow rate from 6.2×10^{-10} m³/s to 7.6×10^{-8} m³/s when constant pressure injection resumes.

- Temporal analysis of pressure data revealed the fault zone's permeability increases during the micro-stimulation from 1.0×10^{-18} to 1.7×10^{-16} m² in linear flow model (A), and 7.2×10^{-20} to 1.4×10^{-17} m² for radial flow model. (B). This is 2 orders of magnitude.
- Fractures-microfractures within the fault zone were assumed to act as effective conduits for fluid migration through impermeable country rock. We can neither ascertain true effective flow volume nor exclude radial flow. This intrinsic uncertainty over effective flow geometry means obtained hydraulic parameters should be taken as estimates accurate to within an order of magnitude.
- Rapid response time in DSS data is evidence for fault aperture opening. In the month following the micro-stimulation, maximum deformation above 200 microstrain was observed in the along-fault strike monitoring boreholes BCS-D3 and BCS-D5.
- Strain was significant but localised along the uppermost fault interface, which in combination with pressure signals, could be interpreted as hydraulic pathways directed along discontinuities orientated approximately parallel and perpendicular to the main fault strike. Lack of pressure sensors along fault zone strike mean along-fault dilatancy cannot be excluded, however down-dip deformation can.
- Fault self-sealing is evidenced by fast decay of flow rate following the micro-stimulation, despite constant pressure injection. However, it's crucial to note that the estimated 50 % reduction in permeability within under a week following the stimulation event may not necessarily indicate a complete recovery to the original state.

This study has confined the evolution of fault zone permeability during long-term exposure to CO₂, and the variation of geo-mechanical response with time. According to hydraulic parameter analysis, injection into a fault zone does not always result in a pathway for fluid to escape at shallow depths, addressing 2 primary escape mechanisms: pressure-induced fault reactivation and free CO₂ leakage up-fault. Our findings suggest a strong link between permeability and leakage flow rate, promising for caprock resealing at the end of injection campaigns. However, it is essential to acknowledge the complexity of fault resealing processes, and that once reactivated, fault integrity may be compromised over extended period. While this study suggests that CO₂ storage security develops over time, the observed decrease in permeability does not necessarily imply complete fault closure over the lifespan of a CO₂ reservoir. In conclusion, the main fault intersecting the MRTL does not appear to impact the barrier function of the OPA as a caprock, and caprock sealing ability appears unaffected by CO₂-saturated water injection. These results hold promise for CO₂ injection campaigns even in reservoirs with imperfect caprocks.

References

- Grab, M., Zappone, A., et al. 2020. Active seismic monitoring of CO₂-saturated brine injection into a fault (CS-D experiment in the Mont Terri Rock Laboratory). <https://doi.org/10.5194/egusphere-egu2020-21588>
- Guglielmi, Y., Birkholzer, J., Rutqvist, J., Jeanne, P. and Nussbaum, C. 2017. Can Fault Leakage Occur Before or Without Reactivation? Results from an in Situ Fault Reactivation Experiment at Mont Terri. *Energy Procedia*, 114, 3167–3174. <https://doi.org/10.1016/j.egypro.2017.03.1445>
- Guglielmi, Y., Nussbaum, C., Jeanne, P., Rutqvist, J., Cappa, F. and Birkholzer, J. 2020. Complexity of Fault Rupture and Fluid Leakage in Shale: Insights from a Controlled Fault Activation Experiment. *Journal of Geophysical Research: Solid Earth*, 125. <https://doi.org/10.1029/2019jb017781>
- Hopp, C., Guglielmi, Y., et al. 2022. The Effect of Fault Architecture on Slip Behavior in Shale Revealed by Distributed Fiber Optic Strain Sensing. *Journal of Geophysical Research: Solid Earth*, 127, <https://doi.org/10.1029/2021jb022432>.
- Laurich, B., Urai, J.L., Vollmer, C. and Nussbaum, C. 2018. Deformation mechanisms and evolution of the microstructure of gouge in the Main Fault in Opalinus Clay in the Mont Terri rock laboratory (CH). *Solid Earth*, 9, 1–24. <https://doi.org/10.5194/se-9-1-2018>
- Wenning, Q.C., Rinaldi, A.P., et al. 2020. Fault hydromechanical characterization and CO₂-saturated water injection at the CS-D experiment (Mont Terri Rock Laboratory). <https://doi.org/10.5194/egusphere-egu2020-19243>
- Zappone, A., Rinaldi, A.P., et al. 2021. Fault sealing and caprock integrity for CO₂ storage: an in situ injection experiment. *Solid Earth*, 12, 319–343. <https://doi.org/10.5194/se-12-319-2021>

Fluid flow driven by rupture growth in low-permeability faults during high-pressure injection in shale caprocks

Yves Guglielmi^{1*}, Frédéric Cappa², Christophe Nussbaum³ and Jens Birkholzer¹

¹ Energy Geosciences Division, Lawrence Berkeley National Laboratory, Berkeley, California, USA

² Université Côte d'Azur, CNRS, Observatoire de la Côte d'Azur, IRD, Géoazur, Sophia Antipolis, France

³ Federal Office of Topography (swisstopo), St-Ursanne, Switzerland

* yguglielmi@lbl.gov

Abstract

High-fluid pressures can penetrate faults and diffuse through channels while activating slip. Here, we use hydromechanical observations from a cross-borehole fluid injection experiment in a low permeability shale-bearing fault at 340 m depth within the Mont Terri Underground Research Laboratory (Switzerland) to show that the fault slips and opens prior to fluid pressure build-up. Reproducing the experimental data with 3D hydromechanical models, we find that the fluid migrates in the fault only after the fault fails and primarily slips beyond the pressurized area. This is creating potential hydraulic pathways that are then widely opened by a large effective normal stress decrease that overtakes the shear-induced dilation. Fault displacements of tens of micrometers are enough to trigger such significant leakage. These results provide new field constraints on mixed rupture processes, which drive the fluid migration in low permeability faults.

1 Introduction

Fluid pressure can reactivate faults and fractures, and have the potential to cause seismicity, as observed in both natural earthquake swarms (Shelly et al., 2016; De Barros et al., 2020) and energy production and storage activities (Ellsworth, 2013; Keranen et Weingarten, 2018). Increase in fluid pressure can also trigger aseismic slip on faults (Guglielmi et al., 2015; Wei et al., 2015; Villarasa et al., 2021). At the same time, the hydraulic properties of faults are an important factor as the evolution of permeability and porosity is coupled with slip and opening, and a consequence of this coupling is the variation of fluid pressure (Sibson, 1990; Zhu et al., 2020).

Recent works have shown that even low-permeability faults can drive and increase of fluid pressure because the fault permeability can increase during slip (Guglielmi et al., 2015; Wu et al., 2017). However, in the absence of *in situ* measurements of fluid pressure and deformation in faults, important questions remain, such as how fluid pressure migrates along faults, and how the fault responds mechanically.

Here, we use an *in situ* cross-borehole experiment with controlled fluid injection into a low-permeability shale fault zone ($k_0 \sim 10^{-17} \text{ m}^2$, Wenning et al., 2020). This experiment was developed at a depth of 340 m in the Mont Terri Underground Research Laboratory, Switzerland (Thury et al., 1999) (Fig. 1). We directly measured the evolution of fluid pressure and fault displacements (Fig. 2-3) at two vertical boreholes, spaced about 3 m horizontally. Reproducing the observations with 3D hydro-mechanical models, we track the fluid diffusion in association with fault deformation, and we give insights into how the decoupling between slip and opening, as well as the shear stress perturbation occurring outside the pressurized zone, control the fluid migration over the fault.

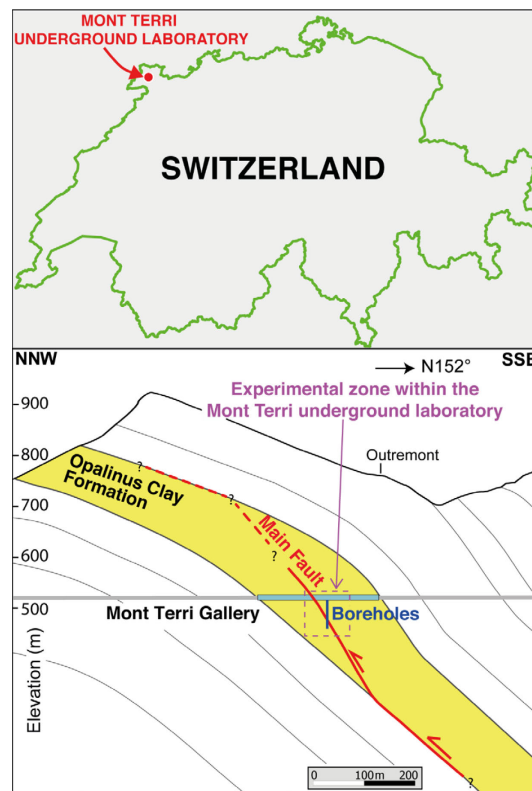


Fig. 1. Geology and location of the Mont Terri underground laboratory in Switzerland.

2 Methodology

The experiment was conducted in a 1.5–3 m thick seismically-inactive thrust fault zone with a mean orientation of N°045 in dip direction, a dip of 45°, and a slip offset of a few meters (Wenning et al., 2020) (Figs. 1, 2 and 3). During the experiment, pressurized water was injected for 645 s with step-increasing rates into a 2.4-m-long packer-isolated borehole interval spanning the main slip plane of the fault zone. The fluid pressure, the fault-normal (opening) and the fault-parallel (slip) displacements were recorded at both the injection and monitoring points with a specially designed borehole (SIMFIP) probe (Guglielmi et al., 2014) (Fig. 2-3), while the flowrate was only monitored at the injection point.

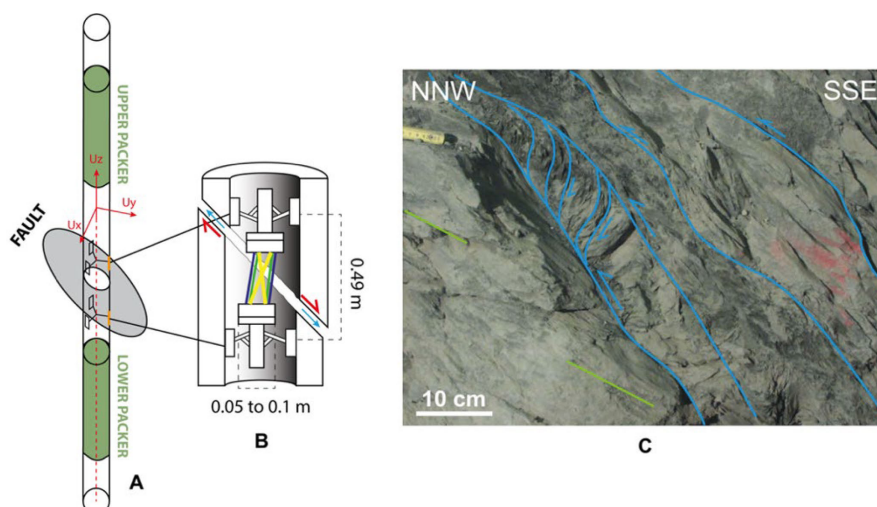


Fig. 2. SIMFIP probing of fault movements and fault geology. (A) Schematic plan of the SIMFIP probe; (B) Details of the three-dimensional displacement sensor; (C) Fault geology from Nussbaum et al. (2011). Green lines show the bedding planes. Blue lines show the main fault shear planes.

3 Results

At the injection point, the fluid pressure was increased step-by-step from the initial value of 0.5 MPa to a maximum value of 5.4 MPa (Fig. 3B), and the fault slip initiates at 555 s, followed by rapid fault opening at 568 s, and flowrate increase at 572 s. Then, the fluid pressure decreases from the peak to a steady-state value of 4.2 MPa. The slip increased to about 18.7 μm , and the opening up to 19.7 μm . At the monitoring point, first, the fault slip initiates at 574 s after the beginning of injection, followed by fault opening at 587 s (Fig. 3C). No fluid pressure change was detected until 31 μm of fault slip, 5 μm of fault opening, about 597 s into the experiment. Thus, at the monitoring point, the fluid pressure starts to increase 23 s after the fault starts to slip. The fluid pressure reaches a maximum value of 4.17 MPa at 623 s. This phase of pressurization is associated with fault closing (10.7 μm from 597 to 618 s) and slip at a slower rate toward the peak value (58.5 μm at 622 s). After the peak of pressurization at the monitoring point, the fluid pressure slightly decreases and stabilizes at a value of 3.85 MPa. This phase is associated with a fault opening of 24 μm from 618 to 645 s. Meanwhile, there is a decrease of fault slip of 20 μm , from 58.5 μm at 622 s to 38.5 μm at 645 s. The measured fluid pressure evolution is reproduced by the numerical solution when the fault first fails and slips while activating permeability change. The injection of fluid increases the pressure, which weakens the fault and initiates failure. Once the fault fails and starts slipping, the fluid enters the ruptured parts and induces a decrease of effective normal stress, causing an intense fault opening and slip acceleration, consistent with field data. Model results (Fig. 3D) show that the fluid pressure front follows the migration of peak shear stress where rupture occurs. Shear stress increases within a highly localized zone at the rim of the region of fluid pressurization. The shear stress perturbation arising from fault slip develops beyond the pressure front.

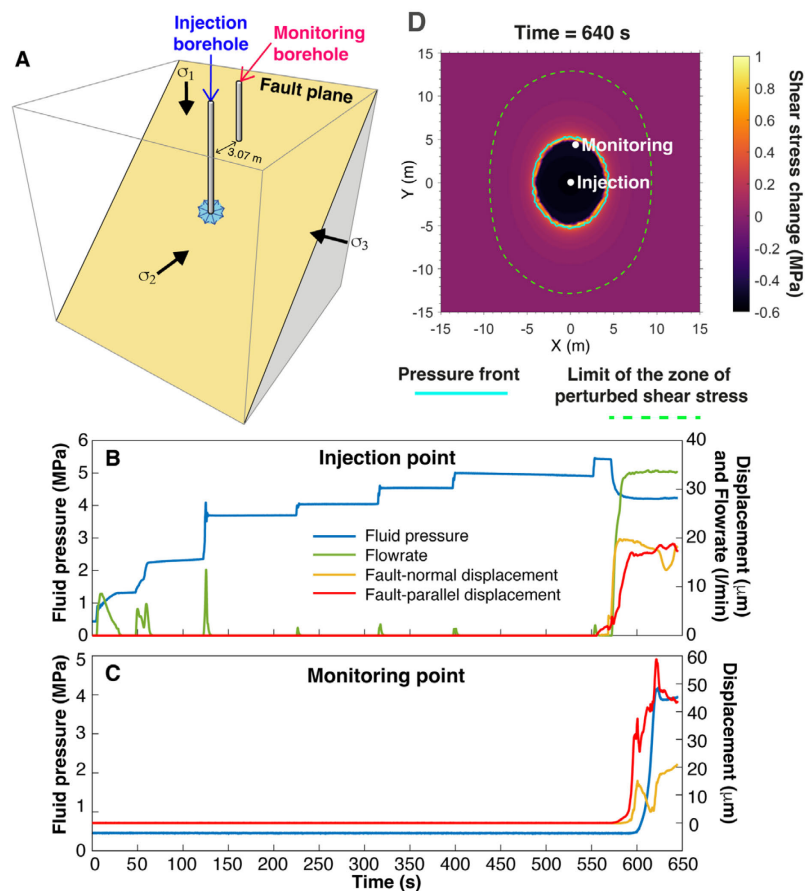


Fig. 3. (A) Fluid is injected through the open section of the injection borehole into the fault. A borehole probe (SIMFIP) was used to simultaneously measure the fault displacement (fault-parallel in red, and fault-normal in gold) and fluid pressure (blue) at the (B) injection and (C) monitoring points. (D) Spatial distribution of the change in shear stress relative to the initial value at 640 s for the best-fit numerical solution.

4 Conclusion

This study demonstrates that fluid pressure migration along low-permeability faults is driven by rupture growth through stress perturbation ahead of the pressurized zone. The fault rupture increases permeability and fluid flows in the preferential direction of fault slip. Our results are consistent with previous laboratory-sized experiments on sawcut rock surfaces, which showed that rupture is a necessary condition to allow fluid flow in low-permeability faults (Rutter and Hackston, 2017).

Our observations also provide clear *in situ* constraints on the physics underlying fault permeability enhancement in shales. Once failure occurs, a large increase in permeability and significant fluid migration can occur in the fault, now mainly driven by fault opening as a result of a strong decrease in effective normal stress. At this point, the fault is at rupture but the contribution of dilation induced by slip to permeability enhancement is minor. This fault response demonstrates that a mixed-mode rupture mechanism favored by a combination of slip propagation and opening explains such rapid fluid migration at high pressure and the apparent decoupling between fault slip and opening in low-permeability shale formations.

References

- De Barros, L., Cappa, F., Deschamps, A., & Dublanchet, P. 2020. Imbricated aseismic slip and fluid diffusion drive a seismic swarm in the Corinth Gulf, Greece. *Geophysical Research Letters*, 47, e2020GL087142. <https://doi.org/10.1029/2020GL087142>
- Ellsworth, W.L. 2013. Injection-induced earthquakes. *Science*, 341, 6142. <https://doi.org/10.1126/science.1225942>
- Guglielmi, Y. et al. 2014. ISRM Suggested Method for Step-Rate Injection Method for Fracture In Situ Properties (SIMFIP): Using a 3-components borehole deformation sensor. *Rock Mech. Rock Eng.*, 47. <https://doi.org/10.1007/s00603-013-0517-1>
- Guglielmi, Y. et al. 2015. Seismicity triggered by fluid injection-induced aseismic slip. *Science*, 348, 1224. <https://doi.org/10.1126/science.aab0476>
- Guglielmi, Y. et al. 2015. In situ observations on the coupling between hydraulic diffusivity and displacements during fault reactivation in shales. *J. Geophys. Res.*, 120. <https://doi.org/10.1002/2015JB012158>
- Keranen, K.M. & Weingarten, M. 2018. Induced seismicity. *Annu. Rev. Earth Planet. Sci.*, 46, 149–174. <https://doi.org/10.1146/annurev-earth-082517-010054>
- Nussbaum, C., P. Bossart, F. Amann, C. Aubourg 2011. Analysis of tectonic structures and excavation induced fractures in the Opalinus Clay, Mont Terri underground rock laboratory (Switzerland). *Swiss J. Geosci.*, 104, 187–210.
- Rutter, E.H. & Hackston, A. 2017. On the effective stress law for rock-on-rock frictional sliding, and fault slip triggered by means of fluid injection. *Philosophical Transactions of the Royal Society of London*, 375. <https://doi.org/10.1098/rsta.2016.0001>
- Shelly, D.R. et al. 2016. Fluid-faulting evolution in high definition: Connecting fault structure and frequency-magnitude variations during the 2014 Long Valley Caldera, California, earthquake swarm. *J. Geophys. Res.*, 121, 1776–1795. <https://doi.org/10.1002/2015JB012719>
- Sibson, R.H. 1990. Conditions for fault-valve behaviour. *Geol. Soc. Lond. Spl. Publ.*, 54, 15–28
- Thury, M. & Bossart, P. 1999. The Mont Terri rock laboratory, a new international research project in a Mesozoic shale formation, in Switzerland. *Engineering Geology*, 52(3–4), 347–359.
- Vilarrasa, V., De Simone, S., Carrera, J., & Villaseñor, A. (2021). Unraveling the causes of the seismicity induced by underground gas storage at Castor, Spain. *Geophysical Research Letters*, 48(7), e2020GL092038
- Wei, S. et al. 2015. The 2012 Brawley swarm triggered by injection-induced aseismic slip. *Earth Planet. Sci. Lett.*, 422, 115–125. <https://doi.org/10.1016/j.epsl.2015.03.054>
- Wenning, Q.C. et al. 2020. Shale fault zone structure and stress dependent anisotropic permeability and seismic velocity properties (Opalinus Clay, Switzerland). *J. Struct. Geol.*, 144, 104273. <https://doi.org/10.1026/j/jsg.2020.104273>
- Wu, W. et al. 2017. Permeability evolution of slowly slipping faults in shale reservoirs. *Geophys. Res. Lett.*, 44, 11,368–11,375. <https://doi.org/10.1002/2017GL075506>
- Zhu, W. et al. 2020. Fault valving and pore pressure evolution in simulations of earthquake sequences and aseismic slip. *Nature Communications*, 11:4833. <https://doi.org/10.1038/s41467-020-18598-z>

Assessing caprock integrity in an acid gas storage project: a Middle East case

Martina Cervelli^{1*}, Nicolás Rangel Jurado^{1,2} and Federico Games¹

¹ Ad Terra Energy, Chemin des Vergers 4, 1208 Geneva, Switzerland

² Geothermal Energy and Geofluids, ETH Zürich, Sonneggstrasse 5, 8092 Zurich, Switzerland

* martina.cervelli@adterra.com

1 Introduction

Acid Gas Storage (AGS) is a mature technology that aligns with the decarbonization goals outlined by the Paris Agreement (Rajamani, 2016). AGS involves the injection and sequestration of acid gases, such as hydrogen sulphide (H₂S) and carbon dioxide (CO₂), in underground reservoirs over geological times. Acid gases are undesirable by-products that often result from the extraction and processing of hydrocarbons. Instead of releasing these acid gases into the atmosphere, thereby contributing to climate change, AGS offers an environmentally responsible solution to mitigate these scope 1 emissions. The success of the technique depends on the selection of suitable geological formations, which can fulfill storage capacity, injectivity, and containment criteria. Whereas the first two requirements are most important for the techno-economic viability of the project, the containment requirement is critical to ensure the safety, risk management, and remediation strategies of the project. At Ad Terra, on behalf of a Middle East field operator, we explore options for acid gas handling and evaluate the related potential for compromising the integrity of a shaly Santonian (late Cretaceous) caprock due to acid gas injection (AGI) in a partially depleted hydrocarbon reservoir (Fig. 1).

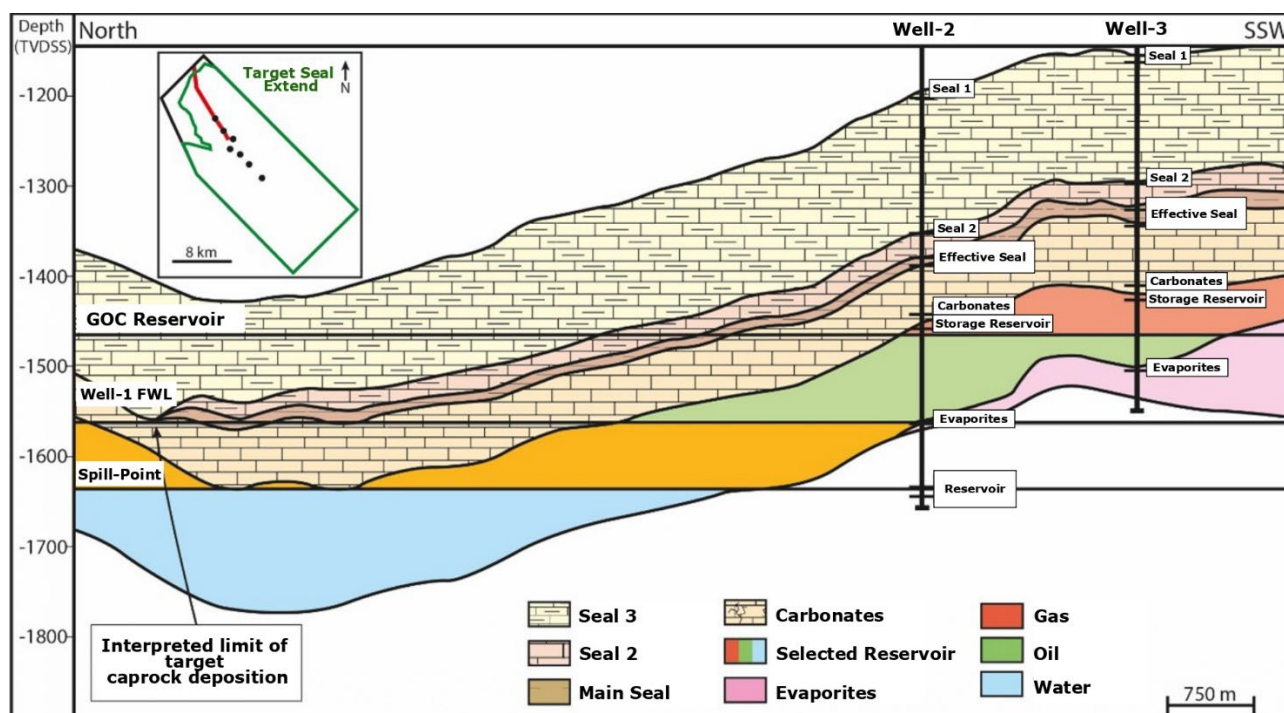


Fig. 1. Cross-section based on seismic image showing the main seal northern limit towards the storage reservoir spill-point.

2 Methods and Discussion

Acid gas sequestration requires long-term confinement of the injected gas within the targeted reservoir formation. Two factors play a crucial role: the caprock's lateral extension and the occurrence of fractures and/or faults within the containment formation. In our specific case, there is a gradual reduction in the shale thickness from the Southeast to the North area of the field (Fig. 1). Even though

the targeted formation is pinching out in the northern portion, there is evidence supporting robust sealing capabilities for AGS across the field: 1. well logs obtained while drilling above and below the suspected caprock suggest the existence of a hydraulic discontinuity between the two sections and 2. the Santonian shale is stratigraphically overlaid by two Maastrichtian thick marly carbonates which could act as a secondary/backup barrier for fluids migration. Structurally, pre-existing compressional and extensional features have been identified. The main thrust along the Southern flank of the anticline appears to be acting as a seal, much like the role played by extensional faults in NW-SE direction. Moreover, in the North-Western part of the field, a dextral strike slip motion has been identified but no vertical displacement has been observed, hence the caprock continuity should not be affected (Fig. 2). Nonetheless, additional studies must be conducted to minimize the risk associated with chemical reactions and/or escape mechanisms that could compromise containment such as seal failure, mineral dissolution, rock-fluid interactions, faults' reactivation, etc. (Schukla et al., 2010; Gasda et al., 2017; Karolyte et al. 2019).

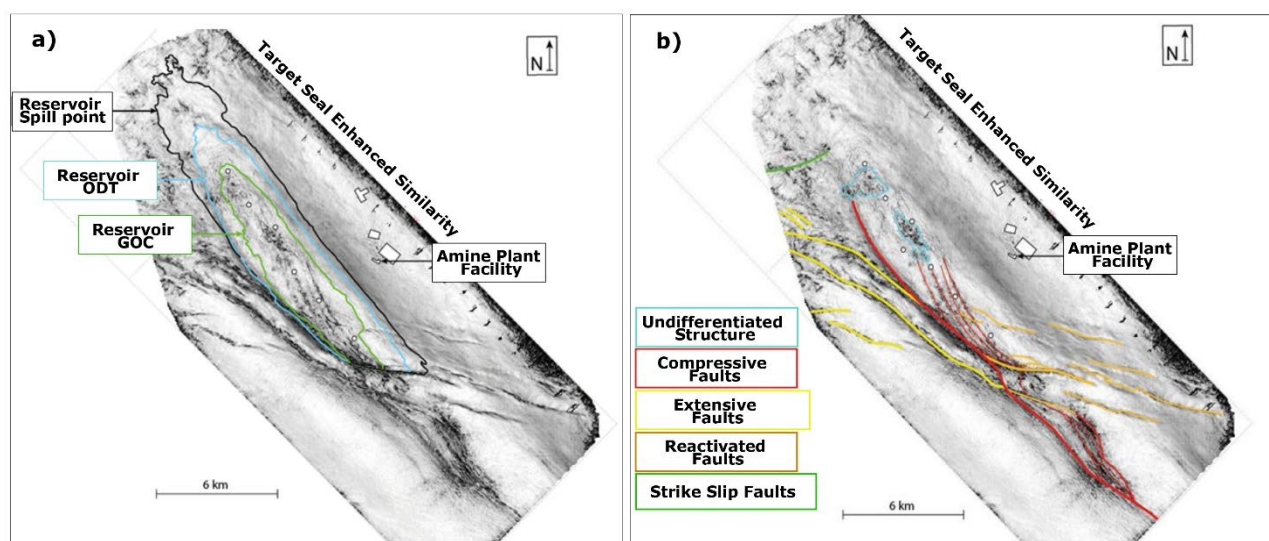


Fig. 2: a) Enhanced similarity map for faults/fractures extracted along the target seal formation. The container reservoir fluids contacts are also displayed. b) Enhanced similarity map with faults/fractures interpreted along the target seal formation.

3 Conclusions

AGS offers a promising solution to address some of the environmental challenges associated with hydrocarbon extraction and processing techniques. The success of AGS is contingent upon the attentive selection of suitable geological formations that meet specific criteria, including capacity, injectivity, and containment.

Our preliminary analyses highlight the robust sealing capabilities of a Santonian shale for AGS in a Middle East partially depleted hydrocarbon reservoir. Despite the shale's non-uniform thickness and the presence of faults, initial results suggest that the containment of acid gas within the formation would not be affected. However, further studies need to be performed to gather information, mitigate uncertainties and minimize the environmental risks associated with acid gas injection.

Our subsequent de-risking strategy includes a core acquisition program to illuminate the specific geochemical and mechanical properties of the selected caprock, a comprehensive study to fully characterize the pre-existing fault network, and numerical modeling of hydraulic fractures propagation through the reservoir and caprock to forecast the acid gas plume migration, induced seismicity and/or potential leakage. This study underscores the importance of conducting rigorous assessments for the secure application of AGS in hydrocarbon fields.

References

- Rajamani, L. (2016). Ambition and differentiation in the 2015 Paris Agreement: Interpretative possibilities and underlying politics. *International & Comparative Law Quarterly*, 65(2), 493–514. <https://doi.org/10.1017/S0020589316000130>
- Gasda, E. et al. (2017). Investigation of Caprock Integrity due to Pressure Build-up During High-volume Injection into the Utsira. *Energy Procedia*, 114, 3157–3166. <https://doi.org/10.1016/j.egypro.2017.03.1444>
- Karolytė, R. et al. (2020). Fault seal modelling – the influence of fluid properties on fault sealing capacity in hydrocarbon and CO₂ systems. *Petroleum Geoscience*, 26(3), 481–497. <https://doi.org/10.1144/PETGEO2019-126>
- Shukla, R. et al. (2010). A review of studies on CO₂ sequestration and caprock integrity. *Fuel*, 89(10), 2651–2664. <https://doi.org/10.1016/J.FUEL.2010.05.012>

CO₂ storage in salt basins: influence of salt tectonics on seal integrity and containment risk

Sian Evans^{1*}, Simon Blondel¹, Torsten Hansen¹, Rikke Bruhn^{1,2} and Alvar Braathen¹

¹ Department of Geosciences, University of Oslo, Norway

² Equinor ASA, Norway

* s.l.evans@geo.uio.no

1 Introduction

Basins with thick, mobile salt deposits, such as the Norwegian-Danish Basin (NDB), provide attractive targets for subsurface storage, as salt-related traps have large capacities and are proven to hold large volumes of fluids (oil and gas fields). The NDB has a strategic location in northern Europe and the potential to be a future energy hub, with diverse sustainable development projects including offshore windfarms and hydrogen storage facilities, as well as CO₂ storage. However, salt basins have complex tectono-stratigraphic histories that pose unique challenges for CO₂ storage evaluations, affecting the capacity, injectivity and containment risk associated with salt-related storage sites (Duffy et al., 2023). In this study we evaluate common salt-related trap types within the NDB and show how their salt tectonic evolution affects their relative risk profile for long-term containment.

2 Geological Setting

During the Permian, a thick, halite-dominated evaporite succession, known as the Zechstein Super-group, was deposited across the southern and central North Sea (Hodgson et al. 1992). Subsequent flow of the mobile salt layer, in response to gravitational instability and active tectonic drivers, generated a variety of thin-skinned, salt-cored structures with highly variable geometries (Hodgson et al. 1992; Stewart and Clark 1999; Rank-Friend and Elders 2004). The deformation of the salt has influenced the distribution of strain and sedimentological heterogeneity of all overlying units, including candidate CO₂ storage complexes. Potential storage units and their associated seals are present at multiple stratigraphic levels within the NDB (e.g., the Triassic Skagerrak and Gassum formations, the Jurassic Sandnes and Bryne formations, the Cretaceous chalk, and the Palaeogene Fiskebank formation; Anthonsen et al., 2013; Halland et al., 2013), but vary in quality across the basin.

3 Data and Analysis

In this study, we use 2D and 3D seismic reflection data to assess the impact of salt tectonic-induced strain on seal integrity, with particular reference to fault development and fracture intensity, within a selected study area in the NDB (Fig. 1a). Depending on their physical and mechanical properties, faults and fracture systems can act as baffles, barriers or conduits for fluid flow (Pei et al. 2015). Where they reduce permeability, they can slow the rate of updip CO₂ migration, provide intra-formational traps, or compartmentalize the storage unit (Stewart 2006). Where they facilitate fluid leakage into stratigraphically shallower units, they compromise the integrity of the seal (Hodgson et al. 1992; Duffy et al. 2023). These structural risks must be assessed and understood in order to reliably constrain storage capacity and ensure the long-term viability of the storage complex. By mapping selected stratigraphic horizons, extracting key surface attributes and interpreting stratigraphic relationships within the overburden, we are able to reconstruct the evolution of the salt-related trap structures and show the key opportunities and challenges for storage sites in the NDB and other salt basins.

4 Results

We show complex patterns of local strain in the crests and flanks of salt structures that could pose a risk to long-term CO₂ containment (Fig. 1b-c). We document the relationship between salt structures and amplitude anomalies interpreted as fluid accumulations in the overburden (Fig. 1d). This

demonstrates widespread fluid leakage through crestal faults associated with large salt diapirs, even where the faulted units are shale-dominated. This indicates that traditional methods for estimating fault seal capacity, such as the shale gouge ratio, may be insufficient for predicting the sealing behaviour of such faults.

However, we also show that the evolutionary history of each structure varies across the study area, and even closely positioned salt structures can exhibit different patterns of deformation, which affects their relative containment risk. This understanding of the salt structural evolution allows us to identify structures that may have a greater sealing capacity, and even predict subseismic attributes such as fracture density in the intervals of interest. We use this analysis to preliminarily categorise structural traps into high or low containment risk, and identify those which could provide optimal targets. Salt structures are unique in their structural complexity, with heterogeneous distributions of strain that vary across relatively short spatial scales, and therefore require a case-by-case risk analysis. Ultimately, we can unlock greater capacity for secure subsurface CO₂ storage in the North Sea, with learnings that can be applied to salt basins globally.

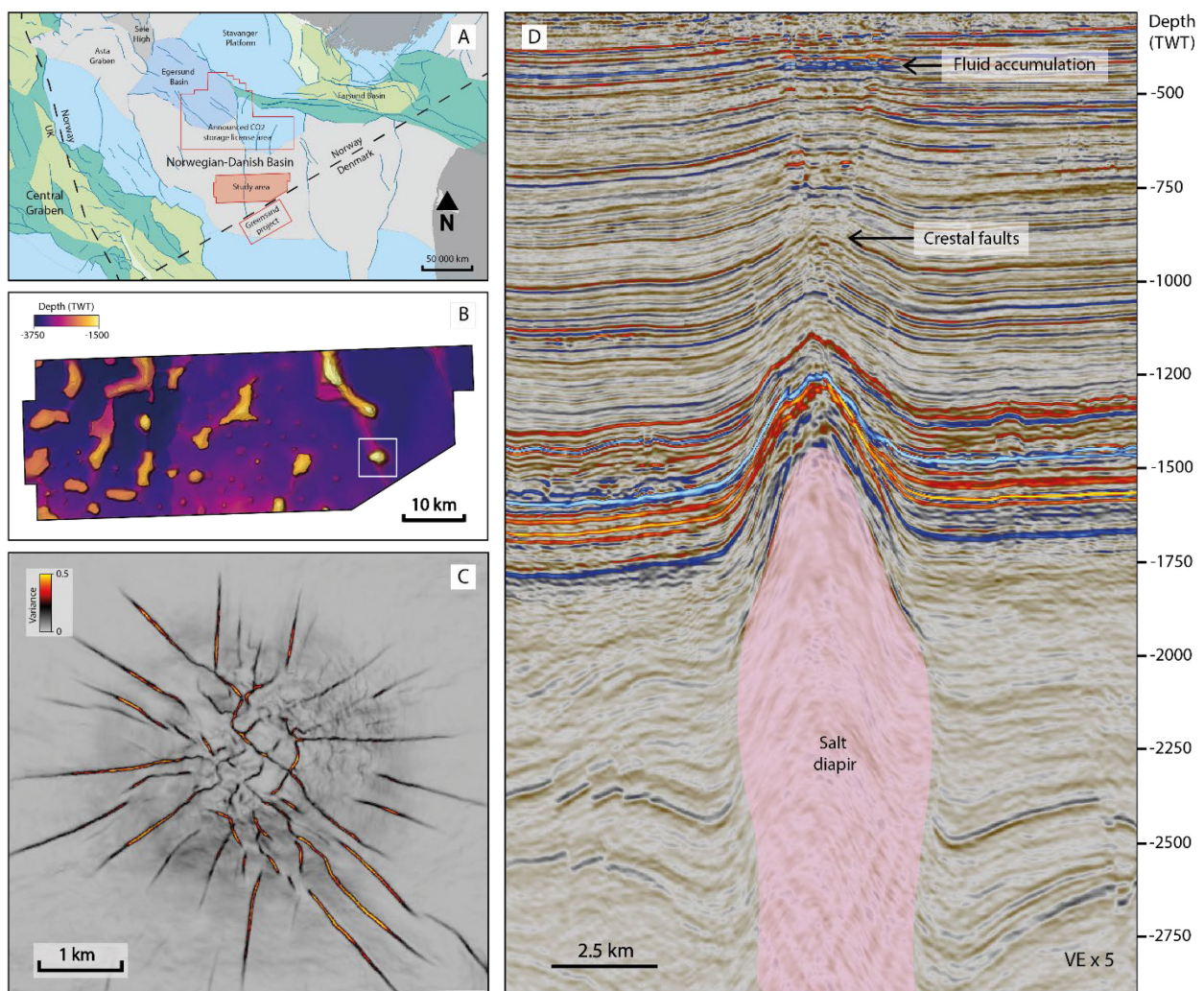


Fig. 1. a) Regional map showing location of study area in the Norwegian-Danish Basin. b) Depth-structure map of the Top Salt surface across the study area showing distribution of major salt structures. c) Variance map across individual diapir showing radial faults around the crest of the structure. d) Seismic cross section of the diapir showing overlying fluid accumulation.

References

- Anthonsen, KL, Aagaard, P, Bergmo, PE, Erlström, M, Fareide, JI, Gislason, SR, Mortensen, GM, and Snæbjörnsdóttir, SÓ. 2013. CO₂ storage potential in the Nordic region. *Energy Procedia*, 37, 5080–5092. <https://doi.org/10.1016/j.egypro.2013.06.421>
- Duffy, OB, Hudec, M, Peel, F, Apps, G, Bump, A, Moscardelli, L, Dooley, T, Bhattacharya, S, Wisian, K, and Shuster, M. 2023. The role of salt tectonics in the energy transition: An overview and future challenges. *Tektonika*, 1, 18–48. <https://doi.org/10.55575/tektonika2023.1.1.11>
- Halland, EK, Riis, F, Magnus, C, Johansen, WT, Tappel, IM, Gjeldvik, IT, Solbakk, T, and Pham, VTH. 2013. CO₂ Storage Atlas of the Norwegian part of the North Sea. *Energy Procedia*, 37, pp.4919–4926. <https://doi.org/10.1016/j.egypro.2013.06.403>
- Hodgson, NA, Farnsworth, J and Fraser, AJ. 1992. Salt-related tectonics, sedimentation and hydrocarbon plays in the Central Graben, North Sea, UKCS. Geological Society, London, Special Publications, 67(1), pp.31–63. <https://doi.org/10.1144/GSL.SP.1992.067.01.03>
- Pei, Y, Paton, DA, Knipe, RJ and Wu, K. 2015. A review of fault sealing behaviour and its evaluation in siliciclastic rocks. *Earth-Science Reviews*, 150, pp.121–138. <https://doi.org/10.1016/j.earscirev.2015.07.011>
- Rank-Friend, M and Elders, CF. 2004. The Evolution and Growth of Central Graben Salt Structures, Salt Dome Province, Danish North Sea. Geological Society, London, Memoirs, 29(1), pp.149–164. <https://doi.org/10.1144/GSL.MEM.2004.029.01.15>
- Stewart, SA. 2006. Implications of passive salt diapir kinematics for reservoir segmentation by radial and concentric faults. *Marine and petroleum geology*, 23(8), pp.843–853. <https://doi.org/10.1016/j.marpetgeo.2006.04.001>
- Stewart, SA and Clark, JA. 1999. Impact of salt on the structure of the Central North Sea hydrocarbon fairways. In Geological Society, London, Petroleum Geology Conference series (Vol. 5, No. 1, pp. 179–200). The Geological Society of London. <https://doi.org/10.1144/0050179>

Increasing process understanding in gas migration: investigations using the TH2M modelling approach

Vinay Kumar^{1*}, Gesa Ziefle¹ and Jobst Maßmann¹

¹ Federal Institute for Geosciences and Natural Resources (BGR), Hannover, Germany

* vinay.kumar@bgr.de

1 Introduction

A sound understanding of gas production and movement in argillaceous rock is key to estimating the safety of the enclosure and efficiency of argillaceous barrier systems. Introduction of gas in fluid saturated argillaceous rock triggers multiple mechanisms of gas transport and alteration of the host- and barrier rock. One such mechanism, two-phase flow, introduces strong non-linearities and potentially affects the integrity of the barrier rock. Another mechanism, namely, the transport of dissolved gas, has a larger spatial extent and is a more secure trapping mechanism over a longer period. Numerical models are commonly utilized to understand gas transport mechanisms in various applications and to optimize the design of repository sites. The BGR follows two approaches to investigate processes affecting barrier integrity: I) non-isothermal two-phase two-component flow in a deformable porous medium (TH2M) and II) reactive transport in saturated flow (HC). This contribution focuses on the TH2M approach.

2 The TH2M Model

The TH2M model (Grunwald et al. 2022) in the open-source simulator OpenGeoSys 6, is a monolithic and fully-coupled FEM implementation. Previous studies have focused on aspects such as equivalence of the model to certain known multiphase formulations (Pitz et al. 2023) and the impact of the gas production rate in the establishment of a multiphase flow regime (Grunwald et al. 2023). Simulation of two ongoing experiments from the Mont Terri Project will be presented here to highlight the application of the model at the field scale to improve the understanding of gas transport mechanisms.

3 Applications of the Model

In the first example, the usage of the model in studying dilatancy controlled gas migration and breakthrough is shown through the simulation of the Gas Transport (GT) Experiment. Here a free gas phase is initially held at a fixed pressure at the inlet. The pressure is then gradually increased until gas breakthrough is recorded in an observation well. In preparation for the modelling of the field-scale experiment, a lab test was also simulated to estimate the predictive capability of the models (cf. Fig. 1). Since the focus of the GT experiment is gas transport and breakthrough, the focus of the presented modelling exercise is to demonstrate the capabilities of the TH2M model in the immiscible two-phase flow regime.

In the second example, a preliminary simulation of the CO₂ Long Term Periodic Injection (CL) Experiment is presented to show the usage of the model in the context of CO₂ injection and migration in argillaceous rock. Since the CL experiment is foreseen to investigate migration of gas as a component dissolved in the liquid phase under periodically changing boundary conditions at the gas inlet, the focus of the presented modelling exercise is, likewise, to demonstrate the component transport modelling capabilities of the TH2M model.

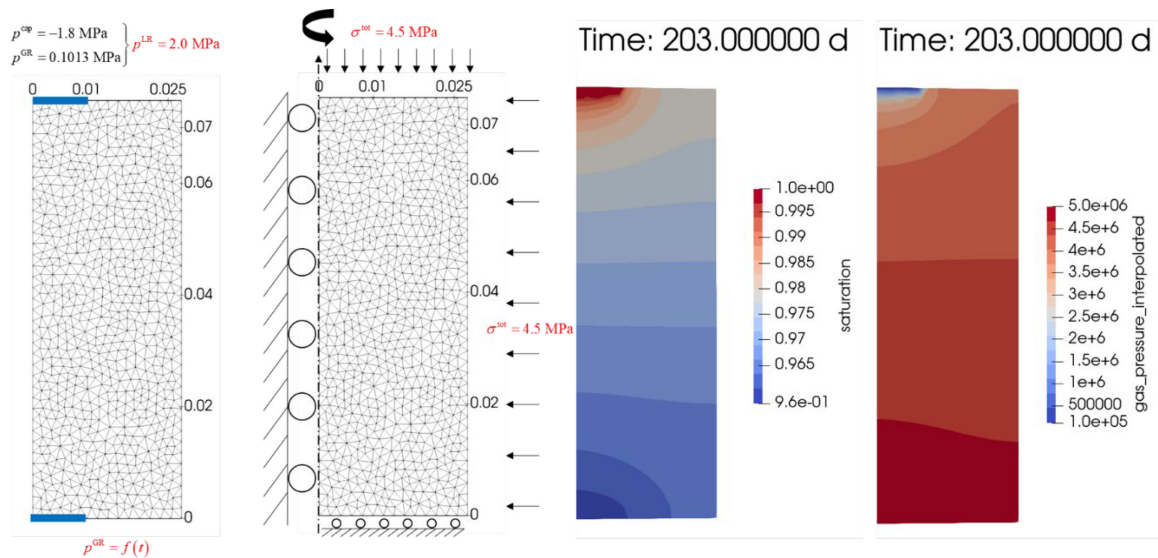


Fig. 1. Boundary conditions and simulation results of the lab-scale experiment showing contours of liquid saturation and gas pressure.

4 Outlook

These examples outline the current efforts of the BGR towards validating the TH2M model for relevant use cases at the field scale. Such studies help in building confidence in the modeling capabilities and are crucial towards model development.

References

- Grunwald, N., Lehmann, C., Maßmann, J., Naumov, D., Kolditz, O., Nagel, T. (2022). Non-isothermal two-phase flow in deformable porous media: systematic open-source implementation and verification procedure. *Geomech. Geophys. Geo-energ. Geo-resour.* 8, 107. <https://doi.org/10.1007/s40948-022-00394-2>.
- Pitz, M., Kaiser, S., Grunwald, N., Kumar, V., Buchwald, J., Wang, W., Naumov, D., Chaudhry, A.A., Maßmann, J., Thiedau, J., Kolditz, O., Nagel, T. (2023). Non-isothermal consolidation: A systematic evaluation of two implementations based on multiphase and Richards equations. *International Journal of Rock Mechanics and Mining Sciences.* 170. <https://doi.org/10.1016/j.ijrmms.2023.105534>.
- Grunwald, N, Nagel, T, Pitz, M & Kolditz, O. (2023). Extended analysis of benchmarks for gas phase appearance in low-permeable rocks, *Geomech. Geophys. Geo-energ. Geo-resour.* (in press).
- OpenGeoSys: www.opengeosys.org
- The Mont Terri Project: <https://www.mont-terri.ch>

Fate of hydrogen gas injected in a clay-rich rock: an *in-situ* experiment

Mélanie Lundy^{1*}, Christian Ostertag-Henning², Myriam Agnel¹, Stefan Wechner³, Yanick Lettry⁴ and Agnès Vinsot¹

¹ Andra, Meuse/Haute-Marne Center, Bure, France

² Federal institute for Geosciences and Natural Resources, Hannover, Germany

³ Hydroisotop GmbH, Schweitenkirchen, Germany

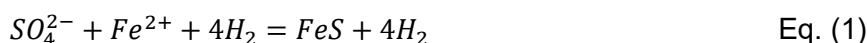
⁴ Solexperts AG, Mönchaltorf, Switzerland

* melanie.lundy@andra.fr

1 Introduction

Deep geological disposal of radioactive waste is foreseen in several countries for long-term isolation of radioactive waste from the environment. Some countries consider claystone formations as the host rock for their disposals: this is the case of France (Callovian-Oxfordian) and Switzerland (Opalinus Clay). After the closure of an underground disposal facility, the anoxic corrosion of steel is expected to produce large amounts of hydrogen gas. The “Hydrogen Transfer” (HT) experiment was implemented in 2009 in the Mont Terri Underground Rock Laboratory (URL) to investigate transport and reactivity (including the potential for microbial consumption) of hydrogen gas injected into a borehole installed within Opalinus Clay formation. This experiment may also provide insights concerning the storage of hydrogen in geological underground or exploitation of natural hydrogen resources.

After a one-time injection repeated twice (the hydrogen partial pressure being at most 60 mbar, total pressure ~1.5 bar), the disappearance rate of hydrogen observed was 20 times larger than the calculated rate considering only dissolution and diffusion. Simultaneously, sulphate and iron concentrations decreased in the water, whereas sulphide became detectable (Vinsot *et al.* 2014). The same disappearance rate was observed over a semi-continuous injection phase which consisted in injecting pure hydrogen regularly to maintain a partial pressure close to 60 mbar for 500 days, then close to 25 mbar for 600 days. The proposed hypothesis is that hydrogen consumption is mainly controlled by hydrogen-fuelled, microbially mediated sulphate reduction, according to the following overall reaction (Eq. 1):



This assumption is supported by microbiological analyses (Bagnoud *et al.* 2016) and geochemical modelling, reproducing the temporal evolution of gas pressure, composition and solute concentrations measured *in situ* (Damiani *et al.* 2021).

To further verify the validity of this hypothesis, pure deuterium (D₂) gas was injected into the borehole. In this paper, the first results obtained during this new experimental phase started in 2021 are presented.

2 Experimental methods

2.1 HT experimental set up

The HT experimental set up is extensively described in Vinsot *et al.* (2014, 2017). The experimental concept is based on gas circulation and water sampling in a 5-m long interval located at the end of a 15-m long, 76-mm diameter borehole. In the drift, a gas circulation module allows to inject pure hydrogen or deuterium at a controlled flow rate and to monitor the gas composition. A water sampling module makes it possible to extract the seepage water to maintain a constant water level in the test interval and to monitor the water composition (Fig. 1).



Fig. 1. Photograph of the experimental equipment of HT experiment inside the Mont Terri URL. From left to right: the water sampling module, the gas circulation module and the Raman spectrometer (photograph by M. Lundy).

2.2 Raman spectroscopy measurements

Online monitoring of the gas composition is carried out using Raman spectroscopy. Raman spectra in the gas phase are acquired using a Raman Rxn2™ analyzer (Endress+Hauser) equipped with a 532 nm Nd-YAG laser, a 5-m long optical fiber and an AirHead™ probe (Endress+Hauser) placed inside the gas circulation module. The spectral coverage range is 150-4350 cm^{-1} with an instrumental spectral resolution of about 5 cm^{-1} . Raman spectral data are acquired by HoloPRO 3.3 software, the exposure time is 3 minutes, and 2 scans are accumulated for each spectrum. The acquisitions are performed continuously during D_2 injection phases. Data are then processed with PEAXACT software, the lines taken into consideration for peak area calculations are indicated in Tab. 1.

Tab. 1. List of characteristic lines analyzed for each spectrum.

Component	Wavenumber cm^{-1}
H_2	4155
HD	3630
D_2	2990

2.3 Chemical analyses

Analyses of the stable hydrogen isotope composition of water ($\delta^2\text{H-H}_2\text{O}$) were done using cavity ring-down spectroscopy (CRDS) instruments.

2.4 Deuterium injection phases

The first deuterium injection was performed in September 2021, the second one in November 2022. In both cases, pure deuterium was added to the circulating gas to obtain a hydrogen partial pressure close to 50 mbar.

3 Experimental results

3.1 Gas composition

After both D_2 injections, we observed a fast decay of the D_2 content, associated with the simultaneous rise of the H_2 , and, to a lesser extent, HD, contents (Fig. 2). Then the generated hydrogen dropped below the detection limit in 65 days, a similar duration as compared to previous H_2 injections (Fig. 3).

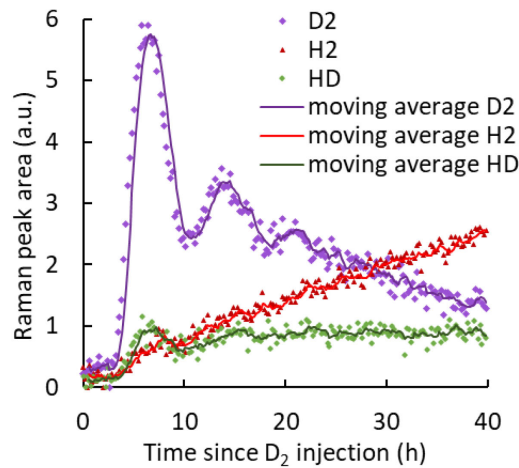


Fig. 2. Evolution of D₂, HD and H₂ in the circulating gas measured by Raman spectroscopy after the second D₂ injection, the initial sinusoidal shape is due to mixing in the gas circuit.

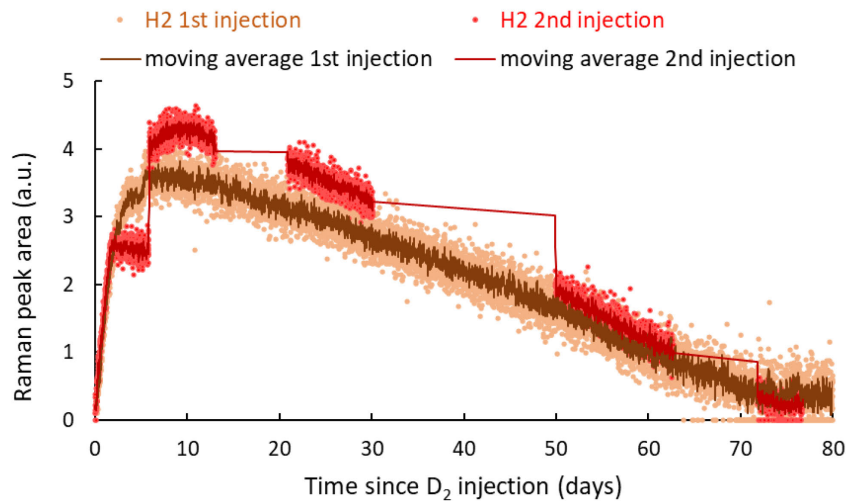


Fig. 3. Evolution of H₂ Raman peak area after D₂ injections into the borehole, Raman measurements were intermittent during the second phase of H₂ decay.

3.2 Water composition

The evolution of the isotope label monitored in the water extracted from the borehole is presented in Fig. 4. Although an increase is clearly visible after the first D₂ injection, mass balance calculations indicate that only 35 % of injected D is recovered in water.

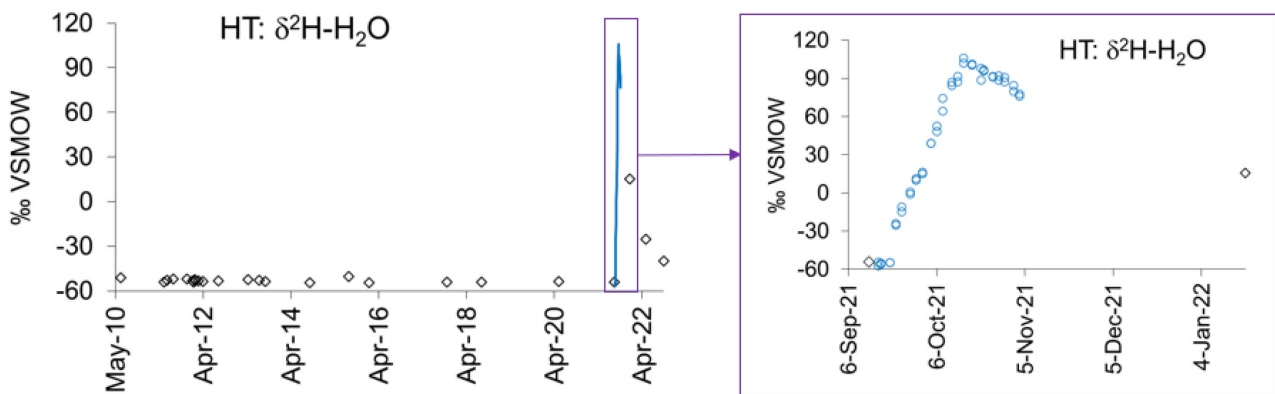


Fig. 4. Evolution of the isotope label in water extracted from the test interval since the beginning of HT experiment. Right side: evolution after the first D₂ gas injection, performed on 9/16/2021.

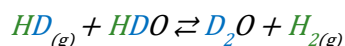
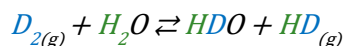
4 Interpretation

4.1 Confirmation of the occurrence of isotopic exchange into the borehole

As isotope exchange processes are expected to be slow at the temperature and pressure conditions prevailing in HT experiment, it was checked that no experimental artifact occurred. The test, started 40 hours after the second D₂ injection, consisted in bypassing the borehole for 4 days while monitoring the evolution of D₂, HD and H₂ Raman peak areas, which remained constant in the gas circulation module. This result confirmed that the fast isotopic exchange observed between D₂ and H₂ is not an experimental artifact.

4.2 The role of hydrogenases

The H/D exchange reaction can be catalyzed by bacteria carrying hydrogenase. This enzyme catalyzes the reversible oxidation of H₂ to proton and possesses the non-physiological functions of H/D exchange and nuclear spin isomer conversion reactions (Vignais 2005). Thus, in the presence of D₂ gas in a D₂/H₂O system, hydrogenases rapidly catalyze the proton/hydrogen-deuterium exchange reaction, which results in the formation of HD and H₂, according to the following reactions:



Furthermore, trends similar to those observed in the gaseous phase of the HT experiment are reported by Kawahara *et al.* (2019) in a work for which Raman spectrometry was used to monitor the activity of a [NiFe] hydrogenase from a sulfate-reducing bacteria.

Consequently, the fast isotopic exchange reactions observed in HT experiment are attributed to hydrogenase enzymes. Then, more slowly, hydrogenases are responsible for the net oxidation of hydrogen to water, resulting in the long-term decrease of H₂.

5 Conclusion and perspectives

Our measurements provide additional evidence that hydrogenase-containing and net H₂-oxidising microorganisms are present and active in the Opalinus Clay. The results of additional analyzes still in progress will allow a more complete interpretation of the H₂ consumption reaction mass balance. Our results suggest that the presence and activity of microorganisms should be investigated in the formations being considered for hydrogen storage, perhaps using methods similar to the ones outlined in this approach.

Acknowledgments

We thank the contribution of the partners of the Mont Terri Project (NWS, NWMO, FANC, BGR).

References

- Bagnoud, A, Chourey, K, Hettich, R, et al. 2016. Reconstructing a hydrogen-driven microbial metabolic network in Opalinus Clay rock. *Nat. Commun.* 7:12770. <https://doi.org/10.1038/ncomms12770>
- Damiani LH, Kosakowski G, Vinsot A, Churakov S. 2021. Hydrogen gas transfer between a borehole and claystone: experiment and geochemical model. *Environmental geotechnics*. <https://doi.org/10.1680/jenge.21.00061>
- Kawahara-Nakagawa, J, Nishikawa, K, Nakashima, S, Inoue, S, et al. 2019. New assay method based on Raman spectroscopy for enzymes reacting with gaseous substrates. *Protein Science* 28, 663-670. <https://doi.org/10.1002/pro.3569>
- Vignais, PM. 2005. H/D exchange reactions and mechanistic aspects of the hydrogenases. *Coord Chem Rev* 249:1677–1690. <https://doi.org/10.1016/j.ccr.2005.01.026>
- Vinsot, A, Appelo, CAJ, Lundy, M, Wechner, S, et al. 2014. In situ diffusion test of hydrogen gas in the Opalinus Clay. Geological Society, London, Special Publications 400(1): 563–578. <http://dx.doi.org/10.1144/SP400.12>
- Vinsot, A, Appelo, CAJ, Lundy, M, Wechner, S, et al. 2017. Natural gas extraction and artificial gas injection experiments in Opalinus Clay, Mont Terri rock laboratory (Switzerland). *Swiss Journal of Geosciences* 110(1): 375–390. <https://doi.org/10.1007/s00015-016-0244-1>

Hydro-geochemical scoping calculations for the CO₂ Long-term Periodic Injection Experiment (CO₂LPIE)

Jin Ma^{1*}, Peter Alt-Epping¹ and Paul Wersin¹

¹ Institute of Geological Sciences, University of Bern, CH-3012 Bern, Switzerland

* jin.ma@unibe.ch

1 Introduction

In the context of reaching net zero carbon emission, the CO₂LPIE project (CO₂ Long-term Periodic Injection Experiment (Rebscher et al., 2020)) is planned to investigate the coupled thermo-hydro-mechanical-chemical processes (THMC) during a periodic CO₂ injection into intact Opalinus Clay in the Swiss Mont Terri rock laboratory. The envisioned time frame is about 15 to 20 years of CO₂ exposure of the rock, with a max. over pressure of 3 MPa (below the fracture pressure). The planned length of the injection borehole is about 15 m to 20 m, with a small active section for injection (e.g., 20 cm), portraying a point source. Monitoring boreholes will be drilled around the injection borehole, to monitor the hydrogeochemical evolution of the pore fluids. However, the optimal distances between these monitoring boreholes and the injection borehole are still under investigation. The distance needs to be within the range of influence radius of the interested parameters during the experiment, and at the same time large enough to avoid inducing interference with the CO₂ transport in the formation. In order to get a general understanding of the hydraulic and geochemical evolution of the system, in particular, the extent of the CO₂ influence zone after a 20-year injection period, a series of scoping calculations have been carried out by the University of Bern using various injection modes and varying a number of rock parameters. These calculations provide important information for understanding CO₂ transport in clay caprocks and for optimizing the distance between the monitoring and injection boreholes in the CO₂LPIE experiment.

2 Model description

A 2D-axisymmetric hydrogeochemical (THC) model has been developed at site-scale using the PFLOTRAN simulator (pflotran.org). The model has a total radius of 10 m and a depth of 25 m. An injection section is located at a depth of 15 m in the center of the cylinder, with a length of 20 cm and a radius of 5 cm. The model represents the Opalinus Clay as a homogeneous medium, with a porosity of 0.15, anisotropic permeabilities of 2e-20 m² in the horizontal and 8e-21 m² in the vertical direction, respectively, and an effective diffusion coefficient (D_e) of 5e-11 m²/s (Wersin et al., 2008). The reactive mineral phases are implemented as 7.5 vol.-% calcite and 2.5 vol.-% dolomite, and the initial porewater in the clay is in equilibrium with these two minerals. Cation exchange reactions with the clay surface are implemented, including major cations, such as Na⁺, Ca²⁺, Mg²⁺, and K⁺. The formation has an initial pressure of 1 MPa and a temperature of 13 °C.

Tab. 1: Main parameters used for the reference case

Model radius	10 m
Model thickness	25 m
Porosity	0.15
Permeability-r	2e-20 m ²
Permeability-z	8e-21 m ²
Effective diffusion coefficient (D_e)	5e-11 m ² /s

A series of scoping calculations have been carried out to explore the impact of different injection options, mineral reactions, and rock transport parameters on the development of the radius of the CO₂ plume over 20 years of injection. Three injection options were tested, including CO₂-charged liquid injection at 3 MPa (“Liquid injection” case), CO₂ gas injection at 3 MPa (“Gas injection” case),

and CO₂-charged liquid diffusion at formation pressure (“Diffusion only” case). In addition, for each injection mode, sensitivity cases with 2x higher and lower D_e were performed.

3 Results

Fig. 1 shows the distributions of dissolved CO₂(aq) concentration, liquid pressure, and pH for the Liquid injection case as an example. Calcite dissolution and small amounts of dolomite precipitation are predicted to occur in a limited area (within ca. 30 cm around the well), leading to notable porosity changes but to almost no impact on the CO₂ distribution. CO₂ plume radii are calculated at selected times using a cut-off CO₂ concentration of 5 mmol/L (Tab. 1). For short-term injection (e.g., after 4 years), the differences of CO₂ plume radii among the three injection options are negligible, due to the diffusion-dominated CO₂(aq) transport in the low-permeable Opalinus Clay. However, after 20 years of injection, the two injection cases (liquid injection and gas injection) show slightly larger CO₂ plume radii than the pure diffusion case. This is because of both slow advection of the fluids and higher CO₂ concentration at the well (due to higher pressure). Interestingly, although in the “Gas injection” case, CO₂ gas can barely enter the rock as a free phase due to the high gas entry pressure of Opalinus Clay, the model predicts a higher CO₂ concentration near the well and thus the largest CO₂ plume after 20 years.

Overall, the model predicts CO₂ plume radii ranging from 0.9 m to 2.0 m after 20 years of injection, accounting for variations in the effective diffusion coefficients (D_e) of a factor of 2. These values reflect the arrival of the CO₂(aq) plume, but a complete breakthrough with steady state is difficult to reach after 20 years, even with a much shorter distance (e.g., 0.35 m) between the injection and observation boreholes (Fig. 2). As an observation distance of less than 1 m would be technically difficult, the placement of the boreholes should be carefully considered and more accurate model settings are needed for the optimal placement of monitoring boreholes.

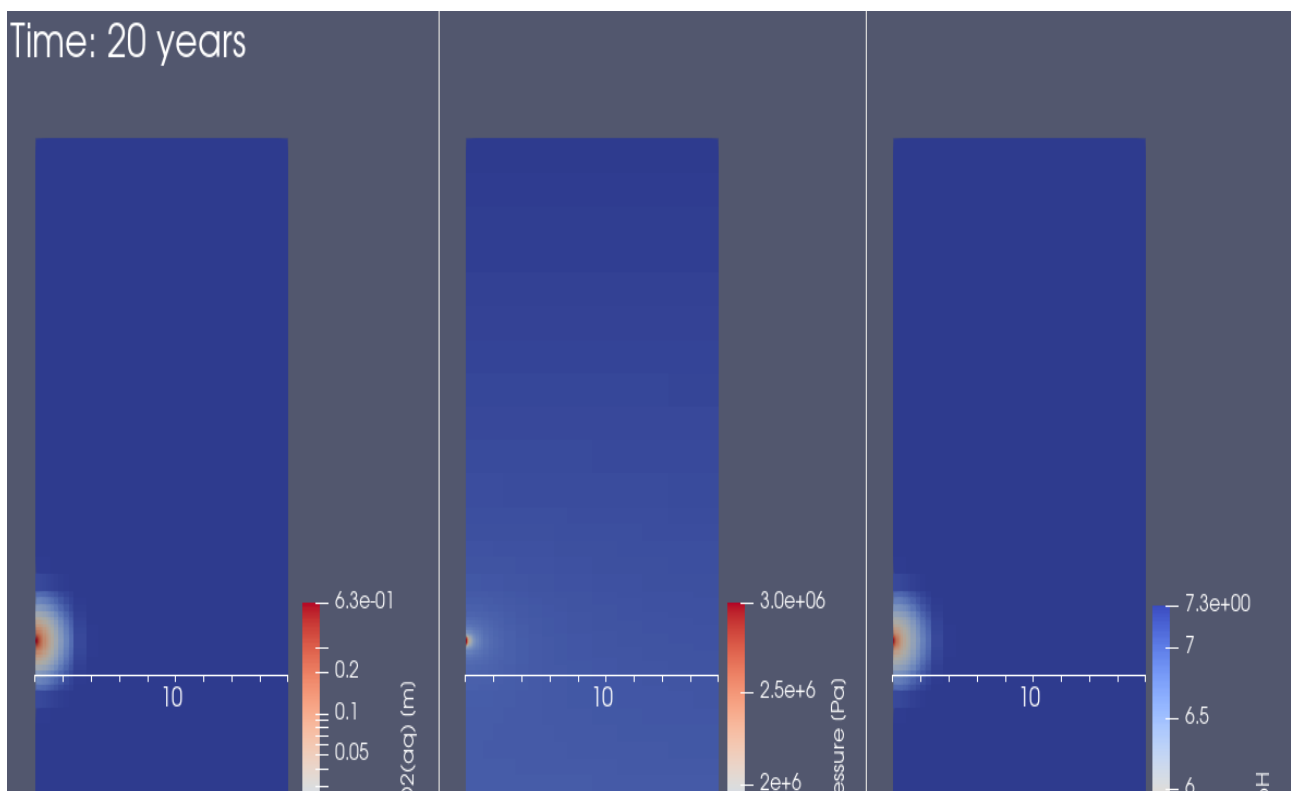


Fig. 1. Distributions of dissolved CO₂(aq) concentration, liquid pressure, and pH for the Liquid injection case.

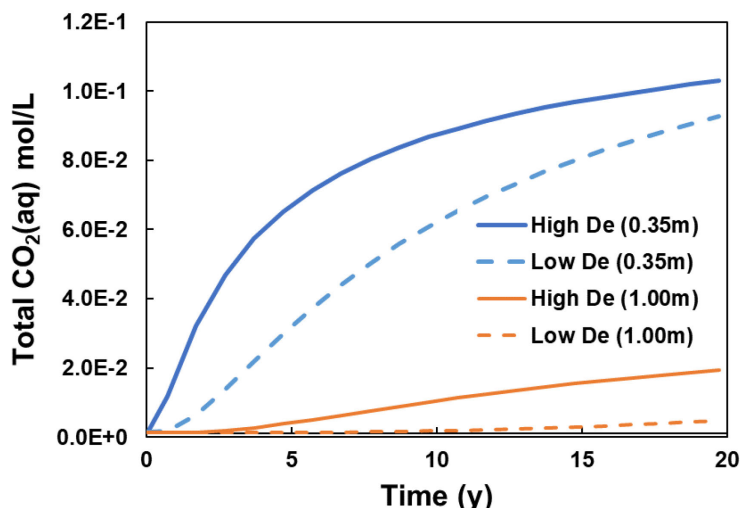


Fig. 2. The time evolution of the concentration of dissolved CO₂(aq) at selected distances from the center of the injection section (at 15 m) for the 2x higher and 2x lower D_e “Diffusion only” cases.

Tab. 2. CO₂ plume radii (C_{CO2}>5 mmol/L) after 4, 10, and 20 years injection for tested cases. Bold: reference cases with D_e= 5e-11 m²/s

	CO ₂ cons. in the well	CO ₂ plume radius		
		After 4 yr	After 10 yr	After 20 yr
Liquid injection	0.63 mol/L	0.70 m	0.90 m	1.29 m
2x higher De	0.67 mol/L	0.90 m	1.30 m	1.49 m
2x lower De	0.63 mol/L	0.50 m	0.70 m	0.90 m
Diffusion only	0.45 mol/L	0.70 m	0.90 m	1.09 m
2x higher De	0.45 mol/L	0.90 m	1.09 m	1.49 m
2x lower De	0.45 mol/L	0.50 m	0.70 m	0.90 m
Gas injection	1.10 mol/L	0.70 m	1.09 m	1.50 m
2x higher De	1.10 mol/L	0.90 m	1.30 m	2.00 m
2x lower De	1.10 mol/L	0.49 m	0.70 m	1.09 m

References

Rebscher, D., Makhnenko, R., Nussbaum, C., & Vilarrasa, V. (2020). CO₂ long-term periodic injection experiment at Mont Terri (CO₂LPIE). Technical Meeting TM-38, 29–30 January 2020, Porrentruy, Switzerland, 2020.

Wersin, Paul, J. M. Soler, L. Van Loon, J. Eikenberg, B. Baeyens, D. Grolimund, Thomas Gimmi, and S. Dewonck. 2008. Diffusion of HTO, Br⁻, I⁻, Cs⁺, ⁸⁵Sr²⁺ and ⁶⁰Co²⁺ in a clay formation: Results and modelling from an in-situ experiment in Opalinus Clay. *Applied Geochemistry* 23, no. 4: 678-691.

Storage capacity assessment for CO₂/H₂S in a depleted gas condensate reservoir

Nicolás Rangel Jurado^{1,2*}, Martina Cervelli¹, Yurianny Rojas¹ and Federico Games¹

¹ Ad Terra Energy, Chemin des Vergers 4, 1208 Geneva, Switzerland.

² Geothermal Energy and Geofluids, ETH Zürich, Sonneggstrasse 5, 8092 Zurich, Switzerland.

* nicolas.rangeljurado@adterra.com

1 Introduction

Acid gas storage (AGS) has emerged as an attractive solution for managing the undesirable by-products generated during natural gas sweetening in hydrocarbon fields. The design of an acid gas injection (AGI) scheme requires large amounts of subsurface information, among which the static and dynamic storage capacity of the targeted reservoir are paramount. In this study, we present two different methodologies for calculating the static storage capacity of a depleted gas-condensate reservoir in the Middle East, which has produced more than 200 billion standard cubic feet (Bscf) of gas as of October 2023. The Cretaceous (Albian) reservoir studied here has been in production since 2015 and produces sour gas, which is sent to gas treatment plants and results in the generation of acid gas as a byproduct of the sweetening process (Fig. 1). The acid gas is currently being flared, thus representing a significant environmental concern for the field operator. The resulting fluid composition of the acid gas varies over time as a function of the sour gas feedstock, nonetheless, here we present a base case for which we consider equal molar compositions of hydrogen sulphide and carbon dioxide (i.e., 50 % H₂S, 50 % CO₂). To support our client's flaring/greenhouse gas emissions reduction strategy, a disposal formation with a proven seal system towards the northeast of the still operational production zone has been identified. The target formation appears to have sufficient injectivity and exhibits approximate reservoir pressure and temperature values of ~140 bar and ~70 °C, respectively. Furthermore, both pressure and temperature at the spill point exceed the critical point of the acid gas to be injected, ensuring its injection in supercritical state. Through material balance and volumetric calculations, we use two different approaches to estimate the available volume within the reservoir that could be devoted for AGS.

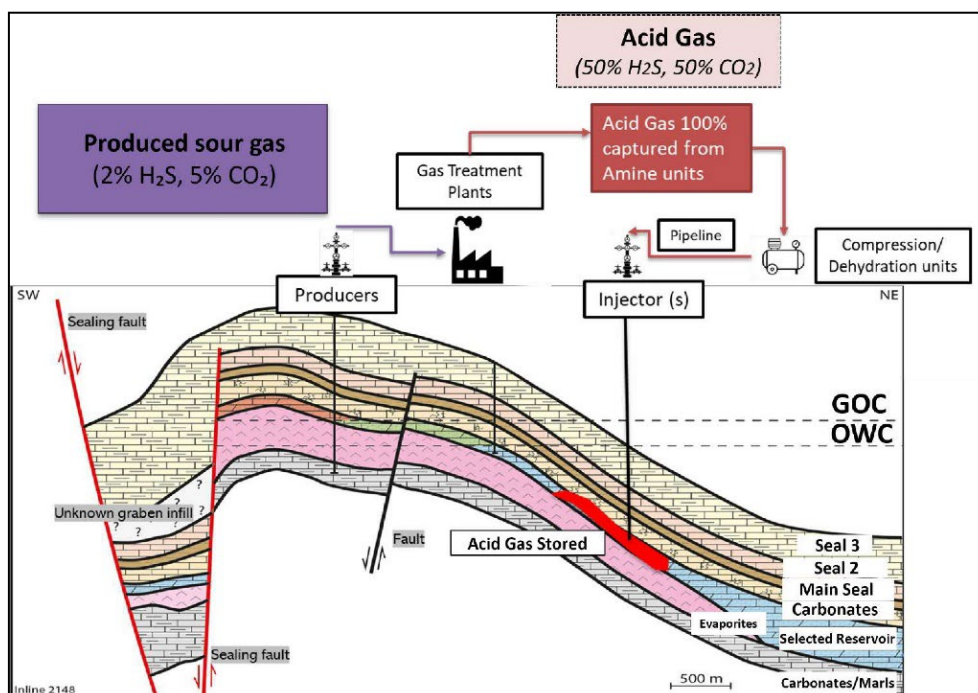


Fig 1. Schematic representation of the planned acid gas injection in the Albian Reservoir.

2 Methods

The hydrocarbon field studied here is composed of more than two compartmentalized units that exhibit varying degrees of hydrocarbon depletion. Based on the criteria collected in Fig. 2, one dolomitic layer from the Albian period (Lower Cretaceous) has been identified as a viable target for the storage and containment of acid gas to the northeast of the production zone.

	Positive Indicators	Cautionary Indicators	Case study
Reservoir storage capacity			
Static	Estimated effective storage capacity much larger than total amount of CO ₂ to be injected	Estimated effective storage capacity similar to total amount of CO ₂ to be injected	>0.85 Bcf at reservoir condition. NB: The reservoir is under production, meaning that capacity is being created day by day.
Dynamic	Predicted injection-induced pressure well below levels likely to induce geomechanical damage to reservoir or caprock	Injection-induced pressures approach geomechanical instability limits	Predicted injection-induced pressure well below levels likely to induce geomechanical damage to reservoir or caprock
Reservoir Properties			
Depth	>1000m <2500m	<800m >2500m	>1200m
Res. thickness (net)	>50m	<20m	25-40m
Porosity	>20%	<10%	15%
Permeability	>500mD	<200mD	2-300mD
Salinity	>100gl ⁻¹	<30gl ⁻¹	200gl ⁻¹
Stratigraphy	Uniform	Complex lateral variation and complex connectivity of reservoir facies	Reservoir thickness' decreases towards the South
Well density	<10	>50	8

Fig 2. Key geological indicators for storage site suitability (modified after Chadwick et al., 2008).

The Albian reservoir's storage capacity is estimated using the following methods:

- 1) Through a bottom-up approach based on historical production data dating back to 2015, correcting for the volumetric expansion—as a result of depressurization—and an expected hydrocarbon replacement factor (Eq. 1)
- 2) Using top-down, volumetric correlations found in literature (e.g., McCabe 1988, Bachu et al., 2007, Bradshaw et al., 2007), which rely on a theoretical sweep efficiency, and the expected geometry and petrophysical properties of the injection formation (Eq. 2).

Following the first method, which considers the cumulative produced volume from the reservoir, a gas formation volume factor (FVF) of 0.94 reservoir barrel per kilo-standard cubic feet (RB/kscf) was calculated using the original temperature and pressure conditions of the now partially depleted reservoir. This volumetric expansion factor is corroborated by the history-matched production model. However, relevant empirical studies for geological CO₂ sequestration suggest that total hydrocarbon replacement is not feasible and that only 75 % of the original oil and gas in place is expected to be replaced by the injected gas (Holloway, 2006; IEAGHG, 2009). As a result, a notional minimum storage capacity can be calculated using the following formula:

$$AGS \text{ volume (Res. conditions)} = \text{Produced volume (Surf. conditions)} * \text{Gas FVF} * 0.75 \quad (\text{Eq. 1})$$

An additional capacity volume was calculated using the well-established resource-reserve pyramid of subsurface volumetric calculations (Fig. 3). This approach quantifies the theoretical pore volume available, corrects for the specific petrophysical and geometric properties—on a first level—and a sweep efficiency factor to derive the maximum viable capacity for gas storage (Eq. 2).

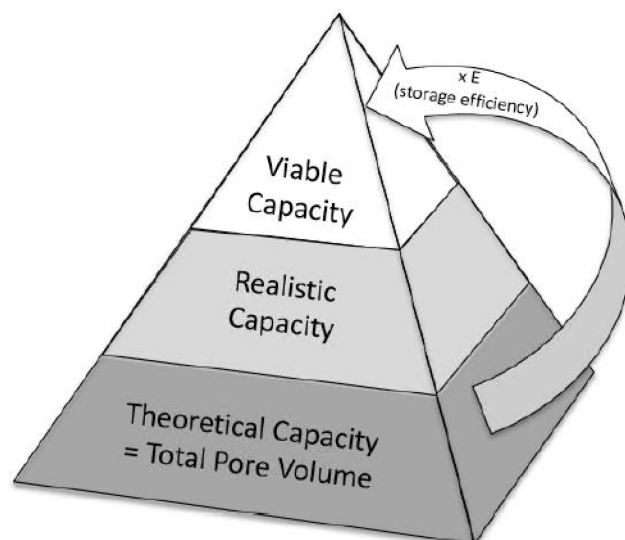


Fig 3. Techno-economic resource-reserve pyramid for gas storage projects (modified after Bradshaw et al., 2007).

This volumetric approach is based on the following formula:

$$AGS \text{ volume (Res. conditions)} = A * h_g * \phi * \rho * E \quad (\text{Eq. 2})$$

where A is the reservoir area, h_g is the gross thickness of the formation, ϕ is the average porosity and E is the storage efficiency factor. The efficiency factor E was varied between 0.5 and 8 % as typically assumed for non-depleted reservoirs in literature.

The injected acid gas density assumed for both methods was calculated using *CoolProp* (Bell et al., 2014) for a gas mixture of 50 % CO_2 and 50 % H_2S molar under the original pressure and temperature conditions of the Albian reservoir, yielding $\sim 670 \text{ kg/m}^3$. This dense acid gas phase would be injected below the hydrocarbon's spill point and would remain below the lighter hydrocarbons, while still providing pressure support for production operations.

3 Results & Discussion

Material balance calculations, relying on historical production data, project a theoretical storage capacity of 13.73 million metric tons (MMtons) or 0.97 billion cubic feet (Bcf) under reservoir conditions for the target formation. In contrast, literature-based correlations yield a more conservative estimate for storage gas capacity, ranging from 0.5 to 10.1 MMtons (0.036 to 0.71 Bcf). This range encapsulates lower and upper bounds linked to typical storage efficiency factors of 0.5 % to 10 %, commonly employed in greenfield development literature. Notably, estimates from historical production data align closely and slightly overestimate the upper bound of literature-based correlations, indicating that the Albian reservoir may allow for slightly higher storage efficiency factors (>10 %).

Based on integrated production modeling — which considers the reservoir's output, injectivity, and the surface facilities' constraints — the AGI project has been sized using an injection rate of 20 million standard cubic feet per day (MMscfd), which would keep the reservoir pressure below the fracturing limits. Under these assumptions and considering the current voidage volume available as of October 2023, the injection scheme will have an expected life of approximately 27 years and potential economic returns that exceed the 550 MMUSD through carbon reduction credits, assuming a carbon avoidance price of 100 USD per ton of CO_2 .

While the volumetric and resulting economic estimates above are already considerable, it is important to note that ongoing hydrocarbon production from the Albian reservoir contributes to a continuous increase in additional volumes available for AGS. As such, the preliminary storage capacity assessment contained here emphasizes a substantial opportunity to store vast quantities of acid gas

that could be further extended in the short-term. Ongoing dynamic and economic modeling aims to refine static storage capacity calculations, ascertain the project's techno-economics, and evaluate the risks associated with fracture propagation, caprock integrity, fault reactivation, and rock-fluid chemical interactions.

4 Conclusions

AGS represents an attractive solution to mitigate the release of CO₂ and other toxic gases produced during hydrocarbon processing. The success of AGS projects is contingent upon the identification of suitable geological formations that meet specific capacity, injectivity, and containment requirements, for which depleted yet fully characterized hydrocarbon fields represent ideal candidates. In this study, we present two different methods to calculate the static storage capacity in partially depleted hydrocarbon fields. Both methods, which rely on different inputs, appear to be in close agreement with each other. Our results suggest that the potential for dedicated AGS in the lower section of the Albian dolomitic reservoir is significant and its injection may provide simultaneous technical, environmental and economic co-benefits.

References

- Bachu S., Bonijoly D., Bradshaw J., Burruss R., Holloway S., Christensen N.P., Mathiassen O.M. 2007. CO₂ storage capacity estimation: methodology and gaps. *International Journal of Greenhouse Gas Control* 1, pp. 430–443.
- Bell, I. H., Wronski, J., Quoilin, S., & Lemort, V. 2014. Pure and Pseudo-pure Fluid Thermophysical Property Evaluation and the Open-Source Thermophysical Property Library CoolProp. *Industrial & Engineering Chemistry Research*.
- Bradshaw J., Bachu S., Bonijoly D., Burruss R., Holloway S., Christensen N.P., Mathiassen O.M. 2007. CO₂ storage capacity estimation: issues and development of standards. *International Journal of Greenhouse Gas Control* v. 1, issue 1, pp. 62–68.
- Chadwick R. A., Arts R., Bernstone C., May F., Thibeau S., Zweigel P. 2008. Best practice for the storage of AG in saline aquifers. *British Geological Survey Occasional Publication* 14, 267 pp.
- Holloway, S., Vincent, C., Kirk, K. 2006. Industrial Carbon Dioxide Emissions and Carbon Dioxide Storage Potential in the UK. DTI Cleaner Fossil Fuels Programme Report. DTI/Pub URN 06/2027.
- IEAGHG. 2009. CO₂ storage in depleted gas fields, IEA Greenhouse Gas R&D Programme.
- McCabe P.J. 1988. Energy Resources – Cornucopia or Empty Barrel? *AAPG Bulletin* v. 82, n°11, pp. 2110–2134.

GCS caprock potential of the Triassic Haisborough Group, Southern North Sea: insights from an onshore UK analogue

Simon Schneider^{1*}, Michael Flowerdew¹, Niall Paterson¹, Colm Pierce¹, Michael Pointon¹, Michelle Shiers¹, Adam Szulc¹, Stephen Vincent¹ and David Warburton²

¹ CASP, Cambridge, United Kingdom

² Anglo American Woodsmith, United Kingdom

* simon.schneider@casp.org.uk

1 Rationale

The Lower Triassic Bunter Sandstone Formation forms an important geological carbon storage (GCS) reservoir target in the Southern North Sea, with the overlying mudstones and evaporites of the Middle to Upper Triassic Haisborough Group and its equivalents forming its primary seal. However, the rocks of the Haisborough Group are poorly characterized because the unit has rarely been cored, and its subdivision into formations and members is largely based on wireline logs (Johnson et al. 1994). The SM14 core from the Anglo American Woodsmith Mine site, situated in the Cleveland Basin north of Scarborough, North Yorkshire, UK (Gibson & Bodman 2021), offers a unique opportunity to study a continuous, near 300-m-thick, direct onshore analogue of these strata.

2 Methods

CASP (a not-for-profit research organisation formerly known as the Cambridge Arctic Shelf Programme) is taking a multi-disciplinary approach to the cored succession to assess the composition, stratigraphy, and caprock suitability of the Haisborough Group. To do so, we combine sedimentary logging, palynostratigraphy, hand-held X-ray fluorescence (XRF), quantitative X-ray diffraction (QXRD), optical petrography, scanning electron microscope energy dispersive spectroscopy (SEM-EDS), porosity-permeability and mercury injection capillary pressure (MICP) analyses. A total of 64 core samples were taken from the entire, nearly 300-m-thick succession of the Haisborough Group, accounting for facies heterogeneity, but also aiming for regular spacing. Results will be integrated with a comprehensive suite of wireline log and geotechnical data to facilitate robust correlation to the offshore subsurface. This project forms part of CASP's wider research strategy, including parallel investigations of the underlying Bunter Sandstone Formation reservoir as well as overlying secondary seal strata of the Lower Jurassic Redcar Mudstone Formation of the Cleveland Basin. Furthermore, the SM14 core dataset will be compared to select cores and samples from offshore wells in the UK and Dutch sectors of the North Sea.

3 Preliminary results

Logging and facies analysis identified a conformal but distinct boundary between the Bunter Sandstone Formation and the Haisborough Group. A lithostratigraphic framework for the latter is being constructed based on sediment textures and the abundances of halite, anhydrite and dolomite cement (see Fig. 1 for select lithology examples). Halite is largely confined to the Röt Halite Member of the Dowsing Formation, where it is pervasive. Throughout the succession, optical petrographic and SEM-EDS analysis identify anhydrite, clay minerals, dolomite, quartz and feldspar as common mineral components at varying proportions. Variation is largely driven by the abundance of anhydrite, which occurs in various crystal shapes (large-acicular, small-acicular, small-equilateral), either finely dispersed, or concentrated in streaks, veins or nodules. Ongoing QXRD analysis will offer the possibility to further characterize the abundance and composition of the clay fraction, and identify mineral components other than feldspar that may react with carbon dioxide. Porosity-permeability and MICP analyses yield encouraging results with regard to validating the suitability of the Haisborough Group as a caprock to injected carbon dioxide within the Bunter Sandstone Formation of the Southern North Sea.

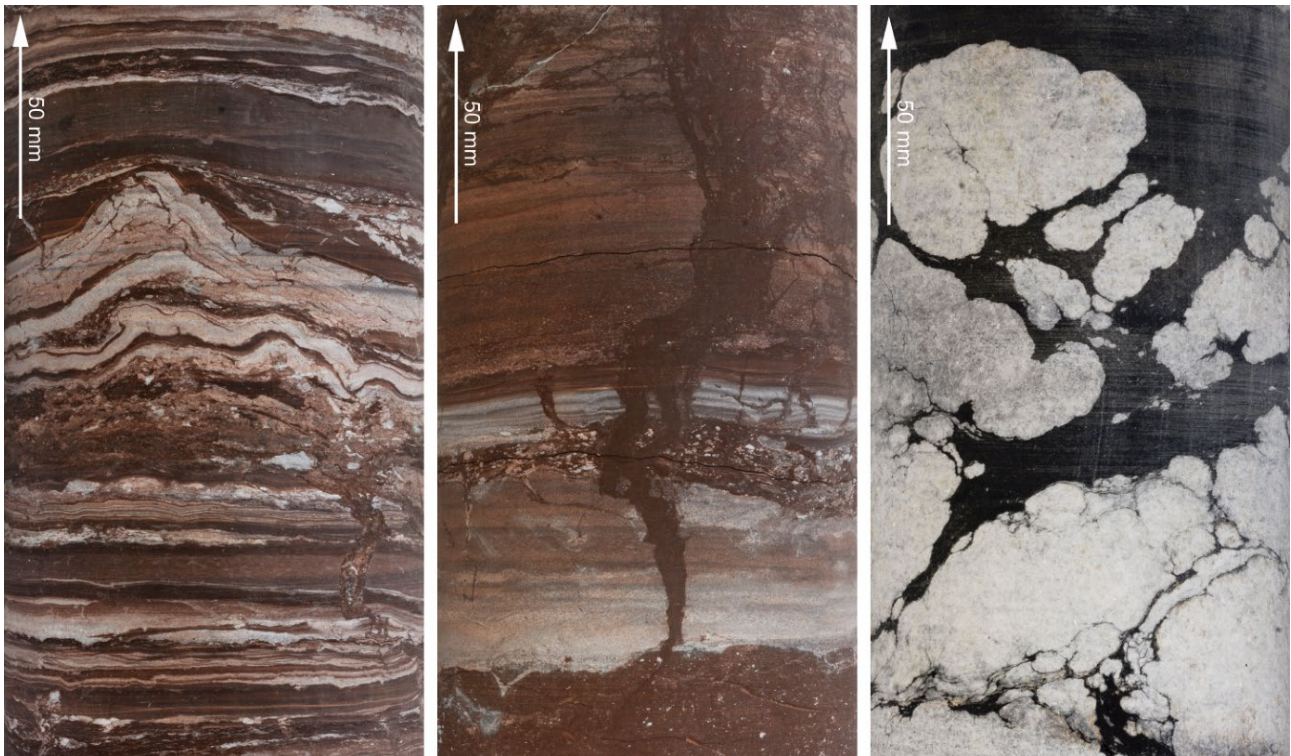


Fig. 1. Examples of sedimentary and diagenetic features in the Haisborough Group of the SM14 core (photographs by first author). Left: Greyish-red mudstone, intercalated with layers or specks of diagenetic dolomite and minor anhydrite, with diagenetic components and potential rootlet traces partly disturbing lamination. Centre: Reddish-brown laminated mudstone with thick reduced, dolomitic interlayers, interrupted by rootlet traces. Right: Homogenous dark grey mudstone surrounding large chicken-wire type anhydrite nodules.

References

- Johnson, H, Warrington, G, Stoker, SJ 1994. 6. Permian and Triassic of the Southern North Sea. In: Knox, RWO'B, Cordey, WG (eds). Lithostratigraphic nomenclature of the UK North Sea. British Geological Survey, Nottingham.
- Gibson, ME, Bodman, DJ 2021. Evaporite palynology: a case study of the Permian (Lopingian) Zechstein Sea. *J. Geol. Soc. London* 178, jgs2020–2174. <https://doi.org/10.1144/jgs2020-174>

Field-scale hydro-mechanical simulation of a novel monitoring system for the CO₂ Long-Term Periodic Injection Experiment (CO₂LPIE) at the Mont Terri rock laboratory

Sri Kalyan Tangirala^{1*}, Martin Ziegler², Roman Y. Makhnenko³ and Victor Vilarrasa¹

¹ Global Change Research Group, IMEDEA, CSIC-UIB, Esporles, Spain

² Federal Office of Topography (swisstopo), Mont Terri URL, Switzerland

³ Department of Civil and Environmental Engineering (CEE), University of Illinois at Urbana-Champaign, Urbana, Illinois, USA

* srikalyan.tangirala@csic.es

Abstract

Monitoring of subsurface operations is essential to gather in situ data of fluid flow and related coupled thermo-hydro-mechanical processes. Such monitoring promotes making on-field decisions that determine the course of a project based on the reservoir-caprock response. With increase in worldwide interest in subsurface CO₂ storage, novel monitoring equipment and methodologies need to be developed to make the operations safe and scalable. Underground laboratories like the Mont Terri Underground Research Laboratory (MT URL) are planning to perform experiments to study the hydro-mechanical (HM) properties of the caprock and assess its long-term sealing capacity when subject to CO₂-induced geochemical reactions. In the CO₂LPIE experiment, assessment of the response of the heterogeneous sandy facies of the Opalinus Clay formation to cyclic injection involves drilling four monitoring boreholes in a square pattern surrounding centrally located injection and extraction boreholes. Among geophysical equipment, the monitoring boreholes have high resolution fiber optic sensors placed in resin between a fiber-reinforced PVC tubing and the borehole wall to measure longitudinal deformations. We run a preliminary field-scale 3D numerical simulation of the HM processes in the rock that would help analyze the injection induced deformations around the wells and quantifying the deformations in and around the optical fiber sensors, which can later be compared to the values recorded during the injection operation. These simulations also assist in designing the layout of future injection and monitoring wells and optimizing the injection conditions to minimize unwanted deformation and improve the safety of the experiment.

1 Introduction

Necessity-driven development of carbon mitigation strategies around the world is increasing as we are getting closer to the deadline set by the Paris Agreement to limit the temperature rise to 1.5 °C. Large amounts of money are being invested into new projects of geologic CO₂ storage (Niemi et al. 2017), H₂ storage, energy storage and other geo-energy applications to reach this goal. To ensure the safety and success of these operations, understanding the coupled thermo-hydro-mechanical (THM) processes in subsurface systems is necessary. Numerical modeling using the data from geophysical surveys and observation wells (if any) serves as a pivotal tool in the study of reservoir response to injection. A detailed field-scale numerical study can help in designing the optimal well layout for maximum performance and safety, suggest safe injection conditions and predict the evolution of various physical parameters with time (Sciandra et al. 2022).

The MT URL in St. Ursanne, Switzerland, well-known for its field scale studies in the frame of nuclear waste disposal through hydrogeological, geochemical and geotechnical characterization of Opalinus Clay, also aims to study the hydro-mechanical (HM) properties and behavior of the Opalinus Clay formation (representative of caprocks) and assess its long-term sealing capacity when subject to CO₂-induced geochemical reactions. The latter will be explored in the CO₂ long-term periodic injection experiment (CO₂LPIE; abstract #615). This long-term experiment will allow us to observe the response of the sandy facies of Opalinus Clay due to exposure to CO₂. This experiment will have four monitoring wells in a square pattern with two centrally located injection and production wells,

which are yet to be drilled. These monitoring boreholes each have two optical fibers placed along the borehole wall and along the exterior of the PVC tubing held in place by a resin to monitor changes in the strain field upon injection (Fig. 1B). Due to computational limitations, we numerically model the field-scale 3-D HM response of the rock using a single injection and a monitoring well to observe the evolution of pore pressure and deformations on the top surface around the monitoring borehole and its internal components as a response to injection. This is an ongoing study and a detailed analysis of the HM response will be published in the near future.

2 Methods

In our model geometry, we consider a 5 m x 5 m top surface and a reservoir depth of 21 m with the wells reaching 16-m deep from the surface. Both the injection and monitoring wells have an outer radius of 10.1 cm. Fig. 1 shows the geometry of the model and a strong simplification of the interior components of the monitoring well. Tab. 1 lists the hydraulic and mechanical properties we use for the rock and components of the monitoring well.

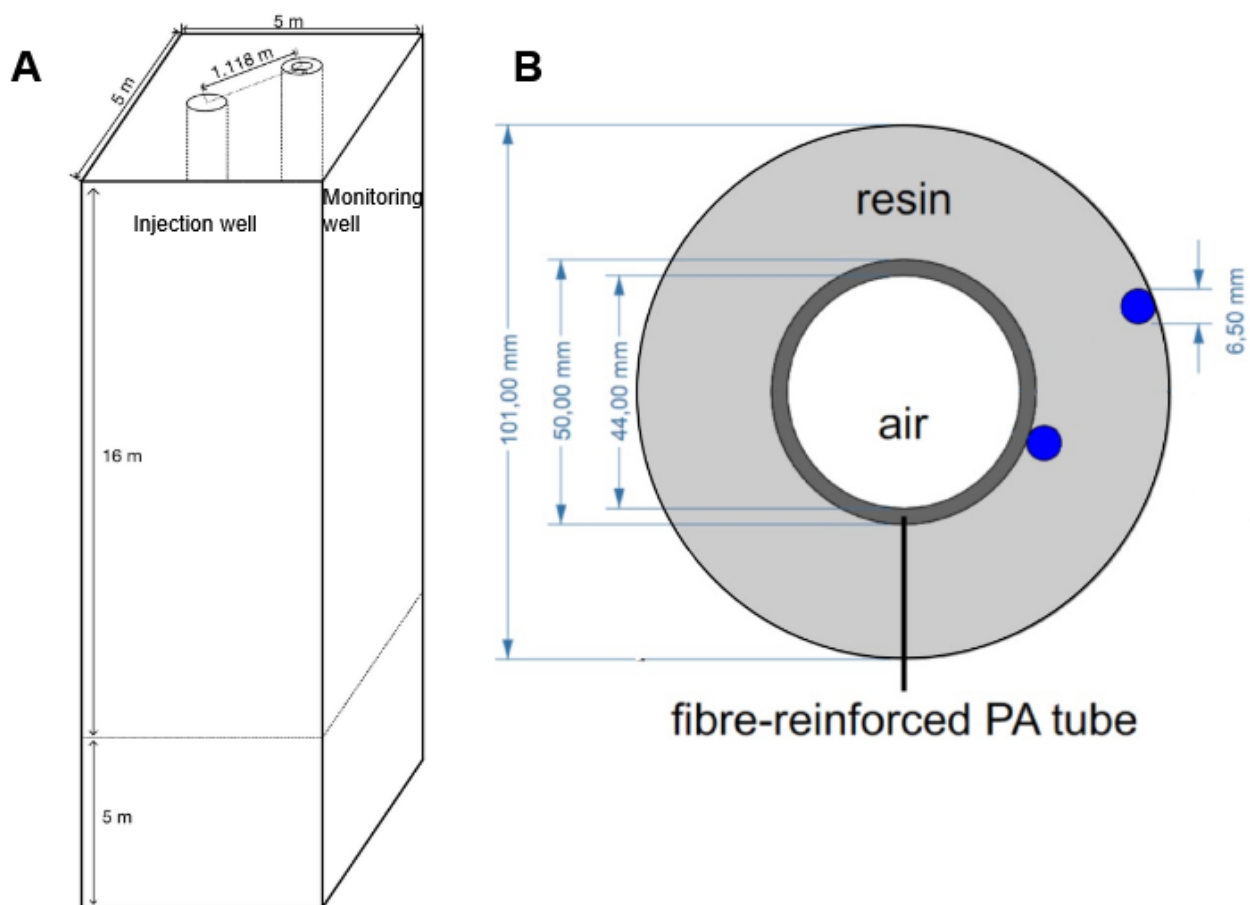


Fig. 1. (A) Geometry of the model, (B) Components (simplified) and dimensions of a monitoring well.

We perform the 3D field-scale numerical simulation using the finite element code CODE_BRIGHT (Olivella et al., 1996). As the wells are drilled perpendicular to the bedding planes, our model considers transverse isotropy and we assign the respective permeability tensor, Young's moduli, and Poisson's ratios along the bedding plane and perpendicular to it (Tab. 1). For our initial conditions, we consider the ambient reservoir pressure as 2 MPa and as the focus is on observing the stress changes, we consider the far field stresses to be 0 MPa. We inject water along the volume of the injection well by increasing its pressure from 2 MPa (initial) to 3 MPa in a span of 10 h. Later, we maintain the pressure at 3 MPa along the injection well for 5 h.

We use structured hexahedral elements to mesh our geometry which consists of 217,303 elements. The dimensions of the mesh elements in the optical fibers are 0.77 mm by 0.74 mm and increase progressively to 0.33 m by 0.33 m along the rock boundaries.

In Tab. 1, E stands for the Young's modulus, ν is the Poisson's ratio, k is the permeability, Φ is the porosity and G is the shear modulus.

Tab. 1. Material properties of rock and equipment in the monitoring well

Material	E (GPa)	ν (-)	k (m^2)	Φ	G (GPa)
Rock (parallel to bedding)	13.8	0.44	$4.8 \cdot 10^{-20}$	0.125	-
Rock (perpendicular to the bedding)	6.0	0.22	$1.6 \cdot 10^{-20}$	0.125	2.45
Resin	0.53	0.45	$1 \cdot 10^{-24}$	0.1	-
PVC	3.0	0.40	$1 \cdot 10^{-22}$	0.2	-
Optical Fiber	0.01989	0.17	$1 \cdot 10^{-20}$	0.3	-
Air	0.0001	0.30	$1 \cdot 10^{-10}$	0.9	-

3 Results

Due to the low permeability of the sandy facies of Opalinus Clay, the pore pressure front appears to still be far away from the monitoring well after 15 hours of injection (Fig. 2).

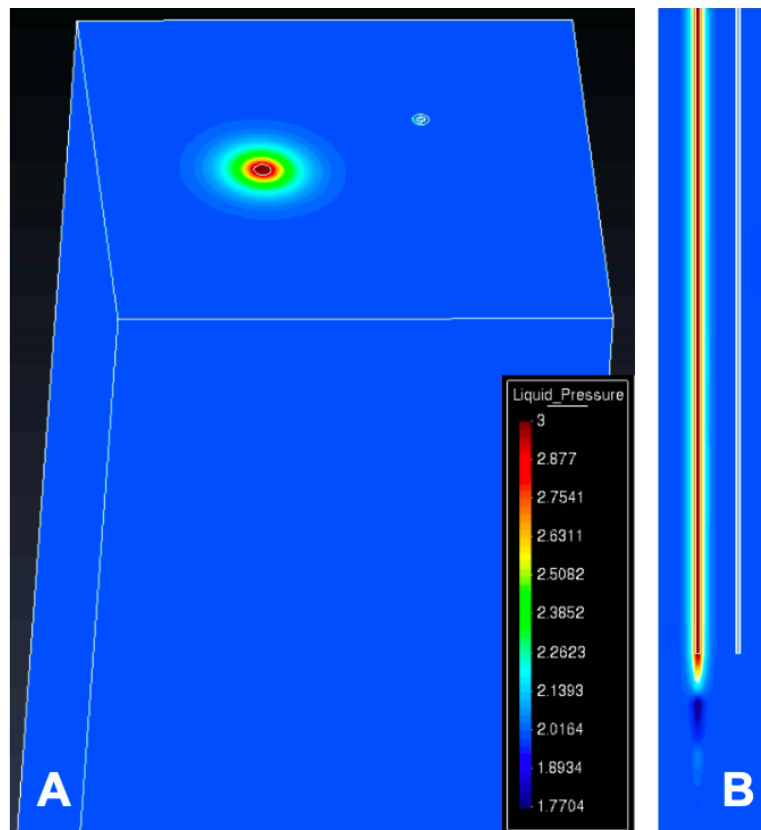


Fig. 2. (A) Pore pressure distribution along the top surface and (B) along a cross section joining the centers of injection and monitoring wells at 15 h from the start of injection.

However, injection-induced volumetric strains in the rock matrix can be observed around the monitoring well and also in the optical fibers (Fig. 3). We use the geomechanics convention of strains in our study with compaction being positive and elongation being negative. We observe that the rock expands around the monitoring well in the blue region on the axis connecting it to the injection well and compresses in the yellow regions (Fig. 3). Due to the very low Young's modulus of the optical fibers, a greater magnitude of strain occurs in the fibers when compared to the rock and resin around them. Interestingly, we can also observe the differential elongation and compression in the cross section of a single optical fiber.

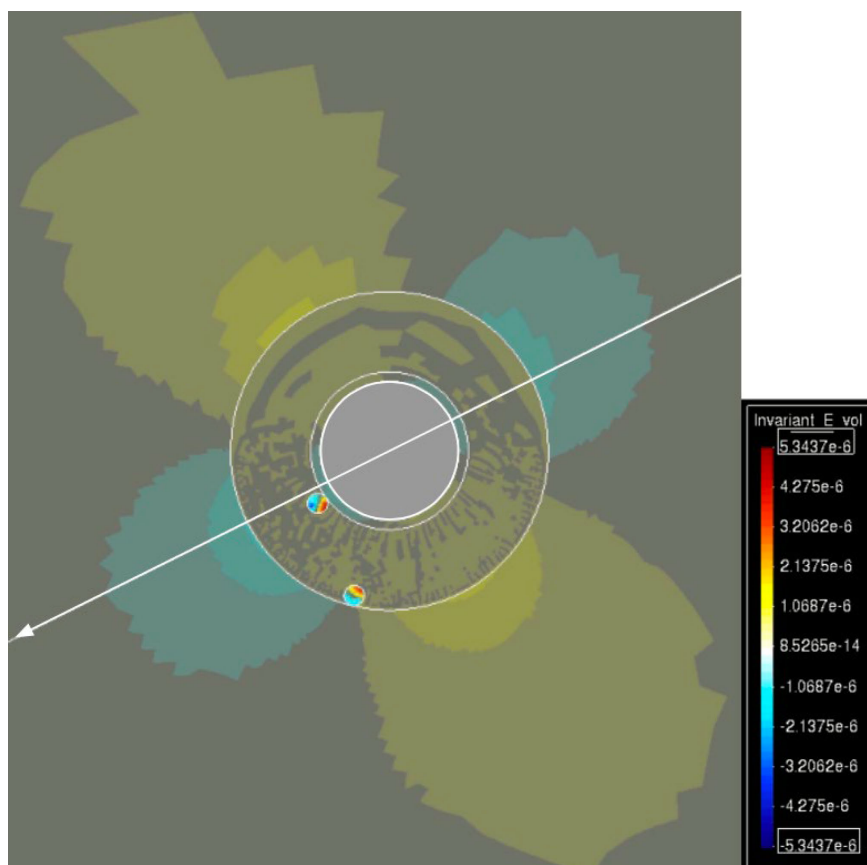


Fig. 3. Calculated volumetric strain distribution over the top surface with the monitoring well and the optical fibers on the walls of the tubing and the borehole. The arrow points towards the center of the injection well.

4 Conclusions

The CO₂LPIE experiment will serve to assess the long-term integrity of a caprock representative when subject to CO₂-fluid-rock interactions with subsequent geochemically-induced changes in the geomechanical properties of the sandy facies of Opalinus Clay. Simulation results of a pretest to measure the rock deformation to pressurization of the injection well reveal that even though pressure diffusion is limited to the vicinity of the injection well because of the low diffusivity of the rock, we observe deformations away from the well as a result of the undrained response of the rock.

Acknowledgements

S.K.T. and V.V. acknowledge funding from the European Research Council (ERC) under the European Union's Horizon 2020 Research and Innovation Program through the Starting Grant G_EO_RE_ST (www.georest.eu) under Grant Agreement No. 801809. IMEDEA is an accredited "Maria de Maeztu Excellence Unit" (Grant CEX2021-001198, funded by MCIN/AEI/10.13039/501100011033). R.M. is funded by US National Science Foundation grant CMMI-2239630.

References

- Niemi, A, Bensabat, J, Bear, J (eds.). 2017. Geological storage of CO₂ in deep saline formations. Springer, Dordrecht. 554 pp.
- Olivella, S, Gens, A, Carrera, J, Alonso E. E. 1996. Numerical formulation for a simulator (CODE_BRIGHT) for the coupled analysis of saline media. *Engineering Computations*. **13**, 87–112.
- Sciandra, D, Kivi, I.R, Vilarrasa, V. *et al.* 2022. Hydro-mechanical response of Opalinus Clay in the CO₂ long-term periodic injection experiment (CO₂LPIE) at the Mont Terri rock laboratory. *Geomech. Geophys. Geo-energ. Geo-resour.* **8**, 166. <https://doi.org/10.1007/s40948-022-00442-x>

Using the miniRUEDI within the context of the Mont Terri Rock Laboratory: potential and challenges

Yama Tomonaga^{1*}, Martin Ziegler² and David Jaeggi²

¹ Entracers GmbH, Dübendorf, Switzerland

² Federal Office of Topography, Mont Terri Underground Rock Laboratory, St. Ursanne, Switzerland

* info@entracers.com

1 Introduction

The miniRUEDI portable mass spectrometer (Brennwald et al. 2016) has been shown to allow in a reliable and robust manner the continuous on-site monitoring of gases in environmental (e.g., Giroud et al. 2023) and engineered systems (e.g., Tomonaga et al. 2019). Recently, an increasing number of miniRUEDIs has been deployed in projects conducted at the Mont Terri Underground Rock Laboratory (MT URL; e.g., Tomonaga et al. 2019; Weber et al. 2023).

Based on our long-term experience in using the miniRUEDI technology to realize gas monitoring strategies, we aim to stimulate a discussion on potential applications and the related technical needs within the context of the Opalinus Clay (OPA), the rock formation hosting most of the experiments at MT URL. Also, we would like to remind potential miniRUEDI users that measurements based on a non-purified gas phase surely have advantages, but also pose challenges. For instance, mass spectrometric overlaps can result in analytical biases that should not be underestimated (Brennwald et al. 2021).

To support the discussion during the 1st Caprock Integrity & Gas Storage Symposium (CIGSS) taking place at St. Ursanne, we performed a gas screening on November 16th 2023 to preliminarily assess the gas composition throughout the MT URL. Furthermore, in the perspective of future experiments targeting the injection of gas tracers at pressures deviating from the atmospheric pressure, we conducted a simple laboratory trial to exemplify the inlet pressure dependency of the miniRUEDI.



Fig. 1. Left panel: Position of the different stations where the gas screening was conducted on Nov. 16th 2023 (picture adapted from the Mont Terri Project website: www.mont-terri.ch). The dotted circle marks the position of the niche of the FE experiment. Right panel: miniRUEDI running on batteries in the niche Passwang (Station 5, picture by Y. Tomonaga).

2 Methods

2.1 On-site gas screening

A miniRUEDI was used to screen the gas composition within the MT URL's galleries at 13 locations (Fig. 1, left). To this end, the portable mass spectrometer system ran on batteries and was transported on a well-cushioned trolley (Fig. 1, right).

At all screening locations, mass spectra (i.e., scans) from a mass (m) to charge (z) ratio of 1 up to $m/z = 200$ were acquired using the Faraday cup detector and the electron multiplier detector to obtain a rough overview on the gas composition. Before each scan, the inlet capillary system of the miniRUEDI was purged with the sample gas at each station for about two minutes. Scans were conducted at a speed of 2.4 s/amu (amu: atomic mass unit). At stations 8, 9, 10, 11, and 13 calibrated measurements were conducted to assess in a quantitative manner the concentrations of H_2 , He, CH_4 , N_2 , O_2 , Ar, CO_2 , and Kr (see e.g., Tomonaga et al. 2019). Each measurement consisted of 20 readings for each item (H_2 , CH_4 , N_2 , O_2 , Ar, CO_2) on the Faraday cup and 30 readings for each item (He, Kr) on the electron multiplier detector.

2.2 Inlet pressure dependency

As far as the analyses of the miniRUEDI can be achieved using an inlet pressure close to the atmospheric pressure, the yield of the respective detectors in terms of peak intensities is almost linear and the measurements have been shown to be robust and reliable (Brennwald et al. 2016). However, experiments targeting the injection/extraction of gases into/from the OPA may need to deal with significant deviations of the inlet pressure from the atmospheric pressure that can lead to important analytical biases.

To exemplify the inlet pressure dependency of the portable mass spectrometer system, we analyzed the gas composition of atmospheric air in a sealed stainless-steel container connected to a miniRUEDI. While the gas composition in the vessel is not expected to change significantly over time, the total gas pressure decreases slowly due to the gas removal necessary for the analyses.

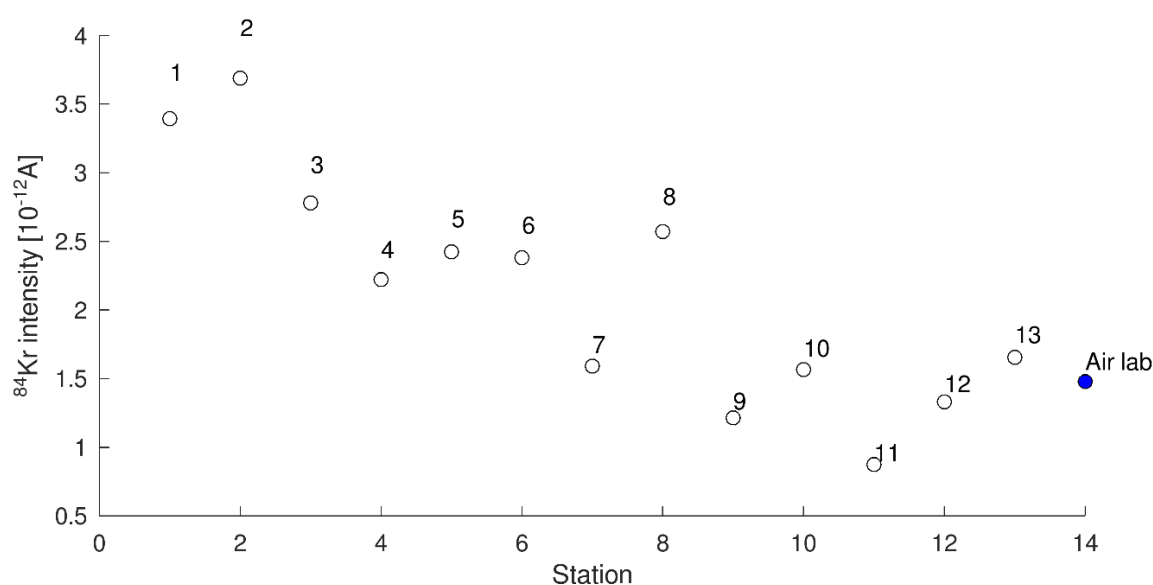


Fig. 2. ^{84}Kr peak intensities of the scans conducted at locations 1–13 in the MT URL (see Fig. 1). “Air lab” marks the value from the measurement of the ambient air in the laboratory of Entracers GmbH in Dübendorf on November 17th 2023 (i.e., immediately after the fieldwork at the MT URL).

3 Results

3.1 On-site gas screening

As the data collected on November 16th 2023 are still under evaluation, for this contribution we decided to focus on the outcome of the scans and, more specifically, on the Kr isotopes. The ⁸⁴Kr peak intensities at each station are plotted in Fig. 2.

From the Full-scale Emplacement (FE) experiment it is known that the ⁸⁴Kr measurements are most likely affected by a mass spectrometric overlap: the ⁸⁴Kr concentrations measured by a miniRUEDI (about $3 \cdot 10^{-6}$ v/v) in the rearmost part of the FE drift are about twice the concentration determined by conventional static mass spectrometry (about $1.5 \cdot 10^{-6}$ v/v; Tomonaga et al. 2019). As during the conventional measurements gases are purified from the reactive species before entering the mass spectrometers, it seems reasonable to attribute the higher ⁸⁴Kr concentrations determined by the miniRUEDI to an interference on $m/z = 84$.

The ⁸²Kr/⁸⁴Kr peak intensity ratios from our gas screening (Fig. 3) hint to a shift with respect to atmospheric air that could imply either a different Kr isotope composition or, as already stated, an analytical bias (on ⁸²Kr or ⁸⁴Kr, or both). Interestingly, the niche of the FE experiment (dotted circle in the left pane of Fig. 1), is characterized by the highest ⁸²Kr/⁸⁴Kr ratio.

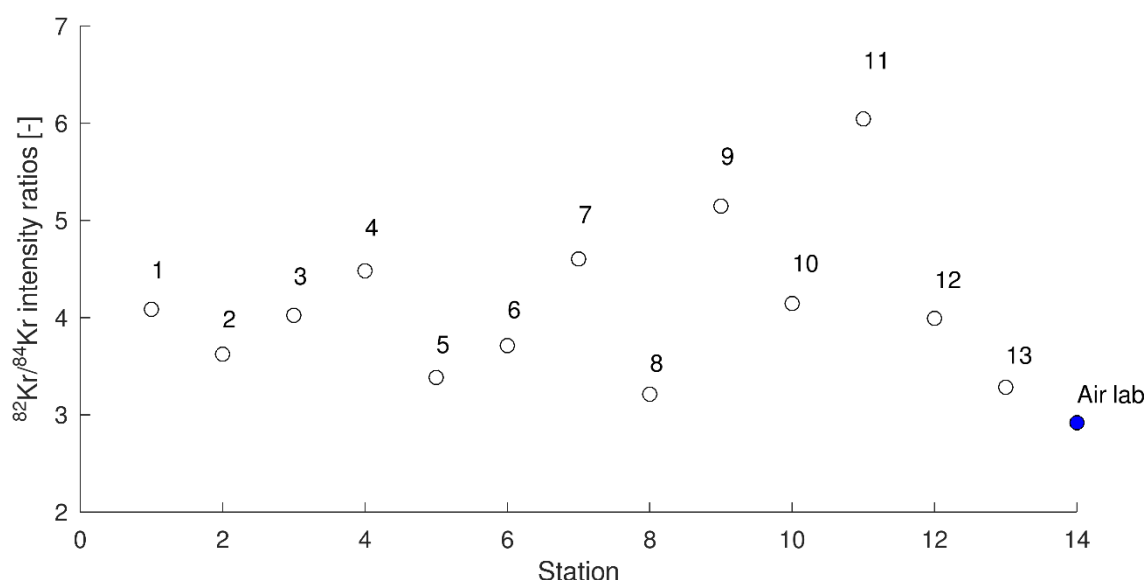


Fig. 3. ⁸²Kr/⁸⁴Kr peak intensity ratios of scans conducted at locations 1–13 (see Fig. 1). “Air lab” marks the value from the measurement of the ambient air in the laboratory of Entracers GmbH in Dübendorf.

3.2 Inlet pressure dependency

The results for N₂ and He of the laboratory trial targeting the inlet pressure dependency of the miniRUEDI measurements are plotted in Fig. 4. While the N₂ values remain virtually constant and within the typical uncertainty range of the miniRUEDI measurements (Fig. 4, blue lines), the He shares deviate significantly from the initial values. The stability of the N₂ shares is due to the predominance of this gas species (together with O₂) in atmospheric air: changes in the respective partial pressures affect almost proportionally the sum of the partial pressures of all measured gas species resulting in no apparent trend. From an inlet pressure difference of slightly more than 50 mbar the He shares start to diverge significantly with respect to the expected values.

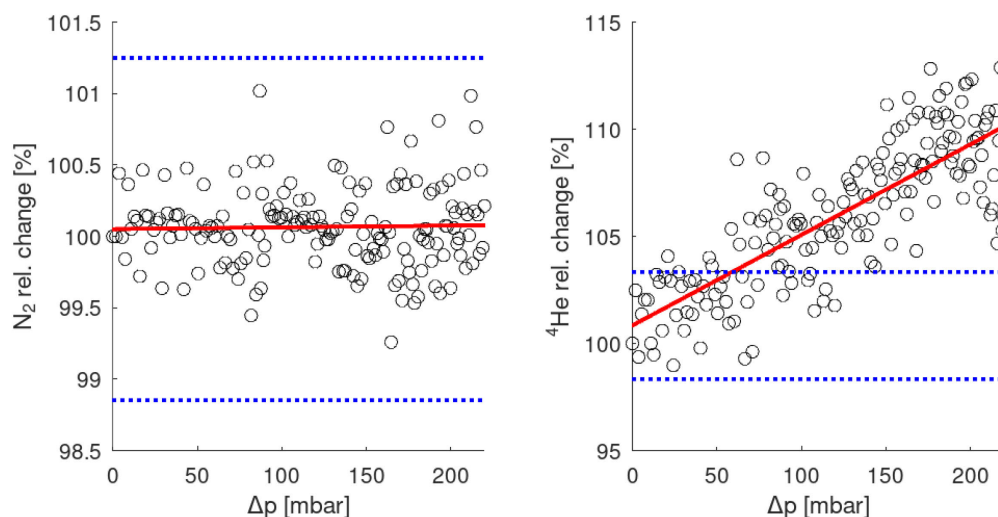


Fig. 4. Examples of inlet pressure dependency of the gas composition determined by the miniRUEDI mass spectrometer system. Δp indicates the negative pressure difference with respect to the atmospheric pressure initially present in the vessel. The relative changes in N₂ and He (y axis) are calculated with respect to the initial gas shares of the respective gases. Red lines: linear regressions of the determined relative changes. Blue lines: typical uncertainty ranges of the miniRUEDI measurements (Brennwald et al. 2016).

4 Remarks

It should be noted that our contribution aims to foster an open scientific discussion on the use of the miniRUEDI technology within the context of the Mont Terri Underground Rock Laboratory. Thus, the data presented here are primarily meant for such a discussion and not to draw final conclusions (for those the inclusion of the data from the calibrated measurements is a minimum requirement).

References

- Brennwald, MS, Schmidt, M, Oser, J, Kipfer, R 2016. A portable and autonomous mass spectrometric system for on-site environmental gas analysis. *Environ. Sci. Technol.* 50(24), 13455–13463.
- Brennwald, MS, Tomonaga, Y, Kipfer, R 2021. Deconvolution and compensation of mass spectrometric overlap interferences with the miniRUEDI portable mass spectrometer. *MethodsX* 7, 101038.
- Giroud, S, Tomonaga, Y, Brennwald, MS, Takahata, N, Shibata, T, Sano, Y, Kipfer, R 2023. New experimental approaches enabling the continuous monitoring of gas species in hydrothermal fluids. *Front. Water* 4, 1032094.
- Tomonaga, Y, Giroud, N, Brennwald, MS, Horstmann, E, Diomidis, N, Kipfer, R, Wersin, P 2019. On-line monitoring of the gas composition in the Full-scale Emplacement experiment at Mont Terri (Switzerland). *Appl. Geochem.* 100, 234–243.
- Weber, UW, Rinaldi, AP, Roques, C, Wenning, QC, Bernasconi, SM, Brennwald, MS, Jaggi, M, Nussbaum, C, Schefer, S, Mazzotti, M, Wiemer, S, Giardini, D, Zappone, A, Kipfer, R 2023. In-situ experiment reveals CO₂ enriched fluid migration in faulted caprock. *Sci. Rep.* 13, 17006. <https://doi.org/10.1038/s41598-023-43231-6>

Fault slip in clay-rich rocks: influence of the interaction between water and clay minerals

Markus Rast^{1*}, Claudio Madonna¹, Paul A. Selvadurai², Antonio Salazar Vásquez^{2,3}, Quinn Wenning⁴ and Jonas B. Ruh⁵

¹ Geological Institute, ETH Zurich, Zurich, Switzerland

² Swiss Seismological Service, ETH Zurich, Zurich, Switzerland

³ Institute for Civil and Environmental Engineering, Eastern Switzerland University of Applied Sciences, Rapperswil Switzerland

⁴ Institute of Geophysics, ETH Zurich, Zurich, Switzerland

⁵ Institute of Marine Sciences, CSIC, Barcelona, Spain

* markus.rast@erdw.ethz.ch

1 Introduction

Clay-rich rocks occur in a wide range of tectonic setting and have attracted interest for practical applications. For example, they are considered as suitable cap rocks in CO₂ storage facilities and as natural barriers in nuclear waste repositories because of their high sealing capacity. The sealing properties of clay-rich rocks result from the low permeability and the natural closure of fractures (self-sealing), where the key factor for the latter is the swelling ability of clay minerals (Wenning et al., 2021). Swelling, in turn, is a consequence of the interaction between electrostatically charged clay minerals and polar fluids (e.g., water), which under confined conditions can lead to the build-up of swelling stress (Madsen & Müller-Vonmoos, 1989). Fault closure by swelling in clay-rich rocks has been the subject of numerous studies (e.g., Bock et al., 2010; Zhang, 2011). However, it remains unclear how water-clay interactions affect the stability of pre-existing faults, considering that in addition to changes in frictional properties, the stress state may also change due to the build-up of swelling stress. This study addresses this gap using triaxial friction experiments.

2 Methods

2.1 Triaxial friction experiments

Triaxial friction experiments were performed using oblique saw-cut cylindrical samples, where the top half consisted of a clay-rich rock (Opalinus claystone, OPA) and the bottom half of a permeable sandstone (Berea sandstone, BER) (Fig. 1). We performed two types of experiments: (1) To estimate the frictional slip envelope of the OPA-BER interface without fluid injection, friction experiments were performed at confining pressures ranging from 4 to 25 MPa and a constant axial loading rate of 0.1 mm/min. (2) Friction experiments with fluid injection were then performed at confining pressures of 10 and 25 MPa with a constant piston position (no axial loading) and an initial differential stress of approximately 70 % of the expected yield stress. The aim was to compare the fluid pressures required to initiate slip in scenarios with and without fluid-clay interactions. This was done by incrementally increasing the fluid pressure by injecting either deionized water (a polar fluid that interacts with the clay minerals) or decan (a non-polar fluid that does not interact with the clay minerals).

2.2 Distributed strain sensing

In one of the decane and one of the water injection experiments, distributed strain sensing (DSS) was performed using fiber-optic (FO) strain sensors that were attached to the sample surface (Salazar Vásquez et al., 2022). Strain parallel to the FO cables was recorded with a spatial resolution of 1.3 mm and a sampling rate of 20 Hz. The DSS data allowed us to differentiate between poroelastic deformation within the matrix, deformation due to water-clay interaction, and elastic relaxation due to slip along the saw cut.

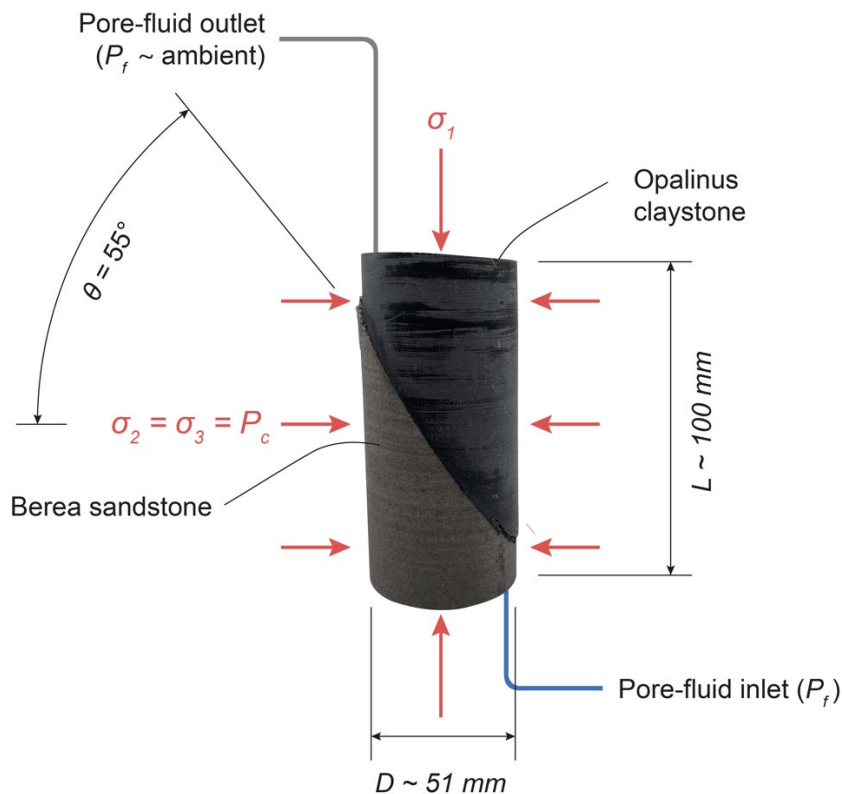


Fig. 1. Post-mortem photograph of the sample assemblage with schematic annotations of the experimental setup.

3 Results and discussion

3.1 Friction experiments without fluid injection

The frictional slip envelope of the OPA-BER interface based on the experiments without fluid injection resulted in a friction coefficient that is well below Byerlee's law and is in the range of previous studies on the frictional properties of OPA (e.g., Orellana et al., 2018). This indicates that the OPA dominates the frictional strength of the bi-material interface, which is consistent with previous studies linking clay minerals to low frictional strength (e.g., Crawford et al., 2008).

3.2 Friction experiments with decane injection

When injecting decane into the axially pre-stressed sample assemblage under stepwise increasing fluid pressure, the mechanical response can be separated into two phases: (Phase I) At relatively low fluid pressures, the effective normal stress decreased but the Mohr circle did not touch the frictional slip envelope and therefore, no slip occurred along the saw-cut (Fig. 2a). Each time the fluid pressure was increased, the DSS data showed poroelastic extension of the BER through which the decane was injected. (Phase II) At higher fluid pressures, the Mohr circle touched the frictional slip envelope causing slip along the saw-cut and a differential stress drop (Fig. 2b). This was supported by the DSS data that showed elastic axial relaxation of both the OPA and BER rock matrix. With further fluid-pressure steps, slip was initiated at progressively lower differential stresses, which allowed us to derive a frictional slip envelope in the presence of decane (Rutter and Hackston, 2017). The resulting frictional slip envelopes for three decane injection experiments are in the range of the frictional slip envelope based on experiments without fluid injection.

3.3 Friction experiments with water injection

When injecting deionized water, applying the same protocol as for the decane injection experiments, a differential stress drop occurred already at initial water injection at ambient fluid pressure

(~ 0.1 MPa), indicating slip along the saw-cut. The DSS data showed a complex deformation behavior at the OPA-BER interface that migrated upward with the fluid front. Slip along the saw-cut is supported by the DSS data after the water wetted the entire interface.

In the subsequent fluid pressure increases, the mechanical responses were qualitatively the same as in the decane injection experiments (Phase I and II, Fig. 2a and 2b). Based on stress data at high fluid pressures (Phase II), we derived frictional slip envelopes for three water injection experiments, which tend to show a slight weakening with respect to the frictional slip envelope based on experiments without fluid injection. Considering this weakening in combination with the post-mortem observation that the OPA transitioned from a solid rock to a mud close to the saw-cut surface, we interpret that water may alter the interface to behave like a hydroplastic fault (Petit and Laville, 1987).

Comparing the stress state at initial hydration with the frictional slip envelope derived at higher fluid pressures shows that slip occurred although the apparent stress state was below the yield stress (Fig. 2c). This suggests the need to consider swelling stress in initial water injection scenarios.

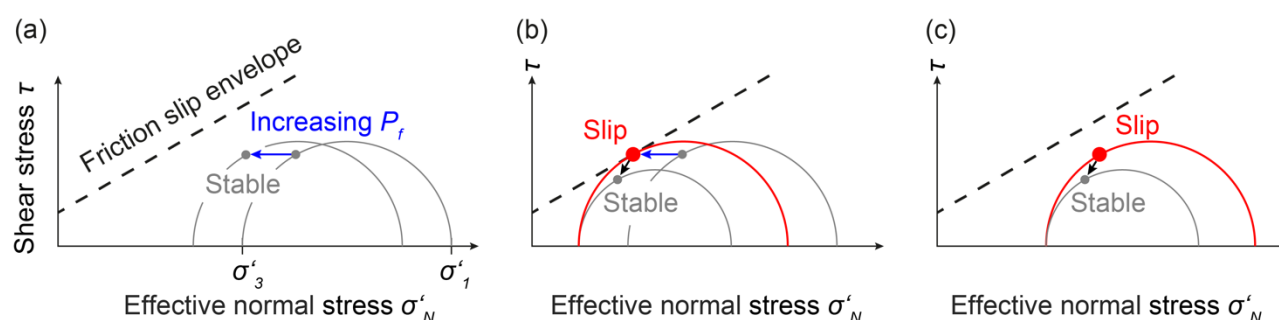


Fig. 2. Schematic representation of the results of the fluid injection experiment (modified from Ye and Ghassemi, 2018). (a) Increasing fluid pressure shifts the Mohr circle to the left without touching the frictional slip envelope. Representative for both decane and water injection experiments (Phase I). (b) Increasing fluid pressure shifts the Mohr circle to the left touching the frictional slip envelope, which causes slip initiation and a differential stress decrease until a stable stress state is reached. Representative for both decane and water injection experiments (Phase II). (c) Slip occurs at initial hydration (water injection experiments only), although the apparent stress state corresponds to a Mohr circle that does not touch the frictional slip envelope.

4 Conclusions

Our data suggest that water-clay interactions can contribute to the reactivation of critically stressed faults by (1) reducing the frictional strength and (2) changing the stress state through the build-up of swelling stress. This has implications for understanding fault zones in clay-rich rocks, where changes in fluid chemistry may lead to effects like those observed in our experiments. Furthermore, the reactivation of faults due to water-clay interactions should be considered when assessing the suitability of clay-rich rocks as a caprocks.

References

- Bock, H., Dehandschutter, B., Martin, D. C., Haller, A. d., Mazurek, M., Skoczylas, F., and Davy, C. (2010). Self-sealing of fractures in argillaceous formations in the context of geological disposal of radioactive waste. Technical report, OECD Publishing, Paris.
- Crawford, B. R., Faulkner, D. R., and Rutter, E. H. (2008). Strength, porosity, and permeability development during hydrostatic and shear loading of synthetic quartz-clay fault gouge. *Journal of Geophysical Research: Solid Earth*, 113(3).
- Madsen, F. T. and Müller-Vonmoos, M. (1989). The Swelling Behaviour of Clays. *Applied Clay Science*, 4:143–156.
- Orellana, L. F., Scuderi, M. M., Colletini, C., and Violay, M. (2018). Frictional Properties of Opalinus Clay: Implications for Nuclear Waste Storage. *Journal of Geophysical Research: Solid Earth*, 123(1):157–175.
- Petit, J.-P. and Laville, E. (1987). Morphology and microstructures of hydroplastic slicken-sides in sandstone. In Jones, M. and Preston, R., editors, *Deformation of Sediments and Sedimentary Rocks*, Geol. Soc. Spec. Publ., volume 29, pages 107–121.

- Rutter, E. and Hackston, A. (2017). On the effective stress law for rock-on-rock frictional sliding, and fault slip triggered by means of fluid injection. *Philosophical Transactions of the Royal Society A: Mathematical, Physical and Engineering Sciences*, 375(2103).
- Salazar Vásquez, A., Rabaiotti, C., Germanovich, L. N., and Puzrin, A. M. (2022). Distributed Fiber Optics Measurements of Rock Deformation and Failure in Triaxial Tests. *Journal of Geophysical Research: Solid Earth*, 127(8).
- Wenning, Q. C., Madonna, C., Kurotori, T., Petrini, C., Hwang, J., Zappone, A., Wiemer, S., Giardini, D., and Pini, R. (2021). Chemo-Mechanical Coupling in Fractured Shale with Water and Hydrocarbon Flow. *Geophysical Research Letters*, 48(5).
- Ye, Z. and Ghassemi, A. (2018). Injection-Induced Shear Slip and Permeability Enhancement in Granite Fractures. *Journal of Geophysical Research: Solid Earth*, 123(10):9009–9032.
- Zhang, C. L. (2011). Experimental evidence for self-sealing of fractures in claystone. *Physics and Chemistry of the Earth*, 36(17-18):1972–1980.

Combined numerical and experimental investigation of injection related effects in the CL experiment

Gesa Ziefle¹, Thies Beilecke¹, Shuang Chen¹, Markus Furche¹, Jürgen Hesser¹, Vinay Kumar¹, Jobst Maßmann¹, Christian Ostertag-Henning¹

¹ Federal Institute for Geosciences and Natural Resources (BGR), Hannover, Germany

* gesa.ziefle@bgr.de

1 Motivation

The CL (CO₂ Long-term Periodic Injection Experiment) Experiment, as well called CO₂LPIE, in the Mont Terri Rock Laboratory focuses on effects related to CO₂ storage and caprock integrity in Opalinus Clay. It aims at an increased understanding of (thermal-hydraulic-mechanical and chemical) TH2MC processes invoked by CO₂ injection and on the further development of monitoring systems. Related physical effects are summarized in Fig. 1. In the context of the CO₂LPIE experiment, the increase of pressure, chemical interactions and the potential development of flow paths is of specific interest. Nevertheless, a couple of basic interactions are similar to the effects that have to be considered in the field of radioactive waste disposal. Open questions in both fields lie in the handling of chemical reactions as well as dilatancy and fracture initiation. In final disposal, the latter should be understood but excluded by an optimization of the repository design. In the context of CO₂ sequestration, these effects also need to be avoided in the barrier (caprock). Therefore, their understanding is of significant importance in both fields.

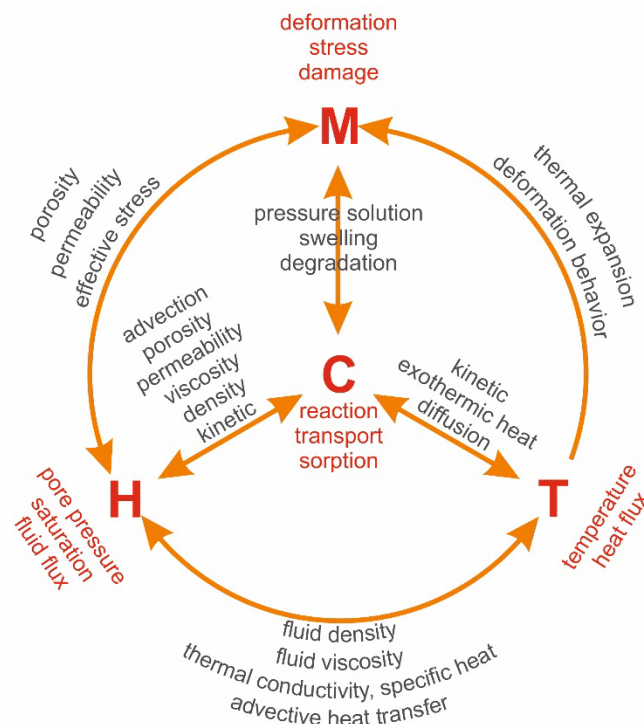


Fig. 1. Schematic presentation of coupled thermal-hydraulic-mechanical and chemical (THMC) processes (Maßmann et al. (2022)).

2 Previous works

BGR is involved in the CO₂LPIE experiment with geophysical measurements and also with numerical simulations combined with geochemical lab experiments, aiming on the interpretation of measurements related to the further development of constitutive models. Numerically, it is planned to use the OpenGeoSys 6 (OGS 6) TH2M model, as presented in the related CIGSS poster by Kumar et al.

(2024). This model has also been used in the GT experiment and for the investigation of gas transport processes on laboratory and repository scale in the EURAD WP “Gas” focusing on advection, diffusion and two-phase flow. Additional modelling is based on the chemical characterization of the claystone as performed in the laboratory and focuses on basic reactions as discussed in the related CIGSS poster by Chen et al. (2024).

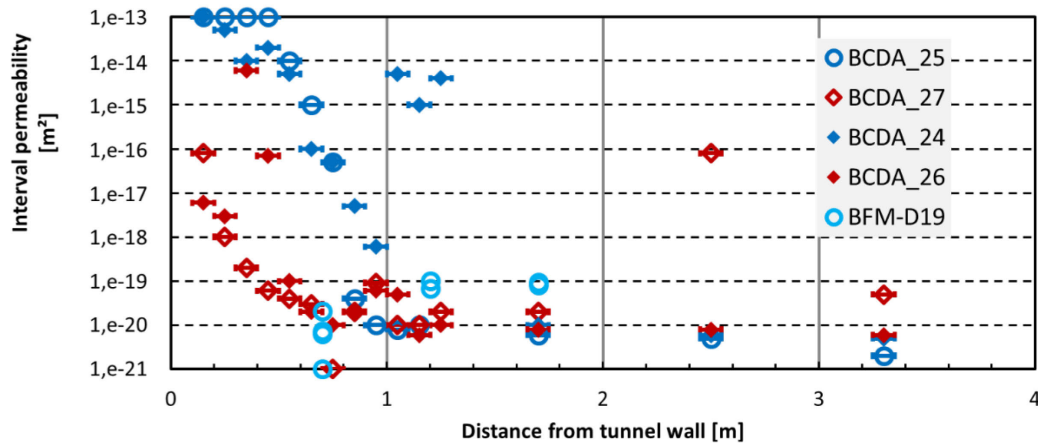


Fig. 2. Measured permeabilities in the open (blue) and closed (red) niche of the CD-A experiment (Ziefle et al. (2024), under review). Pulse tests and evapometer measurements in horizontal (contour) and vertical (filled) drilling direction indicate different conditions in the differently air conditioned niches.

Further development of the numerical model approach is combined with in-situ geophysical measurements like hydraulic pulse tests, electrical resistivity tomography (ERT), and mini-seismic (MSM) measurements, providing a detailed characterization of the Opalinus Clay (Schuster et al. 2019, Kneuker & Furche 2021). Similar investigations in the sandy facies have been carried out on a larger scale in the context of the CD-A experiment (Ziefle et al. 2024, under review). Here, geophysical characterisation of the Opalinus Clay is carried out in horizontal and vertical boreholes around two niches with a diameter of 2.3 m each, which differ only in their climatic conditions. The measured permeabilities received in the course of pulse tests are presented exemplarily in Fig. 2. They show – presumably as a consequence of the different climatic conditions - a clearly different permeability of the host rock within the first meters after 1.5 years. The geometric boundary conditions in the boreholes of the CO₂LPIE experiment differ significantly from the excavation of the twin niches. However, a borehole disturbed zone (BDZ) and also an excavation disturbed zone (EDZ) around the gallery is expected and has to be investigated and considered for modelling.

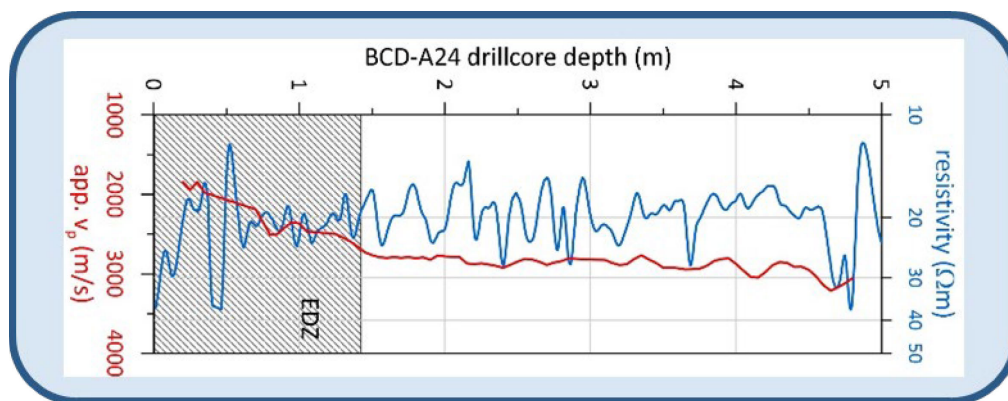


Fig. 3. Borehole measurements of the electrical resistivity in Ω, and seismic velocity in m/s as conducted in the CD-A experiment in a vertical borehole. The electrical resistivity yields information about the distribution of different sub-facies types, while the combined interpretation with the measured seismic velocity allows for statements about the extent of the EDZ.

Fig. 3 yields information about the characterization of the Opalins Clay in the near field of the CD-A twin niches, where the coupled hydraulic-mechanical behavior due to excavation and ventilation is investigated. Statements on the distribution of different sub-facies types can be made by interpreting ERT measurements. The additional interpretation of MSM data allows for statements on the extent of the EDZ. These results are the basic results of an ERT and MSM measurement. However, the extended evaluation of this data is aimed at comparing subsequent measurements with the original measured reference value. This type of evaluation emphasises temporal and spatial differences in the resistivity. These changes can indicate various physical effects: For example, a reduction in the water content as measured in the CD-A experiment (Ziefle et al. 2024) leads to a significant change in the electrical resistance as plotted in Fig. 4. The ongoing information about changes in the electrical resistivity is combined here with NMR measurements, resulting in a time-dependent moisture map. As plotted, the distribution of water content around the ventilated niche indicates the heterogeneous behaviour of near field desaturation effects. The opposite effect of an increasing water content can be seen in the SW-A experiment, investigating the ongoing saturation of a geotechnical barrier system. However, the formation of a loosened zone – potentially coming along with an increase of water content – can also be monitored by the ERT measurements. This effect is observed in the PF experiment (Ziegler et al. 2023), which investigates the progressive failure of the host rock above an excavated borehole with a diameter of 60 cm. In Fig. 5 the ratio of measured data at 03/2022 with respect to the reference measurement carried out in 12/2020 is plotted. One sees a zone (plotted in blue) with significantly lower ratios, potentially indicating a loosened zone. In the CO₂LPIE experiment, a combination of the mentioned effects is expected to arise. Therefore, monitoring the long-term temporal and spatial evolution of the resistivity forms an important source of information and basis for numerical modelling.

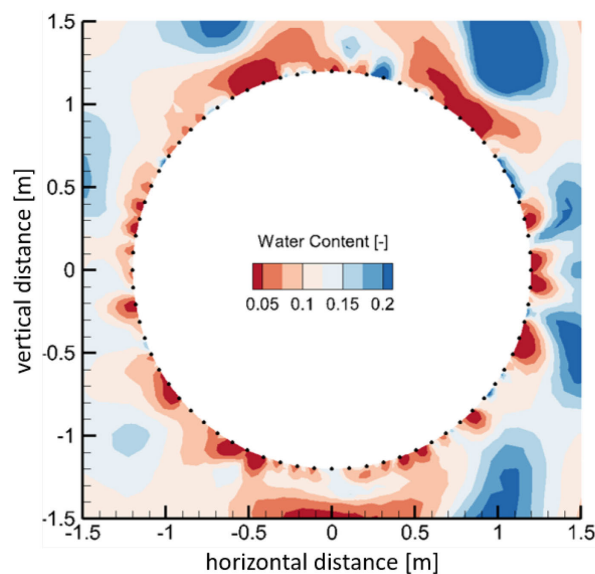


Fig. 4. Distribution of water content, measured in the CD-A experiment around the open twin. The combined interpretation of ERT and NMR measurements yields information about the heterogeneous behavior around the excavation.

Generally, the use of geophysical methods is further developed in the long-term monitoring carried out by the modular multi-sensor monitoring system (MMMS), which is implemented in the CO₂LPIE experiment. These measurements provide comprehensive insights into the long-term development of, e.g., displacements, pressure, seismic transmission, electrical resistivity and thus form the basis for numerically based statements for the design of future CO₂ disposal sites.

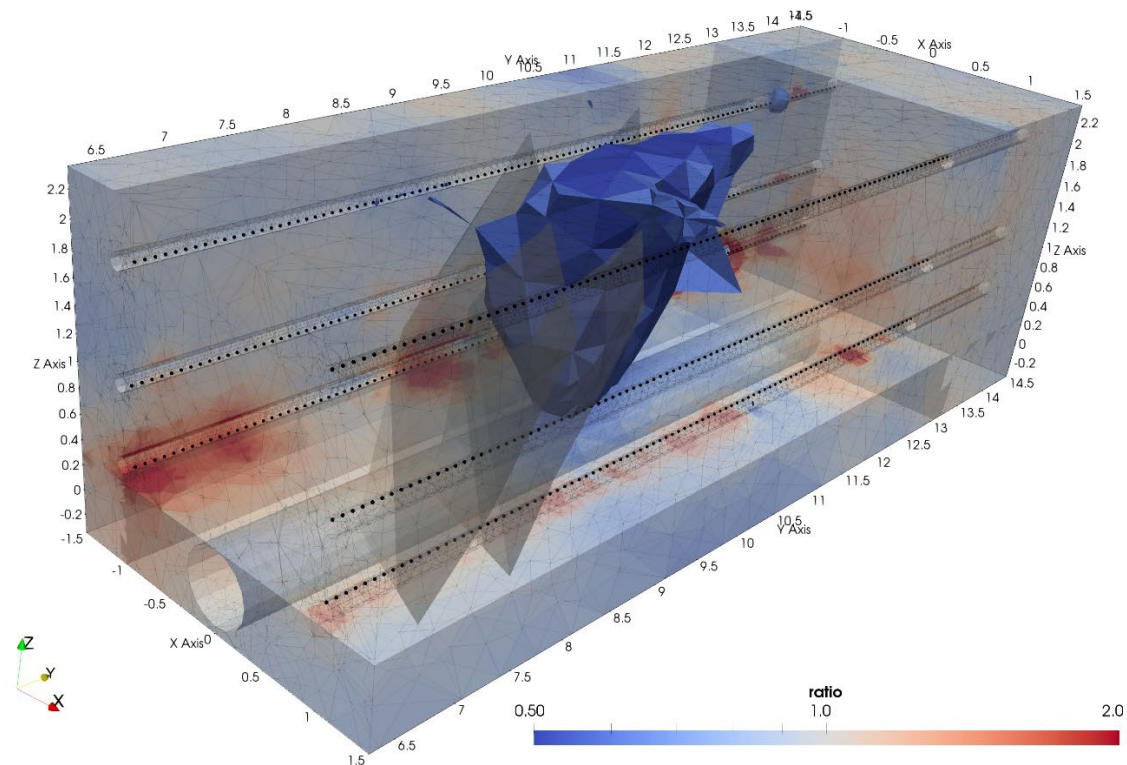


Fig. 5. Measured ratio of electrical resistivity (03/2022) with respect to reference value (12/2020) in the context of the PF experiment (Ziegler et al. 2023). Indicated are the main borehole (tube), the fault zones consisting of scaly clay (slices), the six monitoring boreholes (smaller tubes) and the positions of the ERT sensors (black dots). The resulting ratio indicates zones with higher values in the near field of the observation boreholes and an area with significantly lower ratios, potentially coming along with a loosened zone.

References

- Chen, S, Ostertag-Henning, C, Kumar, V, Shao, H, Ziefle, G, Maßmann, J: Holistic Concept for Analyzing CO₂ Reactions in Opalinus Clay, CIGSS 2024.
- Kneucker, T, Furche, M: Capturing the structural and compositional variability of Opalinus Clay: constraints from multidisciplinary investigations of Mont Terri drill cores (Switzerland), *Environm. Earth Science*, 80, 2021.
- Kumar, V, Ziefle, G, Maßmann, J.: Increasing process understanding in gas migration: investigations using the TH2M modelling approach. CIGSS 2024.
- Schuster, K, Furche, M, Shao, H, Hesser, J, Hertzsch, J-M, Gräsele, W, Rebscher, D: Understanding the evolution of nuclear waste repositories by performing appropriate experiments – selected investigations at Mont Terri rock laboratory, *Adv. Geosci*, 49, 2019.
- Maßmann, J, Thiedau, J Bittens, M, Kumar, V, Tran, TV, Guevara Morel, CR, Kneucker, T, Schumacher, S: Aktualisierung der Sicherheits-und Nachweismethodik für die HAW-Endlagerung im Tongestein in Deutschland : ANSICHT-II - Methode und Berechnungen zur Integritätsanalyse der geologischen Barriere für ein generisches Endlagersystem im Tongestein : Ergebnisbericht, Bundesanstalt für Geowissenschaften und Rohstoffe (BGR), 2022. <https://doi.org/10.25928/n8ac-y452>
- Ziefle, G, Cajuhi, T, Costabel, S, Fourrière, A, Furche, M, Gerowski, J, Kneucker, T, Maßmann, J: CD-A twin niches in the Mont Terri Rock Laboratory: Characterization and interpretation of hydraulic parameters with regard to safety aspects, accepted for RMMS, (2024).
- Ziegler, M, Furche, M, Beilecke, T, Burschil, T, Obermann, A, Lei, Q, Zhao, C, Loew, S. 2023. Monitoring damage evolution in a tectonically faulted clay shale – an experiment of the Mont Terri URL, 15th ISRM congress.

A borehole modular multi-sensor monitoring system (MMMS)

Martin Ziegler^{1*}, Tobias Fritsche² and Stefan Czerner²

¹ Federal Office of Topography, Mont Terri Underground Rock Laboratory, St. Ursanne, Switzerland

² ZHAW School of Engineering, Institute of Product Development and Production Technologies, Winterthur, Switzerland

* martin.ziegler@swisstopo.ch

Abstract

We develop a modular multi-sensor monitoring system (MMMS) for boreholes to allow for comprehensive rock mass instrumentation using a small number of boreholes. In the first version of the system, developed within the frame of the “CO₂LPIE” (CL) project and inspired by the Mont Terri PF project innovation, the MMMS was designed to combine electrical resistivity tomography, active seismic transmission tomography, acoustic emission sensing, strain, temperature, and pore pressure monitoring and improve sensor fixations in boreholes. The MMMS for the CL experiment monitoring boreholes is about 17.5 m long and allows to record baseline data as well as long-term hydromechanical and geophysical changes of the rock mass caused by cyclic CO₂-charged water injections. The fixation system as well as each sensor or group of sensors have specific requirements that the MMMS must meet. All requirements were investigated prior to the design phase, partly together with the manufacturers of individual components. Besides important sensor coupling considerations, the torsion and longitudinal stiffnesses of the fixation system were optimized for the installation into the sandy facies of the Opalinus Clay shale. Essential parts of the MMMS are produced using additive manufacturing technology. In this paper we present design details of the MMMS and test results.

1 Background

For many in-situ experiments at underground rock laboratories it is crucial to obtain datasets of high spatial and temporal resolution, especially when fluid or gas injections are monitored. Sensor location optimizations, the conditions of sensor to rock mass coupling, and potential disturbances on the target rock mass through the drilling of many monitoring boreholes must be considered. Typically, various boreholes used for different monitoring purposes surround an experimental rock mass volume and, thus, may increase drilling and logging costs, may disturb the target rock mass more compared to a smaller number of boreholes, and rock mass states are recorded at different spatial locations that may not always be comparable, e.g., in case of heterogeneous or fractured rock masses. Therefore, combining the monitoring of different state variables (such as temperature, pore pressure, strain, seismic and electrical properties) inside a single borehole may provide benefits but such systems must satisfy requirements of fundamentally different sensor types.

The idea of a modular, multi-sensor monitoring system (MMMS) originated from the Progressive Failure of Structurally-Controlled Overbreaks (PF) experiment where successful monitoring of electrical resistivity was achieved by permanently installed electrodes individually mounted on centralizing springs on the outside of borehole casings allowing for a direct contact with the rock mass (Ziegler et al. 2023). In addition, resin infill of the remaining annulus space and empty casings allow to run seismic surveys along the PF monitoring boreholes (Ziegler and Loew 2020). Based on the experiences obtained from the PF and other experiments, an MMMS was developed recently to monitor over several years the CO₂-charged brine injections into heterogeneous, sandy-facies Opalinus clay rock of the CL experiment (see Ziegler et al., #615).

2 System requirements

Prior to preliminary design studies, the requirements of the sensor fixations for the MMMS and of the sensors themselves were elaborated together with sensor manufacturers and researchers. Tab. 1 lists key requirements for our first version of the MMMS.

Tab. 1. Requirements of the MMMS (version 1)

Item	Requirement
<i>Sensor fixation</i>	<ul style="list-style-type: none"> modular system that can hold different sensors as well as electrical, hydraulic and infill lines in boreholes of 101 mm diameter (alternative 131 mm) allow for different combinations of electrodes, acoustic senders and receivers, and fiber-optic sensor cables 2-m-long modules and monitoring along 10–20 m length temperature-, humidity- and saltwater stable; resistant to corrosion high torsion-resistance but allow for radial and axial deformations to allow for strain transfer from rock formation into the borehole installation (pushing in) by drilling rig (possibility of pulling out of hole in worst case) allow for mounting a hydraulic packer for pore pressure monitoring at lower end optimization for resin infilling (volume reduction, active cooling to control polymerization temperature)
<i>Sensors</i>	<ul style="list-style-type: none"> electrodes for single- and cross-hole electrical resistivity tomography <ul style="list-style-type: none"> axial spacing of 5 cm electrically isolating, stable fixation and bedding (infill) material in contact with rock formation allowing for low contact resistances acoustic sensors and receivers for active transmission monitoring and AE recordings <ul style="list-style-type: none"> axial spacing of 0.5 to 2 m fully embedded and stabilized in the filling material considering acoustic decoupling from fixation system fiber-optical strain (and temperature) sensor cables <ul style="list-style-type: none"> along entire MMMS borehole section fully embedded and stabilized in the filling material in contact with rock formation point temperature sensors orientation sensor to survey sensor positions upon installation
<i>Filling</i>	synthetic resin with <ul style="list-style-type: none"> low viscosity, electrically and hydraulically isolating conditions long processing time (i.e., delayed polymerization) no shrinkage / crack development upon polymerization and later mechanical straining elastic behaviour similar or at least in the same order of Opalinus Clay shale low or controllable exothermal reaction and chemically stable

3 Fixation system design

Based on the system requirements (Tab. 1), and further considerations (e.g., optimizations for additive manufacturing, modular installation into boreholes), the first version MMMS design was developed and improved steadily after multiple prototype tests at ZHAW and the Mont Terri URL. Fig. 1 shows the major components and fixation system designs of the MMMS. Thermoplastic polymers, e.g., ABS and PA, in different modifications have been tested for the 50-mm-long fixation elements, and thermocycles were used to test the polymers aging behaviors to ensure that the elasticity of the spring-like centralizers meet the demands of the installation. The electrode is produced of high-grade steel (1.4404) by Powder Bed Fusion using Laser Beam on Metal (PBF-LB/M) technique. The electrodes' geometry was designed so that it develops a more areal (compared to point) contact with the borehole radius even with different deflections of the spring travel (Fig. 1; cf., Section 4).

Acoustic senders and receiver base plates are made of ABS polymer and located in recesses of the inner tubing made of fiber-glass reinforced PA polymer. To further increase the torsion resistance of the inner tubing, the module ends are interlocking and additionally stabilized with an inside socket. All components are glued to avoid any hole drilling through the tubing system that could lead to leakages. Note that an air injection line is guided down in the annulus space between inner tubing and borehole wall and connects with the inside tube for air flushing reducing the temperature of the exothermal resin polymerization reaction. This temperature control (cooling and or warming) system was developed since all resin-pretests led to too high temperatures upon polymerization and the used resin requires a minimum temperature of about 15 °C.

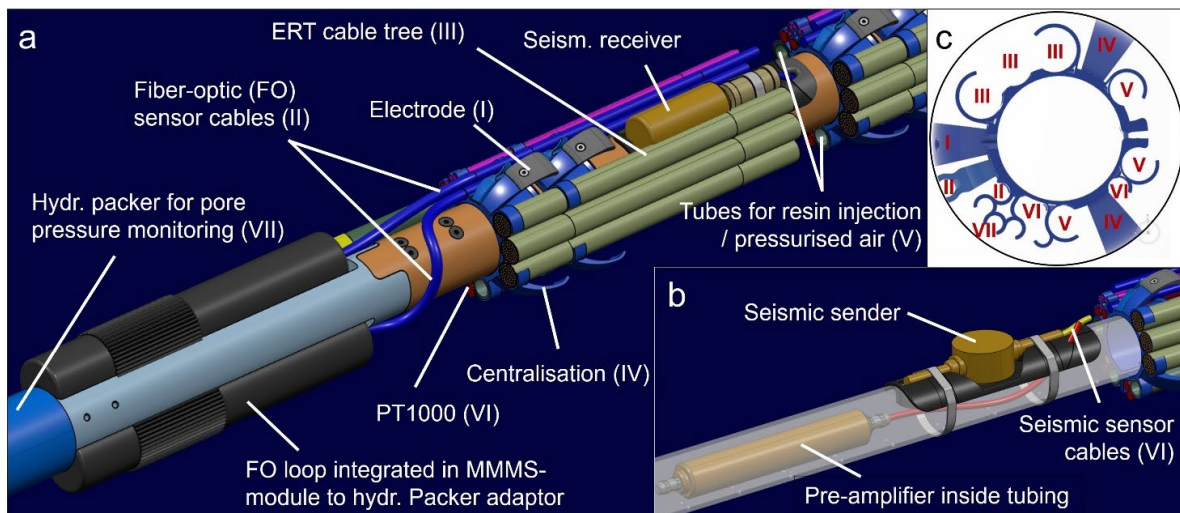


Fig. 1. Major components of the MMMS to be installed inside monitoring boreholes of the CL experiment. (a) Section of MMMS showing a part of the deepest MMMS module and adaptor to the hydraulic packer with location of fiber-optic loops. (b) Detail of a seismic sender and location of pre-amplifier inside the tubing. (c) Cross-section of a single fixation made of PA (length 50 mm), centralized in 101 mm diameter boreholes.

4 In-situ pre-test

After resin selection and tests, we installed MMMSs on November 27th, 2023, in the so-called CL pre-test boreholes BCL-3 and BCL-4, slightly outside the CL niche (Fig. 2). Resin injection of BCL-4 was carried out on November 29th, 2023 (note that BCL-3 is not yet filled with resin at the time of writing). The boreholes of 101 mm diameter were drilled between September 15th and 19th, 2023, to a depth of 3.92 m (BCL-3) and 4.10 m (BCL-4). Only one tectonic fault plane was found by core logging at about 1.0 m depth along bore hole BCL-3.

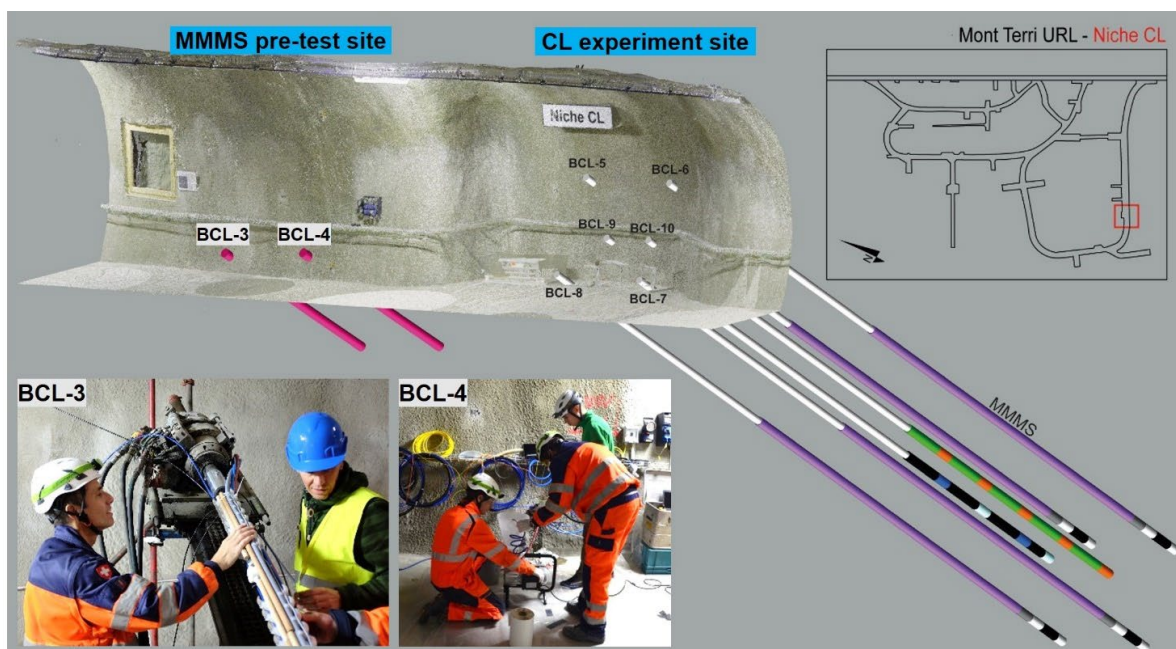


Fig. 2. Locations of the MMMS pre-test inside boreholes BCL-3 and BCL-4 and main CL experiment. The photos show the installation of an MMMS using a drill rig to gently push the system into BCL-3 and resin injection of the system inside BCL-4. The CL main experiment borehole installations are only roughly sketched here. For considerations and details of the main CL experiment borehole installations see Ziegler et al., #615.

During the pre-test of BCL-4 we monitored the temperature evolution inside the annulus space of the borehole (Fig. 3a). The air temperature inside the borehole was about 12.1 °C prior to the start of resin injection with air ventilation at 15–16 °C air temperature and 1–3 m/s air flow through the

inner tubing. The measured temperature inside the injected resin at seven locations was 16 °C at maximum so that the resin polymerization was very gentle. Electrode contact resistances increased upon resin injection and polymerization but stayed within acceptable ranges (<10 kΩ) for most electrodes (Fig. 3b). Curvature adjusted electrodes seem to perform better (electrode #1–12) than “head-shaped” electrodes (electrode #13–36). However, as the electrodes get polished and contact areas with the rock formation may improve during installation, it is yet unclear if the trend of decreasing contact resistance with depth originates from this process. Differences between single-hole ERT profiles prior and after resin injection were small (on average $-0.06 \pm 0.27 \Omega\text{m}$). In addition, FO strains (and temperatures) were recorded but are not presented here. After resin-injection into BCL-3 (planned for mid-December 2023), transmission seismic tests will be carried out.

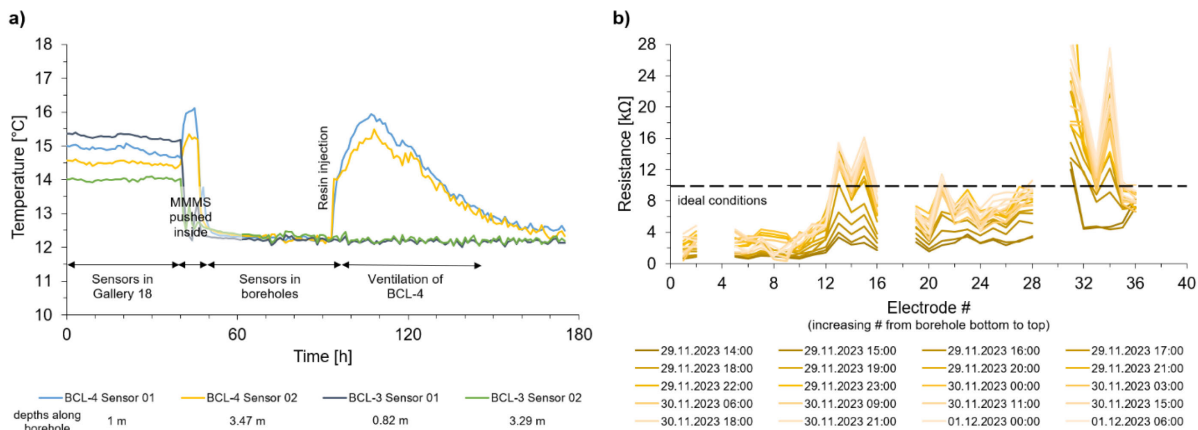


Fig. 3. (a) Monitoring of temperature evolution prior, during, and after resin polymerization showing small increasing and decreasing temperatures (figure provided by J. Windisch, swisstopo). (b) Gently increasing contact resistances of 30 electrodes inside BCL-4 upon resin injection (figure provided by M. Furche, BGR).

5 Conclusions

Within the frame of the CL experiment, we developed an innovative modular, multi-sensor fixation system for borehole monitoring (MMMS) that allows for unprecedented long-term monitoring using only a fraction of boreholes than usually required. MMMS installation and testing in two pre-test boreholes helped to fine-tune the design and proved the concept. Early considerations of sensor requirements, past experiences, several rounds of modifications and prototype tests, as well as flexible additive manufacturing played important roles in improving the MMMS design. The present system relies on a sealed annulus space to allow controlling resin polymerization temperatures inside the borehole with air flushing and to guarantee negligible thermally-induced rock mass disturbances.

Acknowledgement

We are thankful for the contributions of M. Furche (BGR), A. Eul (Eul GmbH), K. Plenkers (GmuG mbH), A. Rinaldi (SED), A. Fasciati (Solifos AG), A. Ammon (Solexperts AG), A. Grignaschi, J. Windisch, D. Jaeggi, S. Schefer, T. Theurillat (swisstopo), and D. Klimjuk (ZHAW). The CL experiment and MMMS development are financially supported by the Swiss Federal Office of Energy (SFOE), the Association of the Swiss Cement Industry (cemuisse), the Association of Swiss Waste Utilization Plant Operators (VBSA), and the German Federal Institute of Geosciences and Natural Resources (BGR).

References

- Ziegler, M., Jaeggi, D., Grignaschi, A., Kipfer, R., Rinaldi, A. 2024. CO₂LPIE: CO₂ Long-term Periodic Injection Experiment (CL). Caprock Integrity & Gas Storage Symposium, St. Ursanne, 24–25 January 2024, abstract #615.
- Ziegler, M., Loew, S. 2020. Mont Terri PF experiment: Progressive Failure of Structurally-Controlled Overbreaks - Project introduction and overview of work program. ENSI annual experience and research report, ENSI-AN-10919, 307–315.
- Ziegler, M., Furche, M., Beilecke, T., Burschil, T., Obermann, O., Lei, Q., Zhao, C., Loew, S. 2023. Monitoring damage evolution in a tectonically faulted clay shale — an experiment of the Mont Terri URL. In: Schubert, W., Kluckner, A. (eds.): Challenges in rock mechanics & rock engineering, 15th ISRM Congress 2023 & 72nd Geomechanics Colloquium, Salzburg (Austria), October 9–14, 953–958.

CO2LPIE: CO₂ Long-term Periodic Injection Experiment (CL)

Martin Ziegler^{1*}, David Jaeggi¹, Alessia Grignaschi¹, Rolf Kipfer^{2,3,4}, Antonio Pio Rinaldi⁵

¹ Federal Office of Topography, Mont Terri Underground Rock Laboratory, St. Ursanne, Switzerland

² Department of Waterresources and Drinkingwater, EAWAG, Dübendorf, Switzerland

³ Institute of Biogeochemistry and Pollutant Dynamics, ETH Zurich, Zurich, Switzerland

⁴ Institute of Geochemistry and Petrology, ETH Zurich, Zurich, Switzerland

⁵ Swiss Seismological Service, ETH Zurich, Zurich, Switzerland

* martin.ziegler@swisstopo.ch

Abstract

The CO₂ Long-term Periodic Injection Experiment (CO2LPIE or CL) investigates hydraulic, mechanical, and chemical (HMC) effects of CO₂ injection into unfractured heterogeneous and anisotropic Opalinus Clay of sandy facies under in-situ conditions at the Mont Terri underground rock laboratory. The experiment aims at enhancing our general understanding of caprock behaviour and its integrity with a focus on CO₂. Here, the insight on geochemical reactions is important due to their influence on clay rock composition and hydro-geomechanical rock properties. Experimental data on reaction rates and barrier properties with adequate accuracy are required to perform reliable reactive transport simulations as a base for storage site characterization and risk assessment of long-term storage integrity. However, as of yet, only data from small-scale (a few cm) laboratory experiments are used and realistic large scale (above the order of meters) data of the heterogeneous rock matrix are not yet available. The CL experiment will close this gap. Another key aspect of CL is its novel monitoring approach, which includes multi-sensor systems allowing for robust characterization of the test volume, baseline measurements, and high temporal and spatial resolution monitoring during the injection phase. This paper presents the in-situ experiment concept, timeline, and planned offsite works.

1 Motivation

Based on the IPCC's report on global warming, the Swiss Federal Council decided in 2019 that Switzerland will reduce its greenhouse gas emissions to net zero by 2050. This net-zero target lays the foundation for the Climate Strategy 2050, which the Federal Council adopted in 2021 and submitted to the UN Climate Change Secretariat. The aim of this strategy is to reduce the Swiss greenhouse gas emissions by 50 % by 2030, compared to 1990, and achieve net zero by 2050. The Energy Perspectives 2050+ show how these targets can be achieved and, in particular, the role of CO₂ avoidance and CO₂ removal.

Research on CO₂ has been carried out since 2010 in the Opalinus Clay shale at the Mont Terri underground rock laboratory (MT URL). With regard to CO₂, research experiments were and are carried out to explore well integrity and fault integrity. These experiments have provided important findings, e.g., measures to seal CO₂ wells (e.g., Goodman et al. 2023) and the hydromechanical conditions that can lead to gas/fluid leakage along tectonic fractures (e.g., Guglielmi et al. 2021; Zappone et al. 2021). However, seismically-identified faults will be avoided in the CO₂ storage concept and intact caprocks will be prospected. The caprock integrity has already been investigated and demonstrated on small-scale samples (e.g., Makhnenko et al., 2017), but this has yet to be demonstrated on the more realistic (i.e., heterogeneous and sandy) intermediate rock laboratory scale. The CO2LPIE (CL) experiment aims at closing this gap.

2 In-situ experiment layout and on-site works

The CL experiment will be conducted at a specific niche at the south-western corner of the MT URL. At this site, anisotropic and heterogeneous Opalinus Clay shale of the upper sandy facies will be tested geophysically and geochemically using six boreholes drilled perpendicular to bedding plane

orientation. The design foresees four monitoring boreholes (BCL-5 to BCL-8) surrounding an injection (BCL-9) and an extraction (BCL-10) well for CO₂ experiments (Fig. 1). The cross-section of the borehole array is shown in the inset of Fig. 1. The major steps of the CL experiment include:

- i. Development of modular multi-sensor monitoring system/s (MMMS; Ziegler et al., #614)
- ii. Testing and fine-tuning of the MMMS design in boreholes (BCL-3 and BCL-4; Ziegler et al., #614)
- iii. Drilling, logging, sampling, and MMMS installation in four monitoring boreholes (BCL-5 to BCL-8)
- iv. Characterization of the local rock formation and baseline monitoring
- v. Drilling, logging, sampling, and installation of CO₂ injection and extraction wells (BCL-9 and BCL-10) as well as hydraulic tests
- vi. CO₂-enriched brine injection labelled with noble gases and long-term chemical, geophysical, and hydromechanical monitoring (3+ years)
- vii. Drilling, sampling and laboratory analyses of rock samples in contact with CO₂ (via future borehole(s))

In each monitoring borehole an MMMS will be installed (Ziegler et al., #614). The four MMMS include, at the target depth range of 10–16 m along hole, about 380 electrodes for electrical resistivity tomography, 12 acoustic sender and receiver pairs for active transmission and AE monitoring, 8 fiber-optical sensor lines for strain and temperature (along 0–16 m), 20 Pt1000 temperature sensors, and four pore pressure intervals (at about 17.3–17.5 m depth).

The layout of the borehole injection and extraction (sampling) system are in discussion and the final positions of CO₂ injection intervals will be decided based on rock mass characterization results. For the injection borehole's base design, two main injection intervals centered at about 12 and 14 m (marked in blue at BCL-9 in Fig. 1) are planned. This allows to inject CO₂ into petrographically and/or hydraulically different rock masses. Furthermore, the pre-design of the injection borehole includes additional control intervals. The latter intervals will be used for pore pressure monitoring, chemical in-line indicators (pH/EC), fluid/gas sampling, or additional injections. Since the main monitoring sensors of the MMMS locate at 10–16 m depth, they embed the injection (and extraction) volume (11–15 m depth) and thus allow to define the ideal position of the injection interval(s).

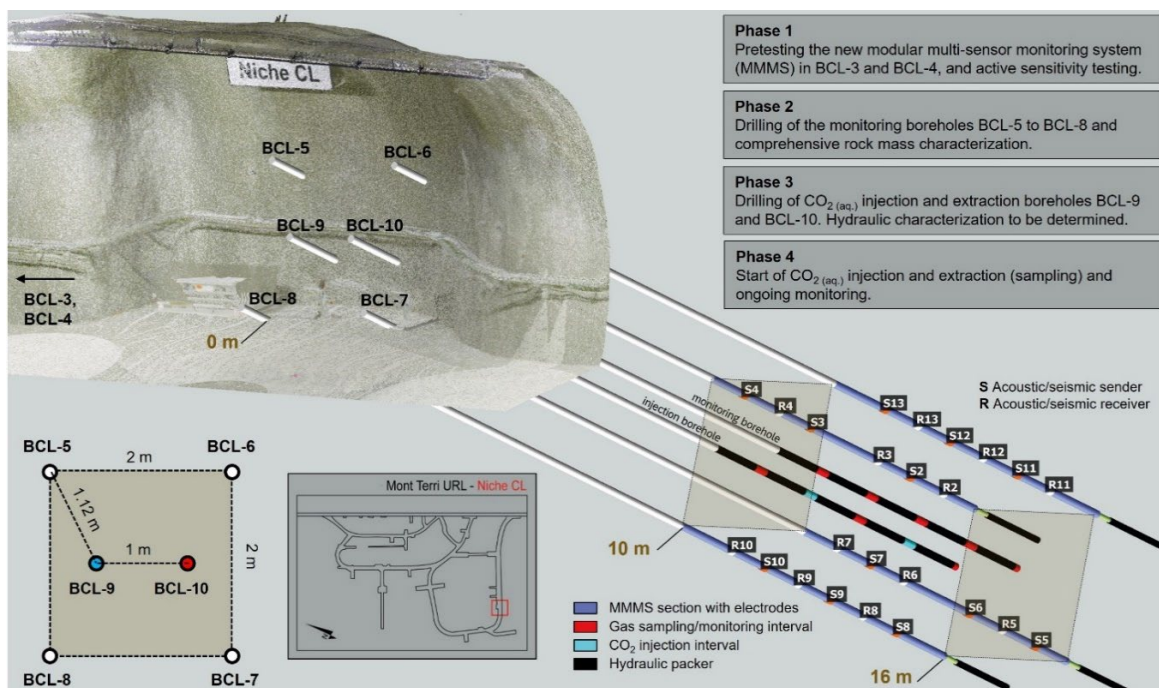


Fig. 1. Laserscan model of the CL experiment niche with the positions of the main experiment boreholes BCL-5 to BCL-10. The monitoring boreholes BCL-5 to BCL-8 with MMMS surround the injection and extraction wells, BCL-9 and BCL-10. The MMMS allows for 3D seismic and electrical resistivity tomography as well as for monitoring of strain and pore pressures in the experiment “far-field” prior and during CO₂ injection.

After filling the injection intervals with artificial pore water and an initial equilibration phase, tailored hydraulic tests will be carried out to characterize the hydraulic properties of the experiment rock mass. The hydraulic test procedure will be selected so that the CO₂ injection protocol can be refined and the rock mass will be prevented from any damage or considerable disturbances. In addition, the injection protocol for diffusion-controlled transport will be compared against results from numerical modelling and analytical results (Ma et al. 2022; Sciandra et al. 2023, submitted).

After hydraulic characterization and an equilibration phase, the actual injection test with CO₂-enriched water will take place. CO₂-enriched brine will be injected into BCL-9 following a precisely defined protocol based on the measured pressure level and magnitude and length of the planned fluid injection oscillations. A simplified sketch is shown in Fig. 2. Maximum pressures of, e.g., 3.5 MPa will be applied in order not to produce fractures (Guglielmi et al. 2021). The CO₂ will be injected dissolved in artificial pore water and labelled with Kr and with a predefined isotopic composition ($\delta^{13}\text{C}$) to be used as tracers for the injected fluid. Finally, the intervals of BCL-10 will be used for gas and hydrochemical on-site monitoring (sampling).

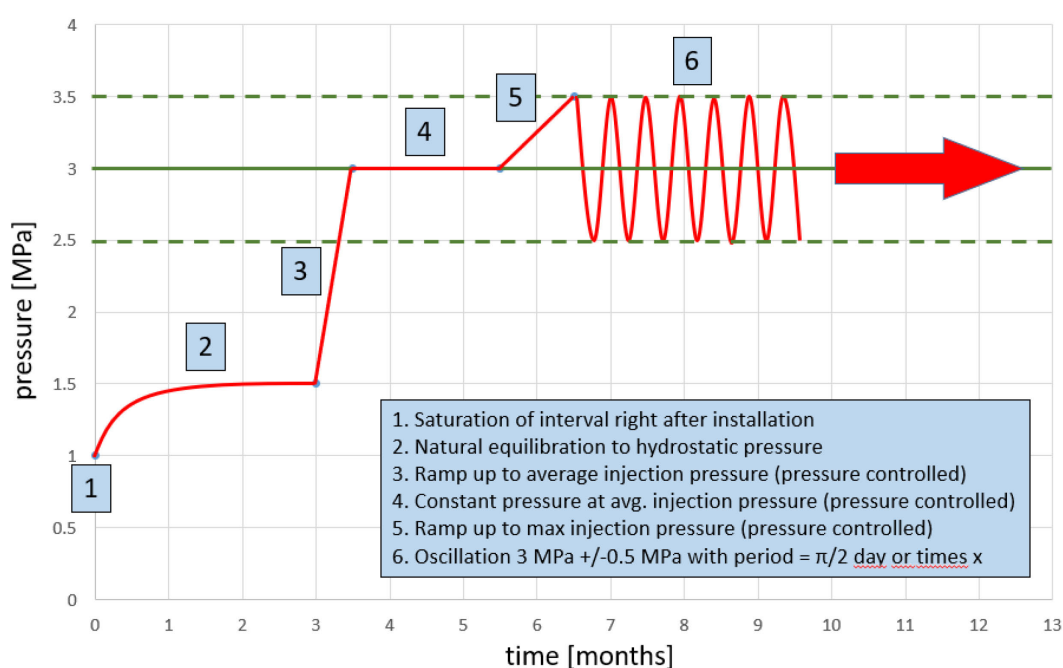


Fig. 2. CL experiment injection scheme of CO₂-enriched brine into BCL-9.

3 Overview of planned off-site works

3.1 Laboratory analyses

Rock, water, and gas samples for off-site laboratory analyses will be taken prior, during, and after CO₂ injection. The analyses will explore:

- i. Mineralogical, petrophysical, and structural rock properties
- ii. Chemistry of pore fluids (CO₂, CO₂ isotopy, water and water isotopy, noble and trace gases)
- iii. Poromechanical and CO₂ transport properties under realistic in-situ conditions

3.2 Numerical simulations

The CL project includes the in-situ experiment at Mont Terri, analytical laboratory programmes, and numerical modelling at a broad range of scales (10⁻³ to 10 m). Modelling will inform about the geochemical, mechanical, and hydraulic processes at different scales, from small-scale injections of CO₂ into core samples at controlled boundary conditions up to the experiment scale on the order of meters that includes rock mass heterogeneities. Different numerical codes (e.g., Code Bright,

PFLOTRAN, and OpenGeoSys) will be applied to study the hydromechanical and geochemical processes that are induced by the CO₂ injection (see Ma et al., Tangirala et al. and Ziefle et al., abstracts #607, #610, and #613). The following questions will be addressed:

- i. What are the mechanical and hydraulic (two-phase flow) processes to be expected during CO₂ injections?
- ii. What are the effects of changes in the process variables gas pressure, fluid pressure, stress and deformation and how do material properties such as porosity and permeability change?
- iii. What are the important in-situ transport processes and geochemical reactions caused by CO₂ injections into the Opalinus Clay shale, how fast are they, and how do these change the hydro-mechanical rock masson properties?
- iv. What is the (long-term) impact of applying different CO₂ injection protocols?
- v. What impact do rock heterogeneities and rock anisotropy have on the (T)HMC-coupled processes?
- vi. What modelling strategy is suitable to upscale the process understanding to the pilot or field scale?

4 Timeline

The CL experiment extends over four years during which five milestones will be achieved in order to complete the experiment (Fig. 3). Technical and scientific results will be discussed and documented in order to steer the complex CL experiment to success.

Steps of the CO ₂ LPIE (CL) experiment	2023		2024				2025				2026				2027	
	4/4	1/4	2/4	3/4	4/4	1/4	2/4	3/4	4/4	1/4	2/4	3/4	4/4	1/4	2/4	3/4
1. Elaboration of final experiment design	█	█	█	█	█	█	█	█	█	█	█	█	█	█	█	█
2. Modeling	█	█	█	█	█	█	█	█	█	█	█	█	█	█	█	█
3. Development of systems (MMSS)	█	█	█	█	█	█	█	█	█	█	█	█	█	█	█	█
4. Drilling of boreholes and sampling			★ M1	█	█									TBD		
5. Characterization of experimental volume																
6. Baseline monitoring																
7. Testing				★ M2	█											
8. CO ₂ brine injection					★ M3	█										
9. Lab analysis on core material													★ M4			
10. Reporting, Publications																★ M5

M1: Installation of 4 MMSS
M2: End of baseline monitoring and start of hydraulic testing
M3: Start of CO₂ injection test sequence
M4: Rock sampling in experimental zone and lab analysis
M5: End of project, synthesis reporting and start of long-term monitoring phase

Fig. 3. CL experiment time plan with detailed steps and milestones (M).

Acknowledgements

The CL experiment is financially supported by the Swiss Federal Office of Energy (SFOE), the Association of the Swiss Cement Industry (cemsuisse), the Association of Swiss Waste Utilization Plant Operators (VBSA), and the German Federal Institute of Geosciences and Natural Resources (BGR). Finally, we are grateful to the initiation of the project by Dorothee Rebscher (former BGR).

References

Goodman, H, Rösli, U, Gisiger, J, Jaeggi, D, Minnig, C. 2023. CS-A Experiment: Synthesis report of CS-A work activities Sealant test outcomes that address seepage of CO₂ behind casing. Mont Terri Technical Report TR2022-02.

Guglielmi, Y, Nussbaum, C, Cappa, F, De Barros, L, Rutqvist, J, Birkholzer, J. 2021. Field-scale fault reactivation experiments by fluid injection highlight aseismic leakage in caprock analogs: Implications for CO₂ sequestration. International Journal of Greenhouse Gas Control, Volume 111. <https://doi.org/10.1016/j.ijggc.2021.103471>

Ma, J, Wersin, P, Alt-Epping P. 2022. Scoping tests on the CL experiment. Mont Terri Technical Note TN2022-65.

Makhnenko, RY, Vilarrasa, V, Mylnikov, D, Laloui, L. 2017. Hydromechanical aspects of CO₂ breakthrough into clay-rich caprock. Energy Procedia, 114, 3282–3290.

Sciandra D, Iman R, Kivi, I, Makhnenko, RY, Rebscher, D, Vilarrasa, V. 2023 (submitted). Characterization of hydraulic rock diffusivity using oscillatory pore pressure. Manuscript submitted to Water Resources Research.

Zappone, A., Rinaldi, AP, Grab, M, Wenning, QC, Roques, C, Madonna, C, Obermann, AC, Bernasconi, SM, Brennwald, MS, Kipfer, R, Soom, F, Cook, P, Guglielmi, Y, Nussbaum, C, Giardini, D, Mazzotti, M, and Wiemer, S. 2021. Fault sealing and caprock integrity for CO₂ storage: an in-situ injection experiment, Solid Earth, 12, 319–343. <https://doi.org/10.5194/se-12-319-2021>

Distributed fibre-optic temperature monitoring in boreholes of a seasonal geothermal energy storage

Matthias Bühler^{1*}, Frank Fischli¹, Michael Iten¹, Falko Bethmann² and Andre El-Alfy²

¹ Marmota Engineering AG, Zurich, Switzerland

² Geo-Energie Suisse AG, Zurich, Switzerland

* matthias.buehler@marmota.com

1 Introduction

1.1 Seasonal geothermal energy storage “Forsthaus”

At the “Forsthaus” energy centre (EZF), the local utility company and energy provider Energie Wasser Bern (ewb) operates a waste incineration plant, a wood-fired heating plant and a gas-fired heating plant. The “Forsthaus” geothermal energy storage project aims to store waste heat of the incinerator as well as the surplus from a possible summer operation of the heating plants in the lower freshwater molasse (USM) aquifer unit at a depth of 250 to 500 metres below surface (ewb, 2023). For this purpose, hot water is circulated between a heat exchanger and the USM to heat (or cool) the sandstone lenses of the so-called “Gümmenen” strata (see Fig. 1; compare Kellerhals et al., 2000). In total, a “seasonal energy reserve” of 12 to 15 gigawatt hours is expected from the geothermal energy storage (ewb, 2023).

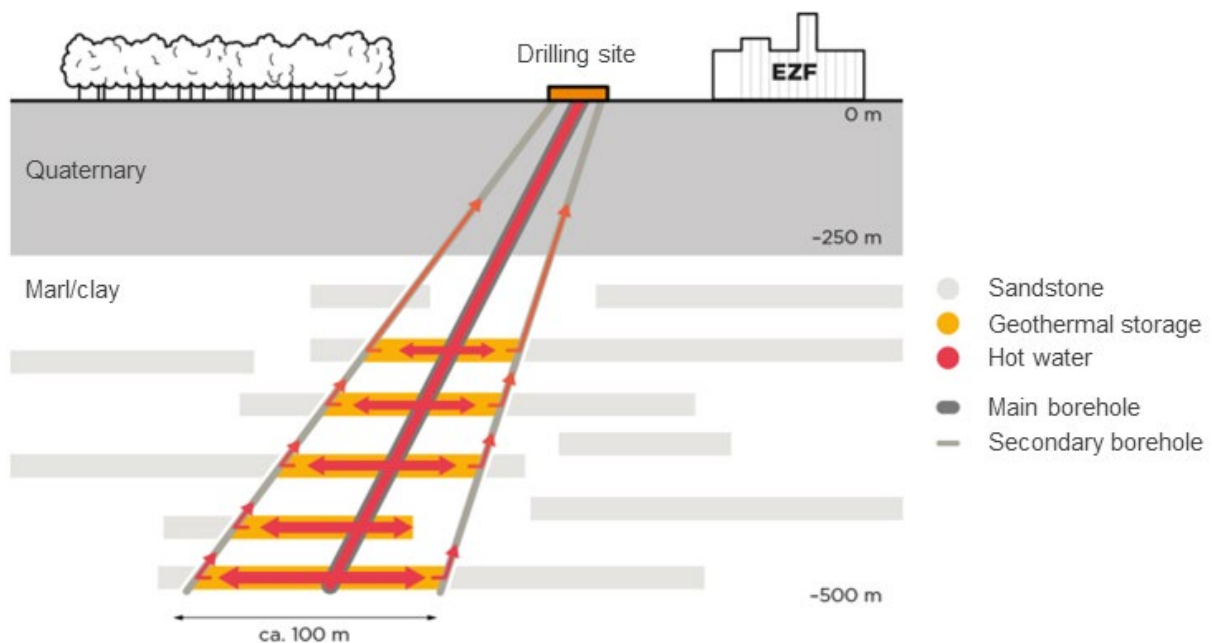


Fig. 1. Schematic of the “Forsthaus” geothermal energy storage (schematic by ewb, 2023).

1.2 Down-borehole fibre-optic temperature sensing

Monitoring the in-situ temperature is key for the characterization of the seasonal geothermal energy storage. For this purpose, a variety of different sensor types are available. When it comes to permanent monitoring of deeper and more complex geothermal systems, fibre-optic distributed temperature sensing (DTS) systems have several advantages. Installed along the casing, DTS provides temporally continuous and spatially distributed measurement data in near real-time that captures borehole temperature dynamics. The DTS system used in this project is based on the principles of Raman scattering that occurs inside the fibre core and enables to calculate the absolute temperature from the intensity ratio of the Anti-Stokes and Stokes band of the back-scattered light (Ukil et al. 2012, Shiota & Wada 1991, Dakin et al. 1985).

2 Instrumentation and measurements

2.1 Technical details of instrumentation

One inclined and two directional boreholes were drilled down to a maximum of 500 metres true vertical depth (mTVD). In all three boreholes, the 2" annulus of both, the surface casing (diameter of 16") and the production casing (10 3/4"), were instrumented with an armoured multi-fibre sensor cable that allows combined DTS, distributed acoustic sensing (DAS) and distributed strain sensing (DSS). To account for the specific requirements of the project with temperatures up to 120 °C, the original cable design was adapted by the manufacturer accordingly. The cable was installed in a loop configuration for redundancy and to allow for temperature calibration using a temperature matching approach. To cope with the single valve available at the wellhead of the pressurized system, the fibres installed along the production casings were looped using a "Mini-Loop" solution at the borehole base¹. Using specially designed spacers, the sensor was held in place to avoid destruction during the perforation of the production casing.

Unfortunately, the sensing cable was ruptured several times during the installation: At borehole GES-F-1 the casing got stuck at a depth of 228 mTVD due to geological instabilities, the sensors remained intact, though. At GES-F2 it is assumed that the curvature of the directionally drilled production casing caused the rupture of the fibre-optics (see Fig. 2). And at GES-F-3 the sensors were destroyed at multiple depths, and thus, this borehole is not further presented in this short report.

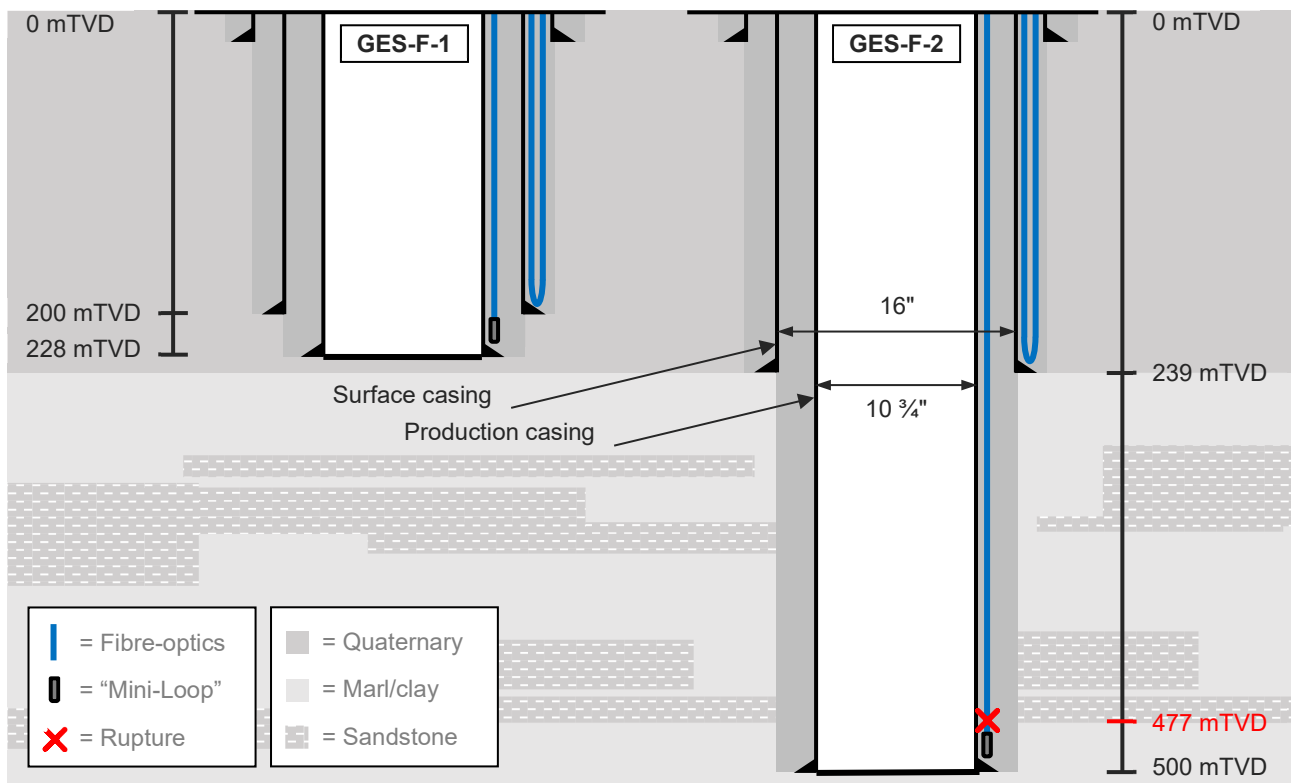


Fig. 2. Schematic of boreholes GES-F-1 and GES-F-2 with the fibre-optic instrumentation along the casings.

2.2 Distributed temperature measurements

After the installation, the fibre-optic sensors were continuously measured with a temporal average over two minutes to monitor the cementation process and the subsequent hardening of the backfill. As Raman-based temperature monitoring can be performed in a single end setup, the intact sections of the cables that got damaged during installation could still be measured.

¹ A "Mini-Loop" solution allows looping a multi-fibre cable at the borehole base where there is limited space available. Therefore, the fibres are looped in a narrow U-turn and spliced in a hermetically sealed housing with an outer diameter of approx. 2 cm only.

3 Results

Fig. 3 and Fig. 4 show the temperature profiles measured during the cementation along the cable inside the annulus of the surface casing of GES-F-1 and GES-F-2, respectively. Please note that the plotted temperature ranges of the two presented boreholes are at a different absolute level due to the varying temperatures of the injection material. This was chosen purposely to better highlight the various effects, consciously accepting a trade-off in comparability between the boreholes. After applying a temperature matching approach to calibrate the differential attenuation along the fibre, the data shows a good correlation between the two strings of the looped cables. The temperature change of a few degrees Celsius induced by the rising grout level is clearly visible in the data. Activities above ground level (e.g., flushing the wellhead) can be observed, too.

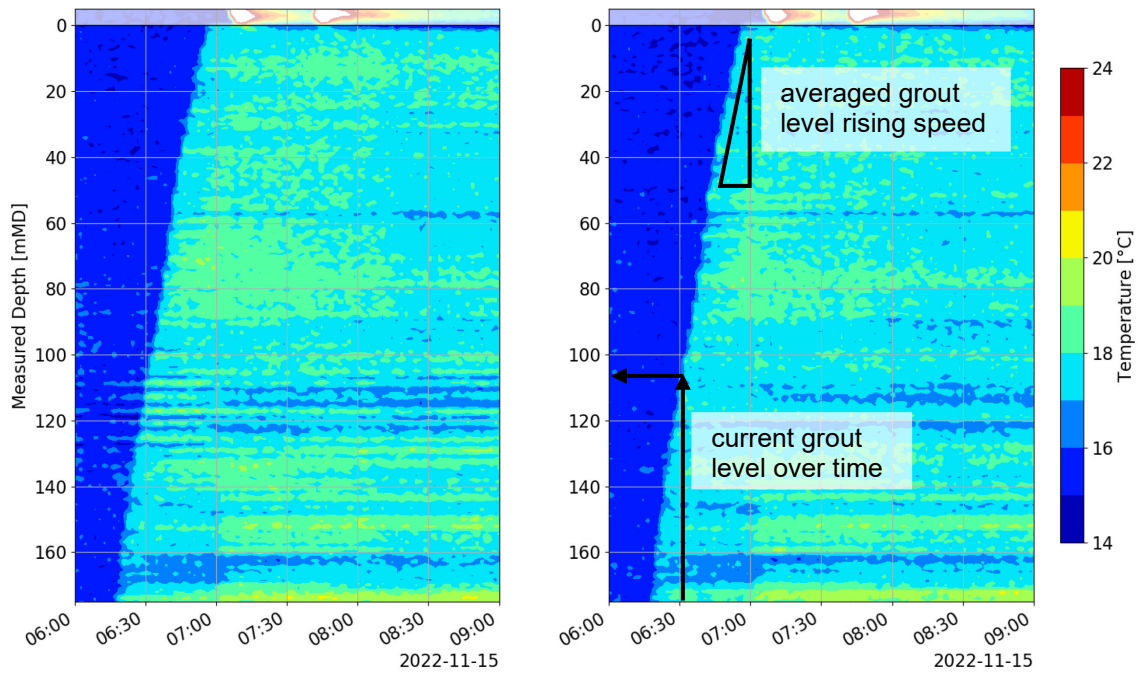


Fig. 3. Temperature measurements during cementation of the surface casing of GES-F-1 on string “A” (left) and “B” (right) of the looped fibre-optic cable.

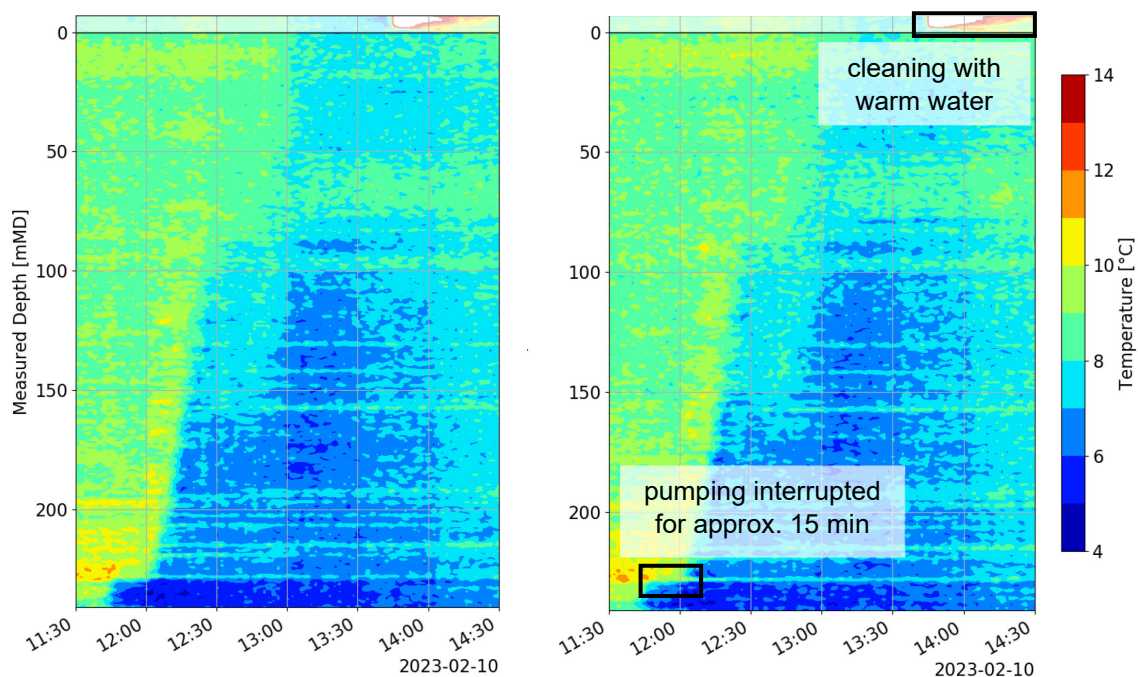


Fig. 4. Temperature measurements during cementation of the surface casing of GES-F-2 on string “A” (left) and “B” (right) of the looped fibre-optic cable.

4 Discussion

The good quality of the acquired data is proven by the congruence between the two respective strings of the looped cables as well as the high temperature resolution. Even though the temperature change induced by the backfill material is limited to a few degrees, the fibre-optic temperature measurements show a clear picture of the cementation progress. In both boreholes, GES-F-1 and GES-F-2, the rising grout level inside the annulus of the surface casing is well detectable which allows to determine the height of the cement at every instant. Short interruptions in the grouting operations are as visible as the wellhead being pressure washed with warm water from the excess cement. The high-level resolution in both spatial and temporal domain combined with the availability of the acquired data in near real-time allows to monitor the cementation process in detail.

Protecting the fibres posed a major challenge in this project. Despite the several cable reinforcement layers and the spacers specially designed to hold the wires as close to the casings as possible, the cables got crushed repeatedly at a similar depth assumingly due to the curvatures of the directionally drilled boreholes. Thus, the concept of protecting of the sensitive fibre-optic sensor cables will have to be revised for possible additional boreholes in the “Forsthaus” geothermal energy storage project considering the enormous forces acting on the inclined casings of this size.

5 Conclusions

The continuous temperature data acquired during cementation of the casings showcases the ability of DTS systems to track small temperature changes in near real-time. During the cementation process, the displacement of the drilling fluid (see Fig. 3 and Fig. 4) and the setting of the cement (not shown in the course of this short report) were captured with distributed temperature measurements. The DTS data was valuable to estimate the depth and setting speed of two different cement compositions. In future, the monitoring system will be used to acquire spatiotemporal temperature data during stimulation treatments and operations of the seasonal geothermal energy storage.

The authors believe that the experience made with this fibre-optic monitoring system can be transferred to geological gas storage applications and in this context provide information for the caprock integrity analysis and risk assessment with the fibre-optic monitoring system providing temperature, strain and acoustic data from a single cable that requires minimal space.

References

- Dakin, JP, Pratt, DJ, Bibby, GW, Ross, JN, 1985. Distributed optical fiber Raman temperature sensor using a semiconductor light source and detector. *Electron. Lett.* 21, 569–570. <https://doi.org/10.1049/el:19850402>
- Energie Wasser Bern, visited on 29.11.2023. Geospeicher: Wärme für den Winter speichern. <https://www.ewb.ch/ueber-uns/unternehmen/kraftwerke/geospeicher.php>
- Kellerhals, P, Haefeli, C, Staeger, D, 2000, Bern (LK 1166): Erläuterungen von A. Isler, Geological Atlas of Switzerland, Federal Office for Water and Geology.
- Shiota, T, Wada, T, 1991. Distributed temperature sensors for single mode fibers. *Proc. SPIE* 1586, 13–18. <https://doi.org/10.1049/el:19850402>
- Ukil, A, Braendle, H, Krippner, P, 2012. Distributed Temperature Sensing: Review of Technology and Applications. *IEEE Sens. J.* 12, 885–892. <https://doi.org/10.1109/JSEN.2011.2162060>

Modelling of factors affecting fault stability

Pierre Cerasi^{1*}, Xiyang Xie² and Anna Stroisz¹

¹ SINTEF Industry, Dept of Applied Geoscience, Trondheim, Norway

² IKM Consultants, Bergen, Norway

* pierre.cerasi@sintef.no

1 Introduction

Faults can be introduced as discontinuities in subsurface models or more explicitly given an internal structure (central core, fractured zones) or as an upscaled homogeneous layer (Fredman et al. 2007). Concepts such as shale gouge ratio (SGR) tune the mechanical and petrophysical properties of the fault (Bjørnarå et al. 2021). The detailed topology of the fault and its surroundings will however be very dependent on the history of deformation that has taken place (e.g., Fig. 1). This in turn will depend on the local and basin-scale stress field, as well as the properties of the different lithologies, including their anisotropy. In fact, the same rock stratum can have differing properties on either side of a fault, or near the fault or deformation bands (A. Varella, pers. comm.). Also, the full 3D structure of the fault has an effect on its activation, which might be different than apparent on a 2D surface cut, as on a visible outcrop (A. Zanella, pers. comm.). In this paper, we review the modelling approaches performed in the last few years at SINTEF, looking at a very simplified geometry with two horizontal sandstone layers at different depths, connected by a bounding fault (Fig. 2). An attempt is made to give structure to the fault by including a process zone (Vilarrasa et al. 2016). The simplest way is to upscale fault core and process zone into one homogeneous layer, assigning it an intact permeability between that of the sandstone layers and the assumed uniform shale elsewhere. SINTEF's in-house Modified Discrete Element tool explores fault reactivation and associated fracturing in the process zone. Coupled with the MRST reservoir simulator, it allows for calculating permeability changes along the fault for different stress hysteresis scenarios, related to injection in a reservoir, with or without prior depletion (Rongved & Cerasi, 2019).

An upscaling is proposed using the explicit finite volume program FLAC3D, where the fault is treated as a homogeneous zone (albeit with given thickness). It is weaker than surrounding shaley formations and given similarly low intact permeability. Upon failure, the permeability is either increased by several orders of magnitude or left unchanged. The finite volume simulations also investigate the role of the process zone width on failure extent, together with the introduction of a layered structure, containing a central core (Xie et al. 2023). Finally, healing of fractures is looked at thanks to shale caprock creep and weakening when exposed to CO₂-brine. The COMSOL Multiphysics software is used to simulate creep vs. fracture opening pressure.



Fig. 1. Photograph of faults in a road cut in the Neuquén province, Argentina (photograph by P. Cerasi).

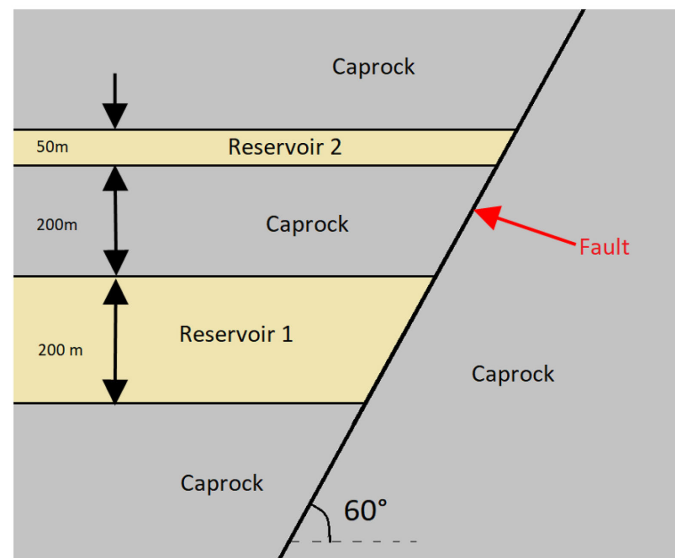


Fig. 2. Idealised case study where a fault potentially connects deeper to shallower sandstone reservoirs.

2 Modelling results

Using SINTEF's MDEM fracturing tool, several simulations were carried out with the geometry given in Fig. 2. The two sandstone reservoirs were assumed to have similar properties, while all the other areas except the fault and its process zone around it were assumed to be shaley with nano-Darcy permeability. Typical values for the petrophysical and mechanical properties were assigned to all regions in the simulation domain, from the Norwegian Continental Shelf, with a variation in permeability for the fault area (including a 20 m wide process zone around it, not shown in the sketch), from equal to the shale's low permeability to in-between shale and sandstone. Although the tool is coupled to a reservoir simulator, TOUGH2 or SINTEF's MRST tool, to save computation time on repeat runs, the pore pressure in the deeper reservoir was changed uniformly across its entirety in steps, rather than simulating injection or production. Comparison of results in terms of stress changes near the fault showed that due to the high contrast in original permeability between fault and reservoir, the changes were similar at the end of each step, compared to injection until the same pore pressure was achieved. This, provided the step change was sufficiently small. Several different scenarios were investigated:

1. Depletion from hydrostatic pore pressure in the lower reservoir;
2. Injection from hydrostatic pore pressure in the lower reservoir;
3. Depletion followed by injection in the lower reservoir;
4. The same as step 3, but in the presence of cross-shaped existing fractures (predefined in the model) in the process zone (no fault core).

Results show that different fracture propagation occurs for the case where the reservoir is on the hanging wall of the fault, versus the footwall. Propagation occurs towards shallower layers for the hanging wall, while towards deeper layers for the footwall. The stress history shows that more fracturing is seen during the depletion of the reservoir than for the inflation phase. Mostly, shear fracturing is recorded, and natural fractures tend to "attract" induced fractures (new fractures connect to the existing ones and propagate further from them at the other end). An arbitrary multiplier was assigned to fault permeability for simplicity, although the code is capable of using a more sophisticated model for calculating permeability based on cubic law for tensile opening and a shear strain-dependent law for shear fracturing. For more details, please see Rongved & Cerasi (2019) and Cardon & Cerasi (2021).

Flac3D simulations were performed to benchmark a commercial Finite Volume software against the in-house MDEM tool, using the same simple 2D geometry. Here, the injection or depletion of the

reservoir is simulated without uniformly changing the pressure. An initial permeability for the up-scaled fault elements was taken to be similar to the shale surroundings, while they were weaker in strength than the shale. Plastic yielding of the fault elements resulted either in unaltered permeability or in arbitrarily larger permeability. A simple Mohr-Coulomb model was used where shear failure of elements is monitored in the domain. Shale, sandstone and fault elements have each their assigned properties (stiffness, cohesion, shear and tensile strength, friction and dilation angles). Results show the same footwall vs. hanging wall behaviour as observed with the SINTEF MDEM tool. Again, failure propagation along the fault towards shallower layers occurs primarily upon depletion of the hanging wall reservoir (Fig. 3). Repeat simulations looked at increasing the fault thickness from 1 to 200 m (Torabi et al. 2020) and adding a low-permeability core. For large faults, the yielding of elements confirmed yet again the footwall/hanging wall propagation direction, whereas for direct injection the picture was less clearcut. For more details, see Xie & Cerasi (2021) and Xie et al. (2023).

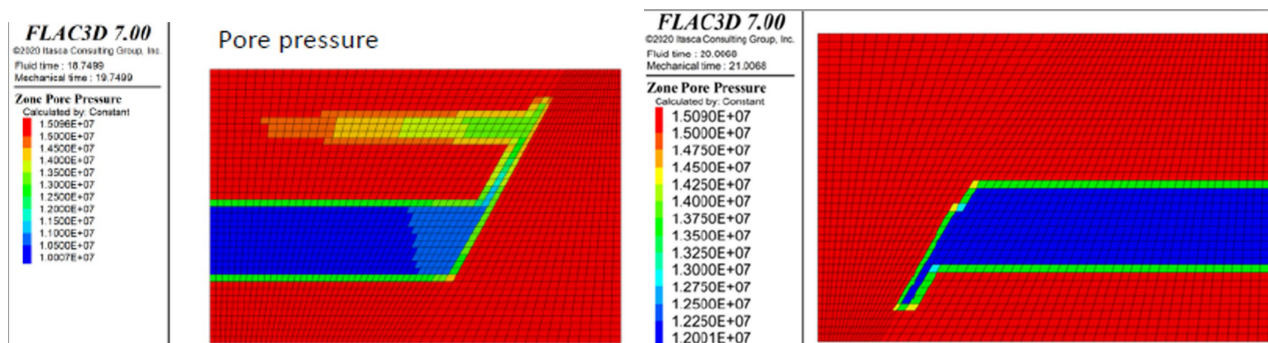


Fig. 3. Pore pressure results for depleting and reinjecting in the lower reservoir, for hanging wall (left) vs. footwall (right).

Another modelling attempt, still in progress, is made at considering long-term deformation at constant stress of a shale, either around a well or in the presence of a fracture, i.e., creep deformation. The purpose of this is to look at the potential of the creep deformation "healing" the shale, or microannulus between well cement and the shale (see Xie et al. 2021), vs. the fluid pressure in the crack keeping it open. A creep model was calibrated using laboratory testing with exposure of shale to CO₂; a time-dependent stiffness was fitted from the laboratory results (Xie et al. 2021). Use is made of the commercial COMSOL Multiphysics FEM tool in the ongoing effort. Initial results (Fig. 4) show how healing occurs after 300 years below a threshold fluid pressure in the crack element (special feature in COMSOL, whereby the opening or closure of a pre-defined crack can be monitored), or for a monotonically reducing crack pressure, mimicking expected overall pressure relaxation after injection stop for a large saline aquifer (Fig. 5).

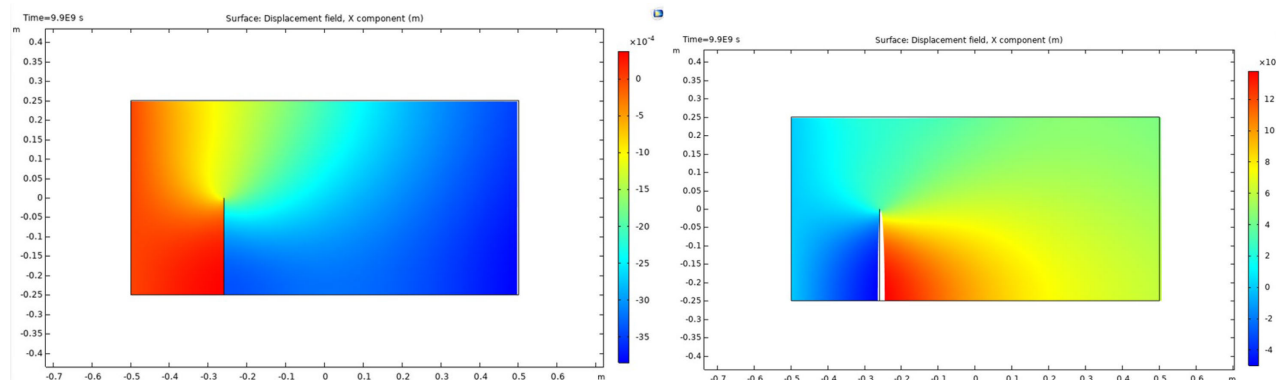


Fig. 4. Horizontal displacement maps for low fluid fracture pressure (left) and high pressure (right). Notice opening tendency for the high pressure case.

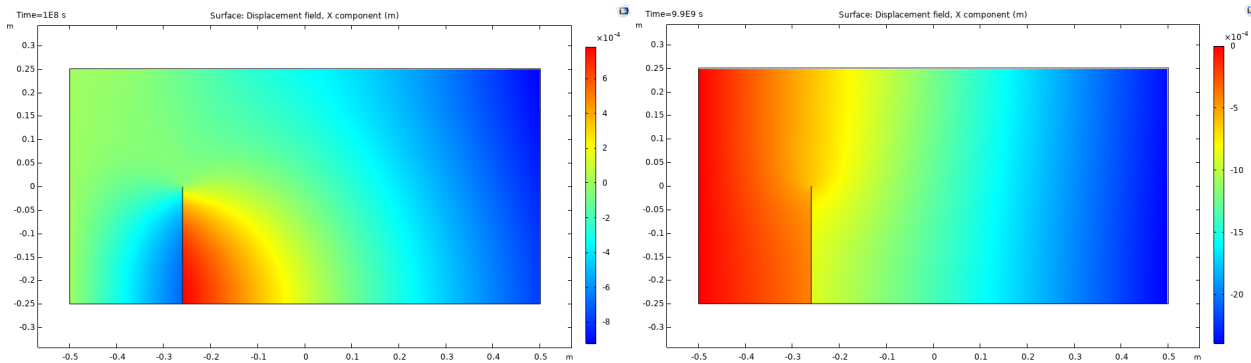


Fig. 5. Horizontal displacement maps for decreasing fluid fracture pressure (left: $t=0$; right: $t=300$ years).

3 Concluding remarks

Simplified models are explored, looking at permeability increase accompanying fault reactivation. This is a step away from models where faults are represented as simple discontinuities. However, introducing more detailed features should agree with geological observations, e.g., type of faulting, presence of repeated sequences of different lithologies in deformation bands, etc. The approach in the different simulations undertaken here is to upscale enough where detailed information is lacking, but without losing the effect of finite fault zone thickness. The results showcase depletion as a main mechanism for shear failure creating potential leakage paths, such as suggesting caution in the case of storing CO_2 in very depleted reservoirs, as opposed to large saline aquifers. A strengthening of confidence in these results is that they are corroborated by different modelling techniques. It is natural to suggest that fractures existing or created in fault process zones or more generally in the caprock may heal or remain open on the long term. More detailed modeling is now required for different cases, with emphasis on 3D features that may challenge the results presented here, such as geometry changes perpendicular to the plane featured in the present 2D simulations. However, for demonstration of principle in fault and fracture behaviour in the mechanical domain, the simplifications performed in the present work seem justified.

4 Acknowledgement

This publication has been produced with support from the NCCS Research Centre, performed under the Norwegian research programme Centre for Environment-friendly Energy Research (FME), the participating industry partners and the Research Council of Norway (257579/E20).

References

- Bjørnarå TI, Haines EM, Skurtveit E. Upscaled geocellular flow model of potential across-and along-fault leakage using shale gouge ratio. InTCCS-11. CO_2 Capture, Transport and Storage. Trondheim 22nd–23rd June 2021. Short Papers from the 11th International Trondheim CCS Conference 2021. SINTEF Academic Press.
- Cardon C, Cerasi P. Fracture propagation along a fault – stress hysteresis effect. Presentation at XXV ICTAM 2020+1 online conference. IUTAM – International Union of Theoretical and Applied Mechanics, 2021.
- Fredman N, Tveranger J, Semshaug S, Braathen A, Sverdrup E. Sensitivity of fluid flow to fault core architecture and petrophysical properties of fault rocks in siliciclastic reservoirs: a synthetic fault model study. *Petroleum Geoscience*. 2007 Nov 1;13(4):305–20.
- Vilarrasa V, Makhnenko R, Gheibi S. Geomechanical analysis of the influence of CO_2 injection location on fault stability. *Journal of Rock Mechanics and Geotechnical Engineering*. 2016 Dec 1;8(6):805–18.
- Rongved M, Cerasi P. Simulation of stress hysteresis effect on permeability increase risk along a fault. *Energies*. 2019 Sep 7;12(18):3458.
- Torabi A, Ellingsen TSS, Johannessen MU, et al. (2020) Fault zone architecture and its scaling laws: where does the damage zone start and stop? Geological Society, London, Special Publications 496:99–124. <https://doi.org/10.1144/SP496-2018-151>
- Xie X, Cerasi P. Impact of a fault on CO_2 reservoir integrity under depletion. In ARMA US Rock Mechanics/Geomechanics Symposium 2021 Jun 18 (pp. ARMA-2021).
- Xie X, Cerasi P, Stroisz A. Reuse a depleted reservoir as a storage site: How may reactivation of a sealing fault affect the storage site's integrity? In ARMA US Rock Mechanics/Geomechanics Symposium 2023 Jun 25 (pp. ARMA-2023).
- Xie X, Edvardsen L, Cerasi P. CO_2 -induced creep on Draupne shale and impact on cemented wellbore integrity. In ARMA US Rock Mechanics/Geomechanics Symposium 2021 Jun 18 (pp. ARMA-2021).

Well integrity monitoring for large-scale CO₂ storage: the LEGACY project

Bastien Dupuy^{1*}, Michael Jordan¹, TJ Ulich^{2,3}, Harvey Goodman^{2,5}, Andrew Delorey², Robert Guyer⁴ and Benjamin Emmel¹

¹ SINTEF, Norway

² Los Alamos National Laboratory, USA

³ Texas A&M, USA

⁴ University of Nevada/Reno, USA

⁵ Goodman Geomechanics LLC, USA

* bastien.dupuy@sintef.no

1 Introduction

Legacy wells are one of the main threats for deployment of large-scale CO₂ and energy storage because, together with geological faults, they constitute one of the main possible leakage paths of injected fluids through the overburden towards the surface. Fig. 1 shows an example of distribution of legacy wells in the shutdown Frigg field offshore Norway where the CO₂ migration will likely reach several of these wells. Potential leakage paths in the well elements are also described. The LEGACY project aims to overcome three main hurdles for CO₂ storage in regions with legacy wells: Assessing the risks and potential leakage rate for each individual legacy well (1), Monitoring and mitigating identified risks efficiently (2), and Enabling use of both legacy and future wells for monitoring for operational and long-term safety (3). The methods, workflows, and tools to be developed will be essential for rapid and reliable assessment, maturation, and later management of a CO₂ storage site in the vast number of locations with legacy wells. Earlier work performed at Mont Terri by the CS-A experiment for CO₂ injection well leakage mitigation, discovered complex near wellbore damage that extended to the outer cement sheath-formation host rock interface. At present, there is no cased hole logging technology available to characterize this complexity quantitatively, i.e., to assess component elastic properties and stiffness, nor to quantify and map damage of the cement sheath itself.

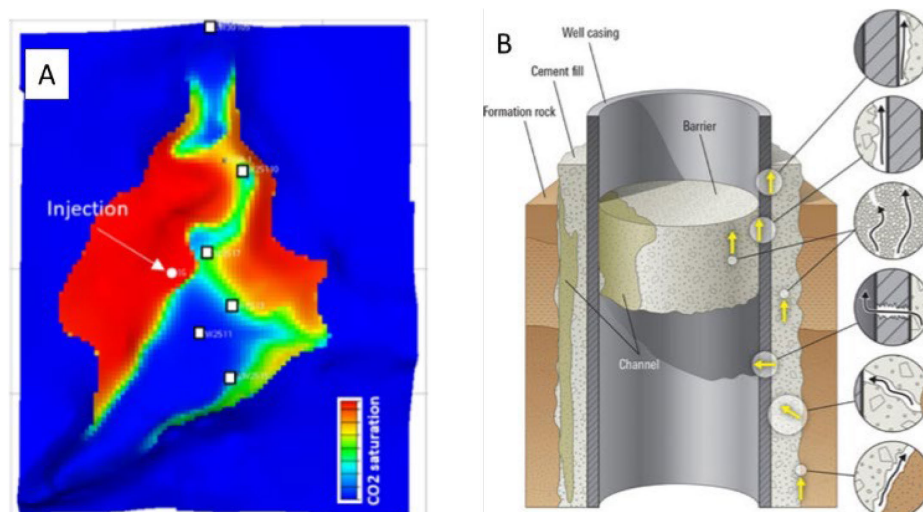


Fig. 1. (A) Reservoir model showing CO₂ migration at Frigg field (Romdhane et al., 2022). White boxes indicate locations of legacy wells and white dot shows the injection location. (B) Description of the different leakage paths between and across well elements (Figure from Gasda et al., 2004).

2 LEGACY project background

The LEGACY project is a newly funded project by the Clean Energy Transition Partnership, Call Module: TRI3 CCU/CCS technologies with support from industry partners. The primary objective of

the LEGACY project is to develop tools and technologies for screening, modelling, monitoring, and mitigation of well integrity issues and leakage, thereby enabling safe and cost-efficient, large-scale storage of CO₂ in areas with legacy wells. The LEGACY project is divided into one administrative and five technical work packages (WPs), as shown in Fig. 2. WP1 develops workflows and tools for rapid and reliable screening of wells and potential well integrity problems. WP2 involves empirical assessment of mechanical field integrity using experimental methods to be tested at Mt Terri. This work is closely linked to the work in WP3 where a framework for leakage modelling is developed, allowing for estimation of potential leakage rates from legacy wells. Options for mitigative actions are developed and evaluated in WP4. WP5 has a lower TRL than the rest of the project with studies of how legacy wells can be an asset and used for improved monitoring of a CO₂ storage site. This WP also contributes by studying and formulating recommendations for future construction and abandonment of wells in such a way that they are more easily monitored.

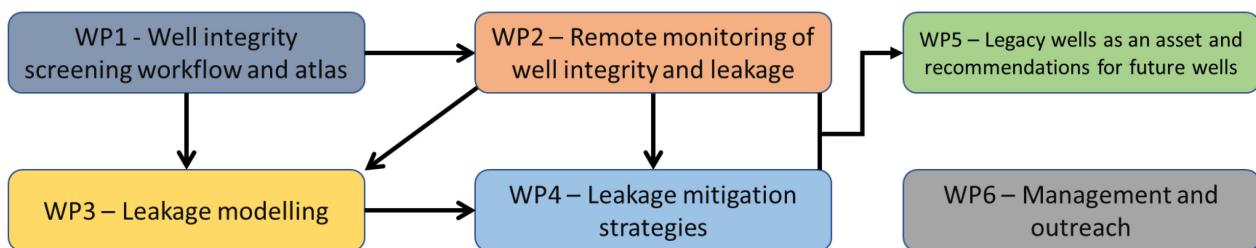


Fig. 2. Work packages and their dependencies in the LEGACY project.

3 Mont Terri experiment

An experiment at Mont Terri will be carried out as part of LEGACY project WP4. There is a near field and a far field component to the empirical studies to be carried out at Mt Terri. The near field component, 1cm to 100cm from borehole, employs time reversal (TR) signal manipulation methods. The far field component, beyond 100cm, employs passive noise methods to find a set of Green functions. The target of both components is information about the local elastic properties, both linear and non-linear. As example in the case of TR experiments the near borehole region is the volume adjacent to the detector (near the d in Fig. 3).

The time reversal (TR) process involves two steps: the forward propagation step, also known as the training step; and the back-propagation step, the focusing step. The training step, described here (to be repeated for each source independently), is

- Broadcast training signal $S(t)$, (i.e., chirp) from source n ($n = 1 \cdot \cdot \cdot N$). All other sources are inactive.
- Record response, $R_n(t)$ at the receiver location, receiver d in Fig. 3. Recorded signal length will be 1-4 times that of the source chirp.
- Compute the impulse response from source n to the receiver d using the cross-correlation of the source signal $S(t)$, and the received signal, $R_n(t)$. This impulse response is called $A(n,t)$.
- Repeat the above 3 steps each n and save all $A(n,t)$ for the focusing step.

The focusing step, described here, (has all sources synchronized and activated simultaneously):

- Time reverse each $A(n,t) \rightarrow TA(n,t)$ (see Fig. 3) and broadcast from the respective source n . Importantly, all $TA(n,t)$ are broadcast from their respective sources simultaneously. Source amplitude (i.e., amplifier gain) will be V and depends upon equipment, signal amplitudes, etc.
- Record TR focused signal $FV(t)$ at location d , i.e., using the original receiver.
- Repeat two steps above for various amplifier gains (i.e., source amplitudes), e.g., $2*V$, $4*V$, $6*V$, $8*V$ and $10*V$ (preferably with 1 to 2 orders of magnitude change in relative broadcast amplitudes).

- The desired information about the elastic properties of the near borehole region resides in the time structure of the focused signal measured at d . The inverse problem, interpreting this signal, is an important part of the TR scheme.

In the borehole far field (1-10m), we will use the same physics to probe the formation away from the borehole. We will calculate Green Functions using sensors in the injection borehole, nearby observation wells, and on the surface using both artificial and natural noise (Fig. 4). The Green function for an elastic wave, $G(x_1t_1|x_2t_2)$, describes the propagation of the elastic wave from x_1 at t_1 to x_2 at t_2 . The Green function contains information about the nature of the elastic system encountered during propagation of the wave from point 1 to point 2. The Green function describes the propagation of a displacement vector field. An x -displacement may be launched from 1 and a y -displacement detected at 2. The Green function can be a very sophisticated probe of the domain traversed.

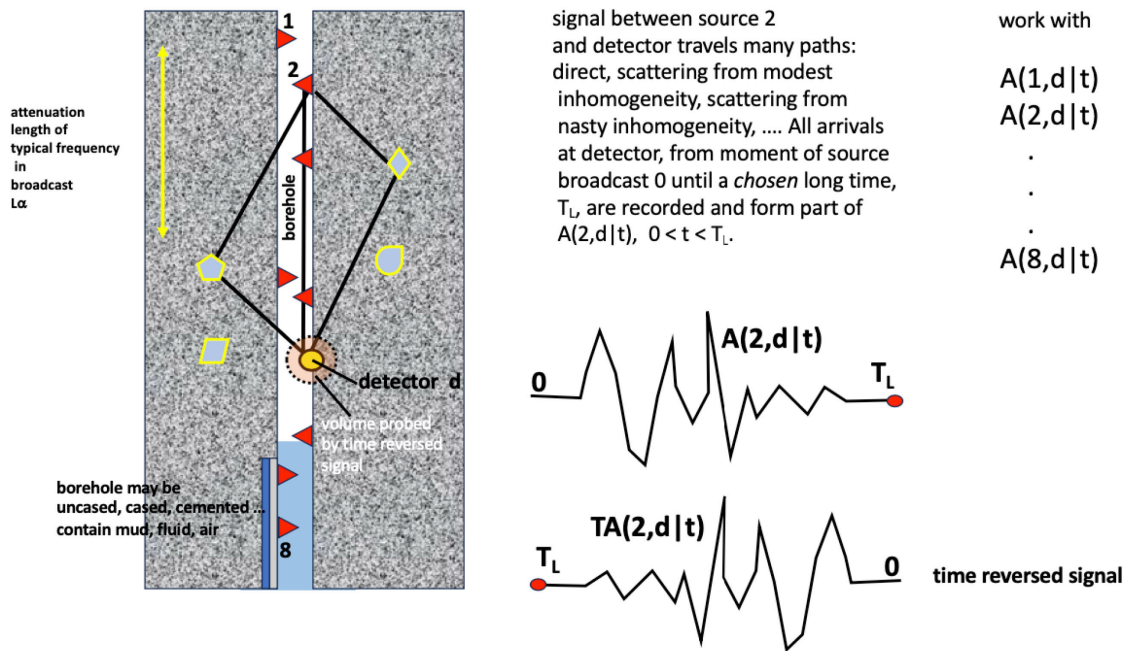
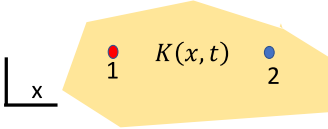


Fig. 3. Well centric near borehole region measurements. The red triangles represent seismic sources and the orange circle represents a detector. Waves generated by the sources take many paths to the detector. Three possible paths are indicated by black lines showing one direct path and two paths that bounce off scatterers.

At a set of sensor sites (on a lattice in $D=2$ to have an explicit example), the Green functions between near neighbor site pairs are determined. For site $(i,j) \rightarrow \alpha$ and site $(m,n) \rightarrow \beta$ the Green function comprises the numbers

$$G_{\alpha\beta}^{\nu}(\omega_{\gamma}) = G_{\alpha\beta}^{\nu\gamma}, \quad \nu = (x,x), (x,y), (y,x), (y,y), \quad (1)$$

where ω_{γ} is a frequency range between ω_1 and ω_M , the range being used to specify the Green function. Empirical Green functions are formed between sensor pairs. A local distortion of the elastic space will change the local Green functions giving a signature of the distortion proportional to $\delta\epsilon$ on each Green function bond (see Fig. 5). Green Functions describe the elasticity of the formation within the sensor array. We can monitor the elastic response to injection activities and to natural and artificial strain cycles over time and space and therefore detect any changes related to fracture and fluid behavior.

$$\frac{\partial^2}{\partial t^2} G(1|2) - \frac{\partial}{\partial x} \left(K(x, t) \frac{\partial}{\partial x} G(1|2) \right) = 0$$


elastic constant of domain through which propagation occurs; for porous media K depends on matrix, porosity, saturation, etc.

Fig. 4. Expression for the Green function G with respect to elastic constant K , time t and position x . Points 1 and 2 are the locations between which the Green function is calculated. The distance between points 1 and 2 are greater than 1 m and less than 10 m.

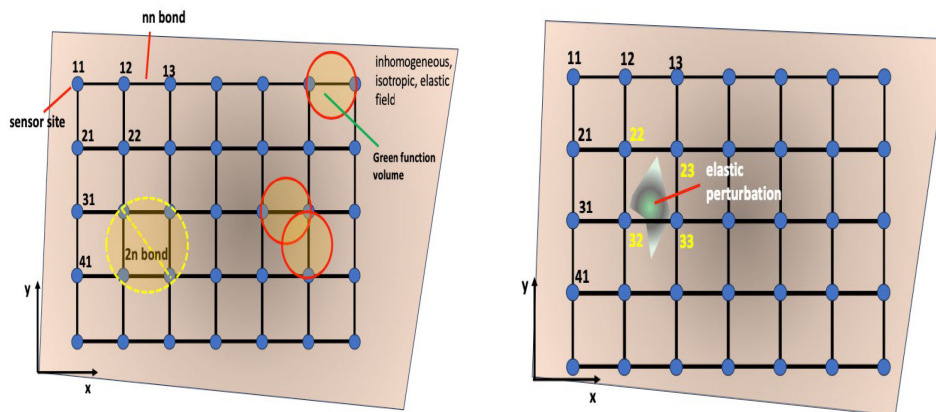


Fig. 5. Far field region measurements. Left: Empirical Green functions are formed between all near neighbor (nn) sensor pairs, a bond is placed in the sensor lattice, between sensor pairs, if an empirical Green function has been formed. Right: A space local distortion of the inhomogeneous isotropic elastic space will change the local Green functions giving a signature of the distortion. Location of perturbation is proportional to $\delta\epsilon$ on each Green function bond.

4 Summary

The LEGACY project is an extensive project focusing on screening, monitoring, modelling and mitigating risks related to legacy wells. As part of WP4, near and far field experiments will be carried out at Mont Terri. In both the near field (<1m) and the far field (>1m), these experiments use seismic waves to probe the material integrity and changes in material integrity of the formation immediately outside the casing (near field), and nearby the well (far field). The TR method can detect and locate small fractures and fluid pathways that have formed within centimeters of the casing. It works by exciting nonlinear features such as fractures and then locating the signal that they produce. The Green Function method can detect changes in mechanical properties associated with damage and fluid pressure between pairs of sensors. The ability of this method to locate changes in the rock formation is by tomographic imaging or by identifying which interstation paths indicate changes. So, its ability to precisely locate features depends upon the ray path coverage.

Acknowledgments

The LEGACY project is funded by the Clean Energy Transition Partnership, call module TRI3 on CCU/CCS Technologies through the Research council of Norway, ADEME and DOE and with support from Equinor, AkerBP, Neptune Energy and Exxon-Mobil.

References

Gasda, S. E., Bachu, S. & Celia, M. A. Spatial characterization of the location of potentially leaky wells penetrating a deep saline aquifer in a mature sedimentary basin. *Env Geol* 46, 707–720 (2004).
 Romdhane, A., Emmel, B., Zonetti, S. and Dupuy, B., 2022. Screening and Non-Invasive Geophysical Monitoring of Legacy Wells Integrity for Offshore CO₂ Storage. Available at SSRN 4276670.

Overview of structure, geometry, fluid flow and seismo-mechanics of clay-rich thrust faults drilled by the International Ocean Discovery Program (IODP) in active subduction margins: insights for fault seal analysis for CCS

Jade Dutilleul^{*1} and Christopher Wibberley¹

¹ TotalEnergies, Avenue Larribau, 64000 Pau, France

* jade.dutilleul@totalenergies.com

Abstract

For CCS development projects, fault seal analysis is essential to reliable evaluations of underground CO₂ containment limits, whether the main trapping mechanism is fault sealing, or whether the reservoir, topseal and/or overburden are faulted. Fault seal analysis at the reservoir scale allows for a better assessment of fault sealing vs. leaking behaviour based on fault geometrical (e.g., fault zone structure and throw, reservoir juxtapositions and/or disconnections), compositional (e.g., shale gouge ratio) and petrophysical (permeability structure) characterization. Additional detailed geomechanical evaluation is critical to assess and mitigate various hydro-mechanically induced phenomena, such as pressure front dissipation/retention and fault reactivation and slip (aseismic vs. seismic slip?), which may, in addition to the induced seismicity risk, breach the integrity of the fault seal and result in across/up-fault leakage beyond the containment limits. However, the fault seal analysis workflow used for CCS site evaluation relies on still poorly understood sealing and leakage mechanisms, with underlying timescales and geological parameters that are commonly weakly-constrained due to a lack of 1) good quality and accessible fault zone outcrops and 2) of core material from drilled faults especially in shales.

Here, we emphasize the valuable contribution of the International Ocean Discovery Program (IODP) to the understanding of the relations between fault geometry, composition, hydraulic structure and seismo-mechanical responses, which is of critical interest for CCS (although the geological context significantly differs), by providing unique access to the characteristics and in situ conditions of clay-rich faults (mostly thrust faults) through decades of coring, drilling and monitoring in active subduction zones. Resulting research results have documented in detail the structure, composition and petrophysical properties of these clay-rich fault zones, and, when possible, associated in-situ conditions (e.g., stress regime, pressure, temperature), showing a critical impact on fault zone hydraulic properties (thus the type of fluid flow such as across-fault or along-fault), fault stability and slip style (thus seismic hazard), which, in turn, affect the properties of the fault zone.

We review the geometry, the distribution of deformation structures, the composition, the petrophysical, the frictional and the mechanical properties of clay-rich thrust fault zones in well documented modern active accretionary (the Nankai margin in southwest Japan, and the Northern Hikurangi margin in New Zealand) and erosive (Japan Trench) margins. The clay-rich faults reviewed consist in basal decollement faults, in-sequence frontal thrusts, and out-of-sequence thrusts crosscutting the accretionary margins called splay or mega-splay faults. We also synthesize the hydraulic information like fluid flow and pore pressure distribution as well as the slip type(s) associated with these clay-rich fault zones. We compare with onland clay-rich fault zones from the Upper Miocene to lower Pliocene outcropping and well-preserved Miura-Boso off-scraped accretionary prism and with the 'Main Fault' subcrop of the Mont Terri rock laboratory in Switzerland.

The structure of the clay-rich thrust fault zones reviewed are strikingly similar whether they come from outcrop/subcrop (Yamamoto et al., 2005; Jaeggi et al., 2017) and core observations (Ujii and Kimura, 2014; Fabbri et al., 2020; Fagereng et al. 2019; Vannucchi, 2019), or borehole data (Pwavodi and Doan, 2024), independently from the clay mineral assemblage. Fault zones comprise:

- Several tens of meters of weak scaly clay or shale, often as a matrix containing large rigid clasts or blocks of weakly-deformed material
- A heterogeneous mixture of fault rocks typically being breccias, gouges and scaly clays;
- A heterogeneous distribution of shear within the fault zone, generally with an increase in shear deformation intensity towards the base of this zone
- A series of thin (mm to cm wide) shale gouges (main slip zones), heterogeneously spaced throughout the shear zone, but becoming more frequent close to the base
- A basal contact shear zone or single fracture/slip surface

The combined analysis of seismic and drilling data reveals a 3D heterogeneous hydraulic structure for the shallow accretionary prisms investigated, with subsequent differences in the seismo-mechanical responses. In the Kumano region of the Nankai margin offshore Kii Peninsula, Pwavodi and Doan (2024) and Pwavodi (2023) documented sealing fault core and large fluid flow channelized in the overpressured footwall damage zone of both the splay faults (Sites C0001-C0004 above the mega-splay fault) and the basal detachment (Site C0024 at the prism toe) that both connect at depths to the mega-splay fault system where a low velocity zone reflecting a high pore pressure patch has been identified (Kitajima & Saffer, 2012). However, at Site C0006 (only ~1 km seaward of Site C0024), both the decollement and the splay fault that branches off the decollement are permeable, allowing updip fluid flow and pore pressure dissipation (Pwavodi, 2023). This implies that when seismic slip nucleates in the seismogenic zone of the mega-splay fault, the released stress may migrate updip either along the mega-splay fault branches or along the decollement almost up to the trench, where it gets further distributed between the main frontal thrust and the accretionary prism. Data from Site U1518 suggest similar situation at the Northern Hikurangi margin (French and Morgan, 2022; Morgan et al., 2020; Dutilleul et al., 2021). In contrast, to the west in the Muroto region of the Nankai margin, the décollement drilled in the prism toe at Sites C0023, 1173 and 808 seems permeable, allowing transient updip migration of fluid sourced in a deeper overpressured zone (Zhang et al., 2021).

The mixture of brittle (e.g., faults, breccia and microbreccia, non-foliated gouge, granular injection veins) and ductile (e.g., foliated gouge) deformation with brittle microstructures commonly overprinting ductile microstructures in both splay faults and the basal decollement suggests that in the shallow part of accretionary prisms, the same fault system has produced both rapid deformation (conventional rapid seismic slip) and slow deformation (e.g., aseismic creep, afterslip or slow slip events) at different times (note however that the type of microstructure depends on the consolidation state of the sediment when it is deformed). In addition, several studies have documented thermal anomalies in the shear zones from <300 °C to 390 °C ± 50 °C depending on the studies (e.g., Sakaguchi et al., 2011; Yamaguchi and Sakaguchi, 2011; Hirono et al., 2009, 2014; Hamada et al., 2015), with diverging conclusions as to their origin, such as coseismic slip-induced frictional heating along the gouge due to one or repeated events, or slow-slip transient event. This frictional heating may have favored the transformation of smectite to illite in the gouge (Yamaguchi et al., 2011). Shear experiments conducted on clay-rich materials commonly show velocity-strengthening frictional behaviors prone to stable sliding at low slip rates (e.g., Ikari & Saffer, 2011), and both velocity-strengthening and velocity-weakening behaviors at intermediate slip rates, at which slow slip events occur (Tsutsumi et al., 2011; Saffer & Wallace, 2015). However, experiments carried out at seismic slip velocity on water-saturated fault gouge samples from Nankai (Ujiie and Tsutsumi, 2010; Tsutsumi et al., 2011) and Hikurangi margins (Aretusini et al., 2021) have shown that together, thermal and mechanical (i.e., compaction-driven) pressurization (enhanced by the low permeability of these clay-rich fault gouges) facilitate faster dynamic fault weakening, thus the propagation of earthquake rupture.

Together, fault rock and well data analyses suggest that after nucleating in the seismogenic zone of the megathrust, seismic slip can propagate to the seafloor either along splay faults or the decollement, with the possible resulting occurrence of a tsunami, as observed in Japan (e.g., Mw 8.2 Tonankai earthquake and tsunami in the Nankai margin off Kii Peninsula in 1944 or Mw 9.1 Tohoku

earthquake and tsunami in the Japan Trench in 2011), in Indonesia (2004 9.2 North Sumatra-Andaman earthquake and devastating tsunami) or New Zealand (Mw 7.0-7.2 tsunami earthquakes of March and May 1947 offshore North Hikurangi margin). In addition, high pore pressure identified near the toe of the Nankai margin (Kumano region) and North Hikurangi margin may favor transitional friction properties and the occurrence of shallow slow slip events, very low frequency earthquakes and/or tremors. Indeed, slow earthquakes have been detected at Site C0006 (located 2 km landward of the Nankai trench; Araki et al., 2017; Edgington et al., 2021) and near Site U1518 at the North Hikurangi margin (e.g., Wallace and Beavan, 2010).

Research conducted by the IODP teams highlights that the understanding of clay-rich fault sealing/leaking behaviour and its relationship with natural hazard (aseismic/seismic slip) benefit from the combined analysis of core, outcrop, drilling and seismic data, and more recently from monitoring data. Although they are of interest for CCS analogs, other types of clay-rich faults in other geological contexts have been weakly documented in comparison. Further monitoring data at the borehole (e.g., Nankai and Hikurangi) and subcrop (e.g., Mont Terri rock laboratory) scales, combined with experiments in the laboratory on samples, under well-known or controlled in situ conditions and fluid flow would further contribute to unravel the details of the interactions between the mechanisms involved in fault reactivation in shales, slip type and extent (thus induced seismicity hazard whose magnitude is even less constrained than that of natural hazards), permeability structure modification, fluid and pressure dissipation/retention for more reliable, safe and sustainable CCS development.

References

- Araki, E, Saffer, DM, Kopf, AJ, Wallace, LM, Kimura, T, Machida, Y, Ide, S and Davis, E. 2017. Recurring and triggered slow-slip events near the trench at the Nankai Trough subduction megathrust, *Science*, 356 (6343), 1157–1160.
- Dutilleul, J, Bourlange, S, Géraud, Y. 2021. Porosity and compaction state at the active Pāpaku thrust fault in the frontal accretionary wedge of the north Hikurangi margin. *Geochemistry, Geophysics, Geosystems*, 22, e2020GC009325. <https://doi.org/10.1029/2020GC009325>
- Edgington, J, Williams, C. and Saffer, D. 2021. Migration of shallow slow slip events to trench: evidence from borehole observatories in the Nankai Trough, in *Proceedings of the AGU Fall Meeting 2021*, held in New Orleans, LA, 13–17 December 2021, id. T25C-0188.
- Fabrizi, O, Goldsby, DL, Chester, F, Karpoff, AM, Morvan, G, Ujiie, K, et al. 2020. Deformation structures from splay and décollement faults in the Nankai accretionary prism, SW Japan (IODP NanTroSEIZE Expedition 316): Evidence for slow and rapid slip in fault rocks. *Geochemistry, Geophysics, Geosystems*, 21, e2019GC008786. <https://doi.org/10.1029/2019GC008786>
- Fagereng, A, Savage, H, Morgan, J, Wang, M, Meneghini, F, Barnes, P, et al. 2019. Mixed deformation styles observed on a shallow subduction thrust, Hikurangi margin, New Zealand. *Geology*, 47(9), 872–876. <https://doi.org/10.1130/g46367.1>
- Festa, A, Dilek, Y, Mitterperger, S, Ogata, K, Pini, GA, Remitti, F. 2018. Does subduction of mass transport deposits (MTDs) control seismic behavior of shallow-level megathrusts at convergent margins? *Gondwana Research* 60, 186–193. <https://doi.org/10.1016/j.gr.2018.05.002>
- French, ME, & Morgan, JK. 2020. Pore fluid pressures and strength contrasts maintain frontal fault activity, Northern Hikurangi Margin, New Zealand. *Geophysical Research Letters*, 47(21), e2020GL089209. <https://doi.org/10.1029/2020gl089209>
- Hamada, Y, Sakaguchi, A, Tanikawa, W et al. 2015. Estimation of slip rate and fault displacement during shallow earthquake rupture in the Nankai subduction zone. *Earth Planets Space*, 67, 39. <https://doi.org/10.1186/s40623-015-02080>
- Hirono, T, Ishikawa, T, Matsumoto, H, Hamada, J, Yabuta, H, & Mukoyoshi, H. 2014. Re-evaluation of frictional heat recorded in the dark gouge of the shallow part of a megasplay fault at the Nankai trough. *Tectonophysics*, 626, 157–169. <https://doi.org/10.1016/j.tecto.2014.04.020>
- Hirono, T, Ujiie, K, Ishikawa, T, Mishima, T, Hamada, Y, Tanimizu, M et al. 2009. Estimation of temperature rise in a shallow slip zone of the megasplay fault in the Nankai Trough. *Tectonophysics*, 478, 215–220. <https://doi.org/10.1016/j.tecto.2009.08.001>
- Ikari, MJ, Saffer, DM. 2011. Comparison of frictional strength and velocity dependence between fault zones in the Nankai accretionary complex, *Geochem. Geophys. Geosyst.*, 12, Q0AD11. <https://doi.org/10.1029/2010GC003442>
- Ikari, MJ. 2019. Laboratory slow slip events in natural geological materials. *Geophysical Journal International*, 218 (1), 354–387. <https://doi.org/10.1093/gji/ggz143>
- Jaeggi, D, Laurich, B, Nussbaum, C et al. 2017. Tectonic structure of the “Main Fault” in the Opalinus Clay, Mont Terri rock laboratory (Switzerland). *Swiss J Geosci* 110, 67–84. <https://doi.org/10.1007/s00015-016-0243-2>

- Kameda, J., 2010. Smectite swelling in the Miura–Boso accretionary prism: Possible cause for incipient décollement zone formation. <https://doi.org/10.1016/j.tecto.2010.08.008>
- Kitajima, H & Saffer, DM. 2012. Elevated pore pressure and anomalously low stress in regions of low frequency earthquakes along the Nankai Trough subduction megathrust. *Geophysical Research Letters* 39(23), 1–5.
- Pwavodi, J. 2023. Integration of borehole geophysical data and core petrophysical properties to model hydrogeological properties of the Nankai subduction zone. *Applied geology*. Université Grenoble Alpes 2023.
- Pwavodi, J, Doan, ML. 2024. Direct assessment of the hydraulic structure of the plate boundary at the toe of the Nankai accretionary prism. *Geophysical Journal International* 236, 1125–1138. <https://doi.org/10.1093/gji/ggad473>
- Mazumder, R., 2016. Soft-sediment deformation structures in the Mio-Pliocene Misaki Formation within alternating deep-sea clays and volcanic ashes (Miura Peninsula, Japan). *Sedimentary Geology*. <http://dx.doi.org/10.1016/j.sedgeo.2016.02.010>
- Morgan, JK, Solomon, EA, Fagereng, A, Savage, HM, Wang, M, Meneghini, F, Barnes, PM, Bell, RE, French, ME, Bangs, NL, Kitajima, H, Saffer, DM, Wallace, LM. 2022. Seafloor overthrusting causes ductile fault deformation and fault sealing along the Northern Hikurangi Margin. *Earth and Planetary Science Letters* 593, 117651. <https://doi.org/10.1016/j.epsl.2022.117651>
- Saffer, D, Wallace, L. 2015. The frictional, hydrologic, metamorphic and thermal habitat of shallow slow earthquakes. *Nature Geosci* 8, 594–600 (2015). <https://doi.org/10.1038/ngeo2490>
- Sakaguchi, A, Chester, F, Curewitz, D, Fabbri, O, Goldsby, D, Kimura, G, et al. 2011. Seismic slip propagation to the up-dip end of plate boundary subduction interface faults: Vitritite reflectance geothermometry on Integrated Ocean Drilling Program NanTro SEIZE cores. *Geology*, 39(4), 395–398. <https://doi.org/10.1130/G31642.1>
- Savage, HM, Shreedharan, S, Fagereng, A, Morgan, JK, Meneghini, F, Wang, M, et al. 2021. Asymmetric brittle deformation at the Pāpaku fault, Hikurangi subduction margin, NZ, IODP Expedition 375. *Geochemistry, Geophysics, Geosystems*, 22, e2021GC009662. <https://doi.org/10.1029/2021GC009662>
- Tsutsumi, A, Fabbri, O, Karpoff, A M, Ujiie, K, & Tsujimoto, A. 2011. Friction velocity dependence of clay-rich fault material along a megasplay fault in the Nankai subduction zone at intermediate to high velocities. *Geophysical Research Letters*, 38, L19301. <https://doi.org/10.1029/2011GL049314>
- Ujiie, K & Tsutsumi, A. 2010. High-velocity frictional properties of clay-rich fault gouge in a megasplay fault zone, Nankai subduction zone. *Geophysical Research Letters*, 37, L24310. <https://doi.org/10.1029/2010GL046002>
- Ujiie, K & Kimura G. 2014. Earthquake faulting in subduction zones: insights from fault rocks in accretionary prisms. *Progress in Earth and Planetary Science*, 1,7. <https://doi.org/10.1186/2197-4284-1-7>
- Vannucchi, P. 2019. Scaly fabric and slip within fault zones. *Geosphere*, 15 (2), 342–356. <https://doi.org/10.1130/GES01651.1>
- Wallace, LM, and Beavan, J. 2010. Diverse slow slip behavior at the Hikurangi subduction margin, New Zealand. *Journal of Geophysical Research: Solid Earth*, 115, B12402. <https://doi.org/10.1029/2010JB007717>
- Yamaguchi, A, Sakaguchi, A, Sakamoto, T, Iijima, K, Kameda, J, Kimura, G, et al. 2011. Progressive illitization in fault gouge caused by seismic slip propagation along a megasplay fault in the Nankai Trough. *Geology*, 39(11), 995–998. <https://doi.org/10.1130/G32038.1>
- Yamamoto, Y., Mukoyoshi, H. & Ogawa, Y., 2005. Structural characteristics of shallowly buried accretionary prism: Rapidly uplifted Neogene accreted sediments on the Miura-Boso Peninsula, central Japan. *Tectonics*, 24, TC5008, <https://doi.org/10.1029/2005TC001823>
- Yamamoto, Y., 2006. Systematic variation of shear-induced physical properties and fabrics in the Miura–Boso accretionary prism: The earliest processes during off-scraping. *Earth and Planetary Science Letters*. <https://doi.org/10.1016/j.epsl.2006.01.049>
- Yamamoto, Y, Okutsu, N, Yamada, Y, Bowden, S, Tonai, S, Yang, K, Tsang, MY, Hirose, T, Kamiya, N, 2017. Structural characteristics of the décollement zone and underthrust sediments in the Nankai accretionary prism: Geologic architectures in the Site C0023, IODP Expedition 370, in: *AGU Fall Meeting Abstracts*. pp. T23A-0591.
- Zhang, J, Hüpers, A, Kreiter, S, & Kopf, AJ 2021. Pore pressure regime and fluid flow processes in the shallow Nankai Trough subduction zone based on experimental and modeling results from IODP Site C0023. *Journal of Geophysical Research: Solid Earth*, 126, e2020JB020248. <https://doi.org/10.1029/2020JB020248>

Evaluation of faulted topseal integrity for CCS: analogues from sub-surface post-mortem well analyses and shale-rich fault outcrops

Maria El Hage Moussa^{1,2*}, Christopher A. J. Wibberley¹, Jade Dutilleul¹, Jean-Paul Callot² and Nicolas E. Beaudoin²

¹ TOTALENERGIES, CSTJF, Av. Larribau 64018 Pau, France

² Université de Pau et des Pays de l'Adour, Institut Pluridisciplinaire de Recherche Appliquée (IPRA), Department of Earth Sciences, Pau, France

* maria.el-hage-moussa@totalenergies.com

1 Project stakes

CO₂ storage in geological reservoirs is considered as the most practical way of isolating it from the atmosphere at the industrial scale, and consequently- it will be an important contribution to mitigating the effect of CO₂ emissions on climate change. The injection and storage of large volumes of CO₂ into subsurface reservoirs need to be evaluated based on the knowledge of how the geological layers surrounding the reservoir will seal the injected fluids, and this is particularly critical in the areas where faults and fractures affect the overburden and reservoirs concerned (Fig 1).

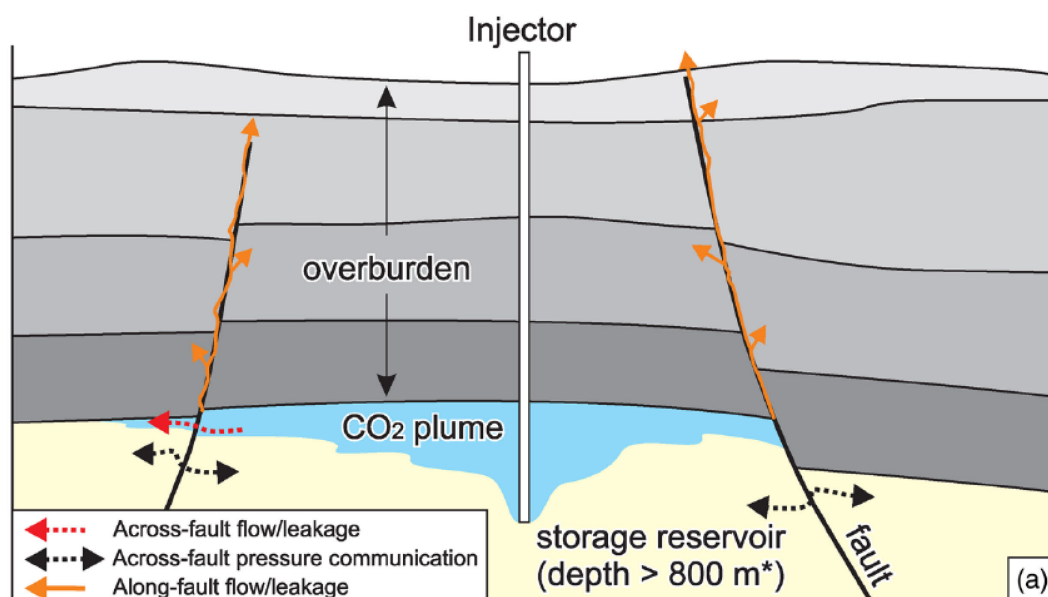


Fig. 1. Potential leakage pathways of a CO₂ plume from a fault-bounded trap. It is important to additionally consider the effect of the aquifer pressure front migrating ahead of the CO₂ plume (from Wu et al. 2022).

One of the critical limits on containment in a CO₂ storage project is the maximum fluid pressure that can be supported by the faults and faulted shale-rich topseal during and after injection. The limits of such maximum pressure are currently relatively uncertain and rely on weakly-constrained in-situ stresses and assumptions on the sealing and leakage mechanisms of the faults and faulted topseal which are poorly understood.

Understanding the mechanisms of fluid retention and leakage through these structures is key to constraining the maximum injection pressure that they can withstand. The analysis of hydrocarbon traps is often used in the hydrocarbon E&P industry by way of post-mortem analysis to understand trapping mechanisms and retention limits.

Whilst these may differ between hydrocarbons and CO₂ in many ways - from fluid thermodynamics and dissolution into the aquifer to migration timescales - such analyses can nevertheless give valuable lessons in understanding and quantifying retention and leakage.

2 Context and thematics

At the scale of a sedimentary basin, various geological factors combine to make a region more, or less, susceptible to vertical fluid escape. At a smaller scale, such as for a potential prospect for CO₂ storage, both the permeability of the seal and the local geological structure (such as a fault acting as a vertical conduit) are critical components for fluid escape in specific conditions. Hence, post-mortem data on in-situ hydrocarbon column heights from exploration wells and fields, can be used to: provide thresholds for maximum fluid pressure supported by topseal / faults in a given play, and better understand the mechanisms of integrity breaching and leakage at the scale of an individual structure.

In order to evaluate the hydrocarbon column heights in prospects, various workflows have been established in the industry for different lithological contexts, fluid pressure regime, tectonic activity and perceived trapping mechanism (e.g., fault capillary sealing vs active leakage). Eventually, the reliability of these workflows depends largely on a regional-to-local calibration (Fig 2), and various external databases provide world-wide algorithms for hydrocarbon column heights, each with several pitfalls and consequently large uncertainties.

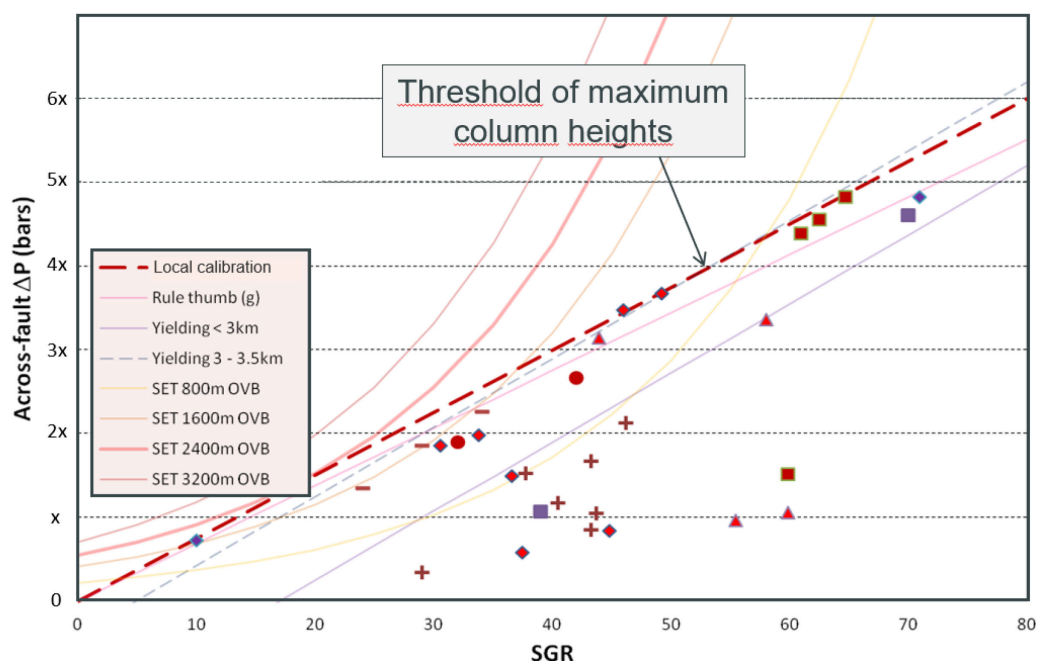


Fig. 2. Example of a locally-calibrated fault seal threshold from a post-mortem analysis of faulted traps in a specific play, sub-basin, depth / Pf range and fluid type (from Nosike et al. 2010).

3 Project overview and Pmax injection review

The doctorate thesis project discussed here capitalizes in-house and published post-mortem data on fluid pressure and hydrocarbon retention limits of in-place hydrocarbon columns trapped against faults and faulted topseal in similar geological contexts. Through careful synthesis work considering the geological parameters in each case, a series of pressure limits will be proposed as a function of the parameters, for different leakage mechanisms identified. However, the first step is to review the state-of-the-art in how to constrain the maximum injection pressure that a fault can support before either leaking, being reactivated, or both. This contribution will present a review and synthesis of the state-of-the-art in evaluation of both fault seal capacity (for across-fault leakage) and fault integrity (for up-fault leakage and/or mechanical reactivation), and the workflows proposed to estimate them. We

find that evaluation of across-fault flow is heavily reliant on the geometry of juxtaposition of reservoir units, hence uncertainties depend largely on geometric definition. Up-fault flow rates, on the other hand, (which can result in loss of containment to the surface or induced seismicity in deeper levels such as in the seismogenic basement) depend not only on vertical fault connectivity but also on the in-situ stress regime. Hence for up-fault leakage the estimation of the local principal stresses, and the hydromechanical behaviour of the fault, are amongst the largest uncertainties.

References

- Nosike, L., Wibberley, C., Jardiné, C., & Pacalin, Y. (2010). The role of tectonics in geopressure compartmentalisation and hydrocarbon leakage in the deep offshore Niger delta. "Trabajos de geologia", 101–106.
- Wu, L., Thorsen, R., Ottesen, S., Meneguolo, R., Hartvedt, K., Ringrose, P., Nazarian, B. 2022. Significance of fault seal in assessing CO₂ storage capacity and containment risks – an example from the Horda Platform, northern North Sea. *Pet. Geosci*, 28. <https://doi.org/10.1144/petgeo2020-102>

Regional characterization of clay formations for multi-barrier CO₂ storage opportunities in North Germany

Franz May^{1*}, Stefan Knopf¹, Alexandra Ruales¹ and Gabriela von Goerne¹

¹ Federal Institute for Geosciences and Natural Resources, Hannover, Germany

* f.may@bgr.de

1 Region and barrier concept

The North of Germany is expected to be the most relevant region for CO₂ storage in the country with the highest CO₂ emissions in Europe. The largest natural gas fields that could be used for storage after depletion are located there and saline water-bearing formations are abundant in the North German Basin (May et al. 2003).

For the subsurface storage of CO₂ at least one porous reservoir formation and one low-permeable caprock are required, though the storage complex (according to the EU CO₂ storage directive) may contain additional secondary barriers. As the efficient storage of compressed CO₂ requires pressures usually found at depths of more than 800 m, the overburden of potential storage sites often includes rock successions of variable hydraulic properties that can serve as aquifers or barriers to fluid flow. Such hydro-stratigraphic successions are present in Northern Germany as well (e.g., Reutter 2011).

General requirements for formations to be candidates for comprising suitable reservoir and barrier rocks have been proposed for Germany (Tab. 1, Reinhold et al. 2011). Information about porosity and permeability of potential reservoir and barrier formations are scarce, especially for the latter. The data density did not allow regional assessments of these properties. Reservoir and barrier formations containing likely suitable lithologies have been identified.

Tab. 1. Minimum requirements for potential reservoir and barrier formation

Reservoir formations	Barrier Formations
Top > 800 m below ground surface	Base > 800 m below ground surface
Net thickness of storage rocks > 10 m	Net thickness of barrier rocks > 20 m
Porosity > 10 %	Porosity, no criterion applied
Permeability > 10 mD	Formations comprising evaporates or clay stones

Using the depth, thickness, and lithology criteria, formations potentially useful for CO₂ storage sites have been identified and were mapped by the German state geological surveys.

Secondary barrier formations can be used for various storage concepts, providing additional safety, facilitating vertically stacked storage concepts, enhancing operational flexibility, e.g., in cases of injectivity issues, providing options for aquifer pressure management, or can be considered for reserve storage, e.g., if corrective measures for storage operations are required. Co-location of deep hydro-geothermal projects and CO₂ storage in reservoirs of different depth, separated by barriers could also be an option for the use of the deep subsurface in North Germany, as potentials for both options overlap in wide regions (Schulz et al. 2013). Barriers in the shallow overburden of storage sites may also be important for preventive risk reduction and groundwater protection.

2 Stratigraphy and spatial extent of reservoir and barrier formations

Formations suitable for storage of CO₂ in North Germany are those containing natural gas reservoirs also. These are predominantly located within Rotliegend and Bunter sandstones. Rotliegend reservoirs are capped by Zechstein evaporites. The Triassic Bunter reservoirs are capped by claystones and evaporites of the Röt-Formation (Upper Bunter). Lower Jurassic and lower Cretaceous barrier formations comprise clay rich lithologies, though regionally, sandstones are intercalated that could provide storage options (Fig. 1).

Period / Epoch	Age / Formation (Fm.)	North German Basin		
		reservoir	barrier	
Quaternary		water		
Tertiary	Pliocene			
	Miocene			
	Oligocene	Chatt		
		Rupel		clay
	Eocene			
Paleocene				
Cretaceous	Upper Cretaceous	Maastricht		
	Lower Cretaceous	Cenoman to Campan	CO ₂	
Jurassic	Upper Jurassic	Oxford to Tithon		
	Middle Jurassic	Aalen to Callov		
	Lower Jurassic (Lias)	Toarc		
Triassic	Keuper	U Rhätkeuper		
		M Steinmergelkeuper		
		M Upper Gipskeuper		
		M Schilfsandstein		
		L Lower Gipskeuper		
	Muschelkalk			
	Buntsandstein	U Röt		
		M Volpriehausen to Solling		
		L		
	Permian	Zechstein	Werra to Fulda	salt
Rotliegend		Upper Rotliegend		

Fig. 1. Stratigraphy of potential reservoir and barrier formations in North Germany, after Reinhold et al. 2011.

In the west and central parts of the North German Basin up to four pairs of formations containing potential storage and reservoir rocks are vertically stacked above each other. The stratigraphically deepest pair is capped by Zechstein salt and anhydrite, a very tight cap rock though geochemically and geomechanically different from clay-rich lithologies. Clay-rich formations of excellent barrier properties have been mapped in North Germany as potential host rocks for radioactive waste (Hoth et al. 2007) and CO₂ storage (Fig. 2, Reinhold et al. 2011, Bense & Jähne-Klingberg 2017).

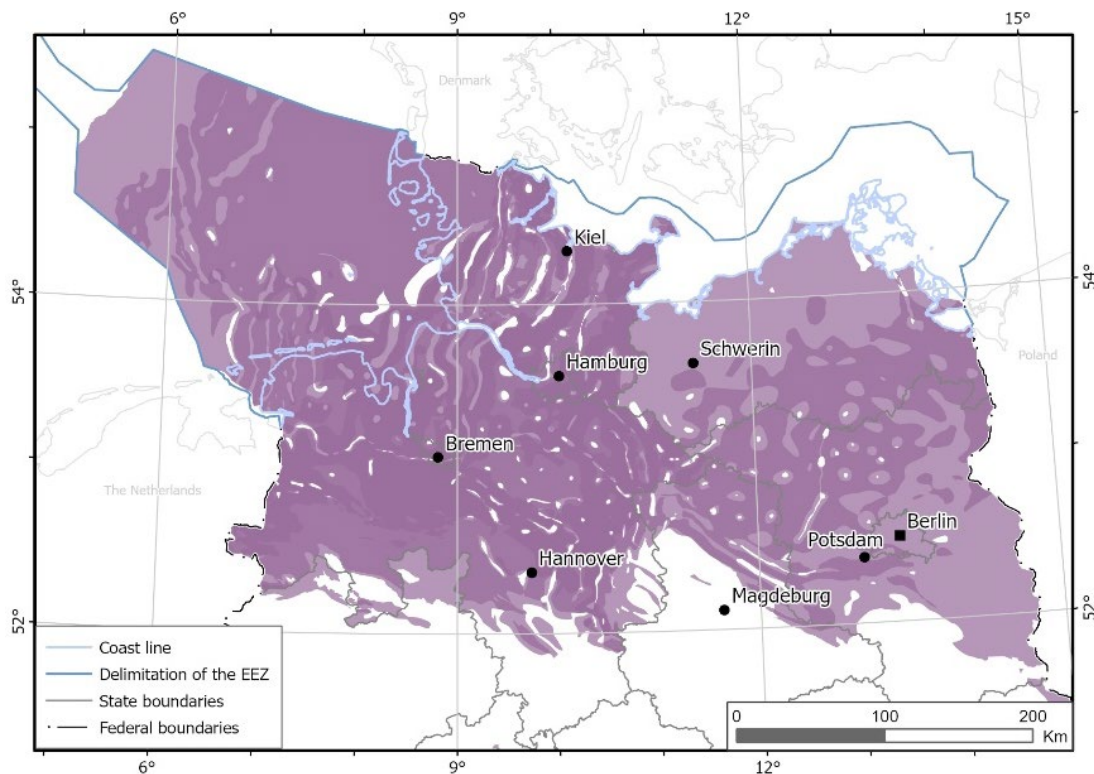


Fig. 2. Distribution of potential barrier formations in North Germany; up to three (darkest colour) clay-rich formations are superimposed.

3 Groundwater protection

Fresh groundwater is the source of 85 - 100 % of the drinking water provided through the public water supply in the North German federal states. In the North German Basin, salinity increases with depth. Below 800 m formation waters often contain more than 100 g/l dissolved solids (e.g., Brasser & Brewitz 2002). These saline aquifers are a potential target for CO₂ storage. Locally, salty formation waters come close to or discharge at the earth surface. These areas can be problematic for agriculture and for drinking water production, e.g., in Brandenburg (Hermsdorf 2010). Fortunately, lower Tertiary clay is abundant in the Oligocene Rupelton formation. These clays frequently separate fresh groundwater above, from saline formation waters below (e.g., Brose & Hermsdorf 2017). As formation waters can be displaced by CO₂ injection and possibly could follow seal bypass pathways into the overburden of CO₂ storage complexes, knowledge of the distribution and properties of the Rupelton-Formation is essential for safety assessments of potential CO₂ storage sites. Locally, erosion due to salt-tectonical movements, glaciations and melt-water runoff has weakened or removed this barrier (e.g., Limberg et al. 2016). Knowledge of such local phenomena is important for site screening. Therefore, BGR has compiled a map of the Rupelium in North Germany 1:500,000, showing distribution and “gaps” within this important barrier for groundwater protection (Fig. 3, Gast 2012).

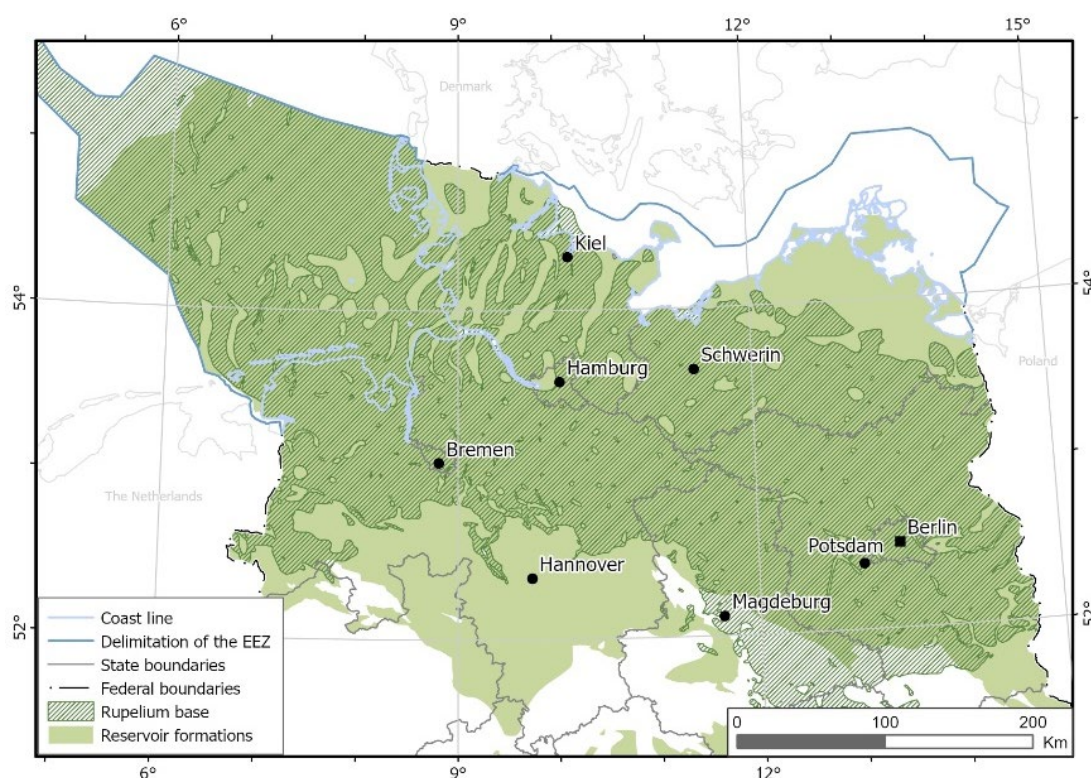


Fig. 3. Distribution of Rupelium above potential reservoir formations for CO₂ storage in North Germany, after Gast 2012.

4 Properties of the Rupelton-Formation

In Lower Saxony, the average thickness of the lower Rupelian is 74 m (Knopf 2011), in Brandenburg the Rupelton Formation typically is 80 to 100 m thick (Brose & Hermsdorf 2017) and between 20 and 200 m in Mecklenburg-Vorpommern (BGE 2020). At the base of the Rupelium sandy sediments occur, followed by silt and clay-bearing ones, which in the centre of the marine basin grade into marl. Plastic Rupelium clay is mined for tile, and brick production in North Germany. Gast et al. (2012) have characterized fresh samples from the upper part of the Rupelton Formation, obtained from a well in the centre of the North German basin, as these have not suffered weathering or desiccation. Cuttings and core samples were obtained from 231 - 249 m depth. The water content of the dark clay is between 20 and 25 vol.-%. Though the name of the Rupelton formation suggest a clay stone, the Rupelian sediments have a much wider grain size spectrum ranging from clay to sand. The

analyzed samples are loamy sand and sandy loam (Fig. 4). Quartz is a main mineral in all of the ten samples. Other main minerals are feldspar, muscovite/illite, mixed layer clay minerals and chlorite. Calcite is the main carbonate. Siderite and dolomite are main minerals in one sample respectively. The carbonate content is 8 - 9 wt.-%. Kaolinite and pyrite occur in traces. The mineralogical composition of the sediments varies on a small scale but also considerably between sites. The abundance of different clay minerals and carbonates can affect the geomechanical and geochemical stability of the barrier and has to be evaluated site-specific. Despite of dominance of the sand fraction, the hydraulic conductivities of the soft rock is very low, $1 - 9 \times 10^{-11}$ m/s, “sehr schwach durchlässig” according to DIN 18130. These low conductivities result from a rather high compaction of the sediments. In general, sediments of the Rupelton formation are more fine-grained than the analyzed sandy samples (e.g., samples from clay pits in Fig. 4). For waste depositories, sediments with clay contents of more than 20 wt.-% are used for geotechnical barriers (Krakow 2012). Thus, good barrier properties for groundwater protection can be assumed for the Rupelton formation throughout Northern Germany.

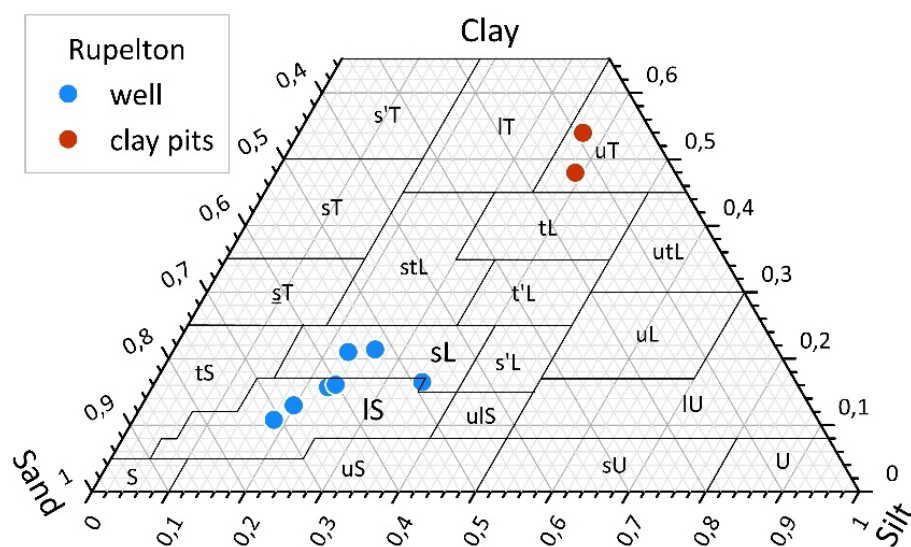


Fig. 4. Grain size classes of Rupelian sediments from well Neuglobsow Hy Ngw 1/2010: loamy sand (IS) and sandy loam (sL) (Gast et al. 2012) and silty clay from open pit mines in Köthen and Haselbach (Krakow 2023).

5 Outlook

Though the distribution of clay-bearing formations is well known in North Germany, their barrier properties for retaining CO₂ streams and reservoir fluids are poorly known. These need to be assessed and verified in specific investigations of potential CO₂ storage sites.

References

- Bense, F, Jähne-Klingberg, F. 2017. Storage potentials in the deeper subsurface of the Central German North Sea. Energy Proced. 114, 4595–4622.
- BGE 2020. Datenbericht Teil 4 von 4 Mindestanforderungen gemäß § 23 StandAG und geowissenschaftlichen Abwägungskriterien gemäß § 24 StandAG. BGE, Peine, 317 pp.
- Brasser, T, Brewitz, W. 2002. Anwendbarkeit der Indikatoren “teufenabhängige Mineralisation / Salzgehalt” für die Erfüllung der allgemeinen Anforderung “keine oder langsame Grundwasserbewegung”. GRS, Braunschweig. 72 pp. GRS-A-Bericht (bundestag.de).
- Brose, D, Hermsdorf, A. 2017. Geogene Versalzung von Grundwasserleitern in Brandenburg. Brandenburg. Geowiss. Beitr. 24 1/2, 7–16.
- Gast, S. 2012. Geologische Übersichtskarte von Norddeutschland – Tiefenlinienkarte der Basis Rupelium 1: 500 000. BGR, Hannover.
- Gast, S, Wirth, H, Fischer, M, Weber, K. 2012. Planungsgrundlagen und geologische Informationen für die Entwicklung potenzieller CO₂-Speichervorhaben. Anhang 1: Mineralogische, geochemische, hydraulische und geomechanische Untersuchungen an Tonen des Rupelium. BGR, Hannover, 46–66 pp.

- Hermesdorf, A. 2010. Überblick über die Grundwasserversalzen im Land Brandenburg und ihre Spezifikation für die Binnensalzstellen. *Naturschutz und Landschaftspflege in Brandenburg* 19, 9–15.
- Hoth, P, Wirth, H, Reinhold, K, Bräuer, V, Krull, P, Feldrappe, H. 2007. Final disposal of radioactive wastes in deep geological formations of Germany. Investigation and evaluation of argillaceous rock formations. BGR, Hannover, 118 pp.
- Knopf, S. 2011. Speicher-Kataster Deutschland: Endbericht für Niedersachsen und Bremen. BGR, Hannover, 104 pp.
- Krakow, L. 2023. Rohstoffdatenblätter Köthen und Haselbach. <https://www.dr-krakow-labor.de/plastische-tone>, download 15.11.2023.
- Krakow, L. 2012. Beim Dichtungsbau zählt Langzeitstabilität. *Gesteinsperspektiven* 6/2012: 18–20.
- Limberg, A, Jonas, O, Kolberg, A. 2016. Detektion möglicher Fehlstellen im Rupelton durch Messung der spezifischen elektrischen Leitfähigkeit in tiefen Grundwassermessstellen im Land Berlin. *Brandenburg. Geowiss. Beitr.* 23, 11–15.
- May, F, Brune, S, Gerling, P, Krull, P. 2003. Möglichkeiten zur untertägigen Speicherung von CO₂ in Deutschland – eine Bestandsaufnahme. *Geotechnik* 2003/3 162–172.
- Reutter, E. 2011. Hydrostratigraphische Gliederung Niedersachsens. *Geofakten* 21, 1–11 pp. https://doi.org/10.48476/geofakt_21_2_2011
- Reinhold, K, Müller, C, Riesenberger. 2011. Informationssystem Speichergesteine für den Standort Deutschland. BGR, Hannover. 134 pp.
- Schulz, R, Suchi, E, Öhlschläger, D, Dittmann, J, Knopf, S, Müller, C. 2013. Geothermie-Atlas zur Darstellung möglicher Nutzungskonkurrenzen zwischen CCS und Tiefer Geothermie. LIAG & BGR, Hannover. 111 pp.

Workflow to determine the potential of leakage from CO₂ storage reservoirs along fractures and faults triggered by uplift

Rafael F. Mesquita^{1,3*}, Sahyuo Achuo Dze¹, Nick Harpers¹, Nathaniel Forbes Inskip¹, Florian Doster² and Andreas Busch¹

¹ The Lyell Centre, Heriot-Watt University, Edinburgh, UK

² Institute of GeoEnergy Engineering, Heriot-Watt University, Edinburgh, UK

³ Reservoir Technology, PETROBRAS - Petróleo Brasileiro S.A., Rio de Janeiro, Brazil

* rfdm2000@hw.ac.uk

1 Introduction

A central operational risk in Carbon Capture and Storage (CCS) projects relates to geomechanical impacts on caprock integrity. The injection of fluids induces pore pressure changes, resulting in the expansion of the storage reservoir. This expansion causes the caprock (primary seal) to deflect, which is leading to uplift, keeping the vertical stress (S_1) unchanged (Kaldi et al. 2011). Depending mainly on the strength of the sealing rock, its deflection can be significant. This can cause changes in the minimum horizontal stress (S_3), which is one of the controls on containing fluids below the low permeability rock. Such changes in stress in the caprock can lead to loss of containment (and thus leakage) by initiating new (micro-)fractures in undamaged rock or by reactivating a fault zone/natural fracture. Once the formation of new or reactivation of fractures are promoted by this uplift, fluid flow behaviour needs to be understood to mitigate the risk of unwanted leakage.

Published studies associated with stress changes of sealing rocks due to their deflection are limited (Li et al. 2015; Wangen et al. 2018; Gravanis & Sarris, 2023). Specific to a defined location, they are always based on the application of containment criteria. In addition, there is limited experimental or numerical studies on stress-dependent fluid flow in induced fractures and reactivated fault zones (Phillips et al. 2020; Snippe et al. 2022; Rizzo et al. 2023).

This work aims at defining a workflow to analyse and identify the potential risk of fluid leakage caused by caprock uplift and its stress changes as well as to characterize the potential flow along fractures/faults. The appropriate workflow for a carbon storage project depends on the project phase, dictating the application of either a generic or detailed workflow. The initial approach employs a linear and straightforward workflow, constrained by the time available for the study's conclusion, emphasizing the verification and utilization of existing data with limited iteration. In contrast, for project implementation, a detailed cyclical workflow is used, demanding additional time and investments. It encompasses various stages, including data acquisition (e.g., analogue cases, outcrops, well logs, well testing data), upscaling information across bench, intermediate, and field scales, and culminating in the development of numerical models and simulations.

2 Distinct approach to project phases

According to the stage of the project, the way of working on a project is distinct (Fig. 1). Typically, in the CCS project appraisal stage, where little information is available, quick but reliable studies are generally carried out to obtain an overview of the possible future results to be achieved. On the other hand, when the project is maturing with more data becoming available, accurate predictions need to be made, which require more detailed and specific studies. In that case, a specific and more detailed workflow must be applied.

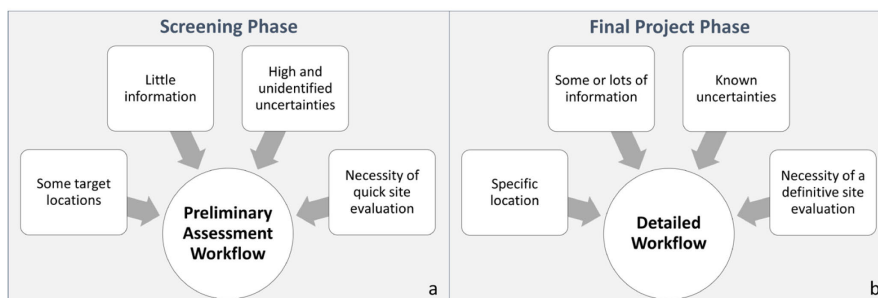


Fig. 1. Different project phases dictating different approaches for project evaluation: (a) initial and (b) final project phase.

3 Preliminary assessment workflow

The generic workflow for CCS project evaluation involves assessing the potential for CO₂ storage, with a focus on caprock integrity. The process aims to identify critical risks, including their acceptability, to determine the need for data acquisition investment for proceeding project phases. Here, seismic data is key to evaluate the storage reservoir and seal. Various techniques are employed to delineate potential storage reservoirs, their limits, and structural features, forming a conceptual structural, alongside stratigraphical, sedimentological, and petrographical models. The time constraints in preliminary assessments allow for minor iterations between disciplines, resulting in one to three deterministic models for engineering porous reservoirs with dynamic properties. In the absence of data, analogue data are utilized, preferably with deterministic scenarios encompassing pessimistic, optimistic, and medium setups at this stage of CCS projects.

In the preliminary assessment workflow, the geomechanical assessment is one of the later stage steps because it obtains information from the fluid flow model, although it directly requires geophysical and geological information to be conducted. Although a geomechanical model can be done in 3D or even in 4D, 1D models are typically conducted initially to understand stress distributions. This allows to develop a primary understanding of how the different formations behave with loading during CO₂ injection.

As can be seen in Fig. 2, the preliminary one-way assessment workflow is as simple as possible without much iteration between the different stages of project appraisal, starting with the geophysical model, followed by the geological model, porous media fluid flow model and finally the geomechanical model.

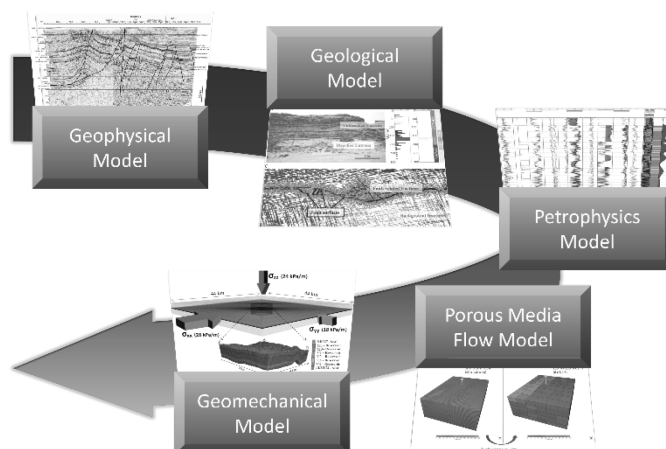


Fig. 2. Preliminary assessment workflow for evaluating a carbon storage project.

4 Detailed workflow

For the implementation phase, the project workflow requires additional elements and increased interdisciplinary iteration beyond the simplified model. This enhancement is essential to bolster project

robustness and reduce uncertainties. The detailed geomechanical aspects of the developed workflow are summarised in Fig. 3.

In geomechanical studies, the preferred approach involves obtaining specific reservoir/caprock data through well logs, cores, laboratory tests, and exploratory wells. The workflow initiates with dedicated data acquisition campaign for subsequent use in numerical models.

The scale of studies varies based on geomechanical effects, with models often utilizing large cell dimensions (e.g., 250 by 250 or 500 by 500 meters), limiting the observation of small dimension fractures and faults. To address this, specific studies focusing on these features are essential. The following sub-items point out the studies at their respective observation scales, exposing the inter-relationship between them.

4.1 *Coupled Hydro-Thermo-Mechanical Numerical Model (HTMNM)*

The comprehensive analysis of stress and deformation changes in the reservoir and caprock using a geomechanical model is crucial. The influence of these rocks on the behaviour of rocks proximal to the reservoir necessitates the incorporation of regions beyond the reservoir in the geomechanical model. This model ideally exhibits full coupling between fluid flow, thermal, and mechanical numerical models (HTMNM), enabling a more precise depiction of physical phenomena relevant to project operationalization. The HTMNM model facilitates a detailed understanding of stress variation due to changes in pore pressure, leading to elastic, plastic, and viscoplastic deformations within the reservoir and, notably, the caprock.

Stress variations in the caprock, especially at the interface with the reservoir, can induce (micro-)fractures or activate small-scale, non-seismic faults, particularly when the rocks are critically stressed. Given the limitations of the fully coupled HTMNM model in representing small features, it is used to identify macroscopic alterations in the stress and deformation field at the reservoir-caprock interface.

4.2 *Fracture studies*

Examinations of hydraulic fractures within caprock necessitate the integration of laboratory and numerical tests, incorporating the coupling of fluid flow, fracture mechanics, continuum mechanics, and, where available, field data. Leveraging the stress change magnitudes derived from the HTMNM model, laboratory tests will be conducted to obtain information of fracture mechanical properties, such as stiffness and intensity factor, as well as the stress-permeability relationships.

Utilizing data derived from laboratory tests and field observations, the numerical fracture model is devised to construct scenarios covering permeability uncertainties and their correlation with stress and stiffness fields, while also verifying the dimensions of the generated fractures. The outcomes of these investigations are crucial for updating the HTMNM model and support decision making regarding project limits, e.g., maximum reservoir pressurization.

4.3 *Fault activation studies*

Investigations into fault activation involve laboratory tests designed to characterize fluid flow behaviour within fractures and its correlation with effective stress. These findings will be extrapolated to a regional scale through the examination and analysis of outcrops containing the fault network. The outcomes of these studies serve a dual purpose: updating the coupled geomechanical model (HTMNM) and, in conjunction with fracture studies, contributing to decisions regarding CO₂ storage pressure limits.

Through the integration of all results, the assessment of caprock integrity and fluid flow behaviour within faults and fractures is conducted across various scenarios, addressing the most critical uncertainties identified in the process.

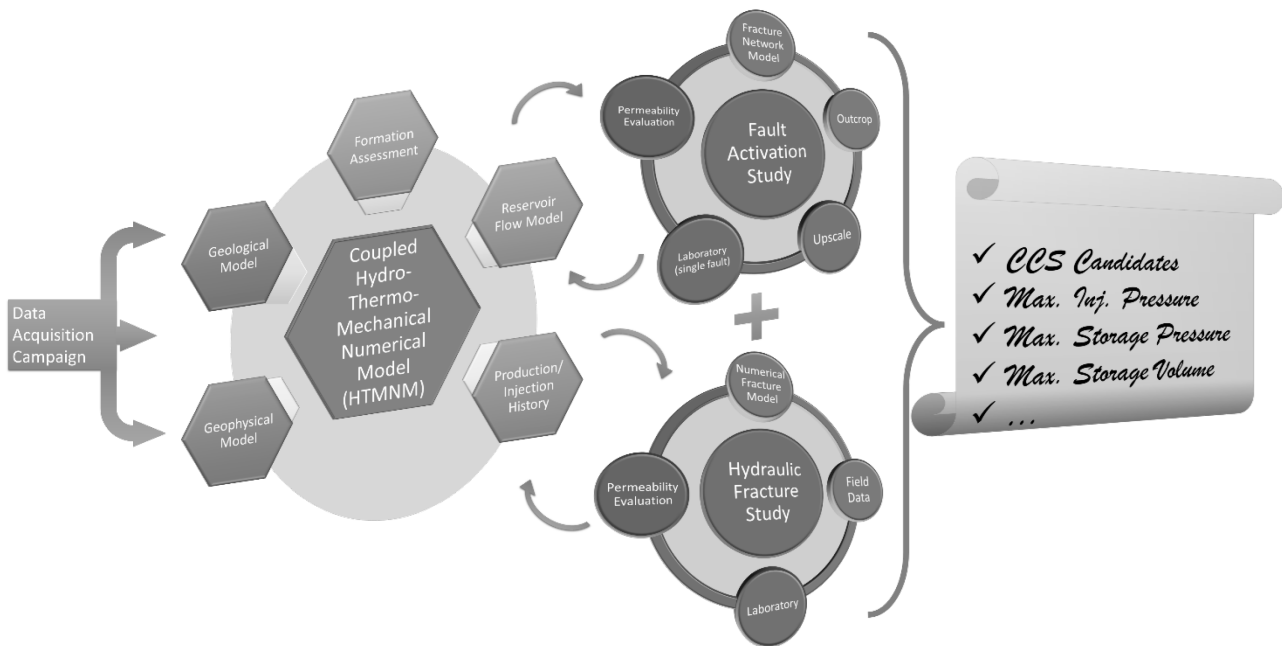


Fig. 3. Steps of the proposal geomechanical workflow to a final CCS project.

5 Conclusion

CCS projects involve geomechanical risks, with caprock integrity being a critical concern. To address these risks, a proposed workflow aims to mitigate caprock integrity issues, ensuring robust and reliable project delivery. The workflow application varies with project stages: a simplified linear workflow is recommended for the initial appraisal stage, given undefined target areas, limited information, and uncertainties. In contrast, during project implementation, a more specific and detailed workflow is essential, considering an already defined storage location, increased data availability, reduced uncertainties, and the necessity for robust and reliable study results.

From a geomechanical perspective, the focus should be on fault reactivation, particularly on those undetectable by seismic acquisition, and induced fractures within the caprock. The workflow presented emphasizes the integration of geomechanical properties with other disciplines to comprehensively characterize and assess caprock integrity. Specific studies aim to determine the triggering point for fluid loss containment from the reservoir and understand fluid flow behaviour in the event of caprock leakage.

References

- Gravanis, E, Sarris, E. 2023. A working model for estimating CO₂-induced uplift of cap rocks under different flow regimes in CO₂ sequestration. *Geomechanics for Energy and the Environment*, 33. <https://doi.org/10.1016/j.gete.2023.100433>
- Kaldi, J, Daniel, R, Tenthorey, E, Michael, K, Schacht, U, Nicol, A, Underschultz, J, Backe, G. 2011. Caprock systems for CO₂ geological storage. IAEHGH Rep 1:149.
- Li, C, Barès, P, Laloui, L. 2015. A hydromechanical approach to assess CO₂ injection-induced surface uplift and caprock deflection. *Geomechanics for Energy and the Environment*, 4, 51-60. <http://dx.doi.org/10.1016/j.gete.2015.06.002>
- Phillips, T, Kampman, N, Bisdom, K, Forbes Inskip, N, den Hartog, SAM, Cnudde, V, Busch, A. 2020. Controls on the intrinsic flow properties of mudrock fractures: A review of their importance in subsurface storage. *Earth-Science Reviews*, 211. <https://doi.org/10.1016/j.earscirev.2020.103390>
- Rizzo, RE, Forbes Inskip, N, Fazeli, H, Betlem, P, Bisdom, K, Kampman, N, et al. 2023. Modelling Geological Co₂ Leakage: Integrating Fracture Permeability and Fault Zone Outcrop Analysis. Available at SSRN.
- Snippe, J, Kampman, N, Bisdom, K, Tambach, T, March, R, Maier, C, Phillips, T, Forbes Inskip, N, Doster, F, Busch, A. 2022. Modelling of long-term along-fault flow of CO₂ from a natural reservoir. *International Journal of Greenhouse Gas Control*, 118. <https://doi.org/10.1016/j.ijggc.2022.103666>
- Wangen, M, Halvorsen, G, Gasda, SE, Bjørnarå, T. 2018. An analytical plane-strain solution for surface uplift due to pressurized reservoirs. *Geomechanics for Energy and the Environment*, 13, 25–34. <https://doi.org/10.1016/j.gete.2018.03.002>

Targeted CO₂ storage monitoring in a multi-layer stratigraphic system

Geetartha Dutta^{1*}, Ricardo Martinez¹, Philip Ringrose¹ and Jo Eidsvik¹

¹ Norwegian University of Science and Technology, Trondheim, Norway

* geetartha.dutta@ntnu.no

1 Introduction

In recent years, there has been much focus on geological storage of CO₂ in subsurface formations. Callioli Santi et al. 2022 suggest a Markovian structure for the leakage probability from one layer to another in a stratigraphic model of m layers. The model assumes a fixed time interval length of the injection program. Here, we extend this to explicitly model the height of the CO₂ column and hence the pore pressure in continuous time, the capillary pressure threshold, and thus extract the time of migration from one layer to another of the m layers.

By modelling the heights in different layers explicitly, we facilitate the linkage to monitoring, assuming that the seismic data are indicative of the heights of the CO₂ columns that build up in various layers over time. We conduct value of information (VOI) analysis to understand when it is optimal to gather seismic data about the CO₂ plume in the stratigraphic layer model.

2 Stochastic model

We build a stochastic model to simulate CO₂ migration based on the invasion-percolation concept. We consider a stratigraphic model having m layers of high porosity and permeability rock, separated by cap rocks having lower permeability (Fig. 1). We assume that CO₂ is injected in the bottom-most layer. The injected volume over time is known, but with the uncertainty in the layer properties, we only have a stochastic model for the volume that builds up in each layer. For each layer, we estimate the height of the CO₂ column and hence the pore pressure function, assuming the capillary threshold pressure as the limiting factor. When the capillary threshold pressure is exceeded, migration to the next layer occurs, and so on to the subsequent layers.

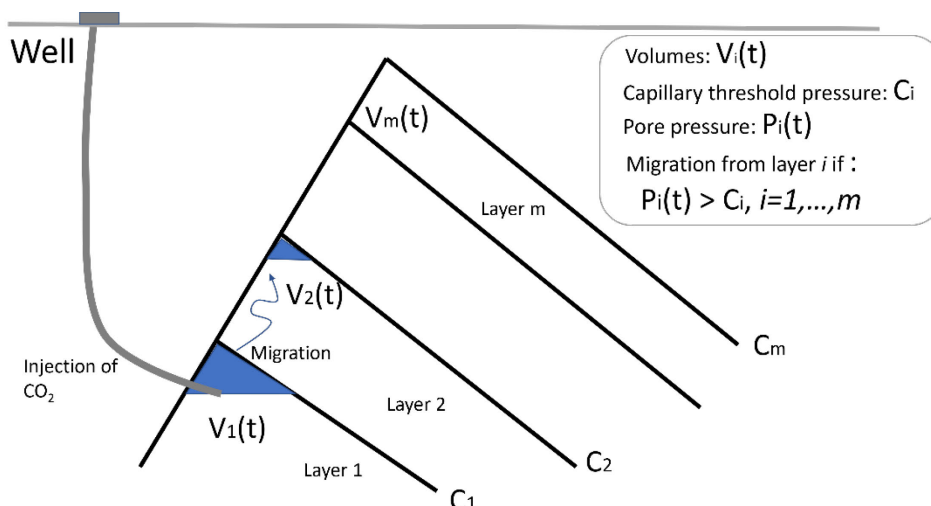


Fig. 1. When the capillary threshold pressure is exceeded, migration to the next layer occurs, and so on to the subsequent layers.

We assume that the capillary threshold pressure for each layer is random and distributed according to a log normal distribution, i.e., $\ln C_j \sim N(\eta_j, \tau_j^2)$. Here j denotes the layer number. The volume of CO₂ in layer j at any point of time t is given by

$$V_j(t) = r_{inj}(t - T_{j-1}). \quad \text{Eq. (1)}$$

Here r_{inj} is the rate of CO₂ injection and T_j is the time of migration from the j^{th} layer. As the buoyancy pressure in each layer is a function of the height of the CO₂ column in that layer, we need a transform between the volume and the height of the CO₂ column. This would depend on the geometry of the formation. In this work, we assume an ellipsoidal cap model (Callioli Santi et al. 2022) for the geometry, which gives the following transform:

$$V_j = \frac{\pi\alpha_j\beta_j}{3\gamma_j^2} h_j^2 (3\gamma_j - h_j). \quad \text{Eq. (2)}$$

Here α_j , β_j and γ_j are the axes of the ellipsoid from which the ellipsoidal cap representing the geometry of layer j has been extracted.

Using equations (1) and (2), we can derive the following relation between time and height, which can be used to compute the height of the CO₂ column in each layer at any point of time:

$$t = \frac{\pi\alpha_j\beta_j}{3r_{inj}\gamma_j^2} h_j^2 (3\gamma_j - h_j) + T_{j-1}. \quad \text{Eq. (3)}$$

We use this in simulating the data for CO₂ monitoring as will be discussed later. Then, to determine the time of migration from each layer, we need to equate the pressure in that layer to the capillary threshold pressure of its sealing layer, and find the time at which that condition would be satisfied.

$$P_j(t) = \delta\rho g h_j(t) = C_j. \quad \text{Eq. (4)}$$

Here $\delta\rho$ is the difference in density between CO₂ and brine, and g is the acceleration due to gravity.

3 Monitoring

3.1 Seismic data on column heights

In Section 2, we discussed how to simulate the heights of the CO₂ columns at any point of time. We assume that seismic data consists of the interpreted heights in each layer. If this data is gathered at time t , we get

$$d_j(t) = \begin{cases} 0 & \text{if } h_j(t) + \delta_j(t) < h_{thres} \\ h_j(t) + \delta_j(t) & \text{if } h_j(t) + \delta_j(t) \geq h_{thres}, \end{cases} \quad \text{Eq. (5)}$$

where $\delta_j(t) \sim N(0, \xi^2)$ for layers $j = 1, \dots, m$ are independent noise terms, and h_{thres} is the threshold height that can be detected. In general, the noise and the threshold height vary with depth and data type (Furre & Eiken 2014; White et al. 2018). But, for simplicity, we use the same h_{thres} for all the layers in this work.

The question is at what time t one gets the most information from the seismic observations. If this is done very early, there is not much happening in the layer model. If this is done very late, one has already injected much CO₂ and there are limited gains by stopping injection. A related VOI analysis was done in Anyosa et al. 2021, who used a situation with scenarios and multiple reservoir simulation models.

3.2 Value of information analysis

We perform a VOI analysis using the simulation-regression approach (Dutta et al. 2019). To do this, we need to frame a decision situation and simulate the data and the prospect values for different decision alternatives. Here we consider a CO₂ storage project where the total time period of injection is initially fixed, but at any given point of time during the project we can decide whether to continue or stop injection.

The prospect value for continuing injection is calculated by adding the cost of injecting CO₂ for the remaining period of time and the cost of possible leakage from the topmost layer. On the other hand, the prospect value for stopping injection at any point of time is equal to the tax that has to be paid for the amount of CO₂ not injected. Thus, we have

$$V_{cont} = -C_{inj}r_{inj}(T - t) - C_{leak}r_{inj} \max(T - T_m, 0), \quad \text{Eq. (6)}$$

$$V_{stop} = -C_{tax}r_{inj}(T - t), \quad \text{Eq. (7)}$$

where V_{cont} and V_{stop} are the prospect values for continuing and stopping injection respectively. Moreover, C_{inj} is the cost of injection per volume, C_{leak} is the cost of leakage per volume, C_{tax} is the tax per volume of CO₂ not injected, r_{inj} is the rate of injection, T is the planned time period of injection, T_m is the time of leakage from the topmost layer, and t is the time at which the decision needs to be made.

In the VOI calculations, we compute values in equations (6) and (7) over simulations of leak times. In addition, we simulate associated seismic data d_j for all $j = 1, \dots, m$, and denote the complete vector of data by $\mathbf{d} = (d_1, \dots, d_m)$. The VOI is obtained as the difference in the posterior value and the prior value, where the conditional values are obtained by regressing the values on the data. We have

$$VOI = \frac{1}{B} \sum_{i=1}^B \max\{\hat{V}_{cont}^i, \hat{V}_{stop}^i\} - \max\left\{\frac{1}{B} \sum_{i=1}^B V_{cont}^i, \frac{1}{B} \sum_{i=1}^B V_{stop}^i\right\}. \quad \text{Eq. (8)}$$

4 Sleipner inspired case

We perform a VOI case study inspired from the Sleipner CO₂ storage project. A 9-layer CO₂ plume has been interpreted at Sleipner (Callioli Santi et al. 2022). So, we try to model this using a 9-layer stratigraphic model. We assume the layer top geometry based on the Sleipner 2019 Benchmark model, and fit ellipsoidal caps to each layer top as shown in Fig. 2. To account for the uncertainty in the layer top geometry, we consider 5000 samples of ellipsoidal caps fitted to different subsets of each layer top.

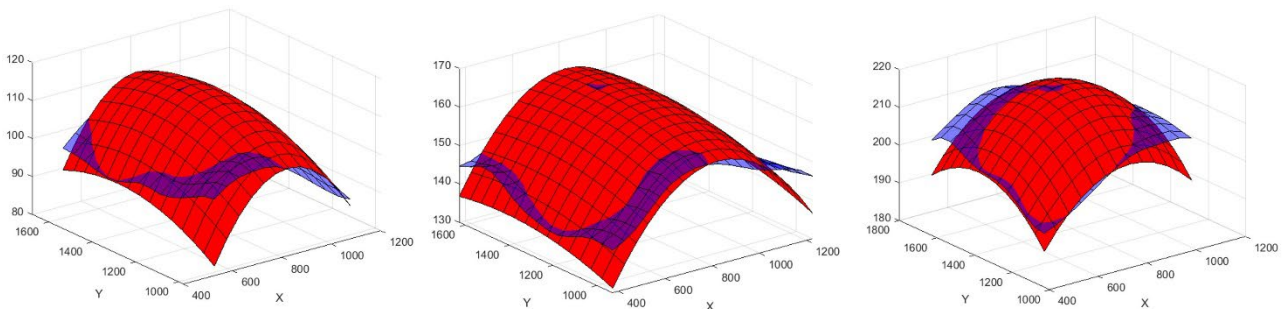


Fig. 2. 5000 samples of ellipsoidal caps are fitted to different subsets of each layer top.

Using this stochastic model, we simulate the times of migration/leakage from each layer, the distributions of which are shown in Fig. 3. We see that there is greater uncertainty in the times of migration for the shallower layers compared to the deeper layers.

We compute the VOI for different points in time using linear regression. Three types of data are considered: perfect data (with no noise), low noise data (with low ξ) and high noise data (with high ξ). Fig. 4 shows how the VOI varies with the time of survey. This seems to indicate that there is high value in collecting data at intermediate times (i.e., after the probability of migration has increased above an initially low value). On the other hand, if data collection is done too late there may be less opportunity to take remedial measures.

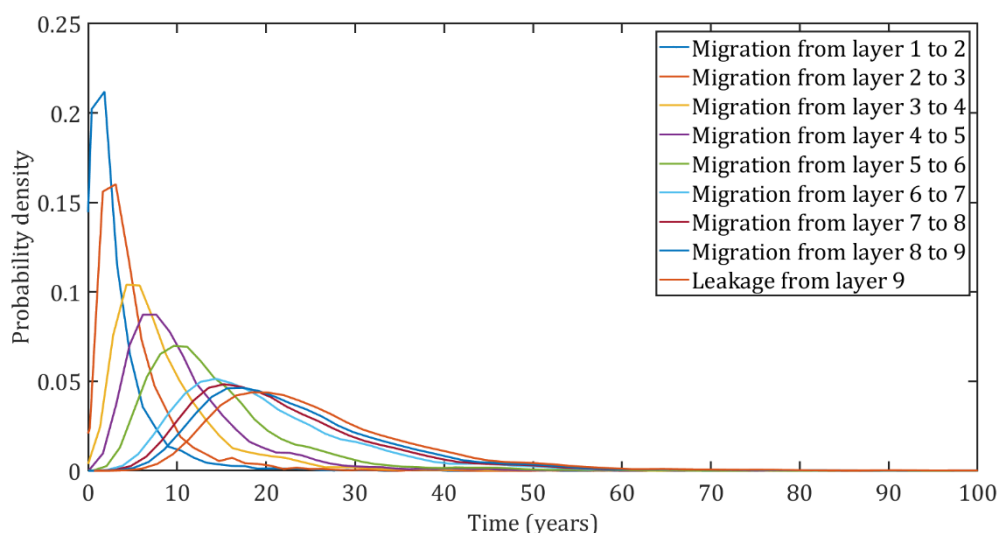


Fig. 3. Distributions for the times of migration/leakage from each layer.

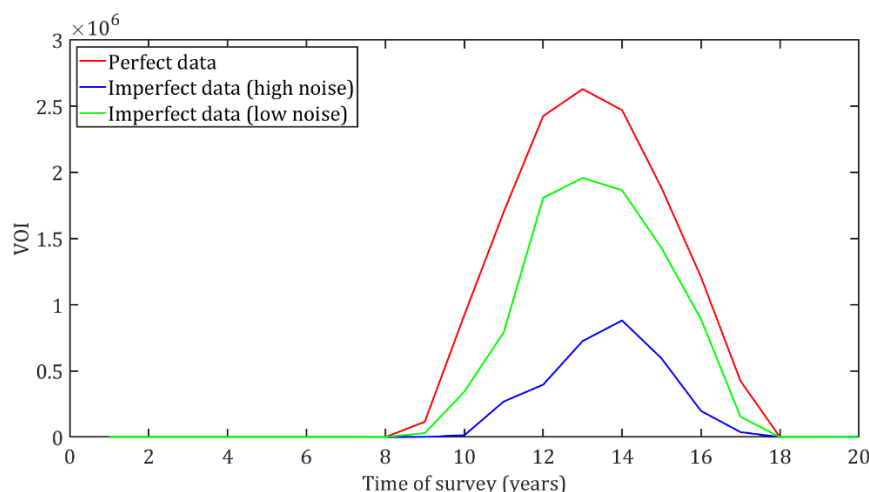


Fig. 4. Variation of VOI with time of survey seems to indicate that there is high value in collecting data at intermediate times.

5 Conclusions

We have developed a framework to estimate the value of information in CO₂ storage monitoring using an illustrative example inspired by the Sleipner case. This VOI framework can be used to find the optimal points in time to collect monitoring data such that the value is maximized. Using plausible CO₂ detection thresholds based on advanced seismic analysis of reflected and refracted wavefields, the VOI framework can be used to target and optimize advanced seismic monitoring strategies.

References

- Anyosa, S, Bunting, S, Eidsvik, J, Romdhane, A, Bergmo, P. 2021. Assessing the value of seismic monitoring of CO₂ storage using simulations and statistical analysis. *Int. J. Greenh. Gas Control*. 105, 103219. <https://doi.org/10.1016/j.ijggc.2020.103219>
- Callioli Santi, A, Ringrose, P, Eidsvik, J, Haugdahl, TA. 2022. Assessing CO₂ Storage Containment Risks Using an Invasion Percolation Markov Chain Concept. *Proceedings of the 16th Greenhouse Gas Control Technologies Conference (GHGT-16)*, 23-24 Oct 2022. <http://dx.doi.org/10.2139/ssrn.4282992>
- Dutta, G, Mukerji, T, Eidsvik, J. 2019. Value of information analysis for subsurface energy resources applications. *Appl. Energy* 252, 113436. <https://doi.org/10.1016/j.apenergy.2019.113436>
- Furre, AK, Eiken, O. 2014. Dual sensor streamer technology used in Sleipner CO₂ injection monitoring. *Geophys. Prospect.* 62, 1075-1088. <https://doi.org/10.1111/1365-2478.12120>
- White, JC, Williams, G, Chadwick, A, Furre, AK, Kiær, A. 2018. Sleipner: The ongoing challenge to determine the thickness of a thin CO₂ layer. *Int. J. Greenh. Gas Control*. 69, 81–95. <https://doi.org/10.1016/j.ijggc.2017.10.006>

The Mont Terri URL: guided tour overview

David Jaeggi¹, Jonas Windsich¹ and Martin Ziegler¹

¹ Swiss Federal Office of Topography (swisstopo), Mont Terri URL, Switzerland

* david.jaeggi@swisstopo.ch

During the guided visit of the Mont Terri underground rock laboratory, we will see and discuss four experiment sites (Fig. 1), which are:

1 CL (CO₂LPIE — CO₂ long-term periodic injection) experiment

The CL experiment investigates hydraulic, mechanical, and chemical (HMC) effects of CO₂ injection into intact Opalinus Clay under in-situ conditions at the Mont Terri underground rock laboratory over a period of 4+ years). The aim is to enhance understanding of caprock behavior and its integrity, both of high relevance for the uses of the subsurface, including geothermal energy and the storage of nuclear waste, energy, and fluids, especially CO₂.

2 CS-E (Mini-fracturing and sealing) experiment

The main goal of the CS-E experiment is to understand the reactivation of single fractures within the Mont Terri Main Fault. The experiment foresees a series of “mini-stimulations” with low flow rate to open pre-existing small fractures, and will be followed by injections of sealants. The experiment will help developing mitigation strategies for caprock failure during storage activities.

3 FS-B (Imaging the long-term loss of faulted host rock integrity) experiment

The FS-B experiment aims at imaging long-term fluid flow as well as permeability and stress variations through a ruptured minor fault to assess the performance of radioactive waste repositories in shale formations. Results from FS-B could also be used to assess CO₂ storage security and the integrity of reservoirs caprocks.

4 HT (Hydrogen transfer in Opalinus Clay) experiment

The aim of the HT experiment is to evaluate if hydrogen consumption processes are measurable in a borehole and to evaluate the role of microbial activity on these processes. The experiment identifies the occurring processes and takes the opportunity of a water producing borehole to get new data on porewater chemistry and natural dissolved gases.

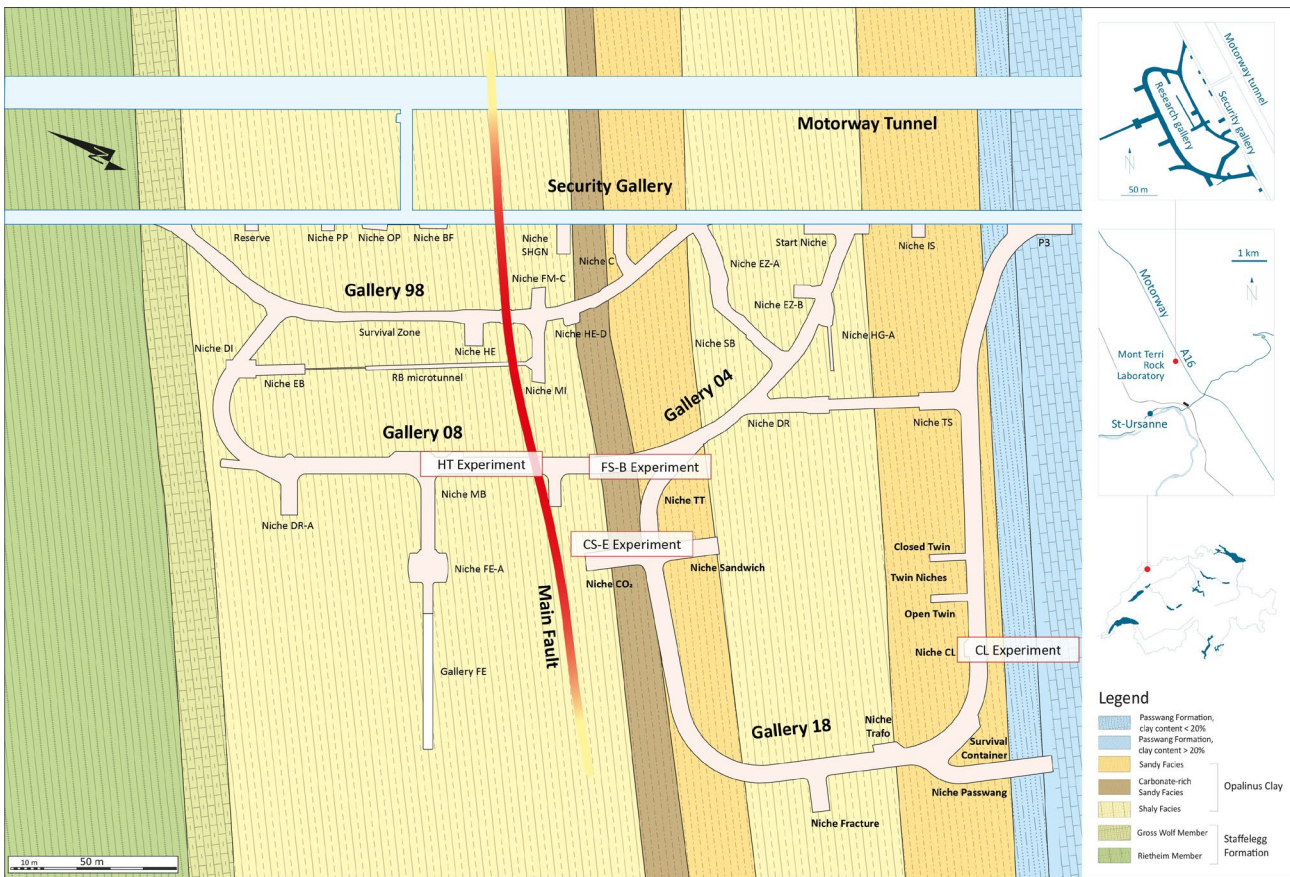


Fig. 1. Geological map of the Mont Terri Underground Rock Laboratory showing the experiment sites (HT, FS-E, CS-E, and CL) that will be visited and discussed during the guided laboratory tour.